



The  
University  
Of  
Sheffield.

# **Regulation of exocytosis and peptide release by synaptotagmins in sensory neurons**

**Judit Mészáros**

A thesis submitted in partial fulfilment of the requirements for  
the degree of Doctor of Philosophy

The University of Sheffield  
Faculty of Science  
Department of Biomedical Sciences

December 2019



## Abstract

In response to inflammation and nerve injury, nociceptive DRG (dorsal root ganglion) neurons become hyperexcitable and this hyperexcitability persists in chronic pain. A key feature of chronic pain states is enhanced secretion of neuropeptides (such as CGRP or Substance P) as a result partly of gene expression changes, and partly changes at the level of regulated secretion. To date however no studies have investigated what changes occur at the level of exocytosis and what changes in the secretory machinery are required to support enhanced neuronal transmission. The research described in this thesis addresses this fundamental question and identifies the role of two regulators of vesicle fusion, synaptotagmin 4 and 7 (syt4/7), in enhanced peptide secretion from nociceptors following exposure to neuronal growth factor (NGF).

Synaptotagmins are vesicular membrane proteins that are known for their role in coupling excitation and increased calcium concentration to vesicle fusion and release of transmitters. In this thesis four synaptotagmin isoforms are described for the first time in DRG neurons using a combination of western blotting and immunofluorescence: syt2, syt4, syt7 and 11. Syt2 and 7 are low and high affinity  $\text{Ca}^{2+}$  sensors respectively that are important regulators of vesicle fusion. Syt4 and 11 are isoforms that are unable to bind calcium, and therefore their role in regulated secretion is unclear. Syt4 is the more well-known isoform of the two, but studies published to date have provided conflicting views, supporting both an inhibitory and potentiating role. Our results have shown that all the above isoforms are expressed in peptide expressing DRG neurons and are present on CGRP containing vesicles.

NGF is a well-known inflammatory mediator of the adult nervous system; it enhances peptide secretion in nociceptive DRG neurons that express its receptor TrkA and contributes to hyperalgesia by sensitising TRPV1 channels. Here we show that syt4 is present in the majority of TrkA positive DRG neurons, and that the enhancement in CGRP secretion following NGF exposure is reduced in neurons isolated from Syt4 knockout (KO) mice. In order to dissect further the role of syt4 and 7 in exocytosis in live DRG neurons, we have established a pHluorin-based fusion assay using total internal reflection (TIRF) microscopy. Using this technique, we found that syt4 and syt7 are functionally targeted to an overlapping population of vesicles, where they mediate fusion events with long fusion pore

open times and slow endocytosis. To our knowledge this is the first study to address directly the role of Syt4 in peptide secretion from nociceptors. Our results provide novel insight into the molecular mechanisms contributing to pain signalling and in particular the secretion of CGRP, a well-known mediator of pain conditions.

## Author's declaration

I declare that the work in this dissertation was carried out in accordance with the requirements of the University's Regulations and Code of Practice for Research Degree Programmes and that it has not been submitted for any other academic award. Except where indicated by specific reference in the text, the work is the candidate's own work. Work done in collaboration with, or with the assistance of, others, is indicated as such. Any views expressed in the dissertation are those of the author.

Signed

Judit Mészáros

Date

14/5/2020

## Acknowledgements

First, I would like to thank my supervisor, Dr Liz Seward for giving me the opportunity of pursuing this PhD. Her guidance and thoughtful insights helped me greatly throughout the past four years to push my project forward. I would also like to thank Dr Mohammed Nassar for giving me help and advice when I needed it, Mark Collins for his help in mass-spectrometry and all my colleagues in the department who contributed to my project through discussions or technical advice.

This thesis would not have been possible without the help of Michelle Bird in the animal house and Maria Pakendorf in the PCR lab. Thank you Michelle for helping me manage the mouse colonies and Maria for helping with the endless genotyping!

I am also grateful for my friends and fellow PhD students, especially Claire Murzeau, Keith Woodley, Toni Carmona and a bit later Kinga Kosim and Sindhu Naik for making my days less gray and rainy and my lunchtime breaks more fun. Angie and all the people in the E floor office, thank you for supplying me with coffee and a good laugh in times of need.

Finally, I would also like to thank you Patrick for putting up with all my complaining during the most difficult times and helping me unwind the stress. Végül de messze nem az utolsó sorban köszönöm a családomnak, főleg szüleimnek és testvéremnek, illetve otthoni barátaimnak a támogatást, Annának és Áginak a távsörözéseket és beszélgetéseket. Pacsi!

## List of figures

<b>Chapter 1 - Introduction</b>	<b>page</b>
Figure 1.1.1 Schematic anatomy of the spinal cord, dorsal root ganglia (DRG) (orange) and attached nerves	19
Figure 1.1.2 DRG neuron types and selected markers as defined by Usoskin et al. (2014)	21
Figure 1.2.1 Neurotrophin receptors and downstream signalling pathways	24
Figure 1.2.2 Processing and synthesis of CGRP	27
Figure 1.2.3 Receptors and signalling pathways activated by CGRP	28
Figure 1.3.1 Electron micrograph showing the synaptic architecture in the spinal dorsal horn	30
Figure 1.3.2 Constitutive and regulated secretory pathways	32
Figure 1.3.3 Steps of regulated exocytosis and main proteins involved	34
Figure 1.3.4 Cartoon of an LDCV with associated SNARES and other vesicular proteins that have been reported in DRG neurons in large scale mRNA and proteomic profiling studies	36
Figure 1.3.5 Schematic showing the classical model of exocytosis (A) and a new model (B) proposed by Chiang et al. (2014)	38
Figure 1.3.6 The role of chromogranin A in chromaffin cells	40
Figure 1.4.1 Example traces of amperometric currents from PC12 cells stimulated with KCl	43
Figure 1.4.2 Cartoons showing the theoretical background of styryl dyes (a, b) and pHluorins (c)	44
Figure 1.4.3 Comparison of mEGFP, pHluorin and mCherry tagged to NPY for reporting vesicle fusion in Ins1 cells	45
Figure 1.4.4 Visualization of DCV fusion pores and hemi-fusion intermediates with STED imaging	47
Figure 1.5.1 Structure of mouse synaptotagmins	49
Figure 1.5.2 Schematic diagram showing the half maximal calcium concentrations, $[Ca^{2+}]_{1/2}$ , of indicated C2 domain containing proteins required for membrane	50

binding	
Figure 1.5.3 Putative roles of syt1 and syt7 in mediating vesicle fusion	53
Figure 1.5.4 Summary figure of known role of syt4 in vesicle trafficking in hippocampal neurons and of TrkA signalling in DRG neurons.	56
<b>Chapter 2 – Materials and Methods</b>	
Figure 2.3.1 Schematic of the syt4 gene structure used to create syt4 KO mice	60
Figure 2.3.2 Schematic showing the “knockout-first” conditional allele targeting strategy for creation of syt7 and syt2 KO mice	61
Figure 2.6.1 DIC images of DRG cultures at different stages	68
Figure 2.6.2 DRG neurons expressing GFP after transfection by electroporation	70
Figure 2.13 Typical layout of ELISA experiments	78
Figure 2.18.1 Schematics of theoretical background of TIRFM compared to epifluorescence microscopy	81
Figure 2.18.2 Calcium signals in DRG neurons after KCl stimulation	83
Figure 2.18.3 Detecting fusion events with pHluorin	85
Figure 2.18.4 Analysis of pHluorin fusion events	86
Figure 2.18.5 Example pHluorin traces and settings for HHD measurements on OriginPro	87
Figure 2.18.6 Example pHluorin traces and settings for HHD measurements in OriginPro	88
<b>Chapter 3 – Characterization of synaptotagmins in cultured DRG neurons</b>	
Figure 3.1 mRNA and protein expression of different synaptotagmin isoforms in DRG neurons	93
Figure 3.2.1 Validation of the specificity of syt2 and syt7 antibodies in knockout brain lysates	94
Figure 3.2.2 Western blots of syt2 and 7 in DRG neurons cultured from syt4 <sup>+/+</sup> and syt4 <sup>-/-</sup> mice	96
Figure 3.2.3 Western blots of syt4 and 11 in DRG neurons cultured from syt4 <sup>+/+</sup> and syt4 <sup>-/-</sup> mice	97
Figure 3.2.4 Syt4 and 11 immunofluorescence in cultured DRG neurons	99
Figure 3.2.5 Syt2 and 7 immunofluorescence in cultured DRG neurons	100

Figure 3.2.6 Quantification of colocalization of syt immunostaining with CGRP	101
Figure 3.3 Further validation of syt2, 4 and 7 antibodies using immunocytochemistry	102
Figure 3.4 Colocalization analysis of CGRP with syt2, 4, 7 and 11	105
Figure 3.5 Basal and evoked CGRP release are unaffected in syt4 and syt7 KO mice	108

#### **Chapter 4 - Studying single vesicle fusion in DRG neurons using pHluorin constructs**

Figure 4.2.1 Detection of VAMP2-pHluorin labelled vesicle fusion events using TIRF microscopy	116
Figure 4.2.2 Graphs of syt2-pHluo amplitude, HHD and decay time	117
Figure 4.3 Tracking peptide release using NPY-pHluorin	119
Figure 4.4.1 Comparison of syt2-pHluorin fusion events on the soma and neurites	121
Figure 4.4.2 Graphs of syt2-pHluo amplitude, HHD and decay time	122
Figure 4.5.1 Comparison of Syt4pHluorin fusion events on the soma and neurites	125
Figure 4.5.2 Graphs of syt4-pHluo amplitude, HHD and decay time	126

#### **Chapter 5 - Investigating the effect of NGF on neuropeptide release**

Figure 5.1 NGF signalling pathways	132
Figure 5.2. Acute NGF treatment enhances KCl induced CGRP release	135
Figure 5.3 Syt4 and CGRP are both co-expressed with TrkA	137
Figure 5.4 The effects of NGF treatment on CGRP release is syt4 dependent	139
Figure 5.5 Identification of the S135 and other phosphorylation sites in syt4 in DRG neurons	141

#### **Chapter 6 - The effects of syt4 and its phosphorylation on syt7-mediated exocytosis and fusion kinetics**

Figure 6.2.1 Syt7-pHluorin fusion events differ on the soma and neurites	146
Figure 6.2.2 Syt4-mCherry favours syt7-mediated events with slower kinetics	147
Figure 6.3 The kinetics of syt7-pHluorin events is altered in syt4 <sup>-/-</sup> mice	149
Figure 6.4.1 Kymograph analysis of syt4-S135A and S135E before stimulation	151
Figure 6.4.2 Syt4 phosphomutants have reduced mobility after stimulation	153
Figure 6.5 Phosphorylation of syt4 at Serine-135 does not alter syt7-mediated fusion	156

---

## Chapter 7 – General discussion

---

Figure 7 Proposed pathways and mechanisms involved in NGF-induced increase of neuropeptide release in sensory neurons

---

162

## List of abbreviations

AIS	axon initial segment
Akt	Protein kinase B
ANOVA	Analysis of variance
APS	ammonium persulfate
ASIC1	Acid-sensing ion channel 1
ATP	Adenosine triphosphate
BDNF	Brain-derived neurotrophic factor
BSA	Bovine serum albumin
Ca <sup>2+</sup>	calcium ions
cAMP	Cyclic adenosine monophosphate
CGRP	Calcitonin gene-related peptide
CIVD	calcium-independent but voltage-dependent
CLR	calcitonin receptor-like receptor
C-LTMR	C-fiber low-threshold mechanoreceptors
CNS	Central nervous system
CREB	cAMP response element binding protein
DAG	diacylglycerol
DAPI	4',6-diamidino-2-phenylindole
DIV	days in vitro
DNA	Deoxyribonucleic acid
DRG	Dorsal root ganglion
dTNP	Deoxynucleoside triphosphate
EGFP	enhanced green fluorescent protein Ethylene glycol-bis(β-aminoethyl ether)-N,N,N',N'-tetra acetic acid
EGTA	acid
ELISA	Enzyme-linked immunosorbent assay
ER	Endoplasmic reticulum
ERK	Extracellular signalling-regulated kinase
FF	Full fusion
HHD	Full-width at half maximum
GABA	Gamma-aminobutyric acid
GAPDH	Glyceraldehyde 3-phosphate dehydrogenase
HEPES	4-(2-hydroxyethyl)-1-piperazineethanesulfonic acid
HET	heterozygous
IB4	Isolectin B4
ICC	immunocytochemistry
Ins1 cells	Insulin secreting beta cell derived line
IP	Immunoprecipitation
IP3	Inositol tris-phosphate
JACoP	Just another co-localisation plugin
JNK	c-Jun N-terminal kinase
KCC2	Potassium chloride cotransporter 2
Kif1a	Kinesin Family Member 1A

KO	Knockout
KR	Kiss-and-run
LDCV	Large dense core vesicle
MAPK	Mitogen-activated protein kinase
MOC	Mander's overlap coefficient
Mrgpr	Mas-related G protein-coupled receptor
MS	Mass spectrometry
Munc13	Protein unc-13 homolog B
Nav	Voltage-gated sodium channels
NDS	Normal donkey serum
NF	Neurofilament
NGF	Nerve growth factor
NMDA	N-methyl-D-aspartate
NP	Non-peptidergic
NPY	neuropeptide Y
NT-3, 4	neurtrophin 3, 4
p75	low-affinity nerve growth factor receptor
PBS	Phosphate-buffered saline
PBS	Phosphate-buffered saline
PBST	Phosphate-buffered saline with 0.1% tween
PC12 cells	Pheochromocytoma-derived cell line
PC12 cells	pheochromocytoma
PEP	Peptidergic
PI3K	Phosphoinositide 3-kinase
PKA	Protein kinase A
PKC	Protein kinase C
PLC	Phospholipase C
PLL	poly-L-lysine
PNS	Peripheral nervous system
Rab3	Ras-related protein
raf	serine/threonine-specific protein kinases
RAMP1	receptor activity modifying protein-1
ras	protein family of small GTPases
RIM	Regulating synaptic membrane exocytosis protein 1
RIPA	Radioimmunoprecipitation assay buffer
RNA	Ribonucleic acid
ROI	region of interest
RPM	revolutions per minute
RRP	Readily releasable pool
SD	Standard deviation
SDS	Sodium dodecyl sulphate
SEM	Standard error of the mean
shRNA	short hairpin RNA
SNAP25	soluble N-ethylmaleimide-sensitive attachment protein 25.
SNARE	N-ethylmaleimide-sensitive factor attachment protein receptor
SP	Substance P

STED	Stimulated emission depletion microscopy
STORM	Stochastic optical reconstruction microscopy
SV	Synaptic vesicle
syt	synaptotagmin
TBST	Tris-buffered saline with 0.1% tween
TEMED	Tetramethylethylenediamine
TGN	Trans-Golgi network
TH	tyrosine hydroxylase
TIRF	Total internal reflection fluorescence
TM	Transmembrane
TM	Transmembrane
tPA	tissue plasminogen activator
TrkA	Tropomyosin receptor kinase A
TRPV1	Vanilloid receptor type 1
VAMP	vesicle-associated membrane protein
VGCC	Voltage-gated calcium channel
WB	Western blot
WT	Wild type

## Table of contents

<b>Abstract</b> .....	3
<b>Author's declaration</b> .....	5
<b>Acknowledgements</b> .....	6
<b>List of figures</b> .....	7
<b>List of abbreviations</b> .....	11
<b>Table of contents</b> .....	14
<b>1. Introduction</b> .....	18
1.1. Sensory processing.....	18
The somatosensory system and nociception .....	18
Classification of dorsal root ganglion neurons .....	19
1.2. Pain – changes occurring in somatosensory neurons in pathological states .....	22
Nerve Growth Factor (NGF) signalling.....	23
Calcitonin-gene related peptide .....	26
1.3. Regulation of exocytosis .....	29
Types of secretory vesicles and their cargo.....	29
The exocytotic machinery.....	33
Somatic secretion in DRG neurons .....	34
The fusion pore and regulation of cargo release.....	37
Modulation of fusion pore dynamics by Ca <sup>2+</sup> .....	41
1.4. Techniques for studying single vesicle exocytosis .....	42
1.5. Synaptotagmins – coupling excitation to Ca <sup>2+</sup> mediated exocytosis .....	48
1.6. Aims and objectives .....	57
<b>2. Materials and Methods</b> .....	58
2.1. List of antibodies.....	58
2.2. DNA constructs .....	59
2.3. Animals.....	59
2.4. Primers.....	61

2.5.	Solutions and buffers .....	62
	Live-cell imaging and ELISA solutions .....	62
	Western blotting solutions .....	63
	Other often used reagents .....	64
	Commercial Kits and devices .....	65
2.6.	Mouse dorsal root ganglia isolation and culture .....	66
	Dissection and culture preparation .....	66
	DRG culture conditions.....	67
	Electroporation of DRG neurons .....	69
2.7.	Western blot .....	71
	Sample lysis.....	71
	Protein quantification and sample preparation for loading.....	71
	SDS-PAGE and protein transfer .....	71
	Antibody staining and visualization .....	72
2.8.	DNA extraction from ear samples.....	72
2.9.	PCR genotyping.....	73
2.10.	Immunoprecipitation .....	74
2.11.	Mass spectrometry .....	74
	Coomassie staining and gel cutting .....	74
	Digestion.....	75
	Protein extraction.....	75
	Mass Spectrometry.....	75
	Proteomics data analysis .....	76
2.12.	Immunocytochemistry.....	76
	Coverslip coating for immunofluorescence.....	76
2.13.	CGRP ELISA.....	77
	Plate coating for western blotting and ELISA .....	77
	ELISA procedure.....	77

2.14.	Bacterial work and DNA preparation .....	79
2.15.	Image deconvolution and colocalization analysis.....	80
2.16.	Epifluorescent imaging for immunocytochemistry.....	80
2.17.	Confocal imaging.....	80
2.18.	Live cell imaging .....	81
	Dye loading for calcium imaging.....	81
	TIRF imaging setup and stimulation .....	81
	Image analysis.....	84
	Kymograph analysis .....	89
	Statistical analysis .....	89
<b>3.</b>	<b>Characterization of synaptotagmins in cultured DRG neurons .....</b>	<b>91</b>
3.1.	Introduction .....	91
3.2.	Syt2, 4, 7 and 11 are expressed in cultured DRG neurons.....	94
3.3.	Antibody validation using syt-pHluorin constructs.....	101
3.4.	Colocalization analysis of synaptotagmins with CGRP in DRG neuron somata .....	103
3.5.	Syt4 or syt7 KO do not affect basic CGRP release.....	106
3.6.	Conclusions .....	109
<b>4.</b>	<b>Studying single vesicle fusion in DRG neurons using pHluorin constructs.....</b>	<b>114</b>
4.1.	Introduction .....	114
4.2.	Establishing exocytosis assay in DRG neurons using VAMP2-pHluorin .....	115
4.3.	Detecting peptide release using NPY-pHluorin.....	118
4.4.	Syt2-pHluorin mediated exocytosis has distinct fusion kinetics between soma and neurites .....	120
4.5.	Syt4-bearing vesicles can release NPY and have differences in their fusion kinetics between soma and neurites .....	123
4.6.	Conclusions .....	127
<b>5.</b>	<b>Investigating the effect of NGF on neuropeptide release.....</b>	<b>132</b>
5.1.	Introduction .....	132

5.2.	30 minutes NGF treatment enhances KCl induced CGRP release in wild type neurons .....	134
5.3.	Syt4 is expressed in the majority of TrkA+ neurons .....	136
5.4.	NGF-enhancement of CGRP release is Syt4 dependent .....	138
5.5.	Identification of Syt4 phosphorylation sites in DRG neurons.....	140
5.6.	Conclusions .....	142
<b>6.</b>	<b>The effects of syt4 and its phosphorylation on syt7-mediated exocytosis and fusion kinetics .....</b>	<b>143</b>
6.1.	Introduction .....	143
6.2.	Overexpressed syt7 and syt4 can be trafficked to the same vesicles, where syt4 may affect syt7-mediated fusion .....	144
6.3.	The kinetics of syt7-pHluorin events are altered in syt4 <sup>-/-</sup> mice.....	148
6.4.	Trafficking dynamics of Syt4-S135A and S135E-mCherry .....	150
6.5.	S135 phosphorylation of syt4 shifts syt7 fusion events towards longer pore open time .....	154
6.6.	Conclusions .....	157
<b>7.</b>	<b>General discussion.....</b>	<b>160</b>
	<b>References .....</b>	<b>165</b>

# 1. Introduction

## 1.1. Sensory processing

### The somatosensory system and nociception

Information from an individual's environment is processed by the somatosensory system which produces the conscious sensation of temperature, touch, body position and pain. This pathway starts with the sensory afferents that are activated by the specific stimuli on the surface or the inside of the body, and then convey this information through the dorsal root ganglia (DRG) to the spinal cord, where they form synapses with second order neurons (figure 1.1). These second order neurons then either pass their information on to other neurons in the spinal cord, or project towards the brain, and finally to the sensory cortex where the sensation is created (Todd, 2010). The sensory neurons in this pathway belong to the peripheral nervous system (PNS); their cell bodies form 31 pairs of DRGs along the spinal cord. DRG neurons are pseudounipolar, which means that a single axon stem bifurcates into two branches, termed peripheral and central axons, and they each grow towards the periphery or the central nervous system (Matsuda *et al.*, 1996; Nascimento, Mar and Sousa, 2018). As opposed to multipolar neurons, where inputs arriving on the somatodendritic compartment summate and elicit an action potential at the axon initial segment (AIS), adult DRG neurons lack a clearly defined AIS (Gumy *et al.*, 2017) though proteins associated with it, such as ankyrin G, are enriched in cultured embryonic DRG neurons (Dzhashvili *et al.*, 2007); instead, action potentials form on their peripheral axon endings and a putative AIS region might serve as a low-pass filter for electrical signals (Carr *et al.*, 2009; Nascimento, Mar and Sousa, 2018).

Different sensory afferents respond to different types of stimuli such as heat, cold, pressure, pH, itch, proprioception and pain, and this feature provides the basis of modality-specific sensation in vertebrates. Whether they respond to one or multiple stimulus modalities, DRG neurons can be unimodal or polymodal, and thus DRG neurons give rise to a uniquely heterogeneous cell population.

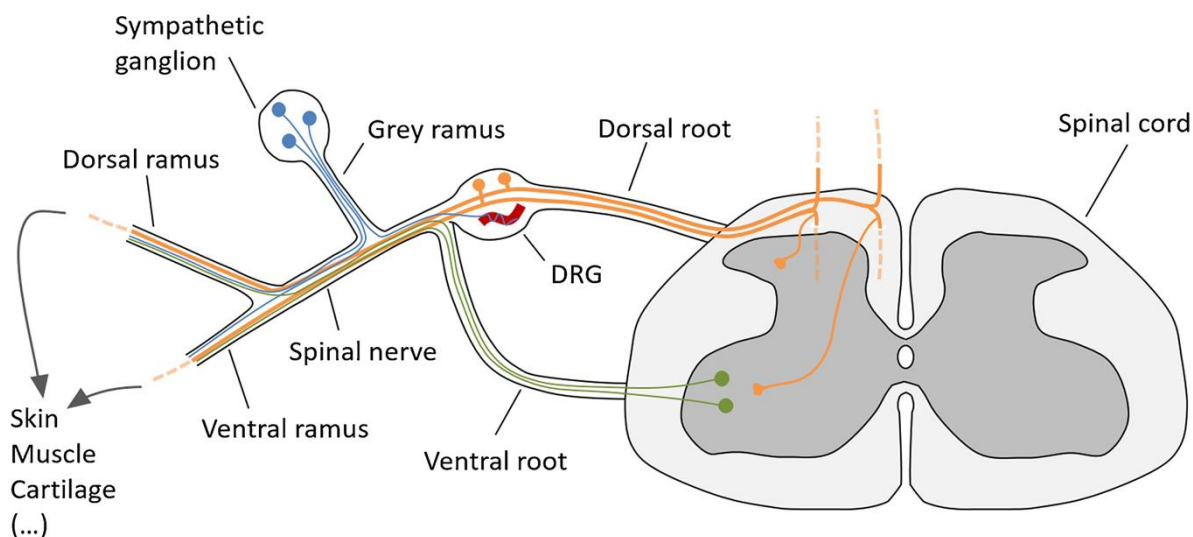


**Figure 1.1.1 Schematic anatomy of the spinal cord, dorsal root ganglia (DRG) (orange) and attached nerves.** From the periphery, signal travel through the spinal nerve where sympathetic (blue) and motor neuron axons (green) run together with the peripheral DRG neuron axons. The central fibres form the dorsal root and enter the spinal dorsal horn, where they synapse onto second order neurons. Image was adapted from Nascimento et al., 2018.

### Classification of dorsal root ganglion neurons

#### *Soma size, conduction velocity and response profiles*

Classically, sensory neurons were categorized based on features such as cell size, axon diameter and myelination (which relates to conduction velocity), firing threshold, neurochemical properties and the type of stimulus they respond to. According to this traditional classification, we can distinguish small, medium and large diameter sensory neurons (recent reviews include Todd, 2010; Le Pichon and Chesler, 2014; Emery and Ernfors, 2018).

Large diameter neurons (>50  $\mu\text{m}$ ) have heavily myelinated fibres (A $\beta$  and proprioceptors), and conduct action potentials at a high speed (70-120 m/s). These are low-threshold mechanoreceptors that specialize on sensations such as light touch, vibration and hair movements, and proprioceptors that help maintain posture and muscle reflexes. Medium diameter neurons (~30-50  $\mu\text{m}$ ) have A $\delta$  fibres that are thinly myelinated, therefore conduct action potentials at a lower speed (5-70 m/s). They are associated with different types of innocuous and also noxious stimuli, and because of their faster conduction velocity

compared to C-fibres, they are thought to result in “fast” pain. Medium diameter axon endings arborize in the superficial laminae of the spinal dorsal horn, while large diameter fibres arborize in the deeper layers (III-V) (Todd, 2010).

Small diameter DRG neurons (between 10 and 30  $\mu\text{m}$ ) give rise to C fibres, which are unmyelinated and have the lowest conduction velocity (around 0.5-2 m/s). Some of these fibres are low-threshold mechanoreceptor (C-LTMRs) activated by light touch, but most C fibres are specialized for painful or noxious stimuli – hence, called nociceptors. These nociceptors can be subdivided into two further groups: peptidergic and non-peptidergic neurons. Peptidergic DRG neurons express neuropeptides such as substance P (SP) or calcitonin-gene related peptide (CGRP) (Nilsson and Pernow, 1975; Wiesenfeld-Hallin *et al.*, 1984), while non-peptidergic neurons are defined by the binding of the lectin IB4 isolated from the plant *Griffonia simplicifolia* (Stucky and Lewin, 1999), and express Mas-related G protein-coupled receptors (Mrgprs), some of which have been linked to the sensation of itch (Dong *et al.*, 2001; Han and Simon, 2011); both types of C fibres arborize in the superficial (I/II) layers of the spinal dorsal horn.

#### *mRNA and protein expression based classification*

The categories described above are not mutually exclusive and there are numerous overlaps between them, eg. some IB4+ neurons also express CGRP and other markers associated with peptidergic neurons (Carr, Yamamoto and Nagy, 1990; Price and Flores, 2007). In the past ~30 years significant efforts have been made to distinguish these neurons by expressional markers such as ion channels and receptors that provide the basis for cellular functions. The gene expression profiles of DRG neurons revealed by these studies provide evidence for a much more complicated picture about sensory neuron function. Bulk RNA sequencing of DRG neuron populations provided useful insights into the variability of genes expressed in the different populations, but these experiments were not unbiased because they involved pre-sorting DRG neurons based on defined markers (Nav1.8+ / IB4+, Nav1.8+/IB4-, Parvalbumin+) (Chiu *et al.*, 2014). Other studies refined these experiments by running single cell RNA sequencing on a large number of cells and thereby eliminating the pre-selection bias. Usoskin *et al.* performed RNA sequencing analysis on 799 cells and

identified 3,574 genes per cell and 4 main neuronal clusters with 11 subclasses in total (Usoskin et al. 2014, Figure 1.1.2). The four main clusters were termed NF (by neurofilament heavy chain), PEP (peptidergic), NP (non-peptidergic) and TH (by tyrosine hydroxylase). The NF cluster could be subdivided into 5 groups and contains proprioceptors and LTMRs (by the expression of, among other markers, parvalbumin, TrkB and TrkC). The NP group could be subdivided into three groups and included the unmyelinated nonpeptidergic C-fibres (although one group expressed CGRP and TrkA). By their expressional profile, these cells likely play a role in neuropathic pain and inflammatory itch. The PEP group on the other hand consists of thermosensitive C-fibres (based on the expression of TRPV1) and myelinated Aδ nociceptors, both of which can be characterized by strong expression of TrkA and CGRP. Finally, the TH group consist of C-LTMRs and sense mechanical pain and pleasant touch as they express the mechanosensitive ion channel piezo 2.

NF1	NF2	NF3	NF4	NF5	NP1	NP2	NP3	PEP1	PEP2	TH
LDHB CACNA1H TRKB <sup>high</sup> NECAB2	LDHB CACNA1H TRKB <sup>low</sup> CALB1 RET	LDHB TRKC <sup>high</sup> FAM19A1 RET	LDHB TRKC <sup>low</sup> PV SPP1 CNTNAP2	LDHB TRKC <sup>low</sup> PV SPP1 CNTNAP2	PLXNC1 <sup>high</sup> P2X3 GFRA2 MRGPRD	PLXNC1 <sup>high</sup> P2X3 TRKA CGRP MRGPRA3	PLXNC1 <sup>high</sup> P2X3 SST	TRKA CGRP KIT TAC1 PLXNC1 <sup>low</sup>	TRKA CGRP KIT CNTNAP2 FAM19A1	PIEZO2 <sup>high</sup> VGLUT3 GFRA2
LTMRs		Proprioceptors			Nonpeptidergic			Peptidergic		C-LTMRs
NEFH		Myelinated NEFH RET	NEFH ASIC1 RUNX3	NEFH ASIC1 RUNX3	Unmyelinated			Myel. NEFH	Unmyel. NEFH	Unmyel. RET
					RET TRPA1 TRPC3 NAV1.8/9	RET TRPV1 TRPA1 TRPC3 NAV1.8/9	RET TRPV1 TRPA1 TRPC3 NAV1.8/9	TRPV1 NAV1.8/9	NAV1.8/9	RET TRPA1 NAV1.8/9

**Figure 1.1.2 DRG neuron types and selected markers as defined by Usoskin et al. (2014).** Abbreviations in the top row are the neuron groups: NF = neurofilament positive cells which represent large diameter, myelinated fibres, NP = nonpeptidergic, unmyelinated fibres, PEP = peptidergic fibres, TH = tyrosine hydroxylase expressing fibres, representing the mechanosensitive C-LTMRs. Selected markers (previously used in black, new ones defined by the study in red) are shown under the neuron groups. Note the expression of CGRP in the NP2 group. Figure was adapted from Usoskin et al., 2014).

Another group performed high coverage RNA sequencing on 197 neurons and identified 10,950 genes per cell, followed by functional characterization using electrophysiology (Li *et al.*, 2016). Due to the deep sequencing used in this study, the

authors found 10 main neuronal clusters termed C1-C10 and overall 14 subtypes. Clusters C1-6 include the small neurons that are generally mechanoheat nociceptors, but some of them are also sensitive to itch and pressure, and one cluster is the C-fibre LTMRs, which corresponds to the TH group in Usoskin et al. Clusters C7-10 are the large neurons and largely consist of mechanoreceptors and nociceptors sensitive to noxious mechanical stimulus (mechano-nociceptors), but some of them are also sensitive to heat due to TRPV1 expression. The same data has been re-analysed by the same authors using a different method that merged two clusters and resulted in 9 groups (Li *et al.*, 2018), and a more recent single cell RNA sequencing of the whole mouse nervous system also identified peptidergic, non-peptidergic and neurofilament type as the three main sensory neuron groups, with several subgroups in each (Zeisel *et al.*, 2018). These studies provide a complex picture of the diversity of sensory neurons and draw attention to the important conclusion that traditional markers used before cannot unequivocally define a certain population, eg. some IB4+ neurons also express CGRP and TRPV1 at high levels. Thus, when defining DRG neuron populations, studies should take into account not just molecular characteristics but also cell size, and physiological function (defined by electrophysiological properties and pharmacological tools, as well as *in vivo* behavioural experiment).

The studies described above mainly focused on the characteristics of DRG neuron populations in normal conditions; however it is well known that sensory neurons undergo various physiological changes during pathological (chronic) pain. In the following section therefore we will define chronic pain and introduce the pathological changes occurring in these conditions, and the current theories of underlying mechanisms.

## 1.2. Pain – changes occurring in somatosensory neurons in pathological states

Pain is an unpleasant sensation that most people experience during their lives. Individuals with a rare disease called Congenital Insensitivity to Pain are unable to feel pain, which leads to injuries (eg. repeated burns or bone fractures) and reduced healing (Katherine Schon, 2018). Acute pain is therefore an important and useful mechanism that alerts the body of damage, diseases and danger. In some cases however, pain persists even after the removal of the painful signal and becomes chronic. Chronic pain is generally

defined as pain that lasts for 12 weeks or longer, and it significantly affects one's quality of life (Aziz *et al.*, 2015).

There are many causes and therefore many types of chronic pain. Neuropathic pain arises from damage to the nervous system (the nerves, spinal cord or the brain), which can be caused by accidents or certain diseases (eg. multiple sclerosis, diabetes, cancerous tissue pressing on a surrounding nerve) (Jensen *et al.*, 2011; von Hehn, Baron and Woolf, 2012). Inflammatory pain on the other hand is caused by peripheral tissue damage and involves inflammatory mediators such as prostaglandins, bradykinin, histamine, nerve growth factors (NGF) and chemokines being released at the site of inflammation by infiltrating immune cells. These inflammatory mediators activate their receptors on nearby nerve terminals, which in turn will also release inflammatory mediators such as CGRP and SP, but this receptor activation also induces signalling pathways which lead to hyperexcitability of the nerve fibre and peripheral sensitization (Ji, Xu and Gao, 2014). Peripheral sensitization is often accompanied by increased pain sensitivity to super-threshold stimulation (stimuli that normally feel painful) termed hyperalgesia, and abnormal pain sensation following innocuous stimuli (mechanical or thermal allodynia). NGF and CGRP are both important mediators of inflammation and have been intensely studied over the last few decades as they can provide efficient ways to alleviate pain using blockers and antibodies directed against them, or their receptors (Edvinsson, 2015; Chang *et al.*, 2016; Bannister, Kucharczyk and Dickenson, 2017).

### Nerve Growth Factor (NGF) signalling

NGF is one of the four neurotrophins along with BDNF, NT-3 and NT-4 that support neuronal survival, neurite growth and synapse assembly during development (Pezet and McMahon, 2006). Neurotrophins are secreted by neurons and their target tissues, which drives the growth of axons towards their targets but it also serves as a "pruning" factor for neurons that are overproduced in the early stages of embryonic development (Yuen *et al.*, 1996).

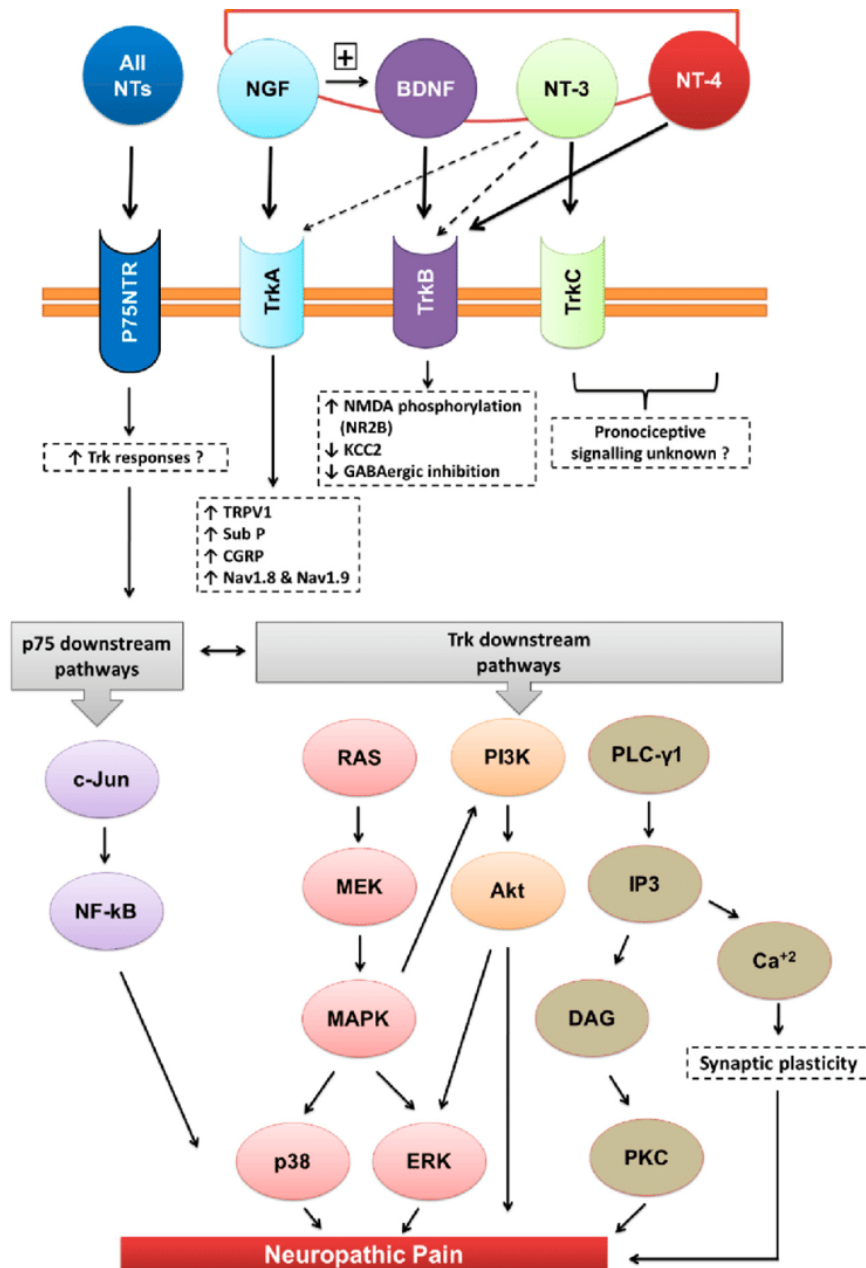


**Figure 1.2.1 Neurotrophin receptors and downstream signalling pathways.** Each neurotrophin activates its high-affinity receptor (arrows with solid lines), and NT-3 can also bind to TrkA and TrkB with low affinity (arrows with dashed lines). All the neurotrophins can bind to the P75 neurotrophin receptor (NTR), but with low affinity. Downstream signalling elements activated by P75 are c-Jun/NFκB, while the three major pathways activated by the Trk receptors are the Ras/MAPK, PI3K/Akt and PLC pathways. For abbreviations, see List of abbreviations on page 9. Figure was adapted from Khan and Smith, 2015.

NGF is synthesised as pro-NGF that binds to the receptor p75 while NGF binds to the tyrosine kinase receptor A (TrkA) with high affinity, but NGF and all other neurotrophins bind p75 with low affinity (Patapoutian and Reichardt, 2001). P75 is a tumor necrosis factor (TNF) receptor and it promotes apoptosis when TrkA signalling is reduced, thus the balance

of TrkA/p75 receptors and the levels of neurotrophins are important in determining the physiological effects of NGF (Chao, 2003). Upon NGF binding, TrkA molecules form dimers and are internalized as NGF-TrkA protein complexes in signalling endosomes through a dynamin-dependent mechanism (Bodmer, Ascaño and Kuruvilla, 2011), and are then retrogradely transported back to the soma along the axon (Delcroix *et al.*, 2003). NGF and other signalling molecules transported with the complex activate the Ras-raf-MAPK, PI3K-akt and PLC-DAG-PKC signalling pathways in the soma (figure 1.2.1).

The constant, baseline production of NGF by innervated tissues ensures that during embryonic development, the NGF-dependent signalling pathways promote axonal growth, sprouting and neuronal survival (White *et al.*, 1996; Patel *et al.*, 2000). In the first two weeks following birth, sensory neurons stop depending on NGF as a survival factor but it can still promote axonal re-growth following injury (Lindsay, 1988). This change of NGF-dependence during development is attributed to a switch in gene expression at these early stages, when about half of the small diameter, nociceptive DRG neurons (those that are IB4 positive) downregulate TrkA and upregulate the GDNF receptor Ret (Bennett *et al.*, 1996; Molliver *et al.*, 1997). The expression of signalling pathway elements and ion channels also changes within the first two post-embryonic weeks, for example ERK/MAPK, PI3K and PKC $\delta$  are all upregulated in the adults, as measured by microarray (Zhu and Oxford, 2011). These changes in gene expression and neuronal phenotype likely underlie the change from the reliance of DRG neurons on NGF for survival to sensitization to noxious stimuli such as heat and capsaicin (Winter *et al.*, 1988; Zhu *et al.*, 2004).

During tissue inflammation, activated immune cells produce cytokines that stimulate other immune and other cells such as neurons, to start producing more NGF. It has been described in multiple inflammatory conditions that local or systemic NGF levels increase in both humans and mouse models (Bonini *et al.*, 1996; Di Mola *et al.*, 2000; Stanzel, Lourenssen and Blennerhassett, 2008). Conversely, administration of NGF induces hyperalgesia and decreases heat pain threshold (Andreev NYu *et al.*, 1995; Dyck *et al.*, 1997) and increases the capsaicin sensitivity of the DRG cultures (Winter *et al.*, 1988), while antagonists can be used to relieve pain (Hefti *et al.*, 2006; Chang *et al.*, 2016). These heat and capsaicin sensitive phenotypes indicate that NGF acts specifically on TRPV1 expressing sensory neurons. One major mechanism of NGF induced hyperalgesia is the upregulation of several pain-related genes such as TRPV1 channels (Ji *et al.*, 2002), sodium channels (Gould

*et al.*, 2000; Kerr *et al.*, 2001; Mamet, Lazdunski and Voilley, 2003), neuropeptides and BDNF (Lindsay and Harmar, 1989; Apfel *et al.*, 1996; Park *et al.*, 2010), which are then transported back through the peripheral axon to the site of inflammation (Lindsay and Harmar, 1989; Park *et al.*, 2010). Moreover, these gene expression changes can result in phenotypic switch, where nerve fibres start expressing neuropeptides or TRPV1 channels that did not do so before, which further contributes to increased pain sensation (Latremoliere and Woolf, 2009). Apart from changing the gene expression, NGF also induces the sensitization of TRPV1 channels locally at the axon endings through direct phosphorylation of the channels by PKC acting downstream of PI3K, causing membrane translocation and increased activity of TRPV1 channels. This, coupled with the increased levels of voltage-gated ion channels leads to neuronal hyperexcitability and increased secretion of already upregulated CGRP, SP and BDNF. These factors further sensitize neurons and contribute to the inflammation and peripheral sensitization (Ji, Xu and Gao, 2014).

### Calcitonin-gene related peptide

As mentioned in section 1.2, CGRP is a neuropeptide expressed in nociceptive sensory neurons in the DRGs and trigeminal ganglia and has been historically used to define this neuron population in studies. Due to its role in inflammatory and neuropathic pain states, CGRP and its receptors have been the subject of intense study over the last few decades in the search for more effective pain management strategies.

#### *Structure, receptor*

CGRP is a small, 37 amino acid peptide that goes through both C- and N-terminal cleavage to create the active peptide. Due to the alternative splicing of its gene, CGRP appears in two forms ( $\alpha$ -CGRP and  $\beta$ -CGRP) that only differ by a few amino acids in mice, rats and human, but  $\alpha$ -CGRP is the main form in the nervous system (Amara *et al.*, 1985; Steenbergh *et al.*, 1986) (figure 1.2.2).

The CGRP receptor, like most other neuropeptide receptors, is a G-protein coupled receptor (GPCR) formed of the calcitonin receptor-like receptor (CLR) and receptor activity modifying protein-1 (RAMP1) (Choksi *et al.*, 2002). CGRP binding to its receptor on neurons and blood vessels activates adenylate cyclase and increases cAMP levels, which activates

several PKA dependent pathways resulting in phosphorylation of ATP-sensitive potassium ( $K_{ATP}$ ) channels and increased nitric oxide levels (Nelson *et al.*, 1990; Russell *et al.*, 2014). CGRP also affects gene expression in an autocrine and paracrine manner in DRG neurons through activation of the cAMP response element binding protein (CREB) (Anderson and Seybold, 2004).

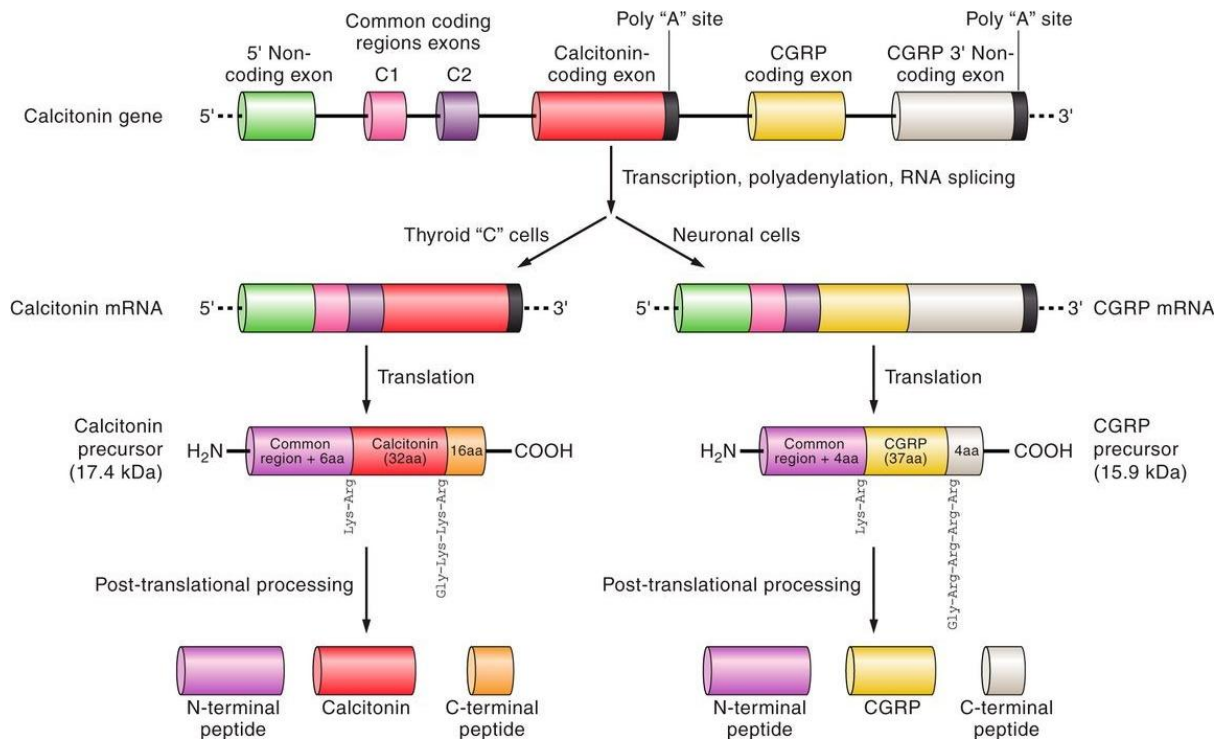


**Figure 1.2.2 Processing and synthesis of CGRP.** The CALC1 gene encodes both Calcitonin and CGRP. The expression of the calcitonin coding exon occurs primarily in the thyroid, while in neuronal cells the CGRP coding exon is expressed. The CGRP mRNA is translated into pro-CGRP, and further processing creates the mature CGRP. Figure was adapted from Russell *et al.*, 2014.

### Pathophysiology

One of the primary physiological roles of CGRP is vasodilatation which can induce swelling and redness at the site of inflammation; immune cells can infiltrate through the dilated blood vessels, secreting inflammatory mediators and contributing to the above described peripheral sensitization (Brain *et al.*, 1985; Russell *et al.*, 2014). CGRP and other neuropeptides are also trafficked anterogradely from the soma to the spinal cord, where they contribute to central sensitization in response to pain signalling. Neurons that become

hyperexcitable following peripheral inflammation, start secreting more transmitters such as CGRP, SP and glutamate in the spinal dorsal horn (Iyengar, Ossipov and Johnson, 2017). CGRP binding to its receptors on second order neurons activates signalling pathways that cause increased evoked and spontaneous activity and altered gene expression, while activation of PKA/PKC pathways lead to phosphorylation of the NR1 subunit of NMDA receptors, increased membrane excitability and central sensitization (South *et al.*, 2003; Latremoliere and Woolf, 2009; Woolf, 2011) (figure 1.2.3). Over time, these and other processes will induce plasticity changes that result in the increased responsiveness of spinal cord neurons to stimulation, which manifests in hyperalgesia and allodynia.

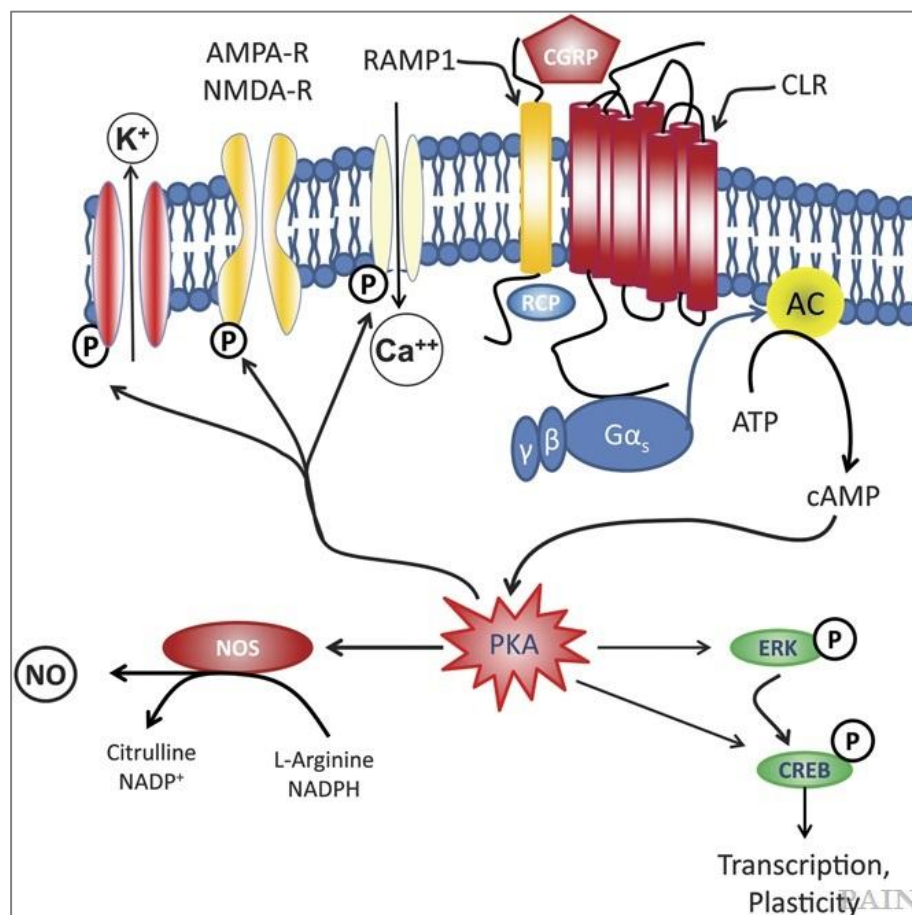


**Figure 1.2.3. Receptors and signalling pathways activated by CGRP.** CGRP first binds to its receptor complex formed by calcitonin receptor-like receptor (CLR), receptor activity modifying protein 1 (RAMP1) and the receptor component protein (RCP). The G<sub>s</sub> protein activates adenylyl cyclase (AC) to produce more cAMP, which leads to the activation of PKA and various downstream signalling targets. Activation of extracellular receptor-activated kinase (ERK) and cAMP response element binding protein (CREB), leads to altered gene expression. PKA may also stimulate the production of nitric oxide (NO) through the activation of nitric oxide synthase (NOS) to promote vasodilatation. An important effect of PKA activation is the phosphorylation of ion channels, which may increase neuronal excitability. Figure was reused from Iyengar, Ossipov and Johnson, 2017.

CGRP is stored in dense core vesicles together with other neuropeptides, BDNF and glutamate (Matteoli *et al.*, 1988; Salio *et al.*, 2007), and its release is stimulated by an increase in intracellular  $\text{Ca}^{2+}$  concentration (L. Y. Huang and Neher, 1996). Most of the knowledge regarding the exocytotic machinery regulating CGRP release comes from studies using botulinum toxins in DRG and trigeminal neurons, which showed that CGRP release is SNARE-regulated and  $\text{Ca}^{2+}$ -dependent (Meng *et al.*, 2007, 2009; Meng, Dolly and Wang, 2014).  $\text{Ca}^{2+}$ -independent mechanisms of CGRP release from DRG neurons have also been reported (Chai, Wang, Huang, Y. Y. Wang, *et al.*, 2017), this type of exocytosis will be described in a later section. Although the physiological effects of CGRP have been extensively studied, there is little detailed knowledge regarding the molecules governing its release. Below is an overview of the current knowledge on of molecules regulating exocytosis, with a focus on peptide secretion from different cell types.

### 1.3. Regulation of exocytosis

#### Types of secretory vesicles and their cargo

In neurons, neuropeptides and other neurotransmitters are stored in different vesicle populations. Low molecular weight “classical” neurotransmitters (such as GABA, glycine, acetylcholine, glutamate, ATP) are released from small (40-50 nm) clear core synaptic vesicles (SV) through fast and spatially localized mechanism at the presynaptic active zone. Larger neuropeptides (such as CGRP, SP or NPY) and some growth factors (BDNF, GDNF) are stored in large dense core vesicles (LDCVs) that are ~75-100 nm in neurons (but can be around 300-400 nm in endocrine/neuroendocrine cells (Albillos *et al.*, 1997; Zhao *et al.*, 2016; Merighi, 2018)), which are characterized by an electron dense core from where their name comes from (figure 1.3.1) (Zhang *et al.*, 1995; Salio *et al.*, 2006; Merighi *et al.*, 2011). A third class of secretory vesicles consists of smaller (~50 nm) dense core vesicles that contain monoamines, though these are less prevalent (recent reviews discussing secretory vesicle classes are (Salio *et al.*, 2006; Merighi, 2017, 2018)).

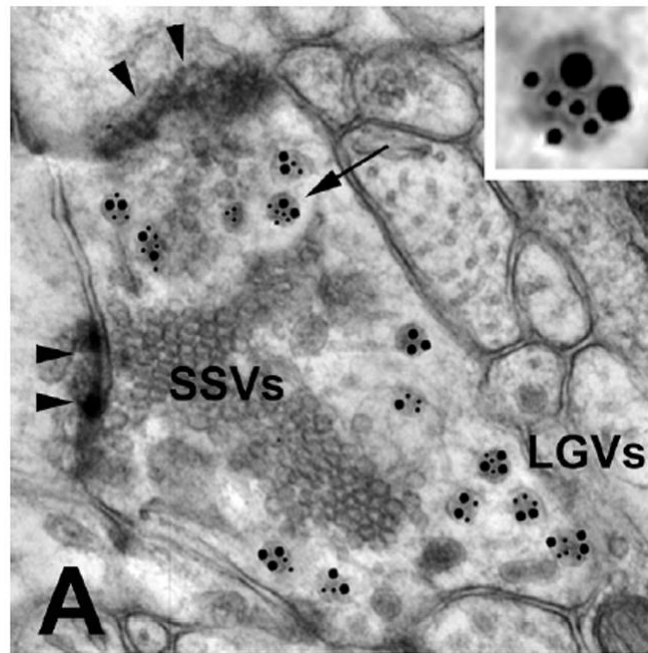


**Figure 1.3.1** Electron micrograph showing the synaptic architecture in the spinal dorsal horn. Clear, small synaptic vesicles (SSV) and dense core vesicles (LGVs, large granular vesicles) are shown in the central terminal of a DRG neuron that is organised in a multisynaptic glomerulus. Immunogold labelling of CGRP (smaller particles) and substance P (larger particles) shows that they are co-stored in LGVs. An enlarged LGV is shown in the inset (arrow). Arrowheads point at the electron dense synapses, where SSVs are packed closely together, while LGVs reside farther away from the synapse. Figure was adapted from Merighi, 2017.

The basic exocytic machinery controlling the fusion of secretory vesicles, including the SNAREs essential for fusion, are thought to be the same or similar for LDCVs and SVs, but there are also some fundamental difference between these vesicle populations. It should be noted that most of the work exploring LDCVs has been done either on non vertebrates or mammalian endocrine cell preparations such as chromaffin cells or cell lines such as PC12 cells or Ins1 cells but there are fewer studies in neurons compared to those addressing SVs (Taraska *et al.*, 2003; Tsuboi and Rutter, 2003; Obermüller *et al.*, 2005; Merighi, 2017). It is unclear at this point if and how neuronal and non-neuronal LDCVs differ, though size seems to be one example (see above).

Neuropeptides are synthesised as pro-peptides in the rough endoplasmic reticulum, and are then transported to the Golgi apparatus where they may undergo further post-translational modifications (figure 1.3.2). The pro-peptides are then packaged into immature secretory vesicles (ISVs) through budding from the trans-Golgi network, a process which is thought to be driven by the interaction of granin molecules, pro-hormones and membrane

lipids (Beuret *et al.*, 2004). The low luminal pH (~6.3) and high calcium concentrations inside the trans-Golgi network induce the aggregation of granins (chromogranins and secretogranins) (Chanat, Weiß and Huttner, 1994; Yoo, 1996), which can also interact with lipid rafts composed of cholesterol, phosphatidylinositol-4-phosphate (PI<sub>4</sub>P) and DAG in the membrane (Hosaka *et al.*, 2002; Sun *et al.*, 2013).

Once the ISV is formed, a crucial part of LDCV biogenesis is the gradual decrease of pH, to ~5-5.5 in mature LDCVs due to increased proton pump density in the vesicle membrane (Wu *et al.*, 2001). This acidification activates the prohormone convertases and carboxypeptidases necessary for cleaving pro-peptides and creating the active neuropeptides (Steiner *et al.*, 1992; Jean Husten and Eipper, 1994). An important morphological difference between immature and mature secretory vesicles is the clathrin coat, which is lost during maturation (Tooze and Tooze, 1986). Clathrin, together with adaptor protein-1 (AP-1) and the neuronal AP-2 helps remove missorted proteins, lysosomal enzymes and membrane proteins such as VAMP4 from immature vesicles through budding of constitutive-like vesicles (Dittié, Hajibagheri and Tooze, 1996; Hinners *et al.*, 2003; Grabner *et al.*, 2006)

Immature and mature secretory vesicles can also differ in size, as ISVs are usually smaller and only contain one type of peptide; they undergo homotypic fusions and content mixing during their maturation process (Tooze, 1991; Wendler *et al.*, 2001). Early studies found that fusion between immature LDCVs is largely regulated by syntaxin-6 (Wendler *et al.*, 2001) and synaptotagmins-4 (Ahras, Otto and Tooze, 2006). More recently, Hid-1 was shown to regulate the process in pancreatic B cells (Du *et al.*, 2016). After homotypic fusion, LDCVs become larger, but this is followed by condensation and size reduction while they are transported to the axon terminals in neurons (Merighi, 2018). During this transport process, LDCV maturation continues and pro-peptides are cleaved to create the bioactive neuropeptides. When they arrive at the release sites, mature LDCVs contain a cocktail of neuropeptides and sometimes, small neurotransmitters that can be released together or separately (Salio *et al.*, 2007; Zhang *et al.*, 2019).

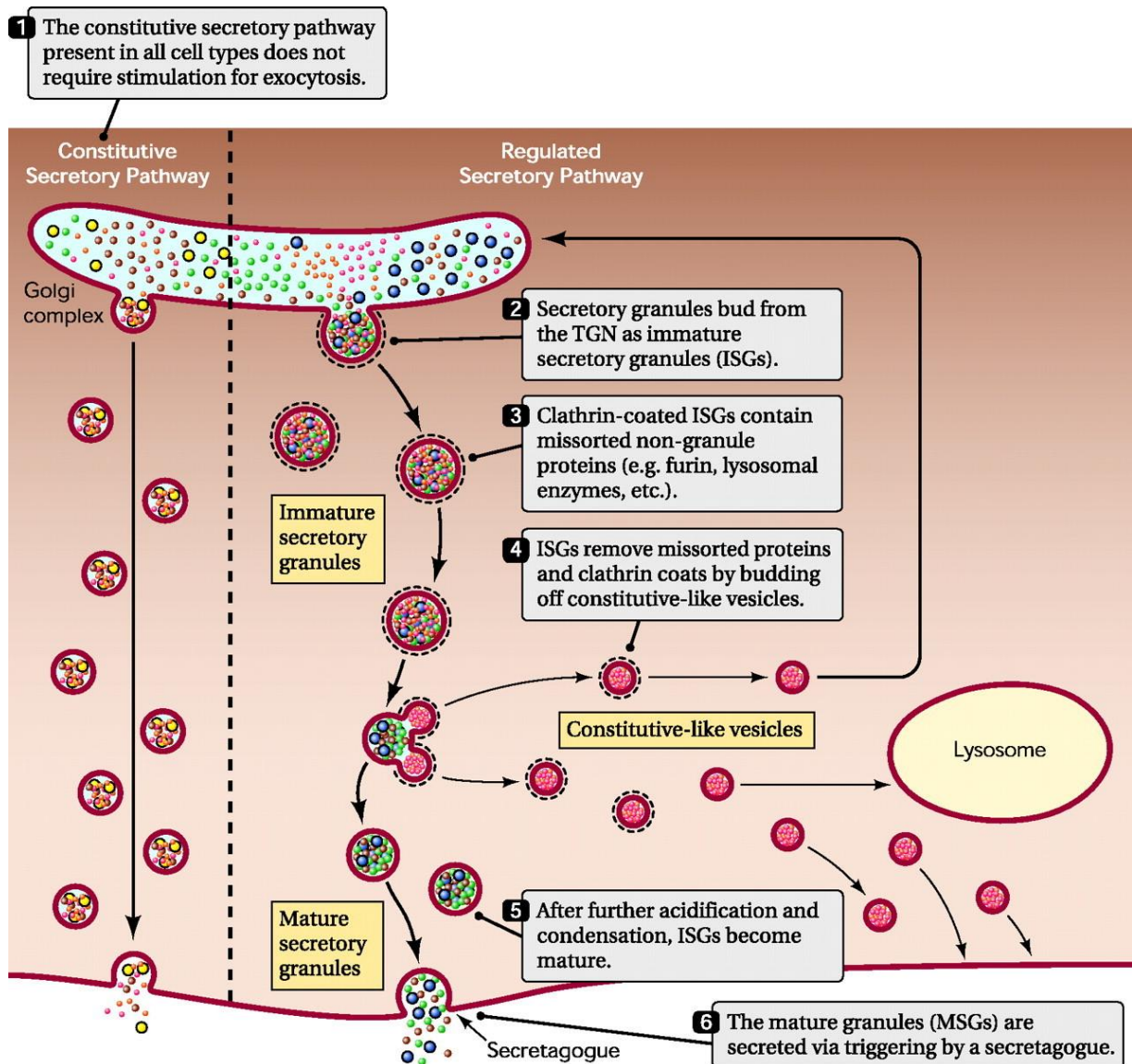


**Figure 1.3.2 Constitutive and regulated secretory pathways.** Figure was reused from Kim *et al.*, 2006.

An important difference between LDCVs and SVs is the release sites: SVs are docked in large clusters called the readily releasable pool (RRP) at the presynaptic sites, while LDCV exocytosis is not spatially restricted and can happen on the soma or along the axons at extra-synaptic sites (figure 1.3.1) (Hökfelt *et al.*, 2000; Salio *et al.*, 2006; Merighi, 2018). As neuropeptides are synthesised in the soma and do not have a known re-uptake mechanism, LDCVs have to be continually resupplied as opposed to SVs that are recycled through kiss-and-run or clathrin-mediated endocytosis, assembled again in the endocytic system and can be reused in several exocytosis-endocytosis cycles (Granseth *et al.*, 2006; Balaji and Ryan, 2007; Rizo and Xu, 2015; Xie *et al.*, 2017).

The difference in the release sites also has important implications in the calcium signals required for exocytosis. SV release requires a robust intracellular calcium increase (10-100  $\mu\text{M}$ ) in the vicinity of voltage gated  $\text{Ca}^{2+}$  channels (VGCCs) (Matthijs Verhage *et al.*, 1991; Acuna *et al.*, 2015), thus a single action potential can be enough to elicit secretion. For LDCV exocytosis, an overall smaller increase in intracellular  $\text{Ca}^{2+}$  concentration is sufficient, but as it can happen far from the active zone and VGCCs, it needs a higher frequency of action potentials to induce a more general elevation of internal  $\text{Ca}^{2+}$  (M Verhage *et al.*, 1991; Matthijs Verhage *et al.*, 1991; Merighi *et al.*, 2011). Such differences in the calcium dependence suggest that there might be differences in the calcium sensors governing the fusion of different vesicle types.

### The exocytotic machinery

Despite the above described differences, the basic mechanisms and proteins governing exocytosis and fusion of membranes are thought to be largely the same. First, for the vesicle fusion with the plasma membrane a major energy barrier has to be overcome due to the negatively charged surfaces of the membranes (figure 1.3.3 A). For this, a core fusion complex at the plasma membrane has to assemble, which consists of membrane linked SNARE proteins (SNAP25, syntaxin-1) and SM proteins (Munc18); the vesicular SNAREs (VAMPs) connect the vesicle to the complex. The exocytotic process involves at least 3 steps: vesicle docking, priming and fusion (figure 1.3.3 B). To create the docking platform, first Munc18 binds to the closed conformation of syntaxin1, which converts to open conformation after the binding of the MUN domain of the priming factor Munc13-1. RIM, like Munc13-1, is an active zone protein which on one hand recruits Munc13-1 to the active zone and activates it by disrupting its homodimerization (Deng *et al.*, 2011). On the other hand, RIM and Munc13 help vesicle tethering by binding to the vesicular Rab3 proteins, and also recruit  $\text{Ca}^{2+}$  channels to the release machinery (Mittelstaedt, Alvaréz-Baron and Schoch, 2010; Han *et al.*, 2015). Primed vesicles are attached to the plasma membrane through the pre-fusion SNARE complex. Complexin, a small soluble protein probably binds to the partially assembled SNAREs and activates the progressive zippering of the trans-SNARE proteins, pulling the membranes closer. It may also act as a “clamp” to keep the proteins in a partially zippered state and prevent early fusion, as deletion of

complexin increases spontaneous release (Schneppenburger and Rosenmund, 2015). The clamp is removed by  $\text{Ca}^{2+}$  binding to vesicular synaptotagmins, which triggers the opening of the fusion-pore (Zhou *et al.*, 2017). This  $\text{Ca}^{2+}$  binding is thought to provide the remaining energy required for membrane fusion and phospholipid mixing (Südhof, 2013). After fusion pore opening, vesicle fusion can go multiple ways. The pore can either briefly open then close; the vesicle is then retrieved and recycled during “kiss-and-run” exocytosis or stays at the membrane during “kiss-and-stay” ready for another vesicle fusion. Alternatively during full fusion, the fusion pore opens wider than the vesicle diameter and the vesicle membrane fully collapses into the plasma membrane.

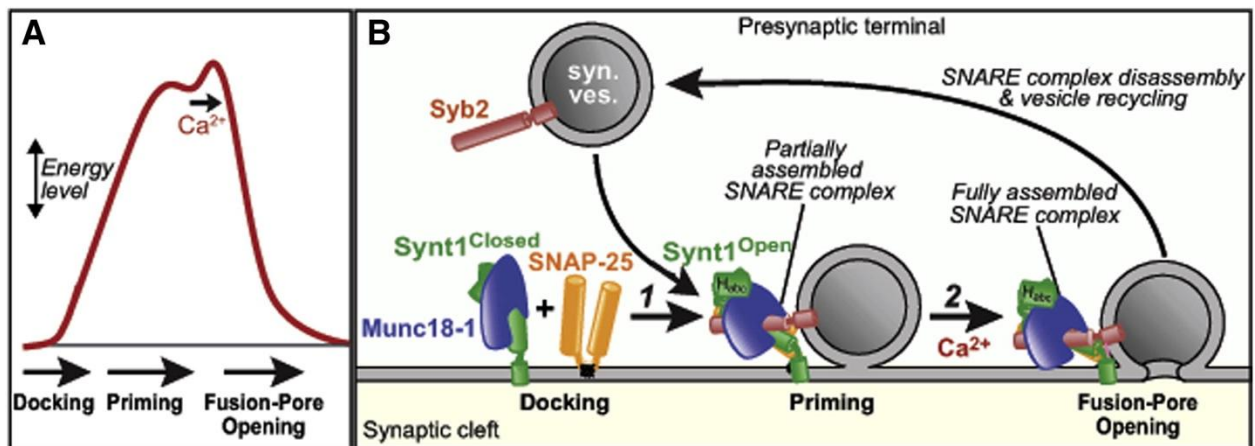


**Figure 1.3.3 Steps of regulated exocytosis and main proteins involved.** A, shows the energy levels of a vesicle undergoing docking, priming and fusion pore opening. Calcium binding to synaptotagmins is thought to provide the energy needed for fusion pore opening. B, Steps of exocytosis. Syntaxin, Munc18 and SNAP25 form a core complex for vesicle docking, followed by the partial assembly of the SNARE complex together with VAMP2 (Syb2). The final fusion step is triggered by increased calcium concentration. Figure was reused from Südhof, 2013.

### Somatic secretion in DRG neurons

There are relatively few studies looking at exocytosis in DRG neurons, due the difficulties they present: most studies on neurons focus on synapses, but DRG neurons in culture do not form synapses unless they are co-cultured with dorsal horn neurons (Ferron *et al.*, 2014; Shaib *et al.*, 2018), limiting studies on pure DRG cultures to somatic secretion. The existence of somatic secretion in DRG neurons used to be in question until Huang & Neher (1996) described  $\text{Ca}^{2+}$ -dependent exocytosis in rat cultured DRG neurons for the first

time. Using capacitance measurements and  $\text{Ca}^{2+}$  chelation they demonstrated that the secretion rate ( $\sim 1.8$  vesicles/s/ $\mu\text{m}^2$ ) and  $\text{Ca}^{2+}$  requirement ( $< 10 \mu\text{M}$ ) were comparable to LDCV secretion from endocrine cells, and were also able to measure SP release from DRG somata in single-cell immunoblotting experiments (L. Y. Huang and Neher, 1996). The function of this somatic secretion remained in question, though they hypothesised that it might play a role in paracrine signalling within the DRGs and since then studies found that it is important for neuro-glia communication within the DRG (Zhang *et al.*, 2007; Kung *et al.*, 2013).

Interestingly, one group found calcium-independent but voltage-dependent (CIVD) secretion from the somata of cultured DRG neurons (Zhang and Zhou, 2002). They demonstrated this using capacitance and amperometry measurements of catecholamine release, and pharmacological block of calcium channels and internal calcium stores and they found some CGRP release in these  $\text{Ca}^{2+}$ -free conditions by radioimmunoassay. Later the same group showed that CIVD was coupled to a rapid calcium and dynamin-independent form of endocytosis that was also regulated by PKA (Zhang *et al.*, 2004), and that CIVD secretion induced by low intensity stimulation ( $< 5$  Hz) only occurred on the soma but not on dorsal horn synapses in co-culture (Zheng *et al.*, 2009). They were also able to identify the machinery involved in CIVD secretion: it involves N-type calcium channels (Cav2.2) as a voltage sensor, which links the SNARE complex and the vesicle to the calcium channel through its synprint region (Chai, Wang, Huang, Y. Wang, *et al.*, 2017). They identified ATP as a cargo of this type of secretion, and showed using TIRF imaging that both SVs and NPY-containing LDCVs undergo CIVD secretion. They suggested that because CIVD secretion dominates during tonic, low-frequency firing, this type of secretion might be more relevant in proprioception and normal sensation rather than pain (Chai, Wang, Huang, Y. Wang, *et al.*, 2017). On figure 1.3.4, we have listed proteins that may be present on LDCVs or have a role in their exocytosis in DRG neurons.

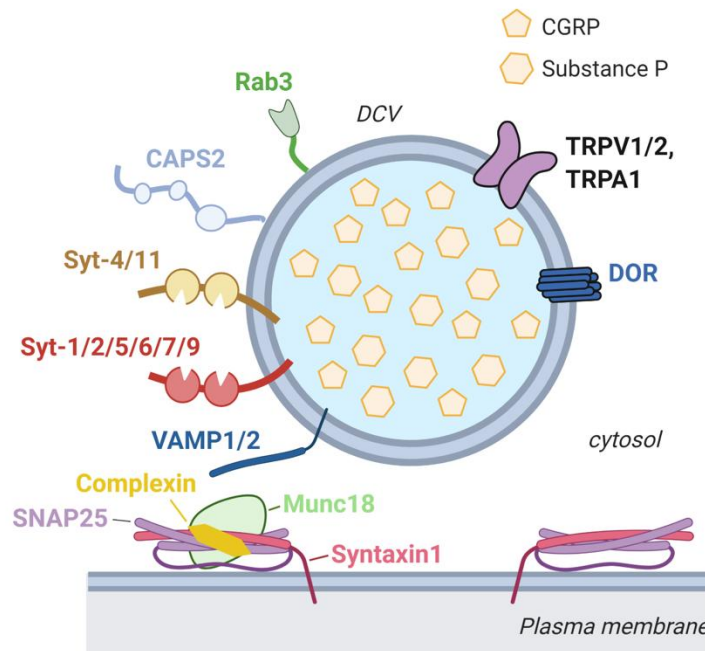


**Figure 1.3.4** Cartoon of an LDCV with associated SNAREs and other vesicular proteins that have been reported in DRG neurons in large scale mRNA and proteomic profiling studies. References that were used for the construction of this figure are in table 1.3.4.

Reference	Selected proteins of interest	Technique
(Shaib <i>et al.</i> , 2018)	CAPS2 (CAPS1)	Single vesicle exocytosis and calcium imaging, TIRF/STED
(Meng <i>et al.</i> , 2016)	Munc18, syntaxin1 and SNAP25 together with VAMP1 mediate CGRP containing of DCVs bearing TRPV1 and TRPA1	Immunocytochemistry, calcium imaging
(Zhao <i>et al.</i> , 2011)	Delta opioid receptor (DOR), TRPV2	Proteomics analysis of DCV fraction
(Goswami <i>et al.</i> , 2014)	SYT1, 5, 7, 9, TRPV1, TRPA1, VAMP1, 2	RNA sequencing of TRPV1 lineage neurons
(Xiao <i>et al.</i> , 2002)	SNAP25, VAMP1, Rab3, Syt4	cDNA array, DNA sequencing of whole DRG
(Rouwette <i>et al.</i> , 2016)	SNAP25, VAMP1, Rab3, Syt1, 2, 11	Proteomic analysis of membrane enriched fraction
(Usoskin <i>et al.</i> , 2014)	CGRP, SP, SNAP25, syntaxin, Munc18, VAMP1,2, complexin, CAPS1, TRPV1, 2, TRPA1, syt1, 2, 4, 5, 6, 7, 9, 11	RNA sequencing of whole DRG
(Reinhold <i>et al.</i> , 2015)	Syt4, VAMP1, SNAP25, Rab1	qPCR analysis of RNA extracts

**Table 1.3.4.** List of references and proteins identified for the construction of figure 1.3.4.

### The fusion pore and regulation of cargo release

The fusion pore that opens during synaptic vesicle fusion with the plasma membrane was originally captured over 30 years ago using snap freezing and electron microscopy in frog neuromuscular junctions (Heuser and Reese, 1981). The formation of the pore was then studied using amperometry and conductance measurements mostly in chromaffin cells, neutrophils and mast cells which established that fusion pores are usually around 1-2 nm in diameter initially and the pore expanded rapidly after opening (Spruce *et al.*, 1990; Lollike, Borregaard and Lindau, 1995; Albillos *et al.*, 1997). With regards to the composition of the pore, some studies argued that it was made of proteins that form a channel between the vesicle and plasma membrane because it had conductance similar to ion channels (Lollike, Borregaard and Lindau, 1995). But because of the high variability in conductance (and size), some proposed a hemi-fusion model, where proteins would merely help in assembling the fusion pore that is entirely lipidic (Nanavati *et al.*, 1992). According to this model, a hemi-fusion state precedes fusion where the cytosolic layer of the vesicle membrane fuses with the cytosolic layer of the plasma membrane. A more recent study provided strong live-cell evidence for this hypothesis using confocal and super-resolution STED imaging in chromaffin cells (Zhao *et al.*, 2016). They found that LDCVs first undergo a hemi-fusion state that can progress to full fusion, full fission, and even full fusion can reverse back to hemi-fusion. It now seems likely that fusion pores are proteolipidic (Bao *et al.*, 2016), and SNARE TM domains actively promote fusion pore formation and expansion. It has been proposed that a minimum of three SNARE complexes are sufficient for fusion but that increasing the number of SNARE complexes will increase the rate of fusion and pore extension (Weber *et al.*, 1998; Dhara *et al.*, 2016; Bao *et al.*, 2018; Sharma and Lindau, 2018).

Some vesicles fuse with full collapse of the vesicle membrane into the plasma membrane (termed full fusion, FF), which allows complete content release into the synaptic cleft but also complete transfer of integral vesicle proteins into the plasma membrane. Another mode of fusion is kiss-and-run (KR), where the vesicle transiently fuses with the plasma membrane and is quickly recovered through dynamin and Ca<sup>2+</sup> dependent endocytosis (figure 1.3.5A) (Fulop, Doreian and Smith, 2008; Chiang *et al.*, 2014; Wen *et al.*, 2016). The significance of controlling vesicle fusion lies in the differential cargo release and the retrieval of integral vesicular proteins if their diffusion through the pore is limited. As

often different sized cargoes are co-stored in vesicles, the fusion pore could serve as a filter for content release based on size and also the type of stimulus. Small neurotransmitters can fit through a small initial fusion pore of  $\sim 1\text{-}2$  nm, as was shown in pancreatic  $\beta$ -cells and chromaffin cells, with larger molecules filtered out (Fulop, 2005; Braun *et al.*, 2007). LDCVs are thought to undergo mostly FF for complete content release, and larger molecules are generally released more slowly than smaller ones (Barg, Olofsson and Rorsman, 2001). For example, NPY-EGFP ( $\sim 40$  kDa) is released rapidly ( $< 200$  ms), while the larger tissue plasminogen activator (tPA-EGFP  $\sim 100$  kDa) is released over several seconds from chromaffin cells (Perrais *et al.*, 2004; Weiss *et al.*, 2014; Bohannon *et al.*, 2017).

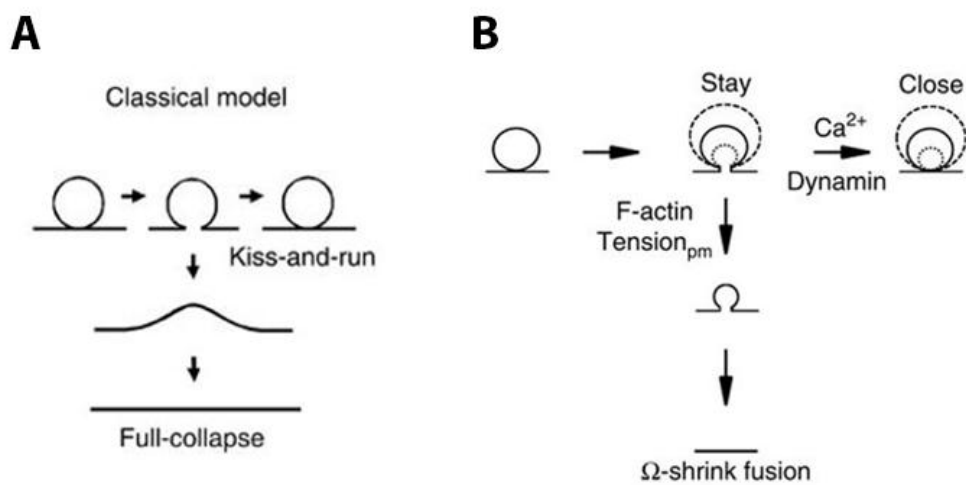


**Figure 1.3.5 Schematic showing the classical model of exocytosis (A) and a new model (B) proposed by Chiang et al. (2014)** (A) According to the classical model, vesicle fusion can go two ways: either full collapse of the vesicle into the plasma membrane, allowing complete content release, or kiss-and-run fusion, where a small (2-5 nm) transient fusion pore opens and closes. According to a different model (B), vesicle fusion is much more dynamic and involves shrinking or enlargement of the vesicle rather than collapsing. The shrinking and eventual full fusion are controlled by membrane tension generated by F-actin, while pore closure is generated by dynamin and  $\text{Ca}^{2+}$ . Figure was adapted from Chiang et al. (2014) and Wen et al. (2016).

Similar relationship between molecular weight and release speed were observed in hippocampal neurons, and the interaction of cargo proteins with the vesicle matrix also seems important, as the release of cargo that binds to the luminal matrix is further slowed down (de Wit, Toonen and Verhage, 2009; Zhang *et al.*, 2019).

The major LDCV matrix protein components are chromogranins and secretogranins. Granins aggregate at acidic pH, which is maintained inside the vesicle by the function of

vesicular ATP-ase proton pumps (Yoo, 1996). The granins, together with other vesicle components such as catecholamines (chromaffin cells and some neurons) and matrix-bound peptides form a dense mixture that can have a significant impact upon transmitter release. The roles of Chromogranin A and B (CgA, CgB) in DCV formation and cargo release have been well studied. One laboratory surveyed the effect of single CgA or CgB KO, and double CgAB KO on catecholamine release in chromaffin cells by amperometry and EM (Domínguez *et al.*, 2012). Catecholamines release is significantly reduced in chromaffin cells of CgA or CgB KO mice, and there is also a reduction in the number of exocytic events (Díaz-Vera *et al.*, 2012). In the absence of CgA, the filling of LDCVs with catecholamines and their capacity to concentrate cargo is disrupted, resulting in reduced release (Montesinos *et al.*, 2008). CgB KO had similar effects in catecholamine release as the CgA KO, and proteomic analysis of LDCVs showed an upregulation of CgA (Díaz-Vera *et al.*, 2010). Double KO of CgA/B resulted in an even more pronounced decrease of catecholamine release, and the average size of LDCVs significantly increased and their catecholamine content was reduced, suggesting impaired LDCV biogenesis (Díaz-Vera *et al.*, 2012). Other studies reported similar results from chromaffin cells, with reduced transmitter release, LDCV number and volume density in the absence of CgA (Kim *et al.*, 2005; Pasqua *et al.*, 2016) (figure 1.3.6 A). Absence of CgB on the other hand in pancreatic islet cells of CgB KO mice resulted in reduced insulin, glucagon and somatostatin secretion, while LDCV morphology and biogenesis appeared normal, suggesting that CgB is more important for exocytosis in these cells (Obermüller *et al.*, 2010).

A recent study in chromaffin cells found that fusion mode (FF or KR) on its own does not necessarily determine the speed of cargo release; whether the cargo is soluble or bound to the LDCV matrix is also important (Zhang *et al.*, 2019) (figure 1.3.6). This study looked at co-release of matrix-bound catecholamines and soluble ATP from LDCVs and found that when the fusion pore is non dilated (ie. during kiss-and-run fusion), the release of ATP molecules is unrestricted but the release of catecholamines is restricted due to their binding to CgA. When CgA was knocked-down however, catecholamine release increased to the same levels as ATP during kiss-and-run fusion. This study demonstrated therefore, the importance of the LDCV matrix in differentially controlling the release of matrix-bound and soluble cargoes.

Despite their importance in neuroendocrine and endocrine cells, double KO of CgA/B did not have a significant effect on LDCV number, morphology or LDCV fusion in hippocampal neurons (Dominguez *et al.*, 2018). In DRG neurons, it would appear that both chromogranins and secretogranins are expressed, as they have been identified on both TRPV1-positive and -negative DRG neurons by RNA sequencing (Goswami *et al.*, 2014); CgB has been successfully used as a LDCV marker in a proteomic study (Zhao *et al.*, 2011). Interestingly, CgA was found downregulated in rat DRG neurons following nerve injury, possibly suggesting altered LDCV biogenesis in these neurons, which could underlie altered peptide release (Xiao *et al.*, 2002).

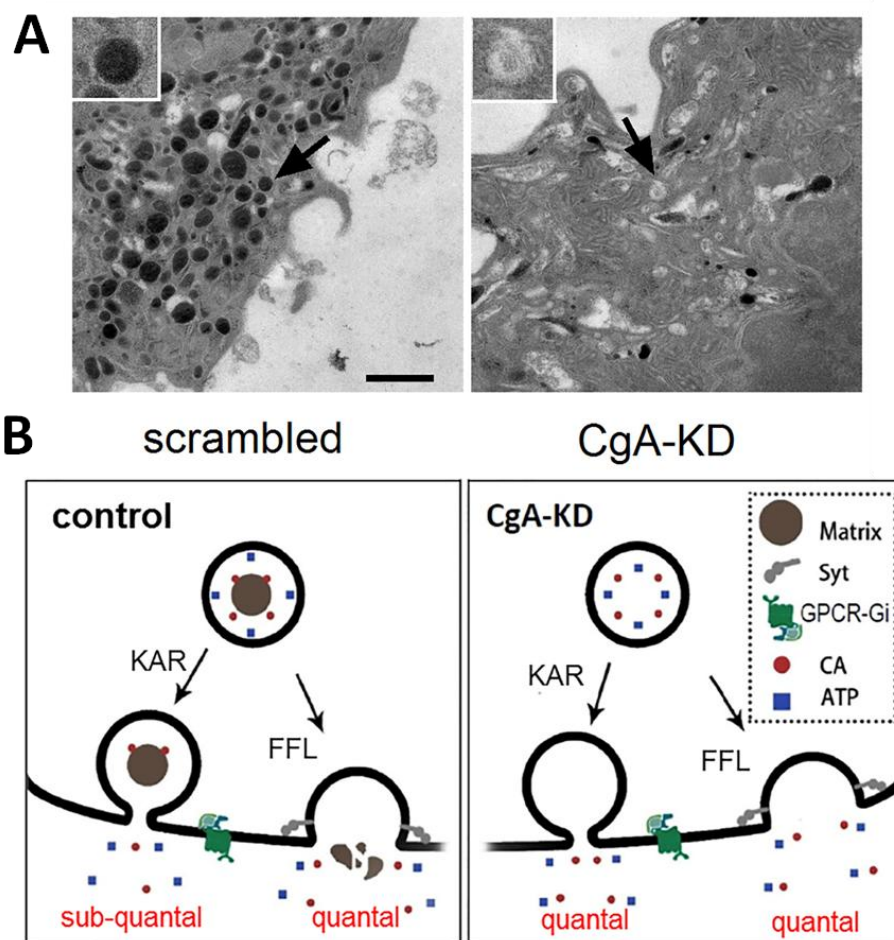


**Figure 1.3.6 The role of chromogranin A in chromaffin cells.** A, EM images of normal and altered LDCVs (arrows) in inactive scrambled shRNA or CgA-shRNA treated chromaffin cells. Note the empty LDCVs in CgA-KD cells. Scale bar = 500 nm. B, proposed role of CgA and vesicle matrix in controlling cargo release in chromaffin cells. In normal control cells, the vesicle matrix retains some catecholamine (CA) from being released during kiss-and-run (KAR) fusion, resulting in its sub-quantal release, while the soluble ATP is fully released. During full fusion (FF), the whole vesicle content is expelled. In CgA-KD cells, the vesicle matrix is disrupted and thus both catecholamines and ATP are

fully released (quantal release), regardless of the types of fusion. Figure was adapted from Zhang *et al.*, 2019.

### Modulation of fusion pore dynamics by Ca<sup>2+</sup>

Ca<sup>2+</sup> concentration and stimulus strength are important regulators of fusion pore dynamics, but there are conflicting findings as to precisely how changes in Ca<sup>2+</sup> affect fusion. Several patch clamping studies on chromaffin cells established that basal firing rates induce KR with a narrow fusion pore that limits content release, while strong firing (15 Hz) or raising intracellular Ca<sup>2+</sup> to >100 μM promoted fusion pore dilation and full content release which were interpreted as FF (Fulop, 2005; Elhamdani, 2006; Fulop and Smith, 2006). As opposed to these results, one earlier study on chromaffin cells found using patch amperometry that increasing Ca<sup>2+</sup> concentrations in the patch pipette promoted faster fusion pore closure and transient KR type fusion (Alés *et al.*, 1999). An important caveat of the latter study is that it was based on spontaneous release while the later ones used physiological stimulation, which might account for the differences.

Using high resolution confocal microscopy, Chiang *et al.* (2014) provided strong evidence in chromaffin cells that, as opposed to the studies above, low Ca<sup>2+</sup> promotes pore expansion while high Ca<sup>2+</sup> promotes pore constriction, and termed their model Ω-exo-endocytosis. According to this model, the Ω fusion profile can change in 7 different ways instead of only two (FF or KR): they redefined FF as vesicle shrinkage and flattening rather than fusion pore dilation, and KR can happen through shrinking, enlarging or without size change, before pore closure, which is triggered by strong Ca<sup>2+</sup> influx, but the transition between different states is flexible (figure 1.3.5 B). The same group later refined this model and proposed a “dynamic pore theory” which says that fusion pore size and cargo release depends on the competing forces of expansion (generated by F-actin) and constriction (generated by dynamin and Ca<sup>2+</sup>) (figure 1.3.5 B) (Shin *et al.*, 2018). In support of this theory they found that fusion pores can expand much more than previously assumed, as a maximum pore size of 490 nm was measured in chromaffin cells. Whether similar fusion pore regulation exists for SVs and in other cell types (eg. neurons) too however remains to be determined.

## 1.4. Techniques for studying single vesicle exocytosis

### Electrophysiological techniques

The two main approaches used for studying neurotransmission and vesicle exocytosis are electrophysiological and optical techniques. Each has its advantages and disadvantages and thus deciding which approach suits one's experimental needs most is crucial for maximizing the advantages. Amperometry can be used to measure the release of oxidizing neurotransmitters, such as catecholamines and monoamines. For this technique, a carbon fibre microelectrode is positioned in close proximity of the cell and is held at a voltage that is higher than the redox potential of the neurotransmitters. When the cell is depolarized and the transmitters are released, they are quickly oxidized on the surface of the electrode, which can be detected as amperometric spikes (figure 1.4.1). These spikes are often preceded by a low amplitude "foot" signal, which is produced by small amounts of transmitter being released through opening of an initial fusion pore. The amplitude and the duration of the pre-spike foot give information about the fusion pore size and life-time/stability, respectively (Chow, von Rüden and Neher, 1992; Albillos *et al.*, 1997).

Capacitance measurements can be used to directly measure both endo- and exocytosis based on the alterations in the cell membrane surface area. However, in contrast to amperometry, it requires a physical connection between the electrode and plasma membrane to establish the patch clamp recording and measurements are restricted to recordings in which electrical parameters of the cell are tightly controlled (Hartmann and Lindau, 1995; Debus and Lindau, 2000). This mostly restricts the technique's applicability to round cell bodies such as chromaffin cells or large nerve terminals; it has been successfully used on isolated DRG neurons, although recordings were restricted to small neurons that had been isolated for only a few hours and lacked processes (L. Y. Huang and Neher, 1996; Zhang and Zhou, 2002; Chai, Wang, Huang, Y. Wang, *et al.*, 2017). Capacitance measurements can suffer from possible artefacts arising from neuronal processes distorting measurements, or gating charge movements and may also be contaminated from fusion of vesicles through the constitutive pathway.

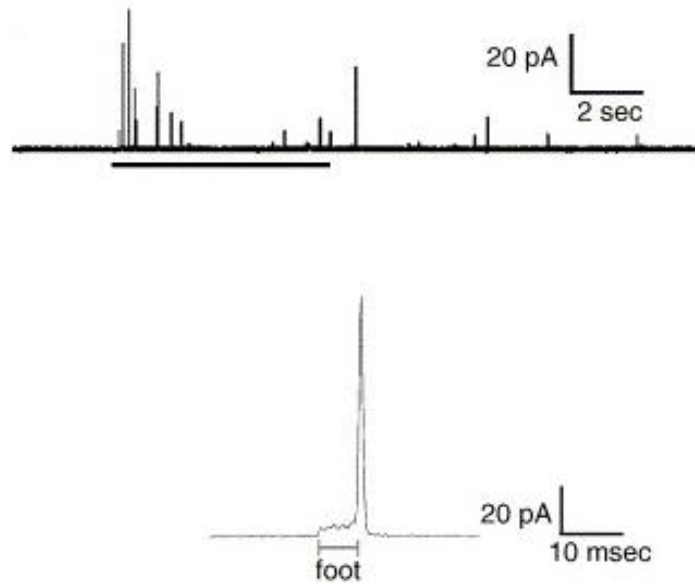


**Figure 1.4.1 Example traces of amperometric currents from PC12 cells stimulated with KCl.** Catecholamine release from single vesicles appears as spikes of various amplitudes on the top trace. The bottom trace shows an individual spike on a larger scale, which start with a pre-spike foot signal, indicating the initial opening of the fusion pore, followed by complete expulsion of vesicle content, indicated by the spike. Figure was adapted from Jackson, 2007.

### **Optical techniques**

In parallel to electrophysiological methods, imaging techniques have also been developed to study vesicle exocytosis. Although electrophysiology has a superior time resolution and is especially useful for studying fast synaptic transmission, to study slower neuropeptide release and vesicle recycling that can happen over seconds-minutes (Betz and Bewick, 1992; Bauer et al., 2004; Perrais et al., 2004), imaging techniques may be better suited. Moreover, the conductance of LDCV fusion pores in chromaffin cells can be higher than what can be measured by electrophysiology but can be measured by a combination of fluorescent dyes (Sharma and Lindau, 2018; Shin et al., 2018). Another advantage of imaging techniques is that they can give valuable information about the location and history of fusing vesicles.

Styryl dyes are amphipathic molecules that increase their fluorescence when bound the membranes and thus can be used to study vesicle cycling (Wu et al., 2009). They bind membranes rapidly but they have different membrane affinities and thus their destaining rate is different. For example, the dye FM2-10 has a faster destaining rate than FM1-42, and this feature has been exploited to study different rates of endocytosis (Klingauf, Kavalali and

Tsien, 1998; Richards, Guatimosim and Betz, 2000). In these experiments, vesicles are loaded with dyes during stimulation, followed by dye washout from the bath solution. During a second round of stimulation, the exocytosis and destaining rate of previously stained vesicles can be measured (figure 1.4.2 B).

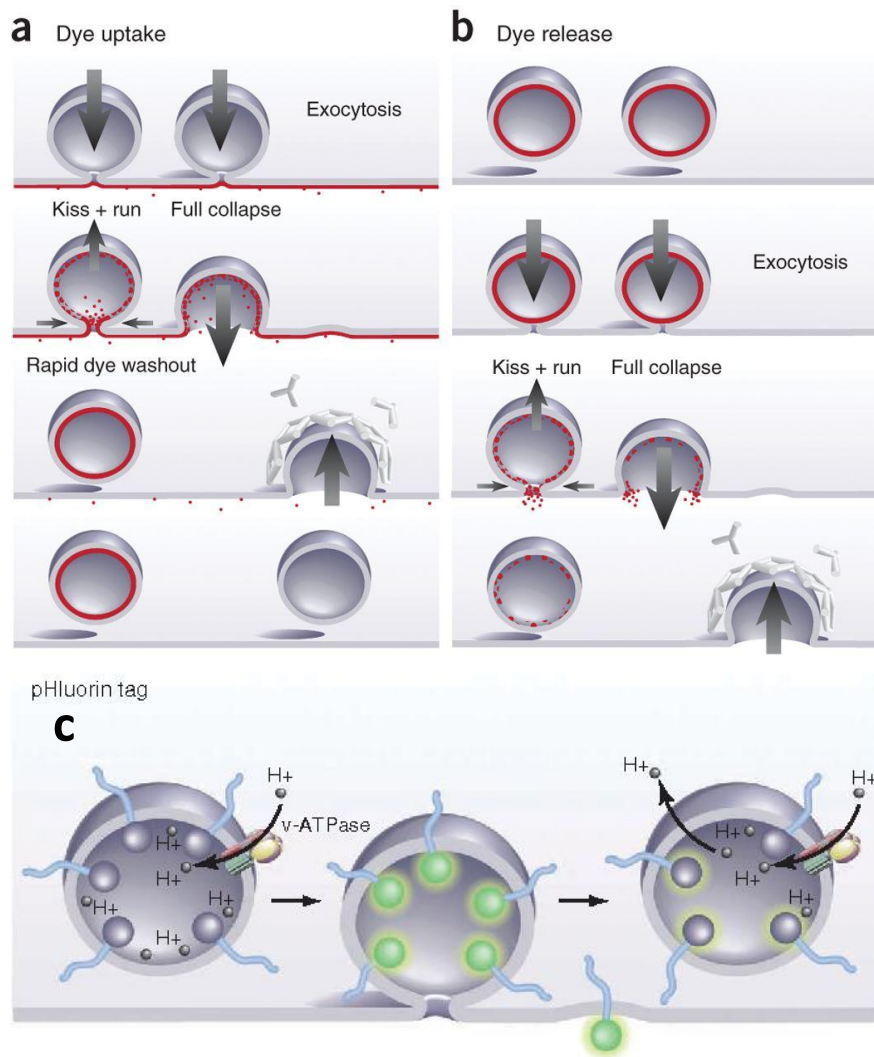


**Figure 1.4.2** Cartoons showing the theoretical background of styryl dyes (a, b) and pHluorins (c). a- b, For experiments using styryl dyes, dye uptake and release can be assessed. During dye uptake, vesicles with different fusion dynamics are loaded with the dye differently, as those fusing with fast transient kiss-and-run fusion will maintain the dye even after washout, compared to vesicles undergoing full fusion and slow endocytosis. Subsequently, dye release can be monitored during vesicle fusion after stimulation. In this case, a short fusion pore opening limits dye release and thus these vesicles stay fluorescent after fusion. C, pHluorin molecules (round tag inside the vesicle) fused to vesicular membrane proteins (shown in blue) or cargo proteins are quenched inside the vesicle, due to the acidic pH, maintained by vesicular proton pumps. Upon fusion, a proton efflux from the vesicle lumen increases the pH and the pHluorin fluorescence swiftly increases. This is followed by vesicle endocytosis and reacidification, and gradual decrease of the fluorescence. Figure was adapted from Kavalali and Jorgensen, 2014.

Dye unloading from vesicles gives an estimate of how long a vesicle is in contact with the plasma membrane and how long a fusion pore is open for. However, one disadvantage of this technique is that dye washout is required after dye loading in order to reduce background fluorescence. As this can take several minutes, the detection of fast vesicle recycling events is limited. Additionally, FM dyes are non-specific and will label all membranes.

A more specific way of studying vesicle exocytosis is the use of fluorescently tagged proteins. One advantage of this approach over styryl dyes is that it allows the tagging and examination of specific vesicular proteins, but it also requires the transfection of cells, which can be done either by transient transfection or by viral vectors. The specificity of the protein tagging also makes the interpretation of fluorescent signals less straightforward, as different fluorescently-tagged proteins can report different fusion characteristics.

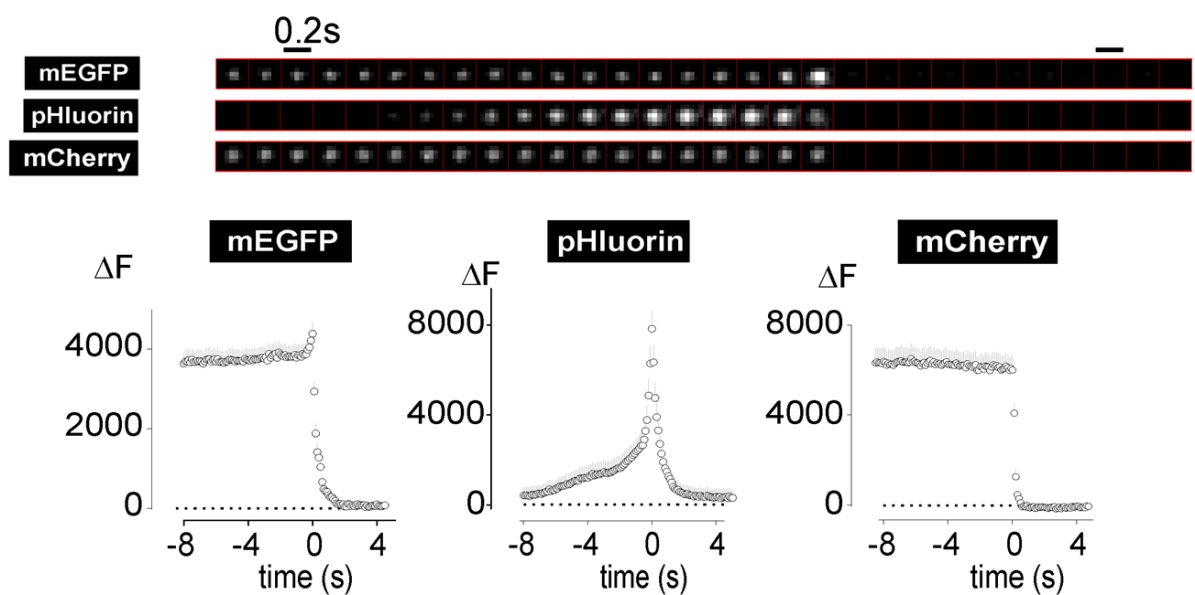


**Figure 1.4.3 Comparison of mEGFP, pHluorin and mCherry tagged to NPY for reporting vesicle fusion in *Ins1* cells.** mEGFP has a pKa of 6 and hence, while the NPY-EGFP is visible before fusion, it exhibits a small increase in fluorescence upon fusion before cargo release and fluorescence loss. pHluorin has the highest pKa among the examined constructs, hence it is invisible before fusion and exhibits a sharp increase in fluorescence before release. mCherry has a pKa of 4.5 and its fluorescence stays the same before dropping, indicating cargo release. Figure was adapted from (Gandasi *et al.*, 2015).

The most widely used among these fluorescent molecules are the pH-sensitive pHluorins (figure 1.4.2 C). Their popularity is due to their neutral pKa ( $\sim 7.4$ ) (Miesenböck, De Angelis and Rothman, 1998), which makes them invisible in the acidic pH of a secretory vesicle prior to fusion, but upon fusion pHluorin fluorescence increases by  $\sim 8-9$  fold, making vesicle fusion events easy to detect (Gandasi *et al.*, 2015). Other fluorescent proteins, such as EGFP, Venus or mCherry have a lower pKa and thus are visible prior to fusion (figure 1.4.3). Fluorescent proteins can be useful to study different aspects of exo/endocytosis and vesicle trafficking depending on their targeting partner. If they are fused to a soluble cargo, such as NPY, then cargo release can be monitored by the disappearance of fluorescence upon fusion. In this case, fluorescent proteins other than pHluorin (such as mCherry or GFP) can be used to monitor the movement of vesicles before and during exocytosis. pHluorins on the other hand are useful when tagged to vesicular membrane proteins to study fusion pore behaviours and endocytosis, as the fate of the vesicle can be followed after exocytosis (Gordon, Leube and Cousin, 2011; Xu *et al.*, 2011; Chanaday and Kavalali, 2018).

In cortical neurons, experiments using pHluorin tagged to different sized cargo proteins (such as semaphoring 3A, tPA, BDNF and NPY) have shown that certain cargoes are retained at the surface of the plasma membrane as stable cargo deposits that can last for minutes (de Wit, Toonen and Verhage, 2009). The appearance of these cargo deposits depends on interaction with the LDCV matrix. Regarding fusion pore behaviours, using a combination of EGFP-tagged PLC1 C $\delta$ 1 PH (PH-EGFP) domain, which selectively labels the cytoplasmic leaflet of both the plasma membrane and vesicular membrane, and Alexa 532 dye in the bath solution, Zhao *et al.* (2016) was able to prove the existence of a hemi-fusion intermediate (figure 1.4.4). They were able to capture fusion states using STED imaging where the PH-EGFP diffused into the vesicular membrane upon contact of the vesicle with the plasma membrane, but the A532 dye did not diffuse into the vesicle, indicating that the fusion pore did not open (figure 1.4.4 A,B). Importantly, the above described electrophysiological techniques would not be able to detect such intermediates. Moreover, using the same technique they were also able to resolve fusion pores of 12-430 nm in size and stable vesicle shapes (Shin *et al.*, 2018) (figure 1.4.4 C).

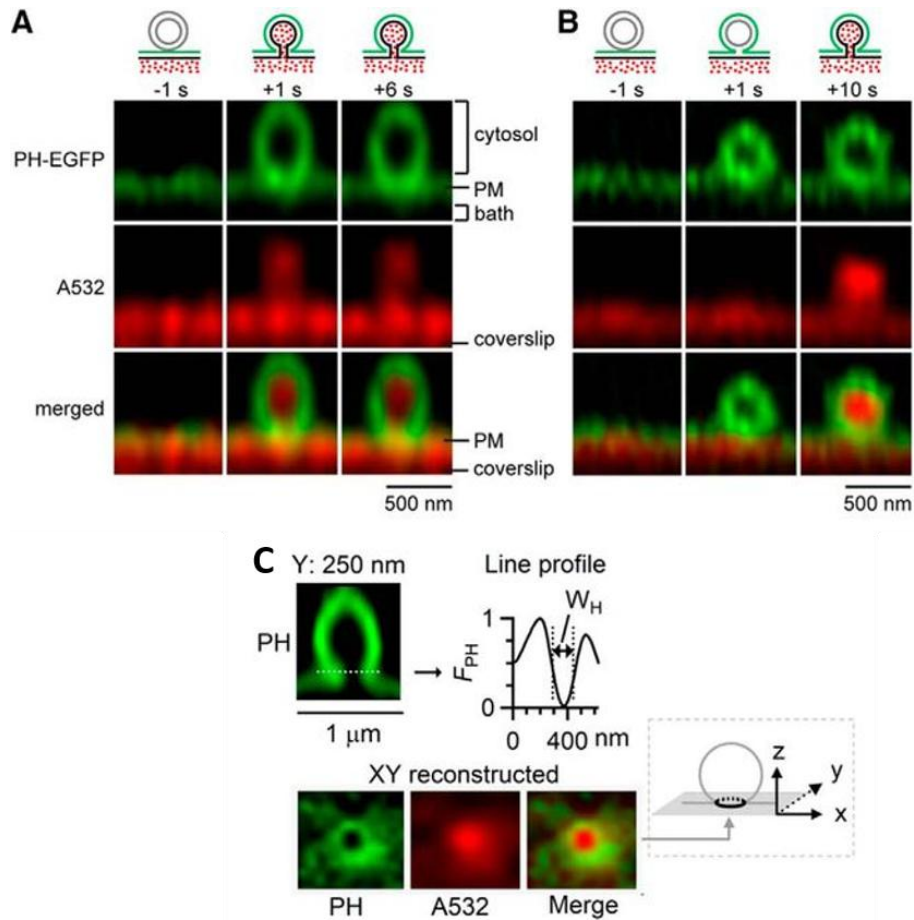


**Figure 1.4.4 Visualization of DCV fusion pores and hemi-fusion intermediates with STED imaging.** Chromaffin cells were transfected with PH-EGFP, which specifically labels the plasma membrane (PM) and the fusing vesicle, while A532 was also present in the bath solution to show fusion pore opening. Cartoons on A and B show the interpretation of the fluorescent images below. A, A vesicle is simultaneously labelled with PH-EGFP and A532 upon fusion with the plasma membrane. B, There is a delay between PH-EGFP and A532 labelling of the vesicle, indicating a hemi-fused intermediate. C *upper left*, an  $\Omega$ -profile of a PH-EGFP labelled vesicle, *upper right*, line profile of the dotted line across the bottom of the vesicle.  $W_H$  = full width at half-maximum. *Bottom*, reconstituted XY plane of the fusing vesicle above, at the fusion pore level (indicated in grey on the inset). Figure was adapted from Shin *et al.*, 2018 and Zhao *et al.*, 2016.

To summarize, the different techniques can report various vesicle fusion characteristics because they each measure different points of the exocytotic process and operate at various time resolutions. A cell-attached capacitance measurement might accurately report the opening and conductance of a fusion pore on the millisecond time scale. An amperometry recording reports the release of oxidizable cargo at similar time scales, but it does not provide information about fusion pore dynamics (only about the initial opening of the fusion pore through the pre-spike foot) or the fate of the vesicle.

Optical measurements on the other hand, might be less accurate to report the initial phase of fusion pore opening, but they report cargo release and fusion dynamics changes with >100 ms to several seconds resolution. Hence, the combination of different techniques should be considered to best understand vesicle fusion and transmitter release.

### 1.5. Synaptotagmins – coupling excitation to Ca<sup>2+</sup> mediated exocytosis

Synaptotagmins (“synapto” refers to a synaptic vesicle protein, “tagmin” refers to its phospholipid binding activity) (M.S. Perin, Johnston, 1991) are a protein family of 17 known isoforms in mammalian cells (figure 1.5.1). They contain a short N-terminal sequence followed by a transmembrane domain and two C2 domains (C2A, C2B), and a C-terminal regions; this structure is highly conserved across species from *Drosophila* to humans, but only the C2 region is homologous across the isoforms (M S Perin *et al.*, 1991; M.S. Perin *et al.*, 1991; Südhof, 2002; Craxton, 2004) (figure 1.5.1). The first discovered isoform, synaptotagmin-1 (syt1), was originally named p65 referring to the molecular weight it was identified at (Matthew, 1981). It contains two Ca<sup>2+</sup>-binding C2 domains homologous to the PKC C2 region (Perin *et al.*, 1990), and its main function was to couple stimulation to calcium dependent exocytosis as shown in *in vitro* fusion assays (Bai *et al.*, 2004; Bhalla, Tucker and Chapman, 2005; Rizo, Chen and Araç, 2006).

Early biochemical studies determined that syts bind phospholipids and syntaxin in a Ca<sup>2+</sup> dependent manner through their C2 domains (Brose *et al.*, 1992; Davletov and Südhof, 1993; Chapman and Jahn, 1994), but the two C2 domains have different functions. While the C2A domain is responsible for Ca<sup>2+</sup>-dependent phospholipid binding (Davletov and Südhof, 1993), the membrane distal C2B domain mediates Ca<sup>2+</sup>-dependent homo- and hetero-oligomerization with other syts (Chapman *et al.*, 1996, 1998; Osborne *et al.*, 1999), Ca<sup>2+</sup> channels (Kim and Catterall, 1997; Sheng, Yokoyama and Catterall, 1997) and synaptic proteins such as syntaxin, AP2 adaptor complex proteins and SNAP25 (Chapman *et al.*, 1995, 1998). The different isoforms also have different Ca<sup>2+</sup>-sensitivities (Li *et al.*, 1995). In the presence of lipids, the Ca<sup>2+</sup> concentration dependence of syt1, 2 and 9 are in the high (>100)

micromolar range, while that of syt3, 5, 7 and 10 are in the low (<10) micromolar range (Sugita *et al.*, 2002; Volynski and Krishnakumar, 2018).

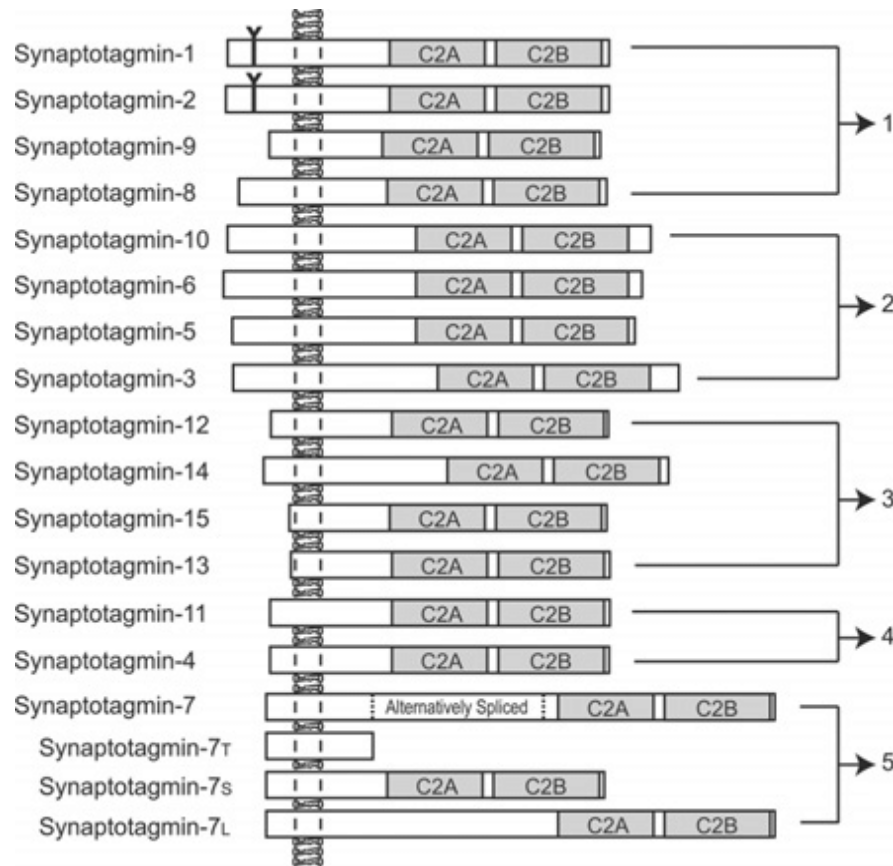


**Figure 1.5.1 Structure of mouse synaptotagmins.** All syts have a TM domain and two C2 domains, but their linker regions between the TMD and C2A domain, and the C/N terminals are variable. Syt7 alternatively spliced forms are shown on the bottom. Syts can be classified into five groups (shown by brackets on the right) based on homology. Image was reused from Gustavsson & Han (2009).

It has thus been proposed that the presence of these low and high-affinity  $\text{Ca}^{2+}$  sensors can accommodate a wide range of  $\text{Ca}^{2+}$  dependence of exocytosis in neurons and endocrine cells (Pinheiro, Houy and Sørensen, 2016) (figure1.5.2). An example for this is the differential distribution of syt1, 2 and 9 in the brain, each of which has slightly different  $\text{Ca}^{2+}$  sensitivities and trigger transmitter release with different kinetics. In the calyx of Held synapses, syt2 is the main  $\text{Ca}^{2+}$  sensor, which triggers neurotransmitter release with the fastest kinetics out of these three isoforms (Xu, Mashimo and Südhof, 2007). In the limbic system syt9 is the dominant isoform and triggers release with relatively slower kinetics while Syt1 dominates in the forebrain (Xu, Mashimo and Südhof, 2007). Thus, their

differential expression in the brain determines the release kinetics of the synapse where they reside.

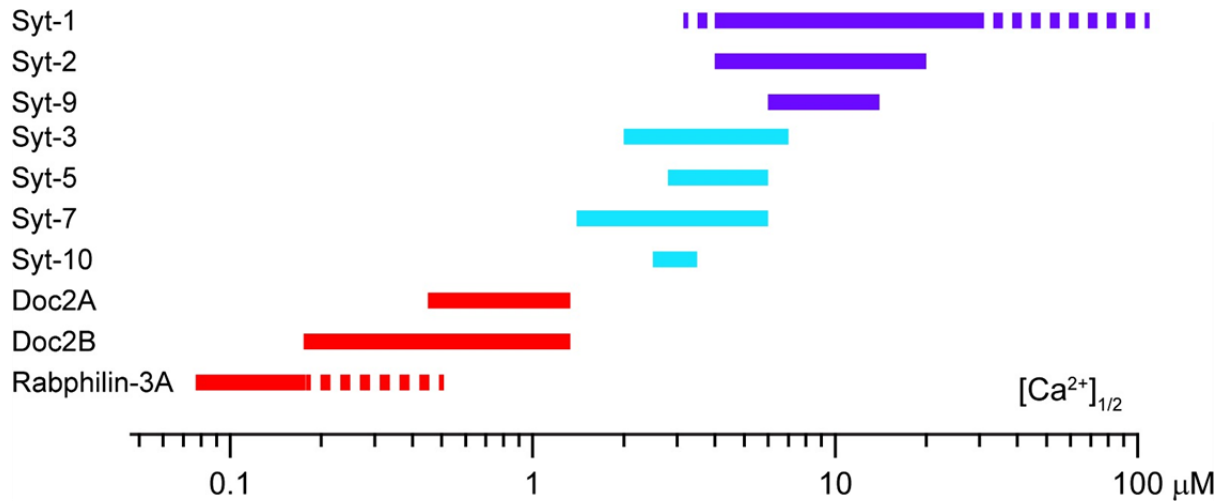


**Figure 1.5.2 Schematic diagram showing the half maximal calcium concentrations,  $[Ca^{2+}]_{1/2}$ , of indicated C2 domain containing proteins required for membrane binding.** Purple indicated low affinity, light blue indicates medium affinity, and red indicated high affinity groups of proteins. Figure was adapted from Pinheiro et al. (2016).

### *syt1*

Being the first identified isoform, *syt1* has been the most extensively studied. Early on, it was identified as the low-affinity  $Ca^{2+}$  sensor of the synchronous component of transmitter release in hippocampal neurons, as synchronous release largely disappears in *syt1* KO mice (Geppert *et al.*, 1994; Goda and Stevens, 1994; Li, Davletov and Südhof, 1995). Later studies confirmed this and solidified *syt1* as the main  $Ca^{2+}$  sensor of transmitter release in neurons and endocrine cells, where the  $Ca^{2+}$  sensitivity of release is largely determined by the  $Ca^{2+}$  affinity of *syt1*, as shown by introducing mutations in the *syt1* C2 domains (Fernández-Chacón *et al.*, 2001; Voets *et al.*, 2001; Rhee *et al.*, 2005). In chromaffin cells, Ca-dependent lipid binding by *syt1* is required for the fusion of vesicles that fuse soon after stimulation (readily releasable pool of vesicles or RRP), as this fast release component disappears in *syt1* KO cells (Voets *et al.*, 2001; Sørensen *et al.*, 2003).

Multiple later studies established that *syt1* likely has other functions, such as clamping  $Ca^{2+}$ -dependent spontaneous “mini” release along with complexin (Xu *et al.*, 2009) and in

vesicle priming/docking to help maintain RRP size in a  $\text{Ca}^{2+}$ -independent manner in hippocampal neurons (Bacaj *et al.*, 2015) and in chromaffin cells (de Wit *et al.*, 2009; Mohrmann *et al.*, 2013). In support of the notion that synaptotagmins might have a role in steps upstream of vesicle fusion is the finding that syt2 (which is highly homologous to syt1) contributes to positional priming (the positioning of SVs close to calcium channels) that is required for synchronous release at rat calyx of Held synapses (Young and Neher, 2009).

### Syt7

Another component of transmitter release is asynchronous (“slow”) release which is maintained over hundreds of milliseconds and has much higher  $\text{Ca}^{2+}$  sensitivity than synchronous release, suggesting that a separate  $\text{Ca}^{2+}$  sensor regulates this type of release (Sun *et al.*, 2007). Syt7 has a high  $\text{Ca}^{2+}$  affinity and the slowest dissociation kinetics from phospholipids among syts (Bhalla, Tucker and Chapman, 2005; Hui *et al.*, 2005), making it an ideal protein to regulate slow release. Syt7 is a  $\text{Ca}^{2+}$  sensor of lysosome exocytosis in fibroblasts (Martinez *et al.*, 2000), the main  $\text{Ca}^{2+}$  sensor of insulin secretion in pancreatic  $\beta$ -cells (Gao *et al.*, 2000; Li *et al.*, 2007; Gustavsson *et al.*, 2008) and is localized on the plasma membrane as well as secretory vesicles (Sugita *et al.*, 2001; Fukuda *et al.*, 2004).

Functional studies using electrophysiology found that syt7 is the main  $\text{Ca}^{2+}$ -sensor of asynchronous SV release in hippocampal neurons, calyx of Held synapses, retinal ribbon synapses and zebrafish neuromuscular junction (Wen *et al.*, 2010; Bacaj *et al.*, 2013; Luo, Bacaj and Südhof, 2015; Li *et al.*, 2017; Luo and Südhof, 2017), although its deletion did not have any effect on SV release at inhibitory synapses between cultured cortical neurons (Maximov *et al.*, 2008). A study examining the role of syt7 on four different facilitating synapses in the mouse brain found that syt7 was required for synaptic facilitation, and suggested that it does so by increasing the probability syt1-mediated SV fusion (Jackman *et al.*, 2016). In chromaffin cells, syt1 and syt7 appear to be the main proteins regulating fast and slow exocytosis of LDCVs respectively, as deletion of syt1 or syt7 eliminated the fast or slow component of release respectively, while double KO eliminated 70-80 % of total secretion (Schonn *et al.*, 2008). There is therefore good evidence that syt7 regulates slow transmitter release in many cell types.

Some suggested that like syt1, syt7 also has a role upstream of fusion triggering, as syt7 was found to work together with calmodulin to replenish SVs during repetitive stimulation in hippocampal neurons (Liu *et al.*, 2014) and LDCVs in chromaffin cells (Schonn *et al.*, 2008). However, other studies found no effect of syt7 on the rate of SV replenishment in hippocampal neurons or retinal ribbon synapses (Bacaj *et al.*, 2015; Luo, Bacaj and Südhof, 2015). The reason for these discrepancies between studies is not clear, but could be due to small differences between experimental procedures, cell types or even the interpretation of results.

Besides the above described roles of syt7, it is also reported to regulate fusion pores and thus selective transmitter release. In mouse embryonic fibroblasts, the release of different sized fluorescent dextran cargo from lysosomes was fuller in syt7 KO cells and it was concluded that syt7 restricts fusion pore expansion (though whether pore size or the speed of opening is affected was inconclusive) (Jaiswal *et al.*, 2004). Additionally, the C2 domains of syt7 were essential for its function in controlling fusion pore dynamics as shown in chromaffin cells. When  $\text{Ca}^{2+}$ -binding to its C2B domain was disrupted by a mutation, more KR and less FF events were observed, suggesting that the C2B domain controls fusion pore expansion, perhaps by stabilizing it, in a  $\text{Ca}^{2+}$ -dependent manner but both C2 domains were needed to open the fusion pore (Segovia *et al.*, 2010).

Due to its high  $\text{Ca}^{2+}$ -sensitivity, syt7 responds to  $\text{Ca}^{2+}$  concentration increase faster than syt1, as evidenced by the fact that syt7-bearing vesicles fuse closer to the time of stimulation than syt1 vesicles in chromaffin cells (Rao *et al.*, 2017). The same group has found that following mild (25 mM KCl) stimulation, syt7 mediated events are favoured compared to syt1 events, and this trend reverses with increasing (56 and 80 mM) KCl concentration (Rao *et al.*, 2014; Bendahmane *et al.*, 2019). The authors concluded that Syt7 is activated by lower  $\text{Ca}^{2+}$  increase after mild stimulation, and restricts fusion pore expansion to slow down cargo release. Syt1 on the other hand can only sense higher  $\text{Ca}^{2+}$  concentration after strong stimulation, and mediates pore widening and fuller cargo release (figure 1.5.3).

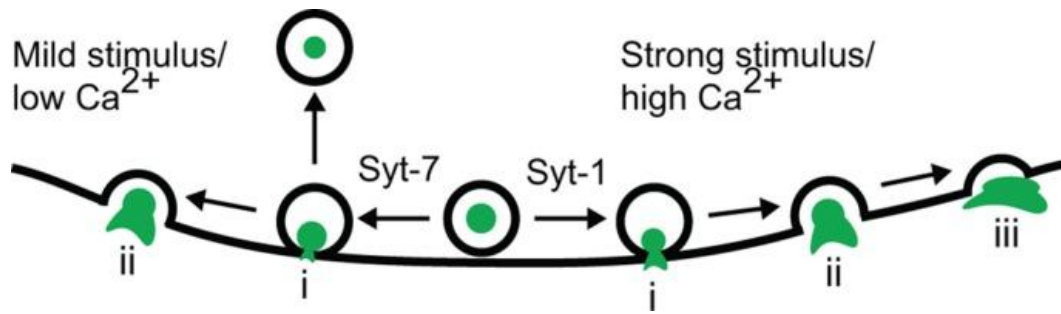


**Figure 1.5.3 Putative roles of syt1 and syt7 in mediating vesicle fusion.** Strong stimulation and higher  $\text{Ca}^{2+}$  rise at nanodomains close to  $\text{Ca}^{2+}$  channels preferentially activated syt1 bearing LDCVs, which mediates fast fusion pore widening and full cargo release. Syt7 on the other is well suited for a lower, more uniform rise in  $\text{Ca}^{2+}$  after milder stimulation due to its higher sensitivity and slow membrane unbinding kinetics, and it restricts fusion pore opening and cargo release. Figure was reused from Rao et al. (2014).

The differences between syt1 and syt7 appear to arise from small differences in their C2B domains, as replacing the syt1 C2B domain with that of syt7 could not rescue the syt1 phenotype (reduced transmitter release) in syt1 KO mice (Xue *et al.*, 2010), and their two C2 domains have different relative importance for their function (Bacaj *et al.*, 2013). Nevertheless, these findings suggest that cells can achieve precise control of fusion pore dynamics and cargo release through sorting different synaptotagmin isoforms onto vesicles, and how accessible their C2 domains are to  $\text{Ca}^{2+}$  (by positioning to  $\text{Ca}^{2+}$ -channels/interaction with other proteins) (the various roles of syt7 were recently reviewed in MacDougall *et al.*, 2018).

#### Syt4

Out of the seven syt isoforms that lack  $\text{Ca}^{2+}$  binding ability (Syt4, 8, 11, 12, 13, 14, 15), syt4 has been the most extensively studied. It harbours a single point mutation resulting in an aspartate to serine substitution in its C2A domain, and thus lacks  $\text{Ca}^{2+}$ -dependent phospholipid binding by this domain in mammalian cells (Ullrich *et al.*, 1994; Poser, Ichtchenko and Shao, 1997), though in *Drosophila* it retained its  $\text{Ca}^{2+}$  binding ability and functions as a postsynaptic  $\text{Ca}^{2+}$  sensor (Dai *et al.*, 2004; Yoshihara *et al.*, 2005; Barber *et al.*, 2009). syt4 can still bind syntaxin through its C2A domain, and interestingly, its C2B domain possesses  $\text{Ca}^{2+}$ -binding properties which promotes its homo- and hetero-oligomerization (Thomas *et al.*, 1999).

The expression of syt4 can be induced by forskolin in PC12 cells and electrical activity in neurons, and its expression levels also change during development (Vician *et al.*, 1995; Ferguson *et al.*, 1999). In the brain, syt4 has important roles in the proper functioning of synaptic transmission in the hippocampus and cerebellum, as syt4 KO mice have impaired learning, memory and motor coordination (Ferguson *et al.*, 2000). On the cellular level, Syt4 is localized to both SVs and LDCVs, as well as the Golgi (Ferguson *et al.*, 1999; Ibata *et al.*, 2000; Zhang *et al.*, 2009), and is generally considered an inhibitory isoform, as it inhibits exocytosis in PC12 cells and neurons (Machado *et al.*, 2004; Moore-Dotson, Papke and Harkins, 2010). In hippocampal neurons, syt4 negatively regulates BDNF release and thus indirectly affects synaptic transmission and plasticity (Dean *et al.*, 2009). However, its function seems more complex than simply inhibiting release, as it was found to regulate the Ca<sup>2+</sup> sensitivity of release by promoting exocytosis at low, and inhibiting it at high Ca<sup>2+</sup> influx at pituitary nerve terminals (Zhang *et al.*, 2009), and by establishing the linear Ca<sup>2+</sup> dependence of transmitter release in cochlear hair cells (Johnson *et al.*, 2010).

It is likely that syt4 functions at least partly through interacting with other isoforms and affecting their Ca<sup>2+</sup>/phospholipid/SNARE binding. In *Drosophila*, it forms hetero-oligomers with syt1 to inhibit neurotransmission (Littleton *et al.*, 1999), while in pancreatic  $\beta$  cells, syt4 developmentally regulates the Ca<sup>2+</sup> -sensitivity of insulin secretion through interacting with syt7 (Huang *et al.*, 2018). This latter study found using proximity ligation assay that syt4 and syt7 interact, and suggested that syt4 increases the Ca sensitivity of insulin secretion in mature  $\beta$  cells through either directly inhibiting syt7 on vesicles or through decreasing the sorting of syt7 onto vesicles at the level of the Golgi. As opposed to the inhibitory roles of syt4 but supporting the notion that it functions together with other Ca<sup>2+</sup> sensors, syt4 and 7 were both required for basal and evoked somatodendritic dopamine release in hippocampal neurons, as measured by radioassay in syt4/syt7 siRNA knockdown neurons (Mendez *et al.*, 2011). It is unknown how the interaction of syt4 with syt7 alters syt7 function, possible mechanisms include changing its Ca<sup>2+</sup> affinity or regulating fusion pore dynamics.

Several studies looking at fusion pore regulation by syt4 were conducted on PC12 cells using amperometry and capacitance recordings. These studies found that overexpression of syt4 resulted in decreased fusion pore stability and reduced pore open time (Wang *et al.*, 2001), and promoted KR events with narrow fusion pores (Wang *et al.*, 2003). A different

study also found that syt4 promoted KR events, but their results indicated that these LDCV fusion events had increased pore size and lifetime (Zhang, Zheng and Jackson, 2010). Experiments in pituitary peptidergic nerve terminals supported this latter study: in wild type nerve terminals, LDCV fusion pores were significantly larger than in those from syt4 knockout mice (Zhang *et al.*, 2009). Thus, it is still not clear how syt4 exactly affect fusion pore kinetics although studies agree that it promotes KR and has no effect on SV fusion.

Interestingly, syt4 is mostly localized to the Golgi in undifferentiated PC12 cells, but following NGF differentiation or forskolin treatment it is trafficked to LDCVs which undergo  $Ca^{2+}$ -dependent exocytosis (Fukuda *et al.*, 2003; Fukuda & Yamamoto, 2004). Since syt4 was shown to be phosphorylated in PC12 cells after NGF treatment (Mori *et al.*, 2008), this points towards the possibility that post-translational modifications may alter its function. Indeed in hippocampal neurons, syt4 phosphorylation on DCVs was found to promote DCV dissociation from microtubules, increased their capture and the release of NPY cargo at presynaptic release sites (Bharat *et al.*, 2017) (figure 1.5.4). However, whether similar mechanisms work in DRG neurons has not been investigated.

In summary, syt4 is a calcium-insensitive isoform that is mostly localized to DCVs but its precise function in secretion and vesicle fusion remains poorly characterized. In DRG neurons, syt1 and 2 are known receptors for botulinum-A but syt4 or syt7 have not been described in these cells, nor have syt4 or syt7 KO mice been assessed for pain behavioural phenotypes. Moreover, while the physiological effects and receptors of NGF on DRG neurons are well characterized, the possible role of syt4 and its phosphorylation in NGF-mediated signalling are unknown.

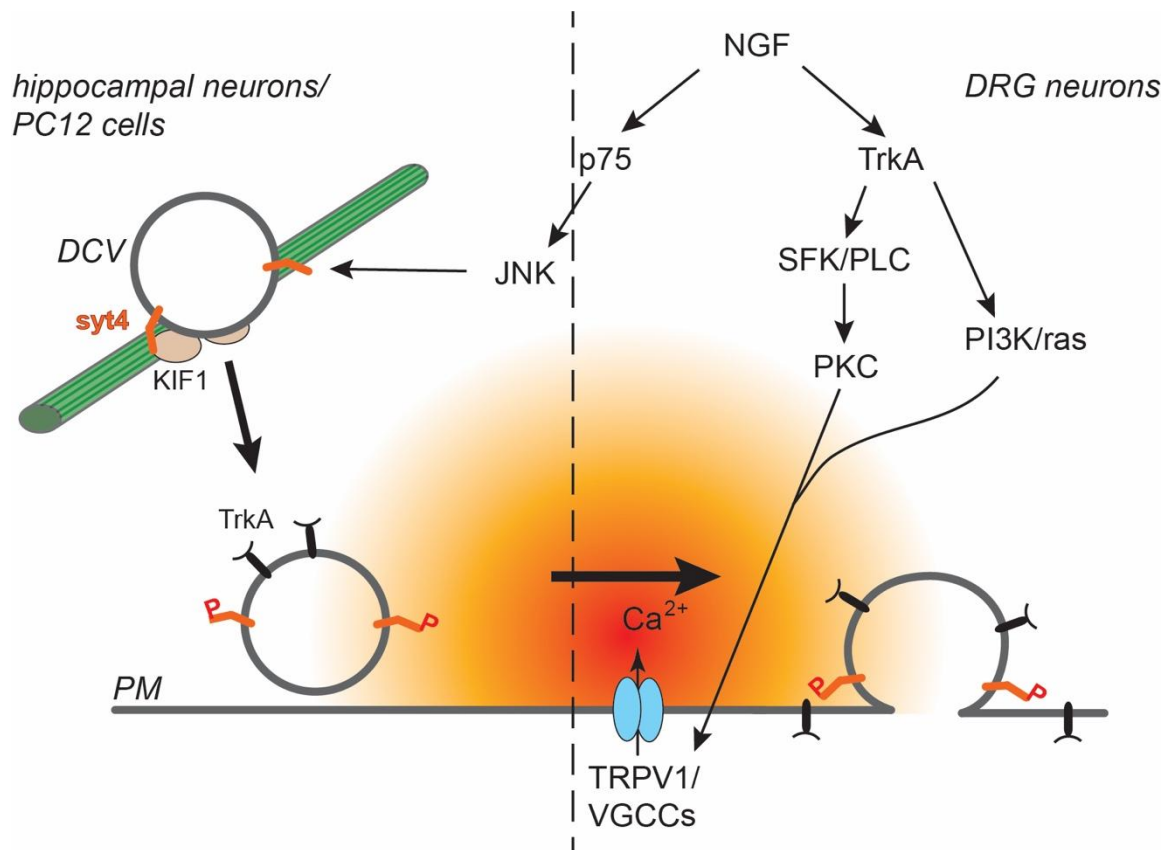


**Figure 1.5.4 Summary figure of known role of syt4 in vesicle trafficking in hippocampal neurons and of TrkA signalling in DRG neurons.** Bharat et al. (2017) found in hippocampal neurons, syt4 located of DCVs is phosphorylated by JNK. The phosphorylation of syt4 promotes detachment of DCVs from microtubules (in green) and from the motor protein KIF1 and increased capture at the plasma membrane (PM). In DRG neurons on the other hand, NGF can bind to its receptors p75 and TrkA, and TrkA activation leads to phosphorylation of TRPV1, which in turn leads to increased neuronal excitability, vesicle fusion and increased surface presentation of TrkA receptors (Tanaka et al., 2016). Whether the activation of p74 by NGF in DRG neurons has similar outcomes as in hippocampal neurons is unknown.

## 1.6. Aims and objectives

Sensory neurons increase their neuropeptide secretion during chronic inflammation both in the periphery and the CNS, but the secretory machinery that enables this maintained secretion is unexplored. This thesis focuses on the role of synaptotagmins in this process as potential calcium sensors that regulate peptide release from DRG neurons. In order to address this question, a second major aim of the work was to establish a method for characterizing and quantifying exocytosis from DRG neurons directly.

Therefore the experimental objectives of the research were to:

- Describe the synaptotagmin isoforms expressed in the peptidergic DRG neurons
- Identify putative isoforms controlling neuropeptide secretion in DRG neurons
- Establish a method for studying synaptotagmin-mediated exocytosis in DRG neurons
- Study the function of identified synaptotagmins in regulating secretion from DRG neurons and explore the impact of phosphorylation of synaptotagmin-4 on exocytosis from DRG neurons

## 2. Materials and Methods

### 2.1. List of antibodies

Primary antibodies			
Name	Host	Application	Source
Synaptotagmin 2	Rabbit	ICC (1/500) WB (1/1000)	Synaptic systems, 105123
Synaptotagmin 4	Rabbit	ICC (1/1000) WB (1/1000)	Synaptic Systems, 105143
Synaptotagmin 4 H-4	Mouse	ICC (1/200)	Santa Cruz, sc271936
Synaptotagmin 4	Rabbit	IP, WB (1/1000)	Synaptic Systems, 105 043
Synaptotagmin 7	Rabbit	ICC (1/200) WB (1/1000)	Synaptic systems, 105173
Synaptotagmin 11 H-79	Rabbit	ICC (1/500) WB (1/1000)	Santa Cruz, sc135411
TrkA	Rabbit	ICC (1/100)	Alomone labs ANT-018
CGRP	Mouse	ICC (1/1000)	Sigma-Aldrich C71113
TRPV1	Goat	ICC (1/200)	Santa Cruz sc-12498
Substance P	Guinea pig	ICC (1/100)	Abcam ab10353
GAPDH	Mouse	WB (1/1000)	Thermo Fisher
Anti-GFP	Camelid single domain antibody	ICC (1/1000)	Synaptic Systems, N0301-At488-S
Secondary antibodies			
Name	Host	Application	Source
Alexa Fluor 488 anti-rabbit	Donkey	ICC (1/1000)	Thermo Fisher A-21206

Alexa Fluor 594 anti-goat	Donkey	ICC (1/1000)	Thermo Fisher 23235
Alexa Fluor 488 anti-mouse	Donkey	ICC (1/1000)	Thermo Fisher A-21203

## 2.2. DNA constructs

Plasmid name	Details
Synaptotagmin 2-pHluorin	Synaptotagmin 4 gene was replaced by synaptotagmin 2 in the syt4-phluorin construct; cloning done by GenScript
Synaptotagmin 4-phluorin	From Anantharam lab (University of Michigan, US)
Synaptotagmin 7-pHluorin	From Anantharam lab (University of Michigan, US)
NPY-mCherry	From Barg lab (Uppsala University, Sweden)
VAMP2-pHluorin	From Barg lab (Uppsala University, Sweden)
NPY-pHluorin	From Anantharam lab (University of Michigan, US)
Synaptotagmin 4-mCherry	pHluorin gene was replaced by mCherry in the syt4-pHluorin construct; cloning done by GenScript
1, Synaptotagmin 4-S135A-mCherry 2, Synaptotagmin 4-S135E-mCherry	Site directed mutagenesis was done by Genscript to change the Serine at the 135 site to Alanine in the phosphodeficient, or to a Glutamic acid in the phosphomimetic construct.

## 2.3. Animals

All animals had free access to food and water prior to sacrifice. C57BL/6 mice were from an in-house breeding colony and were originally purchased from Charles River (UK).

Synaptotagmin-4 mutant mice used in this project were from the in-house breeding colony of Professor Walter Marcotti and Dr Stuart Johnson and were originally obtained from H. Herschman (UCLA). Syt4 KO mice were generated by replacing a section of the syt4 gene encoding the C2A domain with a targeting construct containing the same gene sequence, but which was disrupted using a neomycin resistance cassette (Ferguson *et al.*,

2000) (figure 2.3.1). 129SvJ embryos containing the *Syt4/neo<sup>R</sup>* gene fragment were raised and then crossed with C57BL/6 mice, to obtain heterozygous mice for the mutation. *Syt4* heterozygous (+/-) mice were then crossed to obtain homozygous mutants.

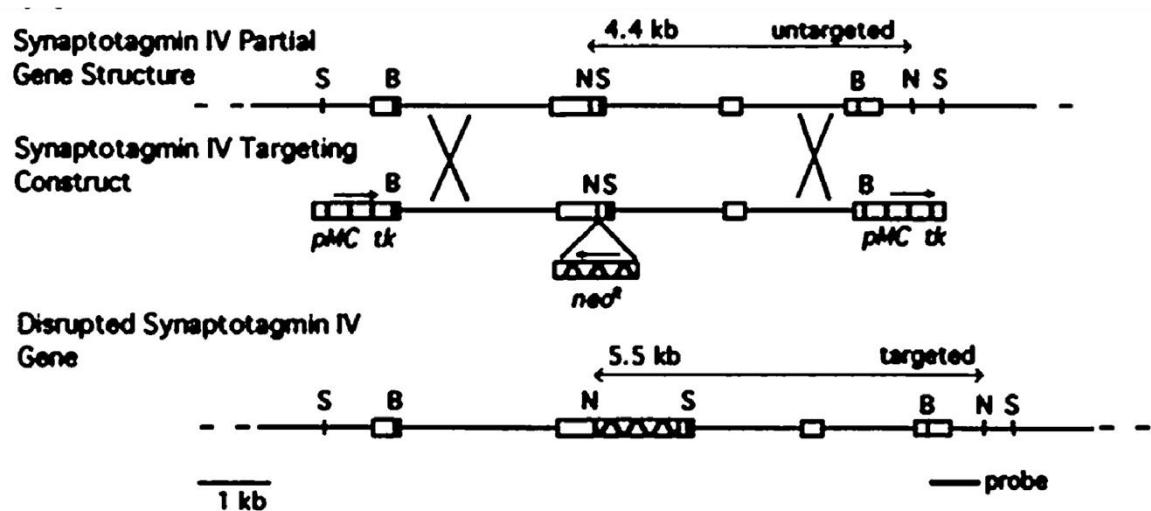


Figure 2.3.1 Schematic of the *syt4* gene structure used to create *syt4* KO mice. Figure from Ferguson *et al.*, 2000.

*Syt7* mutant mice (used for ELISAs and antibody validation in chapter 3) and *syt2* mutant mice (used for antibody validation in chapter 3) were from the breeding colony of Professor Walter Marcotti and were purchased from the MRC Harwell Institute. Both gene knockouts were generated by “knockout-first” conditional allele targeting strategy (Coleman *et al.*, 2015). Briefly, a “targeted mutation 1a” (tm1a) allele containing a *lacZ* cassette, *FRT* sites and *loxP* sites upstream of a critical exon (a gene sequence that is essential for protein function) was inserted into the *syt2* or *syt7* genes by homologous recombination. A *syt7*<tm1b> allele was then generated by crossing <tm1a> mice with global “Cre deleter” mice, resulting in the deletion of the critical exon (exon 7). Due to the remaining *lacZ* cassette,  $\beta$ -galactosidase is expressed in the relevant tissues instead of *syt7*. The *syt2*<tm1d> mice were generated by crossing *syt2*<tm1a> mice with mice globally expressing *FLP1* recombinase, followed by crossing with “Cre deleter” mice, resulting in full knockout of the critical exon (exon 3) without the expression of  $\beta$ -galactosidase.

Adult, 6-12 weeks old C57BL/6, *syt7*<tm1b> and *syt4* mice were sacrificed using a Schedule 1 method in accordance with the animals (Scientific Procedures) Act 1986.

Synaptotagmin 2 <tm1d> mice were sacrificed at P14, as syt2 KO mice are only viable for ~20 days (Pang *et al.*, 2006).

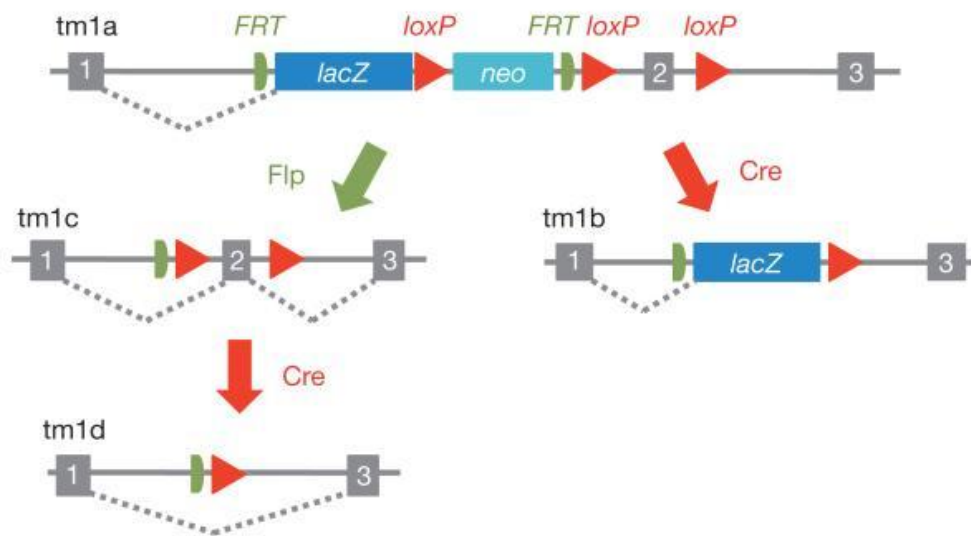


Figure 2.3.2 Schematic showing the “knockout-first” conditional allele targeting strategy for creation of syt7 and syt2 KO mice. Figure reused from (Skarnes *et al.*, 2011).

## 2.4. Primers

Name	Sequence	Details
Reverse	5' GCAAGGAGAGCTCTTGGATGTG 3'	Syt 4 genotyping
Forward 1 (mutant, expected band at 250 bp)	5' AAC CAC ACT GCT CGA CAT TGG G 3'	Syt 4 genotyping
Forward 2 (wild type, expected band at 300 bp)	5' CAC TTC CCT CAC GTC AGA GGA G 3'	Syt 4 genotyping
SYT2,4,7 forward 1	5' C TACTCTTGTGCCAGGGTGTGGTC 3'	Sequencing
SYT2,4,7 SYT forward 2	5' CAGGCGGAAGCGGAGGC 3'	Sequencing
SYT2,4,7 SYT forward 3	5' GGTGGCACTTTTCGGGGAAATG 3'	Sequencing
SYT2,4,7 SYT reverse	5' CATGTCTGCTCGAAGCGGC 3'	Sequencing

NPY forward 1	5' GAGACCCAAGCTGGCTAGCC 3'	Sequencing
NPY forward 2	5' CGGCATGACTTTTTCAAGAGTG 3'	Sequencing
NPY reverse 1	5' GTGGCTAGCCAGCTTGGGTCTC 3'	Sequencing

## 2.5. Solutions and buffers

### Live-cell imaging and ELISA solutions

<b>Normal external solution – pH=7.3-7.4</b>	
KCl	2 mM
NaCl	145 mM
MgCl <sub>2</sub>	1 mM
NaHCO <sub>3</sub>	5 mM
CaCl <sub>2</sub>	2.5 mM
HEPES	10 mM
Glucose	10 mM
<b>High potassium external solution – pH=7.3-7.4</b>	
KCl	40 mM
NaCl	107 mM
MgCl <sub>2</sub>	1 mM
NaHCO <sub>3</sub>	5 mM
CaCl <sub>2</sub>	2.5 mM
HEPES	10 mM
Glucose	10 mM

Western blotting solutions

Running buffer	
Tris Base	25 mM
Glycine	192 mM
SDS	1 %
Transfer buffer	
Tris Base	25 mM
Glycine	192 mM
Methanol	20 %
TBS (Tris-Buffer Saline)	
Tris base	20 mM
NaCl	137 mM
Tween-20	0.1 %
pH = 7.6, adjusted with HCl	

Stack Gel		Gel percentage	
Reagent	Stock concentration	4 %	6 %
Acrylamide	30 %	666 µl	1 ml
Tris-HCl (pH=6.8)	0.5 M	1.25 ml	1.25 ml
SDS	10 %	50 µl	50 µl
H <sub>2</sub> O	-	3.3 ml	3 ml
APS	10 %	30 µl	30 µl
TEMED	-	15 µl	15 µl

Resolving gel		Gel percentage				
Reagent	Stock concentration	7.50%	10%	12%	14%	15%
Acrylamide	30 %	6.25 ml	8.33 ml	10 ml	11.67 ml	12.5 ml
Tris-HCl (pH=8.8)	1.5 M	6.25 ml	6.25 ml	6.25 ml	6.25 ml	6.25 ml
SDS	10 %	250 µl	250 µl	250 µl	250 µl	250 µl
H2O	-	12 ml	10 ml	8.2 ml	6.6 ml	5.7 ml
APS	10 %	250 µl	250 µl	250 µl	250 µl	250 µl
TEMED	-	25 µl	25 µl	25 µl	25 µl	25 µl

Other often used reagents

Name	Supplier	Catalog number
DMEM/F12	Thermo Fisher	31331-028
Heat inactivated fetal bovine serum	Sigma-Aldrich	F0804-50ML
Pen/Strep	Millipore	TMSAB2C
HBSS	Thermo Fisher	14170-088
Laminin	Sigma-Aldrich	L2020
Poly-L-lysine	Sigma-Aldrich	P1274
Normal donkey serum (NDS)	Sigma-Aldrich	D9663
NGF-β from rat	Sigma-Aldrich	N2513
RPMI-1640	GE Healthcare	SH30027.01
Trypsin	Sigma-Aldrich	T7409-1G

Collagenase	Sigma-Aldrich	C5138-100MG
RIPA buffer	Sigma-Aldrich	R0278-50ML
Protease inhibitor cocktail III	Thermo Fisher	12841640
Laemlli buffer	Bio-Rad	161-0747
$\beta$ -Mercaptoethanol	Sigma-Aldrich	M7522

Commercial Kits and devices

CGRP ELISA kit	Phoenix Pharmaceuticals	EK-015-09
ZymoPURE II Plasmid Kits	Zymo Research	D4200
Micro BCA assay kit	Thermo Fisher	23235
AMAXA Basic Nucleofector Kit	Lonza	VPI-1003
Nucleofector 2b device	Lonza	AAB-1001

## 2.6. Mouse dorsal root ganglia isolation and culture

### Dissection and culture preparation

The mouse DRG dissection and dissociation procedure used in this thesis was modified based on (Malin, Davis and Molliver, 2007). Following schedule 1 sacrifice, mice were moved to the dissection area. The skin in the back, starting from the neck was cut open using iris scissors. The skin was pulled to the sides using surgical forceps to expose the spine, which was removed by cutting through the ribs, muscles and any connective tissue. After removal of the spine, it was cleared from excess tissues using scissors until the midline of the spine was visible, where it was then cut into two halves and one of them was placed onto a tissue paper. The other half was placed on a plastic 100 mm Petri dish and moved under a stereomicroscope, where the rest of the dissection was carried out. To remove the ganglia, starting at the cervical region, the dorsal root was grasped using fine forceps and pulled to lift the DRG slightly, then the spinal nerve (located underneath the ganglion) was carefully cut using vannas scissors. Care was taken not to touch or damage the DRG itself in the process. After most of the spinal nerve and dorsal/ventral roots were cut away from the DRG, it was carefully placed in an Eppendorf tube containing ice cold Hank's Balanced Salt Solution (HBSS). This isolation procedure was repeated for all DRGs in both halves of the spine.

After dissection, the tube containing the ganglia was transferred into a laminar flow hood. For enzymatic digestion, ganglia were first incubated in 1.25mg/ml collagenase solution for 30 minutes inside a 37°C incubator, after which collagenase was removed and 2.5mg/ml trypsin solution was added for further 30 minutes. After digestion, ganglia were washed with full culture media (DMEM/F12 containing 10% fetal bovine serum and 1% pen/strep) to deactivate enzymes, and spun down at 1000 RPM for 1 minute. The wash step was repeated, followed by mechanical dissociation of ganglia by triturating with a 19G needle about 3 times, followed by triturating with a 23G needle about 3-4 times. Cell suspension was topped up with additional culture media and spun down at 1000 RPM for 3 minutes. Supernatant was discarded and cell pellet resuspended in full culture media, after which cells were seeded for experiments. Half the media was changed the following day, and cultures were normally maintained for 2 or 3 days, depending on the experiment.

### DRG culture conditions

Different protocols exist for culturing primary DRG neurons which differ in isolation process and culture media, depending on how long the culture needs to be maintained for and on experimental context. As primary DRG cultures contain a mixture of primary non-dividing neurons as well as dividing cells, including glial cells, conditions must be adapted accordingly to ensure adequate support of neuronal survival. To prevent the proliferation of dividing cells that would consume nutrients from the media, mitotic inhibitors can be used in long-term (more than ~3 days) culture media (Malin, Davis and Molliver, 2007; Owen and Egerton, 2012). Moreover, although growth factors are not necessary for the survival of adult DRG neurons, they affect axon growth and can modulate the expression of receptors and ion channels and in turn the neuronal phenotype (Lindsay, 1988; Winter *et al.*, 1988). Therefore long-term (more than ~3 days) cultures often need to be supplemented with growth factors such as NGF or BDNF depending on experimental context. In this thesis we used short term (<3 days) cultures, as in early experiments we determined that using our culture protocol neuronal survival was high, and cells grew extensive neurites within 2-3 days *in vitro* (DIV) (figure 2.6.1). Non-neuronal cells only became more abundant after 4 days and they could be distinguished from DRG neurons by their elongated morphology (figure 2.6.1).

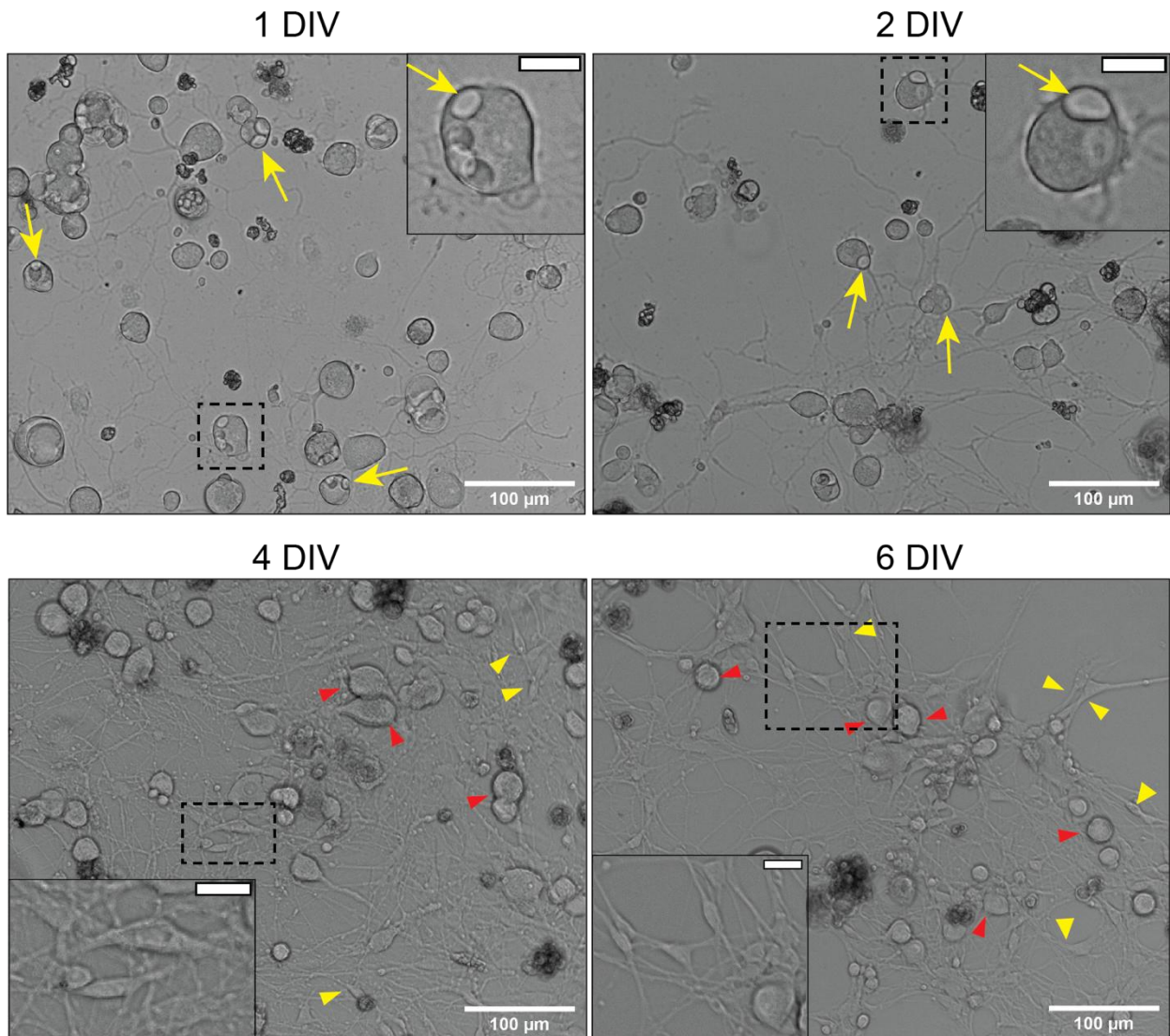


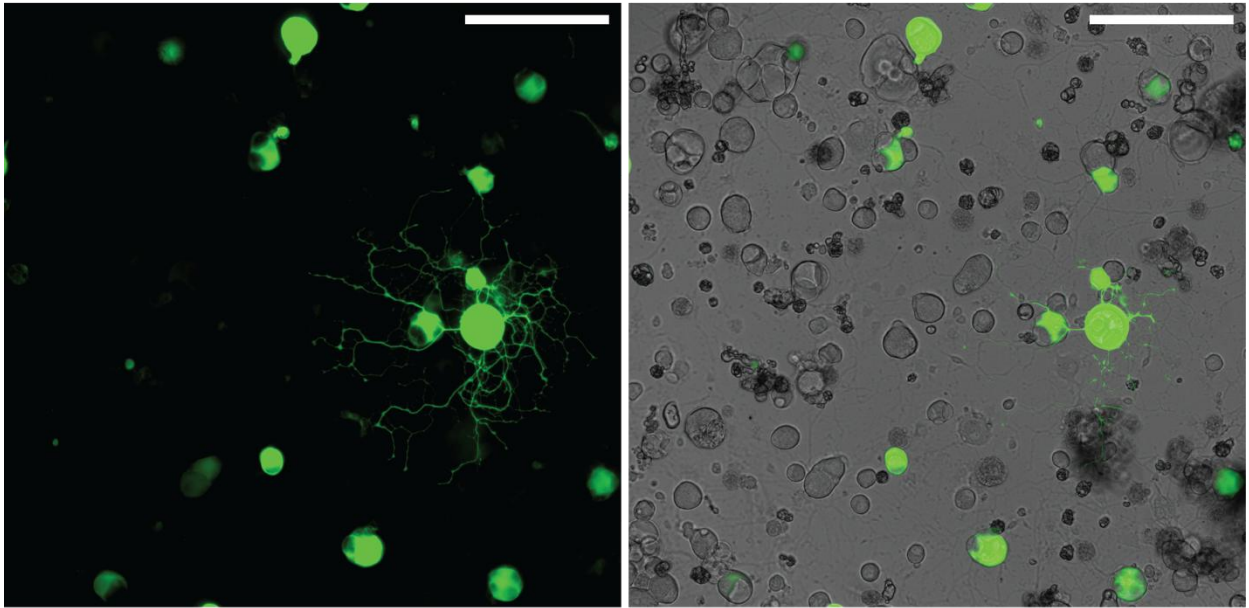
**Figure 2.6.1 DIC images of DRG cultures at different stages.** 1, 2, 4 or 6 days in vitro (DIV) cultures develop progressively more complex neurite network. (top) At 1DIV, neurons start growing neurites that become more extensive by 2 DIV. Satellite supporting cells can be observed on many neuron soma at this stage (shown on insets and yellow arrows). (bottom) By 4DIV, the neurons grow an even more extensive neurite net but non-neuronal cells are also more abundant. DRG neurons can be morphologically distinguished from glial cells: healthy DRG neurons have a well outlined, round cell bodies while glial cells are elongated, less well-defined and smaller than DRG neurons. Yellow arrowheads point out glial cells, while red arrowheads point out neurons. Rectangles with dashed lines indicate sections that have been enlarged in the insets. Inset at 4 DIV shows glial cells, while the inset at 6 DIV shows glial cells and a neuron. Scale bars on large imaged are 100  $\mu\text{m}$ , and on the insets are 20  $\mu\text{m}$ .

### Electroporation of DRG neurons

Mouse DRG neurons were transfected using Amaxa Basic Nucleofector Kit (VPI-1003) using a protocol that was modified from the manufacturer's instructions. In initial experiments, the number of DRG neurons was estimated using a hemocytometer and it was determined that on average  $1.5-2 \times 10^5$  cells were harvested from one mouse. After the last centrifugation step of the culture preparation protocol, the whole cell pellet was resuspended in 30  $\mu$ l transfection mixture (containing 82% Nucleofector solution and 18% Supplement solution, both of which were included in the Nucleofector Kit) for each slide or dish (for example, if 4 slides were used then  $4 \times 30 = 120$   $\mu$ l transfection mixture was prepared). The cell suspension was divided into separate tubes if multiple transfections were carried out, and between 2-3  $\mu$ g total DNA was added to them for each DNA construct.

The cell/DNA suspensions were then transferred to glass cuvettes, inserted into a Nucleofector device and the "Rat DRG neurons G-013" program was applied to transfect the neurons. The cuvette was taken out of the device and recovery media (RPMI 1640 + 1% FBS) was added to the cell mixture to 500  $\mu$ l final volume, after which the cells were carefully transferred to a 500  $\mu$ l Eppendorf tube and placed to the incubator for about 5-10 minutes, or until the laminin coating was washed off the slides or dishes. After the recovery step, cells were spun down on a small bench centrifuge for about 10 seconds, then resuspended in full DRG media and seeded onto TIRF slides or dishes. When cells were plated onto dishes, initially only a 100  $\mu$ l cell suspension was plated to leave cells to settle on the surface, and they were flooded with additional 2 ml of full media after an hour. The next day, half the media was changed to fresh media. It was determined using a GFP construct included in the transfection kit that after 1 DIV, most transfected neurons expressed GFP in only the soma and occasionally in neurites, and by 4 DIV GFP expression increased substantially, and it appeared in the extensive neurite net (figure 2.6.2). The transfection efficiency was on average 20% (measured after 1 DIV and 4 DIV from one culture). In subsequent experiments it was determined that 2 DIV (~ 40 hours) was sufficient to express the pHluorin and mCherry constructs and therefore cultures were used at this time point for live-cell imaging experiments.

1 DIV



4 DIV

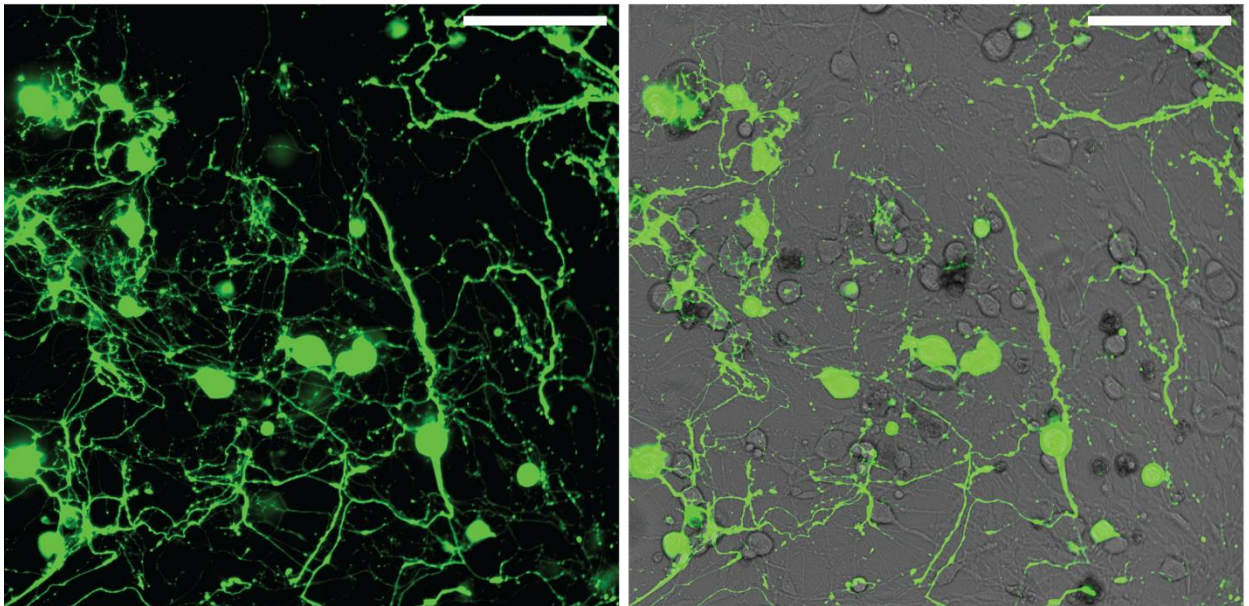


**Figure 2.6.2 DRG neurons expressing GFP after transfection by electroporation.** GFP expression is shown after 1 and 4 DIV on the left, and merged with DIC on the right to show expression in the whole culture. After 1 DIV (top), GFP expression is largely restricted to the soma. After 4 DIV (bottom), GFP is strongly expressed in the neurites. Scale bars are 150  $\mu\text{m}$ .

## 2.7. Western blot

### Sample lysis

2 DIV neurons were washed with PBS once then lysed with ice cold RIPA buffer containing protease inhibitors. The volume of lysis buffer used depended on the well format cells were cultured in, eg. DRG neurons from one mouse on two wells of a 12 well plate were lysed with 150  $\mu$ l lysis buffer. Cell lysate was collected into a 1.5ml tube and vortexed for one minute. In case of whole brain lysates, mouse brains were cut into smaller pieces and homogenized for about two minutes using a motor pestle. Tubes were incubated at 4°C in an end-over-end rotator for an hour, and were vortexed for one minute every 15 minutes. Samples were then spun down at 11,000 x g for 20 minutes at 4°C and supernatants were stored at -20°C until protein quantification.

### Protein quantification and sample preparation for loading

Samples were analysed using a BCA kit according to manufacturer's instructions. Briefly, DRG or brain lysates were diluted to 1/50 or 1/100 respectively, then samples and BSA standards were pipetted into a 96 well plate in triplicates. Following the addition of the BCA reagent, the plate was incubated at 37°C for 2 hours, and the optical density at 595 nm was measured using a plate reader. Sample protein concentrations were interpolated from a standard curve that was generated in Prism software using a second order polynomial fit.

Samples were kept on ice at all times. To prepare sample for loading, the required amount of protein from lysates was mixed with 25% Laemmli buffer containing 10%  $\beta$ -Mercaptoethanol as a reducing agent and lysis buffer to have the same final volume for all samples. Samples were then heated up to 95°C for 5 minutes, then briefly spun down and cooled on ice for another five minutes or frozen down at -20°C before loading.

### SDS-PAGE and protein transfer

12% resolving gel and 4% stacking gel was made according to the recipes in section 2.5.2 above. Gels were then placed in a gel tank, which was filled up with running buffer and samples were then loaded on to the gel. Samples were then run at 100-120V typically for 2 – 2.5 hours.

For protein transfer, transfer buffer was made according to the recipe in section 2.5.2. The sponges, filter papers and nitrocellulose membrane were soaked in the transfer buffer, and assembled with the gel in a plastic cassette. This transfer sandwich was then placed in a tank and topped up with 1 litre of transfer buffer, and ran for 1 hour at 100V.

#### Antibody staining and visualization

Following protein transfer, the membrane was blocked using milk-TBST for 1 hour at room temperature, and then incubated with primary antibodies in milk-TBST overnight at 4°C. Next day the membrane was washed three times for 15 minutes in TBST and incubated in the secondary antibody mixture (1/5000 dilution in milk TBST) for 1 hour at room temperature. The membrane was washed three times for 15 minutes in TBST, then dried and imaged in a LI-COR device.

## 2.8. DNA extraction from ear samples

Ear samples were obtained from Syt4 mice for genotyping. The tissue was digested in 200µl lysis buffer (100mM Tris, 5mM EDTA, 200mM NaCl, 0.2% SDS) containing 0.5 mg/ml Proteinase K (03115 836 001, Roche) at 55°C for about 3 hours or until the tissue was completely dispersed. To inactivate the enzyme, the temperature was increased to 95°C for 5 minutes, then the samples were placed on ice for 5 minutes and centrifuged at 13,000xg for 10 minutes at 4°C. Supernatants were retained and had 200µl ice cold isopropanol added. Tubes were gently inverted a few times until DNA fibres appeared, followed by centrifugation at 13,000xg for 15 minutes at 4°C. Supernatants were discarded and the DNA pellets washed with 70% ethanol, followed by a final centrifugation step for 10 minutes at 4°C. Supernatants were discarded and DNA pellet resuspended in 40µl endotoxin free H<sub>2</sub>O and incubated at 55°C for 1 hour to dissolve the DNA without shearing.

## 2.9. PCR genotyping

The following master mix was used for the Syt4 PCR reactions:

Master mix recipe	Final concentration
5x Taq Buffer (M891A, Promega)	1x
MgCl <sub>2</sub> (25mM, A351H, Promega)	1.5mM
Forward primer (10 $\mu$ M, wt / mutant)	0.4 $\mu$ M
Reverse primer (10 $\mu$ M)	0.4 $\mu$ M
dNTP(10mM)	0.2mM
GoTaq Flexi (5 U/ $\mu$ l, M7808, Promega)	0.07 U/ $\mu$ l
H <sub>2</sub> O	NA
DNA	NA (1 $\mu$ l/reaction)

For each DNA sample, two PCR reactions were set up (one for each forward primer), then the reaction was carried out using the following program:

1) Denaturation:	94°C	5 min
2) Denaturation:	94°C	1 min
3) Annealing:	55°C	1 min
4) Elongation:	72°C	1 min
5) 30 cycles (29 times go to step 2)		
6) Final elongation	72°C	5 min
7) Final hold	12°C	
8) End		$\infty$

Samples were then loaded on to a 2% agarose gel containing SYBRsafe DNA gel stain (S33102, Invitrogen) and ran for about 1 hour at 120V.

## 2.10. Immunoprecipitation

For syt4 immunoprecipitation and mass spectrometry analysis, cultured DRG neurons (1DIV) were treated with external solution containing 100ng/ml NGF for 30 minutes. Cells were washed with PBS once and then cell lysate and protein quantification was done as described above (2.7.2). Typically 30-50 $\mu$ g (3-4%) of protein was retained for western blotting as input lysate. The rest of the lysate, containing about 800  $\mu$ g protein was then pre-cleared with 25 $\mu$ l of sepharose A/G beads (ab193262, Abcam) for 1 hour at room temperature with end-over-end rotation. The sample was spun at 800 x g for 1 minute and the supernatant retained. 5  $\mu$ g anti-synaptotagmin 4 antibody was added and incubated for 1 hour at room temperature with end-over-end rotation, after which the pre-cleared sepharose beads were added back and left overnight at 4°C with end-over-end rotation. Next day the sample was spun at 800 x g for 1 minute and the supernatant retained. Beads were washed three times with lysis buffer, then proteins were eluted by heating at 70°C for 20 minutes in 100  $\mu$ l laemmli buffer with 25mM Tris(2-carboxyethyl)phosphine hydrochloride (TCEP, Sigma-Aldrich, 646547). Eluted proteins were then either frozen down or further processed for mass spectrometry.

## 2.11. Mass spectrometry

The below protocol was provided by and used with the help of Mark Collins at The University of Sheffield. All steps described in sections “Mass Spectrometry” and “Proteomics data analysis” were carried out by Mark Collins in the Biological Mass Spectrometry Facility.

### Coomassie staining and gel cutting

Before gel loading, eluted samples were alkylated by incubating with 50mM iodoacetamide (Sigma-Aldrich, I6125) for 30 minutes at room temperature. Samples were then loaded onto a 12% acrylamide/SDS gel and ran at 120V for about 2 hours. Gels were

then fixed in a 40% methanol/2% acetic acid solution for 30 minutes and stained overnight with colloidal coomassie solution containing 20% methanol and 20% coomassie stain (B-2025, Sigma-Aldrich) in H<sub>2</sub>O to visualise protein bands. The next day gels were destained with 20% methanol for an hour before cutting out the syt4 bands at around 50 kDa. The gel pieces were then collected in Eppendorf tubes containing 50% acetonitrile/50mM ammonium bicarbonate, and destaining was continued at 37°C with shaking at 600 rpm. The destaining solution was replaced every hour, five times in total until gel pieces were colourless, at which point 1 ml of 100% acetonitrile was added to the gel pieces for 15 minutes.

### Digestion

Enzyme solution was prepared from bovine trypsin (90057, Pierce MS grade) and used at 1 ng/μl in 50 mM ammonium bicarbonate solution. Gel pieces were digested for 1 hour at 37°C with shaking at 700 RPM, then temperature was reduced to 25°C and digestion continued overnight.

### Protein extraction

The next morning, 100% acetonitrile was added to each sample and incubated at 37°C with shaking at 600 RPM for 20 minutes. Supernatants were collected, and 0.5% formic acid was added to the gel pieces and incubated at 37°C with shaking at 600 RPM for 20 minutes. 100% acetonitrile was then added to the samples, followed by a further incubation at 37°C for 20 minutes. Supernatants were collected and the procedure repeated twice, after which 100 ul 100% acetonitrile was added to each sample and incubated at 37°C for a further 15 minutes. Supernatants were once more collected and peptide mixtures dried down.

### Mass Spectrometry

Extracted peptides were re-suspended in 0.5% formic acid and analysed by nano-liquid chromatography tandem mass spectrometry (LC-MS/MS) on an Orbitrap Elite (Thermo Fisher) hybrid mass spectrometer equipped with a nanospray source, coupled with an Ultimate RSLCnano LC System (Dionex). The system was controlled by Xcalibur 2.1 (Thermo Fisher) and DCMSLink 2.08 (Dionex). Peptides were desalted on-line using a micro-Precolumn cartridge (C18 Pepmap 100, LC Packings) and then separated using a 60 min

reversed phase gradient (4-32% acetonitrile/0.1% formic acid) on a PepMap C18 column, 15 cm x 50 µm ID, 2 µm particles, 100 Å pore size (Thermo). The Orbitrap Elite was operated with a cycle of one MS (in the Orbitrap) acquired at a resolution of 60,000 at m/z 400, with the top 20 most abundant multiply-charged (2+ and higher) ions in a given chromatographic window subjected to MS/MS fragmentation in the linear ion trap. A Fourier-transform mass-spectrometry (FTMS) target value of 1E6 and an ion trap MSn target value of 1E4 was used and with the lock mass (445.120025) enabled. Maximum FTMS scan accumulation time of 500 ms and maximum ion trap MSn scan accumulation time of 100 ms were used. Dynamic exclusion was enabled with a repeat duration of 45 s with an exclusion list of 500 and exclusion duration of 30 s.

### Proteomics data analysis

MS data were analysed using MaxQuant version 1.6.0.16 (PMID: 19029910). Data was searched against a mouse UniProt sequence database (downloaded June 2015) using the following search parameters: trypsin with a maximum of 2 missed cleavages, 7 ppm for MS mass tolerance, 0.5 Da for MS/MS mass tolerance, with acetyl (Protein N-term), oxidation (M) and phosphor (STY) set as variable modifications and carbamidomethylation (C) set as a fixed modification. A protein false discovery rate (FDR) of 0.01 and a peptide FDR of 0.01 were used for identification level cut offs. Label free quantification was performed using MaxQuant calculated protein intensities with matching between runs (with a 2-minute retention time window) enabled.

## 2.12. Immunocytochemistry

### Coverslip coating for immunofluorescence

For methods requiring cells being plated onto a glass surface, the culture surface was coated with 0.1% (2.5mg/µl) poly-L-lysine (PLL). PLL drops were pipetted on the glass and incubated for 1 hour at room temperature, after which the plates or dishes were washed with water three times and placed inside a 37°C incubator to dry.

Prior to fixation, cells were washed once with PBS and then fixed with 4% paraformaldehyde/4% sucrose for 10 minutes on ice. Cells were washed again with PBS 3 times and permeabilised with PBS containing 0.2% Triton for 15 minutes, followed by blocking for 2 hours with a mix of 1% bovine serum albumin and 5% normal donkey serum (NDS) in 0.02% of PBS-Triton. Primary antibodies were prepared in blocking solution containing 2% NDS and cells were incubated overnight at 4°C. Next day the cells were washed 3 times for 15 minutes in 0.02% PBS-Triton and incubated in secondary antibodies for 2 hours at room temperature. They were washed again 3 times for 15 minutes in PBS, and the coverslips mounted on glass slides in mounting media (Vectashield, Vector labs, H-1000).

## 2.13. CGRP ELISA

### Plate coating for western blotting and ELISA

For Western blotting and ELISA, cells were plated onto laminin-coated 12- or 96 well plates, respectively. 20  $\mu$ M laminin was pipetted in the centre of the wells and kept at 37°C for two hours. Wells were washed with PBS twice, then plates were kept in incubator with PBS in the wells to prevent laminin coating from drying out.

### ELISA procedure

To measure CGRP release from DRG neuron cultures, for each experiment, cells from one mouse were plated on to a 96 well plate into 9 wells, to have 3 replicate wells for each stimulation condition: control, KCl treated and capsaicin treated (figure 2.13). Plating DRG neurons from each mouse into the same number of wells (9) ensured lower variability in the number of cells between experiments. Neurons were maintained for three days in full culture media.

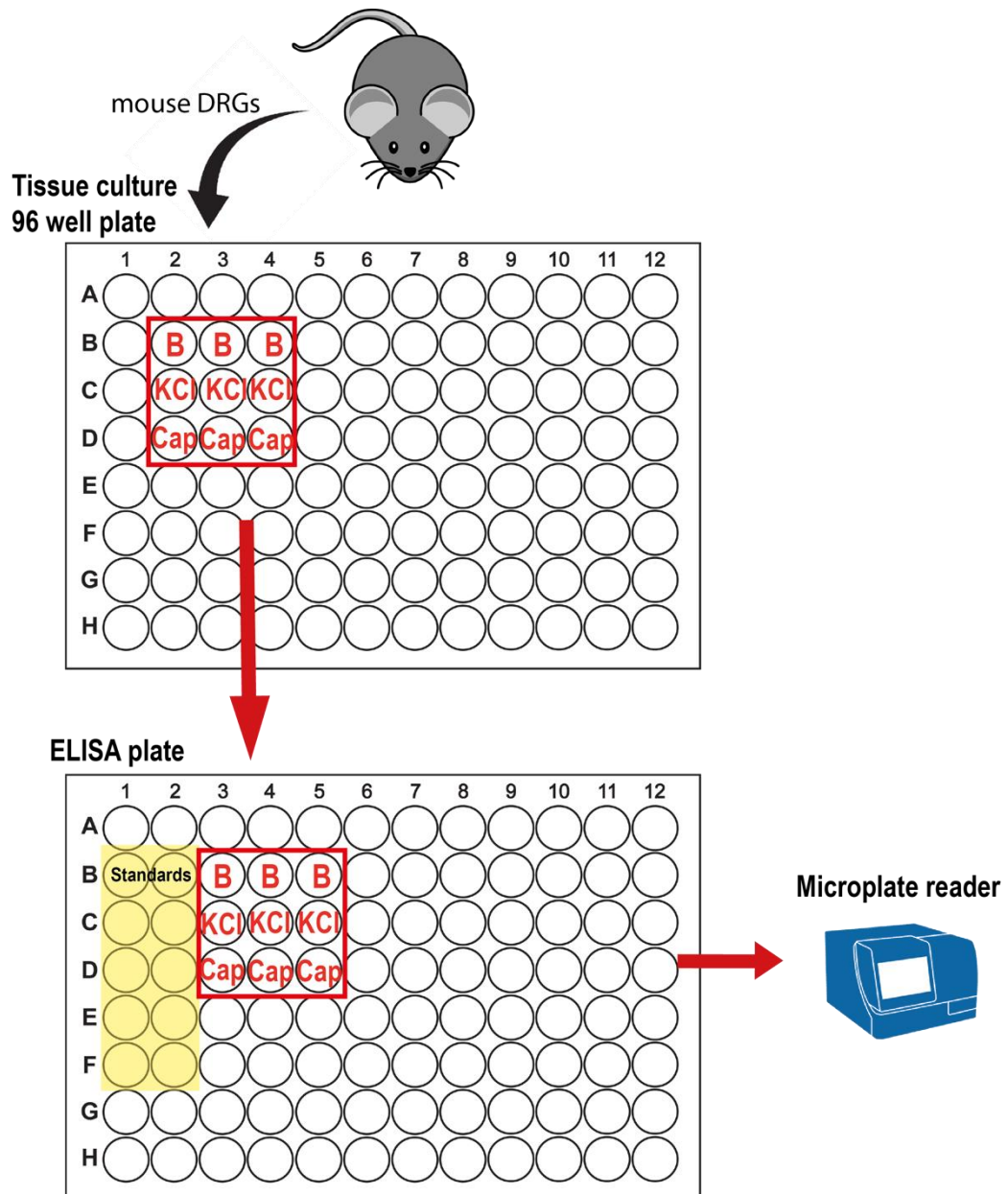


**Figure 2.13 Typical layout of ELISA experiments.** All DRG neurons from one mouse were plated onto 9 well in a 96 well plate and cultured for 3 days. At 3 DIV, wells were treated with control solution (“B” – basal), KCl solution (“KCl”) or capsaicin solution (“Cap”) in triplicates. Supernatants from each well were transferred to a corresponding designated well on the ELISA plate to measure CGRP content.

For the stimulation, media was removed and cells were washed with pre-warmed external solution once, followed by 30 minutes incubation at 37°C in either 60 µl normal external solution, high potassium solution or normal external solution containing capsaicin. For NGF treatment experiments, cells were first incubated with external solution containing 100 ng/ml NGF or control external solution for the indicated times, then the supernatants from 3 random wells were retained and the rest discarded. Supernatants were then either

directly added to the ELISA plates, or were spun at 13,000xg at 4°C for 30 minutes and frozen at -80°C for short term storage.

ELISA experiments were carried out according to manufacturer's protocol. Briefly, samples and standards of known concentration were added to wells coated with anti-CGRP along with biotinylated CGRP and anti-CGRP antibody and were incubated for 2 hours. Wells were then washed and incubated with streptavidin-horseradish peroxidase for an hour, followed by incubation with the substrate solution. The colour reaction was stopped after an hour using 2N HCl solution and the optical density read at 450 nm using a microplate reader. Results were analysed using GraphPad Prism software where the sample CGRP concentrations were interpolated from the 5 point standard curve with the sigmoidal curve fit function.

## 2.14. Bacterial work and DNA preparation

DNA used to transfection experiments were prepared using DH5alpha competent bacteria (Invitrogen, 18265-017). LB media was prepared from LB Broth granules (Fisher Scientific, BPE9723-2) by dissolving 25 g of granules in 1 L of distilled water. Agar plates were prepared from LB agar tablets (Sigma-Aldrich, L7025). Bacteria were transformed by adding 2µl DNA to 50µl of competent cells that were heat shocked at 42°C for 20 seconds, and recovered in LB media for 1 hour at 37°C without antibiotics. Bacteria were then streaked on agar plates containing the appropriate antibiotics and grown overnight at 37°C. The next day single colonies were isolated and grown in liquid culture containing antibiotics for 15-18 hours at 37°C. Midiprep was performed using a ZymoPURE II plasmid midiprep kit according to manufacturer's instructions. Briefly, 50 ml bacterial culture per prep was centrifuged and the pellet lysed and passed through a DNA binding matrix, from which plasmid DNA was eluted using an elution buffer. Cleared plasmid DNA were then stored at -20°C.

## 2.15. Image deconvolution and colocalization analysis

Fixed cells were imaged on a DeltaVision/GE OMX optical microscope, using 488 nm and 568 nm lasers, and 60x oil planapochromat objective lense (NA 1.42). Image deconvolution was done automatically on the z-stacks using the DeltaVision OMX softWoRx 6.0 software.

Colocalization analysis was performed using the JACoP plugin (Bolte and Cordelieres, 2006) in ImageJ. In each cell, three regions were selected near the plasma membrane, where Pearson's correlations ( $r$  values) and Mander's coefficients (MOC) were calculated on the image stacks. Pearson's correlation provides an initial estimate of colocalization based on a scatter plot of pixel intensities in the two channels, while Mander's coefficient gives the fraction of each channel that has positive values on the other channel, ie. fraction of channel A overlapping with channel B and vica versa. Pearson's correlation values range from -1 to 1 for complete negative or positive correlation, while Mander's coefficient gives values between 0 and 1 for completely non-overlapping or overlapping images. The resulting numbers from each cell were then pooled and statistically compared.

## 2.16. Epifluorescent imaging for immunocytochemistry

Epifluorescent images used for figures in chapters 3 and 5.3 were collected using a Leica DMIRB inverted epifluorescent microscope equipped with a Hamamatsu C4742-95 CCD camera and a 40x objective lens with 0.7 NA. The camera was controlled using MicroManager software version 1.4.14. Care was taken to use the same exposure time for each channel between images in each experiment.

## 2.17. Confocal imaging

Confocal imaging was performed using an inverted Nikon A1 microscope, with a CFI Plan Achromat VC 60x oil objective (NA 1.4) at a resolution of 4.83 pixels/ $\mu\text{m}$  using Nikon Elements software.

## 2.18. Live cell imaging

For live cell imaging experiments, a combination of PLL and laminin coating was used to improve cell adhesion and survival during perfusion. TIRF grade slides (Ibidi 80196) or dishes (Ibidi, 81158) were first coated with PLL as described earlier, followed by laminin coating.

### Dye loading for calcium imaging

For calcium imaging on figure 2.18.2, Cal-520 AM dye was used (21130, AAT Bioquest). 1  $\mu\text{l}$  2mM (1000x) stock of Cal-520 was mixed with 1 ml of external solution and triturated for  $\sim 30$  seconds with a P1000 pipette. Care was taken to protect the dye from light. Cells were removed from the CO<sub>2</sub> incubator and the culture media was aspirated, followed by washing with external solution once. Then, 250  $\mu\text{l}$  of Cal-520 AM (1x) was added to the imaging slide and neurons were incubated at 37 °C for 30 minutes. Cal-520 was then removed and replaced with external solution. Cells were recovered at 37 °C for 30 minutes before imaging at 31 °C.

### TIRF imaging setup and stimulation

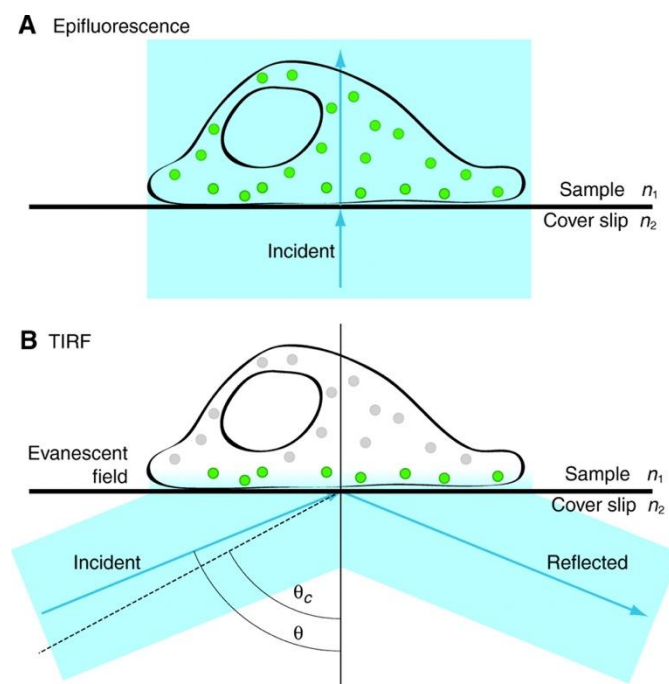


**Figure 2.18.1 Schematics of theoretical background of TIRFM compared to epifluorescence microscopy.**  $\Theta$ =incident angle,  $\Theta_c$ =critical angle,  $n_1$  = sample refractive index,  $n_2$  = coverslip refractive index. Image reused from (Mattheyses, Simon and Rappoport, 2010).

All live-cell imaging in this thesis was done using TIRF microscopy. This technique allows the visualization of objects very close (within  $\sim 100$  nm) to the solid imaging surface (eg. coverslip or bottom of the tissue culture dish) in the evanescent field generated by a laser light (Axelrod, 2003). By only exciting fluorophores in this thin region, we can achieve very low background fluorescence and can image only those vesicles that are in the close proximity of the cell membrane with high resolution and low photobleaching of the cells. To achieve total internal reflection, the incident angle of the laser beam has to be larger than a critical angle. In this case the laser beam reflected back from the sample without crossing through it, but the energy of the laser generates an electromagnetic field called the evanescent field. The width of the evanescent field depends on the incident angle and the sample refractive index must be less than the coverglass refractive index to achieve TIRF. In our case, the refractive index of the slides used was 1.52, while the refractive index of aqueous solutions (such as the external solution used) is  $\sim 1.3$ .

For experiments in this thesis, a Ti-NS N-STORM microscope was used, equipped with 488nm, 561nm and 647nm lasers and a Semrock Quad filter. The microscope was connected to an Andor DU-897 X-8714 camera and cells were viewed using a SR Apo TIRF 100x objective lens. Temperature was maintained at  $\sim 31^\circ\text{C}$ . Exposure time was set to 50 ms for each experiment, to get a 10 fps acquisition rate for each of the two channels (red and green) for the dual colour experiments; for single colour experiments, this was set to 100 ms. Image size was set to 512x512 with no binning. Laser alignments and TIRF illumination were done manually before each experiment. For laser alignment, the laser light was switched on and then dials connected to mirrors that direct the laser beam were used to correct the laser path to hit a reference point above the microscope. At this point, the microscope was in epifluorescent mode. The TIRF illumination was set up on the computer software using a scrolling wheel controlling a motor to gradually increase the incidence angle, while the sample illumination was visually observed. TIRF illumination was achieved when the background fluorescence suddenly dropped, the sample appeared bright and contrasted, and further increase of the incidence angle resulted in no fluorescence excitation being observed.

Cells were carefully chosen for each experiment that had the optimal level of protein expression (cells that were not too bright). A perfusion pump was used to perfuse the external or KCl solution on the cells. It was determined empirically that it took ~3 min 40 seconds for the solution to reach the imaging chamber using slow, 1 ml/s perfusion speed, and a valve was used to manually switch between the solutions that were running in the same tube. Due to this, the KCl solution mixed with the external solution (this was visualised using a blue dye) and likely resulted in a gradual rather than abrupt increase in KCl concentration around the cells and non-synchronised stimulation of the culture, which was visualised using calcium imaging (figure 2.18 below). Thus, for each experiment the imaging was started about 3 minutes after switching to the KCl solution, resulting in a ~30-40 seconds baseline followed by recording for another 2-3 minutes. Because the exact time at which KCl reached and stimulated the cells could not be precisely determined, we were unable to analyse the timing of fusion events with respect to stimulation. Typically 3-4 cells were recorded from each chamber and 10-15 minutes washout/rest period was allowed between cells using continuous perfusion of external solution.

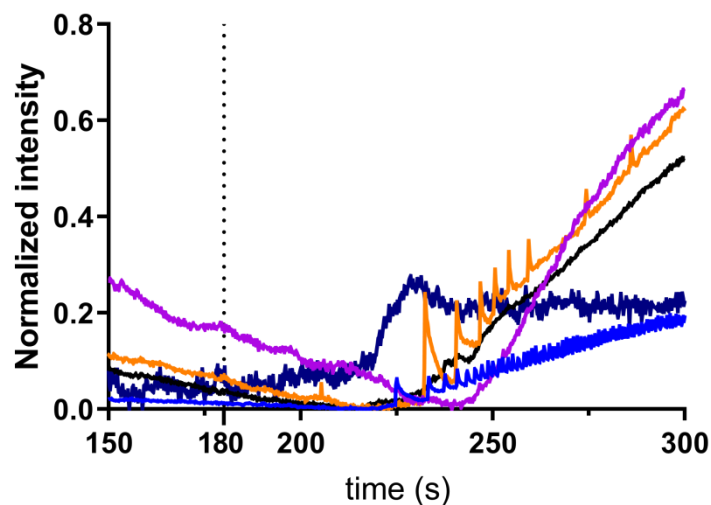


**Figure 2.18.2 Calcium signals in DRG neurons after KCl stimulation.** Cells that were loaded with Cal-520 were used to test our stimulation setup. Cells were continuously imaged after opening 40 mM KCl, dotted line at 3 minutes shows when the recording was normally started for the live-cell imaging experiments in this thesis. The KCl reached cells after about an additional minute and induced calcium responses which were not synchronised.

## Image analysis

Live-cell recordings were analysed in ImageJ 1.52n. To analyse pHluorin recordings, a circular region of interest (ROI) was manually drawn around each event (typically 0.6-0.8  $\mu\text{m}$  in size, but this depended on the size of the event which in some cases was around 1.3  $\mu\text{m}$ ) using the oval selection tool. The fluorescence time course from each channel was measured from each ROI using the multi measure function in ImageJ, and exported into Excel. For background subtraction, to correct for photobleaching and also for fluorescence changes originating from outside the ROI, rectangular ROIs were selected near the fusion events at a cellular region that did not have any detectable vesicle fusion events or vesicle movements within it. Fluorescence from the background ROIs was also exported into Excel, and subtracted frame-by-frame from the fusion event time-courses. As the fusion events on our videos were not temporally synchronized and occurred at different times after stimulation, they were manually aligned in Excel using the “offset” function for the initial peak of fluorescence to start at 4 seconds (figure 2.18.3).

Previous studies have shown that the fluorescence increase upon VAMP2-pHluorin fusion occurs in a fraction of a second ( $<100$  ms), and it may have a plateau phase lasting from 1 s to several seconds, followed by an exponential decay phase (Gandhi and Stevens, 2003; Tsuboi and Rutter, 2003; Obermüller *et al.*, 2005). To examine whether similar behaviour can be observed in sensory neurons, we measured three parameters to describe an event: the absolute fluorescence increase upon fusion (amplitude), the half-height duration (HHD or event width) and the decay time-constant ( $\tau$ ), figure 2.18.3 C. The fluorescence increase at fusion was almost always rapid and occurred within 1-2 frames; this is due to the fact the protons escaping through the fusion pore are less likely to be limited by pore size (proton diameter=0.1 nm, compared to initial pore diameter of 1-2 nm (Barg, Olofsson and Rorsman, 2001). The HHD of the fluorescence trace can be used to describe the time while the fluorescence stayed near maximum, and is thought to approximate the fusion pore open time (Malarkey and Parpura, 2011). The fluorescence decay time may represent either vesicle endocytosis and reacidification during KR fusion, or vesicle collapse into the membrane during FF (Wang *et al.*, 2017). Bafilomycin, a vesicular  $\text{H}^+$  ATP-ase inhibitor can be used to distinguish between these two fusion types, as during KR events bafilomycin prevents vesicle reacidification, slowing down the decay of the

fluorescence signal but will not affect FF events (Dean *et al.*, 2009; Rao *et al.*, 2014). In this thesis however, we did not distinguish between FF or KR events and used the above described three parameters (amplitude, decay time and HHD) to describe fusion events using different pHluorin constructs.

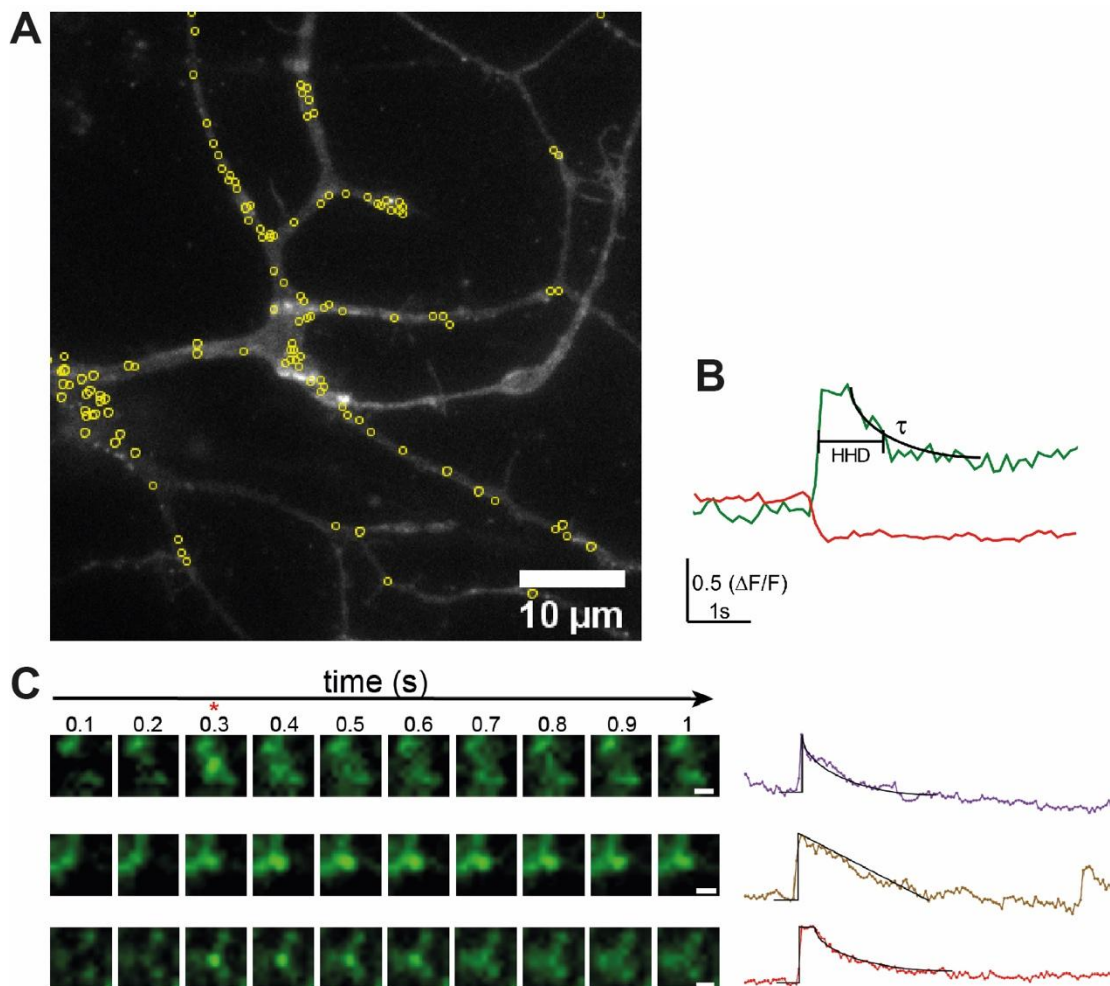


**Figure 2.18.3 Detecting fusion events with pHluorin.** A, neurites from a DRG neuron that was transfected with syt7-pHluorin. Yellow circles (ROIs) indicate regions where vesicle fusion events were detected (ie. sharp increase in fluorescence). B, An example pHluorin trace in green, showing the HHD and exponential decay fit for decay time-constants ( $\tau$ ) in black. Red trace shows the corresponding NPY-mCherry signal decreasing upon fusion as the NPY cargo is released. C, montages on the left show three examples of events with different fusion/endocytosis kinetics (scale bars = 0.5  $\mu\text{m}$ , red star indicates fusion), the corresponding traces are shown on the right. Top: the event disappears abruptly with a fast exponential decay back to baseline, middle: the fluorescence decays linearly after fusion with slightly slower kinetics, bottom: the fluorescence stays at its maximum after fusion before exponential decay.

Another important consideration when interpreting decay time constant is that the diffusion rate of the pHluorin-tagged proteins from the vesicle membrane to the plasma membrane will affect the fluorescence signal. The diffusion rate of syt7 is  $\sim 1 \mu\text{m}^2/\text{sec}$  in artificial liposomes, while it is faster, around  $2.5 \mu\text{m}^2/\text{s}$  for VAMP and other SNAREs (Bacia *et al.*, 2004; Dittman and Kaplan, 2006; Vasquez *et al.*, 2014). These diffusion rates will be affected by interactions with other proteins in a cellular environment; but nevertheless our measurements of syt- and VAMP-pHluorin decay times in chapters 4 and 6 might partly reflect differences in the protein diffusion rates.

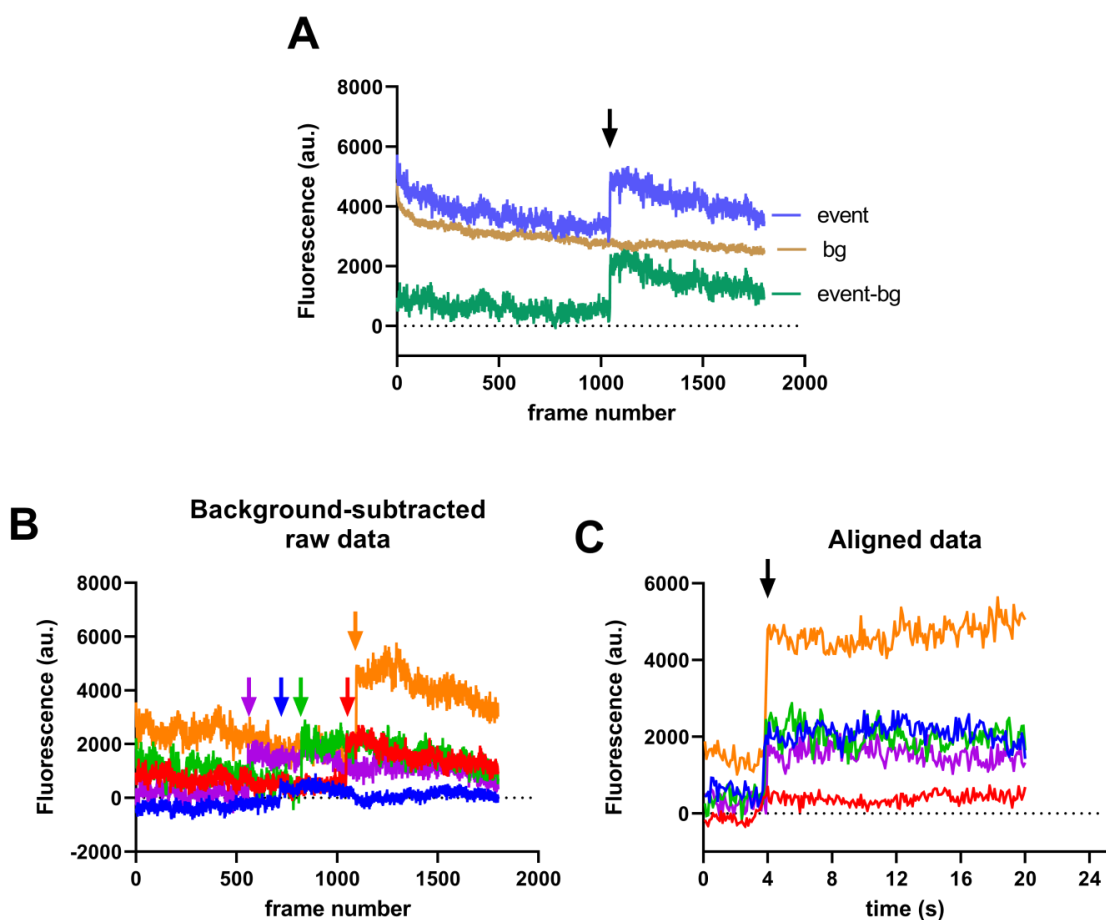


**Figure 2.18.4 Analysis of pHluorin fusion events.** A, example of an event (shown over the total recording period, 1800 frames or 180 seconds) before background subtraction (purple line, “event”), after background subtraction (green line, “event-bg”) and the local background (bg) in light brown. Arrow indicated the time of fusion. B, examples of several background-subtracted events before temporal alignment, coloured arrows show the time of fusion for each colour-matched event. C, the same events as on B after temporal alignment, shown on a 20 s (or 200 frame) time scale. Arrow shows time of fusion, which was set to 4 s.

Amplitude and HHD were calculated in Origin Pro, and decay time was calculated in GraphPad Prism from the background subtracted fluorescent traces. To measure amplitude and HHD, the traces were plotted and analysed using the “quick peak finder” function in Origin (figure 2.18.5). Amplitudes were measured inside an ROI window from 3-5 s, using the following settings:

ROI box:

3-5, fixed

Baseline:

Mode: constant ( $Y_{\text{minimum}}$ )

Range: Curve within ROI

Find Peaks:

Direction: Positive

Peak finding settings: Local maximum (1)

Peak filtering: By number (1)

Rest of the settings were automatic; in the quantities tab, make sure “Height” is ticked.

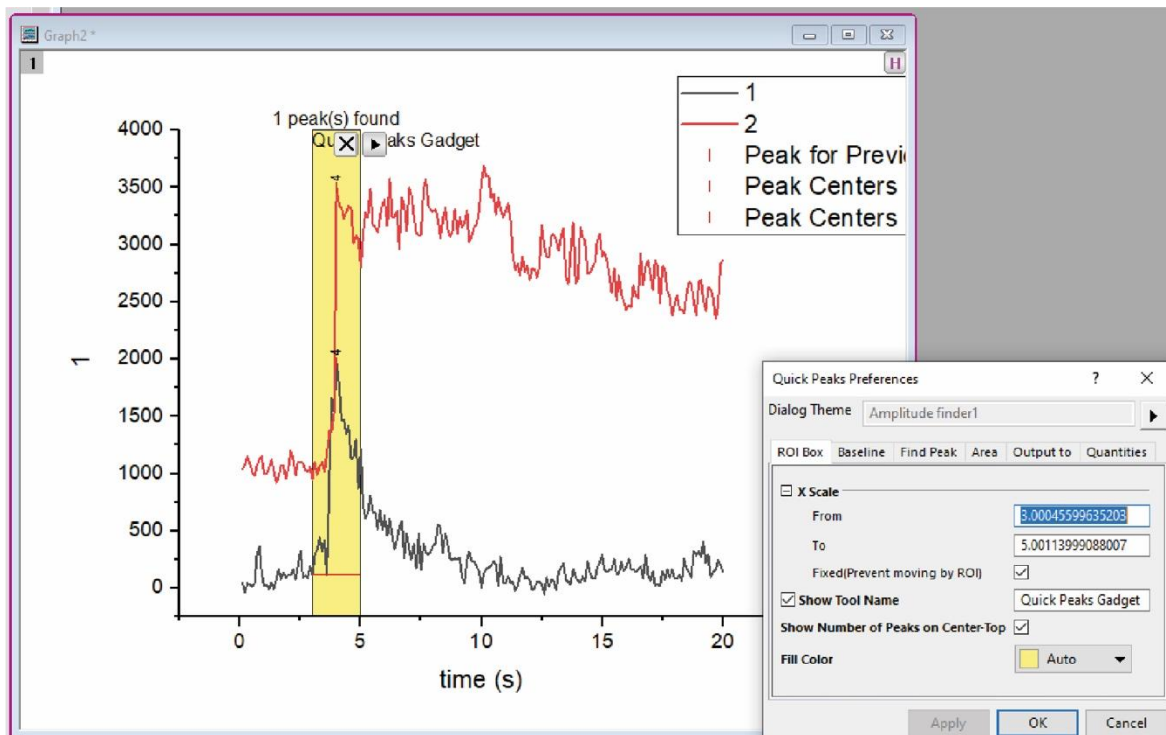


**Figure 2.18.5 Example pHluorin traces and settings for HHD measurements on OriginPro. Yellow box indicates the “ROI” box.**

Therefore, the absolute values of fluorescence increase were measured and reported as amplitude. The same “quick peak finder” function was used to calculate HHD but with the following settings:

ROI box:

2.5-15, fixed

Baseline:

Mode: constant ( $Y_{\text{minimum}}$ )

Range: Curve within ROI

Find Peaks:

Direction: Positive

Peak finding settings: Local maximum (1)

Peak filtering: By number (1)

Area:

Integration from Baseline

Rest of the settings were automatic; in the quantities tab, make sure “HHD” is ticked.

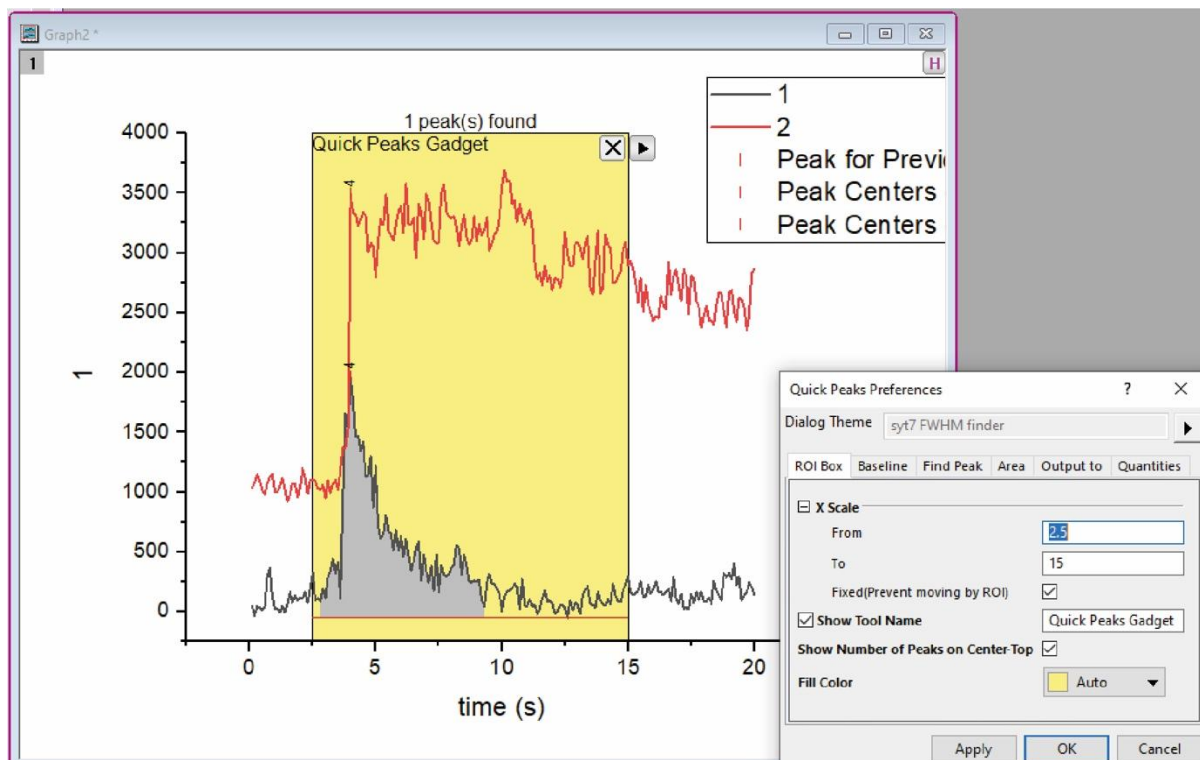


**Figure 2.18.6 Example pFluorin traces and settings for HHD measurements in OriginPro. Yellow box indicates the “ROI” box.**

As the above example shows, the HHD measurements were reliable with fast decaying events (eg. the HHD result for event 1 on figure 2.18.6 was 1.35), but in case of very slowly decaying events, these measurements had a cut-off due to the fixed ROI and were less reliable (eg. the HHD result for event 2 on figure 2.18.6 was 10.2 s).

Exponential decay time constants were measured in GraphPad Prism by fitting the background-subtracted traces with a “one-phase decay” function, with the starting point set to 4 s (peak of fluorescence). In case of slowly decaying events that could not be fit with an exponential curve within our time window (4-20 s), those were placed in a 40 s bin. Frequency histograms were also plotted in GraphPad Prism using the bin sizes specified in each figure legend. To generate averaged traces for figures, the background-subtracted traces were first normalized in GraphPad Prism using the built-in “normalize” function where 0 and 1 was defined as the first and the largest value in each dataset.

#### Kymograph analysis

KymoAnalyzer v1.01 plugin in ImageJ was used to analyse Syt4mCherry trafficking dynamics. KymoAnalyzer is an open source plugin that was developed by Neumann et al. (Neumann *et al.*, 2017) that is available at <https://www.encalada.scripps.edu/kymoanalyzer>, and the analysis was performed according to the authors’ user’s manual. Briefly, kymographs were generated from neurites and vesicle movements were tracked using the polyline tool in ImageJ. The software then calculated the vesicle motility parameters (velocity, pause duration and frequency, mobile vesicles, etc.) from each kymograph, which were then pooled from different experiments for statistical analysis in GraphPad Prism. Data distribution normality was tested in the software, and Mann-Whitney test was used to compare data sets.

#### Statistical analysis

All statistical analysis was done in GraphPad Prism software and mean  $\pm$  SD is shown on in results unless otherwise stated. To calculate significance between soma and neurites in chapter 4, due to the smaller n numbers student’s two-tailed t-test was used. In cases of larger data sets in chapter 6, normality distribution was determined using the built-in “Normality and lognormality test” in Prism, as well as by visually inspecting the frequency

histograms of each dataset. As most of the data in this chapter was non-normally distributed, non-parametric Mann-Whitney test was used to compare results between two conditions. For figure 6.5, Kruskal-Wallis test (non-parametric one-way ANOVA) was used with Dunn's *post hoc* test. For ELISA experiments, results for different conditions from independent experiments (the number of these is specified in results) were compared using ordinary one-way ANOVA with Sidak *post-hoc* test.

### 3. Characterization of synaptotagmins in cultured DRG neurons

#### 3.1. Introduction

A limited number of studies have examined the presence of synaptotagmins in DRG neurons, there are only a few studies about specific isoforms (Morenilla-Palao *et al.*, 2004; Wang *et al.*, 2016; López-Benito *et al.*, 2018). Several high throughput gene expression and proteomics studies done on sensory neurons found multiple isoforms expressed, though none looked at their role specifically. According to a large-scale RNA sequencing analysis done by Usoskin *et al.*, several isoforms are expressed in the CGRP expressing DRG neuron populations (figure 3.1A) (Usoskin *et al.*, 2014). Interestingly, syt4 and syt11, two non-calcium binding isoforms were ubiquitously expressed in almost all peptidergic populations. Moreover, two studies found that syt4 mRNA was 2-fold upregulated in damaged neurons in neuropathic pain models. Loose ligation of the sciatic nerve in mice, and tight ligation of the spinal nerve in rats resulted in the upregulation of syt4 (Xiao *et al.*, 2002; Reinhold *et al.*, 2015). In the latter study they suggested that, since other synaptic proteins (SNAP25, VAMP1 and Rab3) were downregulated, and syt4 is generally considered an inhibitory isoform, perhaps the changes occurring after nerve damage serve to reduce synaptic activity.

One study that performed proteomic profiling of the membrane-enriched fraction of DRG neuron lysates did identify syt1, 2 and 11 in this fraction, but their protein abundance only slightly but not significantly changed in neuropathic (spared nerve injury, meaning the transection of two branches of the sciatic nerve) and inflammatory (Complete Freund's Adjuvant (CFA) administration) pain models (Rouwette *et al.*, 2016). In this study, the authors also identified SNAP25, VAMP1 and Rab3 but only Rab3 was significantly downregulated and only in the neuropathic pain model. The reason for these differences between studies is not clear but it is possible that these proteins are more strongly downregulated on the mRNA level following injury but their protein levels are more even at the membrane, which the study by Rouwette *et al.* focused on.

Another proteomic study that analysed the protein content of the LDCV fraction in DRG neurons identified syt2 (Zhao *et al.*, 2011). Furthermore, in an unpublished proteomics study from M. Nassar and M. Collins at the University of Sheffield, syt11, 2, 4, 6 and 5 were

identified in order of abundance in DRG neuron lysates (figure 3.1B). Based on the findings of the above studies we decided to initially focus on two  $\text{Ca}^{2+}$ -binding and two non- $\text{Ca}^{2+}$ -binding isoforms. As syt4 was identified as a possible target in the neuropathic pain models (Xiao *et al.*, 2002; Reinhold *et al.*, 2015) and that both syt4 and syt11 proteins were ubiquitously expressed in the neuropeptide expressing population (figure 3.1A) and were abundant in full DRG lysates (figure 3.1B), we decided to pursue these two proteins further despite the fact that they are non- $\text{Ca}^{2+}$  binders. As for the  $\text{Ca}^{2+}$ -binders, syt2 was both abundant in whole DRG lysates (figure 3.1B) and was specifically expressed in the peptidergic population that express high levels of CGRP (figure 3.1A), moreover this protein is known to be abundant in the spinal cord (Marquèze *et al.*, 1995; Berton *et al.*, 1997). Finally, although it wasn't identified in the above mentioned studies, we also decided to focus on syt7 as its mRNA was expressed in all of the peptide expressing DRG neurons (figure 3.1A), and its  $\text{Ca}^{2+}$ -binding properties make it an ideal candidate for slower LDCV exocytosis (section 1.2.6). We started our investigation by using immunocytochemistry and western blotting to characterize syt expression in our culture system. Our main goal was to identify possible candidates that might have a role in controlling peptide secretion, therefore we carried out colocalization analysis with CGRP and functional CGRP ELISA experiments.

**A**

	PEP2	PEP1	NP2
CGRP	Yellow	Yellow	Yellow
Substance P	Blue	Yellow	Grey
Syt1	Grey	Grey	Yellow
Syt2	Grey	Purple	Blue
Syt5	Blue	Grey	Yellow
Syt6	Yellow	Purple	Grey
Syt7	Grey	Grey	Yellow
Syt9	Grey	Grey	Yellow
Syt4	Grey	Yellow	Yellow
Syt11	Yellow	Yellow	Yellow

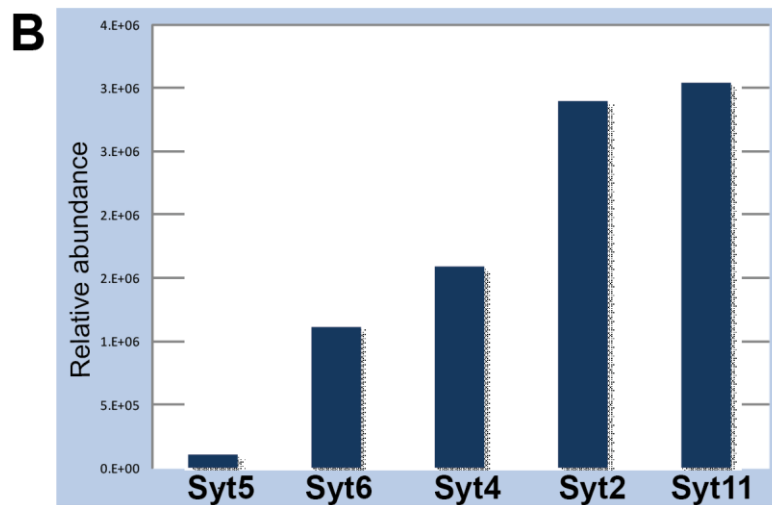


**Figure 3.1 mRNA and protein expression of different synaptotagmin isoforms in DRG neurons.** A, mRNA expression of the indicated syt isoforms in the DRG neuron populations that express the neuropeptides CGRP (*Calca*) and Substance P (*Tac1*). The populations defined by Usoskin et. al(Usoskin et al., 2014) are peptidergic (PEP) and nonpeptidergic (NP). Colour coding from blue to bright yellow indicate the level of mRNA expression. Synaptotagmins shown have been selected as the isoforms that have the highest expression in peptidergic neurons and are of interest. B, syt11, 2, 4, 6 and 5 (in order of abundance) were identified in a proteomic study done by M. Nassar and M. Collins at the University of Sheffield, where they analysed the proteome of whole mouse DRG lysates. Relative abundance is the IBAQ number that was plotted for each protein (the total protein intensities divided by the number of peptides identified for each protein).

### 3.2. Syt2, 4, 7 and 11 are expressed in cultured DRG neurons

We assessed syt expression in cultured DRG neurons using two techniques. Western blotting was used to validate antibodies in cells cultured from knockout (KO) mice and to assess general protein expression in the syt4 mouse strain which was used in later chapters (see Methods). All of the syt antibodies recognize the more easily accessible, cytoplasmic part of the proteins (see details about antibodies in Materials). The syt2, 4 and 7 antibodies were validated using KO mice (figure 3.2.1 and 3.2.2). For syt2 and 7, whole brain lysates were used for this purpose due to their known strong expression in this tissue, and GAPDH was used as a loading control. The syt2 antibody recognized a band at ~60 kDa, which disappeared in the KOs, while GAPDH was unaffected. Although the molecular weight of all synaptotagmins is around 47 kDa, they often appear at higher molecular weights due to oligomerization with other proteins (see section 1.2.6), and according to the antibody specifications, the syt2 antibody products on our blots were at the expected weight. It also weakly labelled two additional bands at lower molecular weights which are probably nonspecific labelling, as they persisted in the knockouts. The syt7 antibody recognized multiple bands between ~40-60 kDa, corresponding to the various splice variants of syt7 (Sugita *et al.*, 2001), which disappeared in the KOs. Once again one strong band at ~40 kDa persisted in the KO lysate, while GAPDH labelling was unaffected. Thus, both of these antibodies exhibited some non-specific activity.

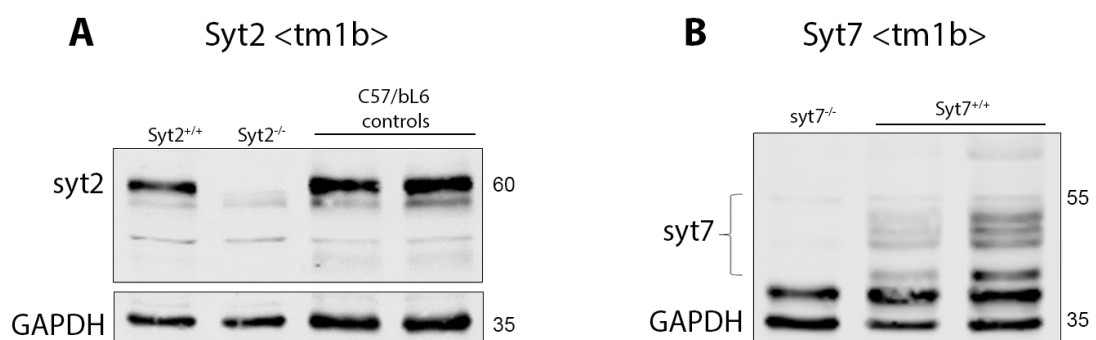


**Figure 3.2.1 Validation of the specificity of syt2 and syt7 antibodies in knockout brain lysates.** A, syt2 western blot of wild type (syt2<sup>+/+</sup>), knockout (syt2<sup>-/-</sup>) syt2<tm1b>, and also C57/BL6 wild type mouse brain lysates. D, syt7 western blots of knockout (syt7<sup>-/-</sup>) and wild type (Syt7<sup>+/+</sup>) syt7<tm1b> mouse brain lysates. GAPDH staining was used as loading control.

The syt4 antibody was validated in DRG neurons cultured from KO syt4 mice, as part of the experiments to determine the expression of the various syt isoforms in the DRG neurons. In these experiments, various amounts of protein from the DRG lysates were loaded onto the gels, and the t-SNARE syntaxin 1 (STXN1) was used as a neuron specific loading control; unexpectedly however, STXN1 staining appeared consistently weaker in syt4 KO DRG lysates (figure 3.2.2 and 3.2.3). Whether this is genuinely due to down-regulation of STXN1 in syt4 KO mice is unclear, as is why or how the expression of syt4 would affect STXN1 expression (for discussion, see section 3.5).

Similarly to syt2 and syt7 antibodies, the syt4 antibody also labelled several non-specific bands in the DRG lysates (figure 3.2.3A). At the expected molecular size of ~42 kDa, just below a persistent band at ~45 kDa, the syt4 staining disappeared in the KOs, indicating the location of the syt4-specific band. Unfortunately we were unable to validate the syt11 antibody, but according to source specifications the antibody recognizes a band at ~65 kDa corresponding to syt11, although several additional bands were observed in our blots (figure 3.2.2B). Interestingly, especially the syt11 but also the syt2 staining was weaker in the cells cultured from syt4 KO mice, while syt7 signal was largely unaffected by genotype (figures 3.2.2B and 3.2.3B). Regarding overall expression in cultures, Syt2 and 7 required more protein lysate to be loaded on the gels for strong bands (40-60  $\mu$ g protein, figure 3.2.2A) while syt4 and 11 produced strong bands in ~ 10  $\mu$ g protein lysate (figure 3.2.3A), suggesting that syt2 and 7 have lower expression levels compared to syt4 and 11. This agrees with the mRNA levels detected by Usoskin et al. (figure 3.1A), and suggest that syt2 and 7 may have more specialized functions that require lower protein levels.

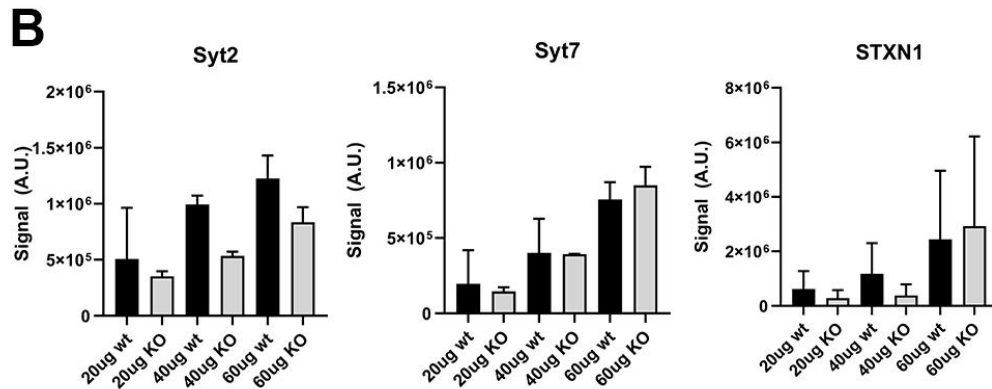
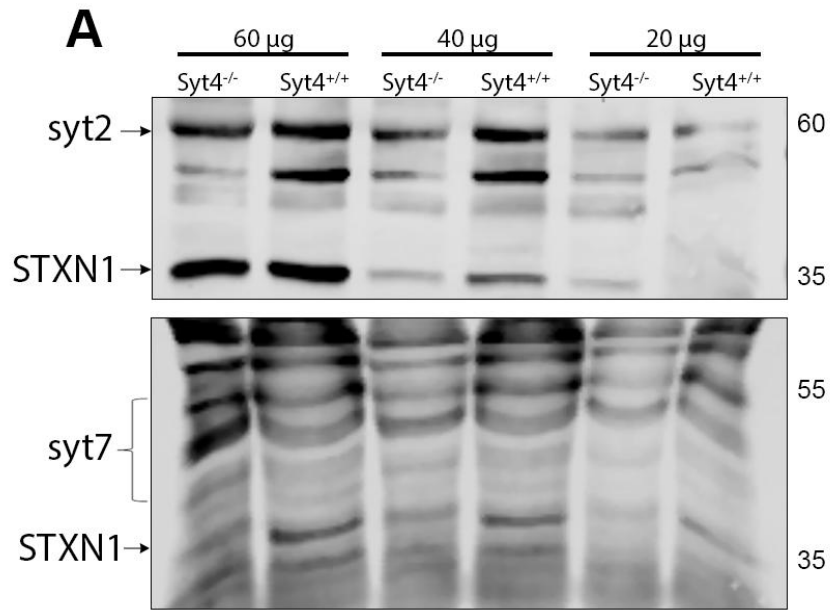


**Figure 3.2.2** Western blots of syt2 and 7 in DRG neurons cultured from syt4<sup>+/+</sup> and syt4<sup>-/-</sup> mice. A, blots of the calcium-binding syt2 and syt7. 20, 40, 60  $\mu$ g protein was loaded as indicated above the blots. Note the multiple syt7 bands corresponding to multiple splice variants. Syntaxin 1 (STX1) was used a neuronal loading control. B, Quantification of syt2 and syt7 protein expression (n=2 blots). Their signal was not normalized to STX1, as STXN1 expression was affected by the genotype, we presented the raw signal values instead (STX1 values were pooled from the 4 blots).

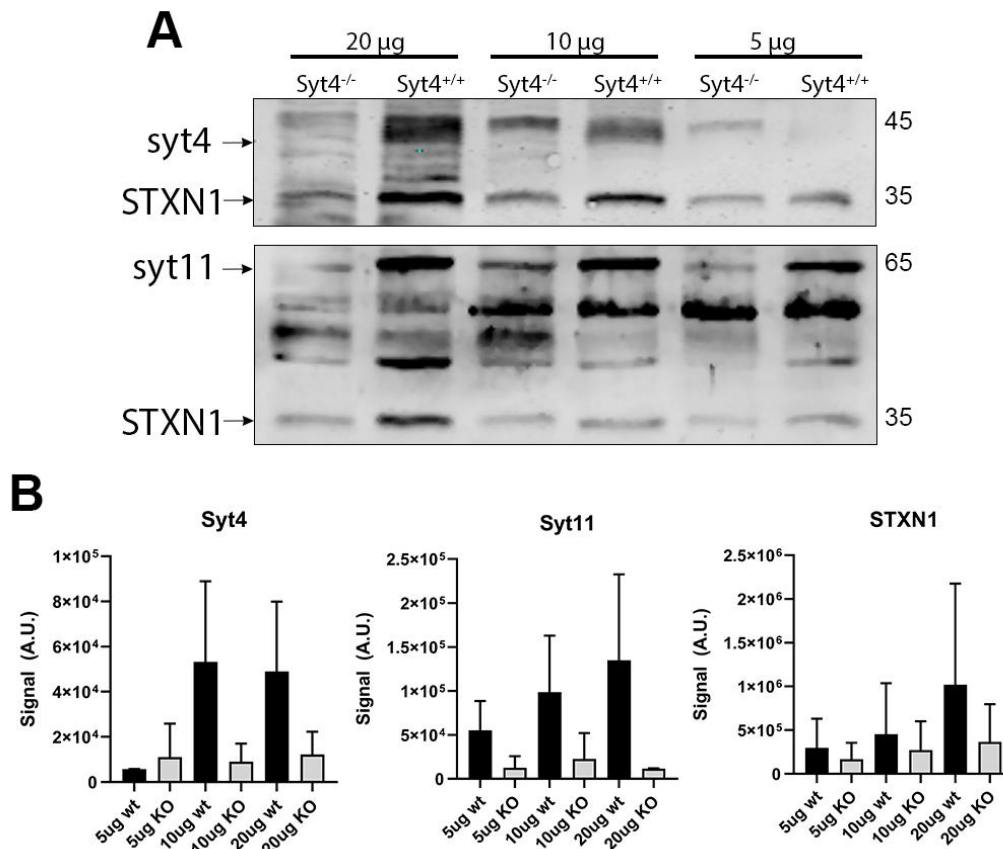


**Figure 3.2.3 Western blots of syt4 and 11 in DRG neurons cultured from syt4<sup>+/+</sup> and syt4<sup>-/-</sup> mice.** A, blots of the non calcium-binding syt4 and 11. 5, 10, 20  $\mu$ g protein was loaded as indicated above the blots. Note on the syt4 blot, the antibody recognizes a double band at 45 kDa but only the lower band is absent in the knockout. Syntaxin 1 (STXN1) was used as neuronal loading control. B, Quantification of syt4 and syt11 protein expression (n=2 blots). Their signal was not normalized to STXN1, as STXN1 expression was affected by the genotype, we presented the raw signal values instead (STXN1 values were pooled from the 4 blots).

To assess the population-level expression of synaptotagmin isoforms, DRG neurons were cultured from wild type C57/bL6 mice and immunostained for syt2, 4, 7 or 11 and CGRP, a marker of peptidergic neurons. Cells were initially imaged on an epifluorescent microscope, but as synaptotagmin expression was low as suggested from western blots above and antibody specificity was poor, the fluorescence signal was weak and therefore we switched to using confocal microscopy. All images were then analysed by comparing the cell fluorescence to the mean no primary control fluorescence + 3 times SD to decide whether a cell was positive for a marker. These results showed that the co-expression of syt2 with CGRP was the highest, 54% on average (n = 89 cells from 3 cultures), while syt4, 7 and 11 had a co-expression of 30, 39 and 33% respectively (n = 68, 77 and 44 cells from 2

experiments, figure 3.2.6A). We can conclude that while all isoforms colocalized with CGRP in the culture to an extent, they were expressed at varying degree in CGRP negative cells as well. As expected from high protein levels in DRG lysates, syt4 had a ubiquitous expression in the culture, suggesting that its function is not limited to a certain population. As expected for a vesicular localization, all isoforms had a punctate staining pattern, but syt4 also had a strong Golgi/ER-like staining pattern in most cells (arrows on figure 3.2.4 A), as reported previously in other cell types (Ibata *et al.*, 2000), consistent with it having a role in vesicle maturation and trafficking in multiple populations of DRG neurons as supported by the ubiquitous expression (Ahras, Otto and Tooze, 2006). Interestingly, we consistently observed syt2 staining in the nucleus (figure 3.2.4 B). At this point it is unclear whether this is real staining or non-specific binding of the antibody, as to our knowledge syt2 nuclear staining has not been observed before but the antibody clearly has non-specific targets (figure 3.2.1A).

Soma size is a common descriptor used to categorize DRG neuron populations (see section 1.1.2), thus we also looked at the size distributions by measuring the Feret diameters of differently labelled cells. This showed that most of the examined proteins were expressed in small to medium size neurons (20-30  $\mu\text{m}$  in diameter). Syt7 and syt11 mostly marked small diameter neurons (<20  $\mu\text{m}$ ), while CGRP, syt2 and syt4 marker a wider range of soma diameters (figure 3.2.6 B). Taken together, syt2, 4, 7 and 11 are all expressed in cultured DRG neurons as detected by western blots and immunofluorescence, and are all present in small diameter, peptidergic neurons.

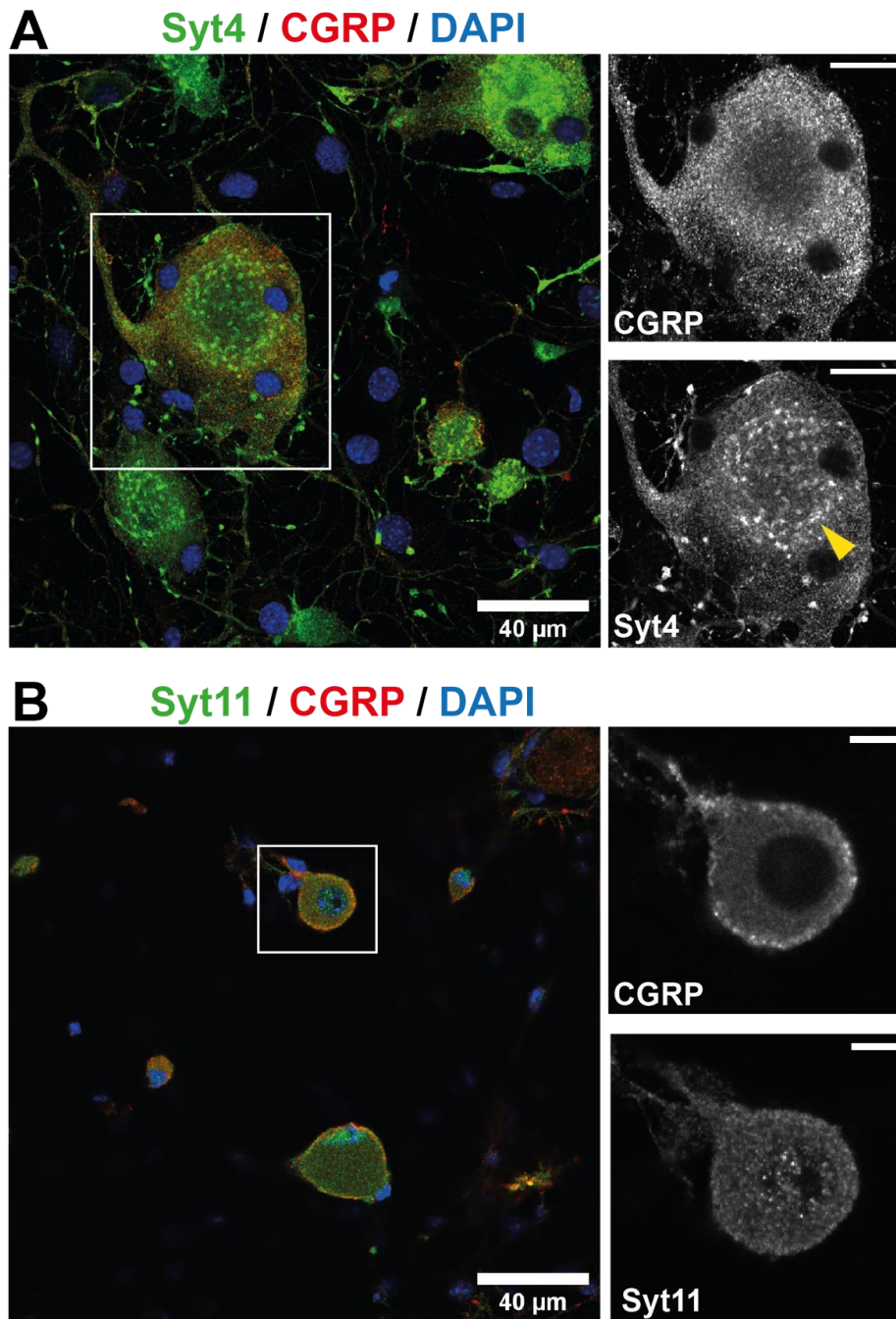


**Figure 3.2.4 Syt4 and 11 immunofluorescence in cultured DRG neurons.** A-B, confocal images of neurons immunostained for CGRP and syt4 or syt11. Areas on merged images indicated with white rectangles have been enlarged and are shown as gray-scale images on the right. Arrow on the bottom right image on A point at Golgi structures in the syt4 staining. Images have been contrast enhanced by 0.3% for clarity. Scale bars = 40 µm in large images, 20 µm on insets on A and 10 µm on insets on B.

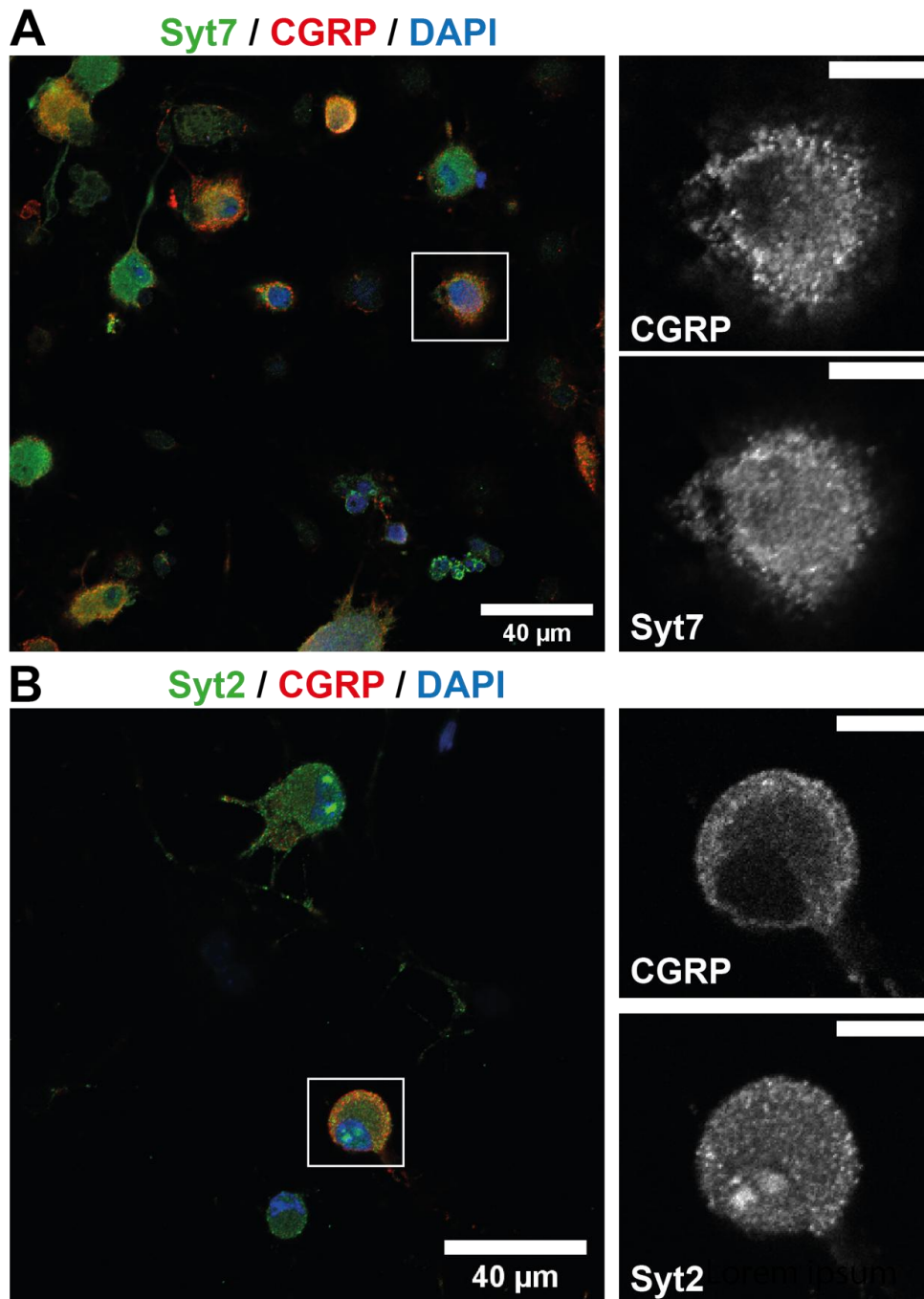


**Figure 3.2.5 Syt2 and 7 immunofluorescence in cultured DRG neurons.** A-B, confocal images of neurons immunostained for CGRP and syt7 or syt2. Areas on merged images indicated with white rectangles have been enlarged and are shown as gray-scale images on the right. Images have been contrast enhanced by 0.3% for clarity. Scale bars = 40  $\mu\text{m}$  in large images and 10  $\mu\text{m}$  on insets.

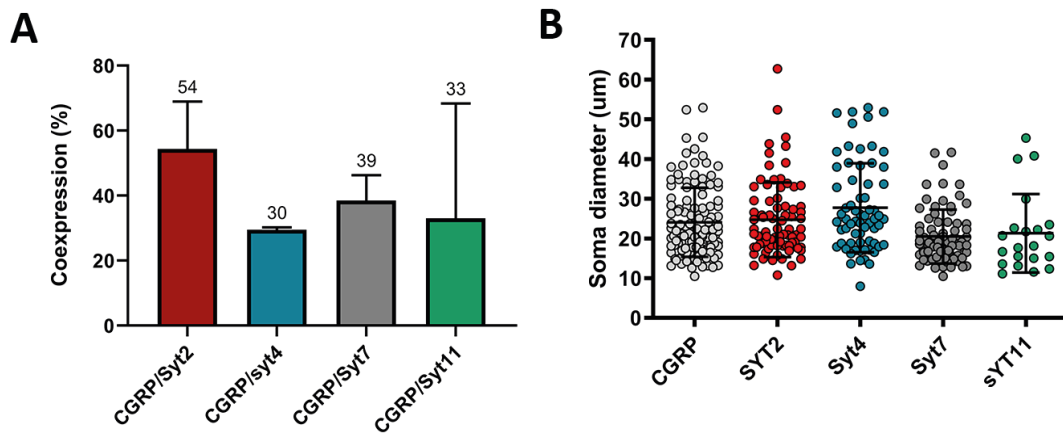


**Figure 3.2.6 Quantification of colocalization of syt immunostaining with CGRP.** A, bar graphs showing % of all stained neurons that were positive for both syt2, 4, 7 or 11 and CGRP (mean  $\pm$  SD). Means are shown above the bars. B, scatter dot plot of soma diameters ( $\mu\text{m}$ ) of cells positive for CGRP, syt2, 4, 7 or 11 (means  $\pm$  SD are shown).

### 3.3. Antibody validation using syt-pHluorin constructs

In order to further validate our syt2, 4 and 7 antibodies in immunocytochemistry, cells were transfected with syt2, 4 and 7-pHluorin constructs that were used in later chapters, and labelled for the same synaptotagmins with the antibodies used above and for anti-GFP (figure 3.3). During imaging, the transfected cells were easily recognisable compared to non-transfected ones by the strong GFP signal. The red synaptotagmin signal (which indicated both endogenous and overexpressed syts) mostly overlapped with the green anti-GFP signal. This was especially striking on the neurites, where most individual puncta were clearly stained for both red and green (see arrows on figure 3.3 A and C). In the cell body of transfected cells, the overexpressed proteins accumulated around the nucleus, presumably in the Golgi/ER compartments, while the synaptotagmin stain also appeared spread out in the soma, perhaps indicating some endogenous staining. In summary, the syt antibodies could be used reliably to recognize the overexpressed proteins.

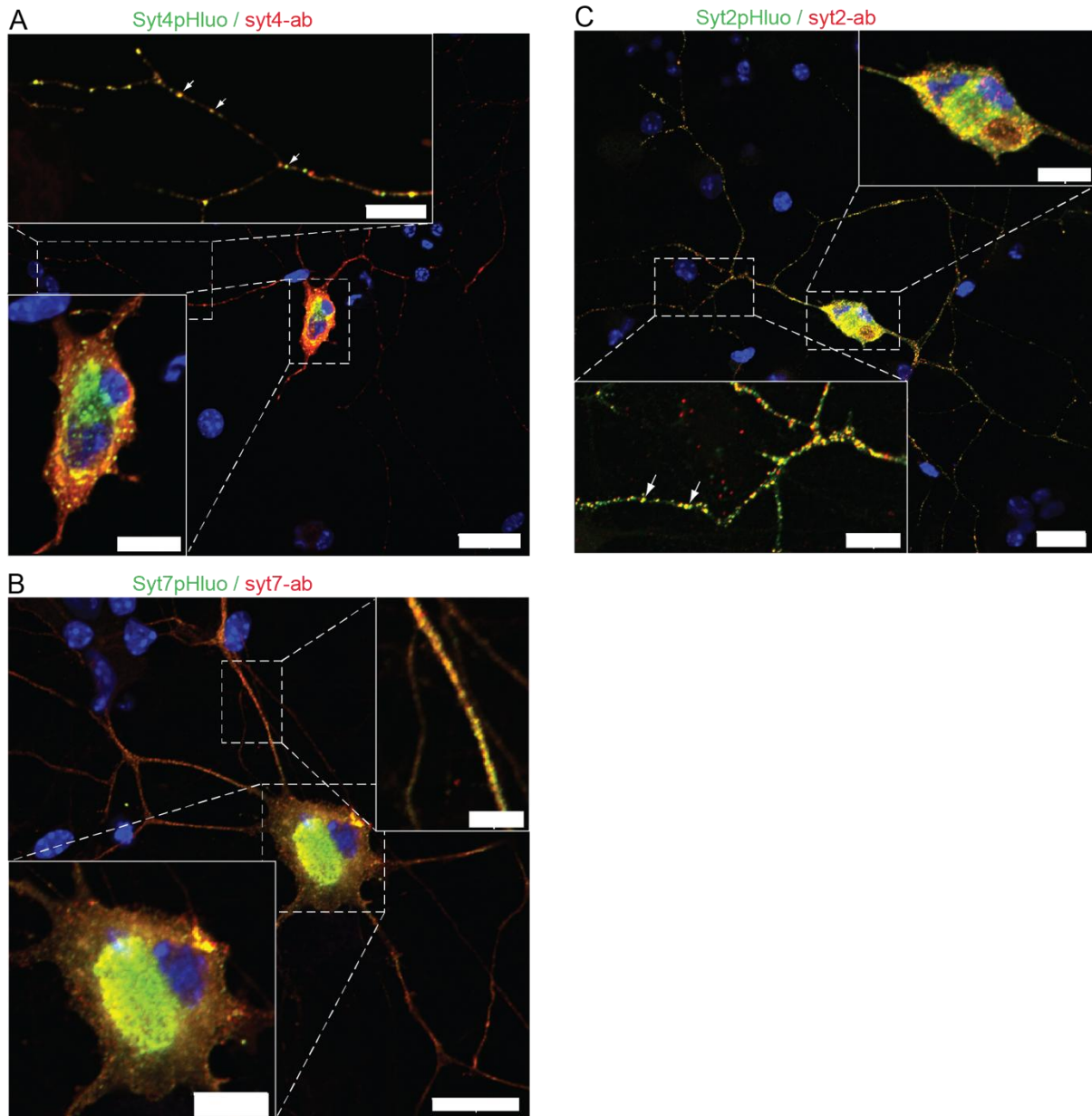


**Figure 3.3 Further validation of syt2, 4 and 7 antibodies using immunocytochemistry.** A-C show DRG neurons that were transfected with syt4-, 7- or 2-pHluorin (green) and were stained with antibodies for the same synaptotagmins (red). Scale bars: A: 25  $\mu\text{m}$  on large image and 10  $\mu\text{m}$  on insets. B: 20  $\mu\text{m}$  on large image and 5  $\mu\text{m}$  on insets. C: 20  $\mu\text{m}$  on large image and 10  $\mu\text{m}$  on insets.

### 3.4. Colocalization analysis of synaptotagmins with CGRP in DRG neuron somata

So far we have established expression of four syt isoforms in DRG neuron cultures and examined more specifically their expression in peptidergic neurons. As our aim was to identify the isoform(s) that might control peptide secretion, we next performed colocalization analysis of CGRP and syt labelled vesicles.

2 DIV DRG neurons were immunolabelled for CGRP and syt2, 4, 7 or 11 and automatic imaging-coupled deconvolution was used to improve the resolution. Pearson's correlation and Manders overlap coefficient (MOC) were used to quantify colocalization on z-stacks; we selected 2-3 rectangular ROIs (depending on cell size and shape) on each neuron near the plasma membrane for analysis, reasoning that vesicles in close proximity to the plasma membrane are more likely to represent a mature, releasable pool of peptidergic vesicles. These colocalization algorithms are sensitive to background noise and therefore positioning ROIs to certain regions with good contrast and many vesicles (eg. away from the nucleus) helped improve accuracy. Running the analysis on smaller image stacks also required less computing power and was therefore faster. TRPV1 has been previously reported to localize to CGRP containing vesicles (Meng *et al.*, 2007) and here we used it as a control for our analysis of colocalization.

We found that most isoforms had a low and occasional colocalization with CGRP which was highly variable between ROIs (figure 3.4 A-H). Figure 3.4I-L shows a visualization of this, where we plotted the red and green fluorescence along a line that was drawn through one of the representative ROIs, each peak represents a fluorescence puncta. These line scans also show that the red and green fluorescence peaks rarely overlap. The results of the Pearson's correlation were  $0.23 \pm 0.2$  for syt2 (n = 71 ROIs),  $0.37 \pm 0.1$  for syt11 (n = 33 ROIs),  $0.26 \pm 0.2$  for syt7 (n = 70 ROIs),  $0.28 \pm 0.2$  for syt4 (n = 41 ROIs) and  $0.26 \pm 0.2$  for TRPV1 (n = 41 ROIs, figure 3.4M), which shows low correlation between CGRP and the respective proteins. We used MOC to assess the fraction of CGRP vesicles overlapping with the different syt isoforms, in other words what percentage of CGRP can be found on the respective syt-labelled vesicles. Again this was highly variable probably due to variability in signal/noise ratio and the automatic threshold assigned by the program; the mean MOCs were  $0.4 \pm 0.3$  for syt2,  $0.5 \pm 0.2$  for syt11,  $0.52 \pm 0.2$  for syt7,  $0.4 \pm 0.2$  for syt4 and  $0.4 \pm 0.2$

for TRPV1 (figure 3.4N). This would suggest that in each dual labelled group, roughly 40-50% of CGRP would be in the respective syt-labelled vesicles, implying that multiple syt isoforms could reside in the same peptide-containing vesicle population. We also examined the soma diameters of the corresponding neurons used in the analysis and found similar results as before (figure 3.2.6 B); most labelled cells represented small/medium diameter range neurons. In conclusion, all the examined syt isoforms colocalized with CGRP to an extent but none was correlated with it strongly, and although syt11 had the highest Pearson's correlation and syt7 the highest MOC, TRPV1 also only poorly colocalized with CGRP. However, as these experiments are highly dependent on antibody specificity and signal/noise ratio, one should take the above results with caution.

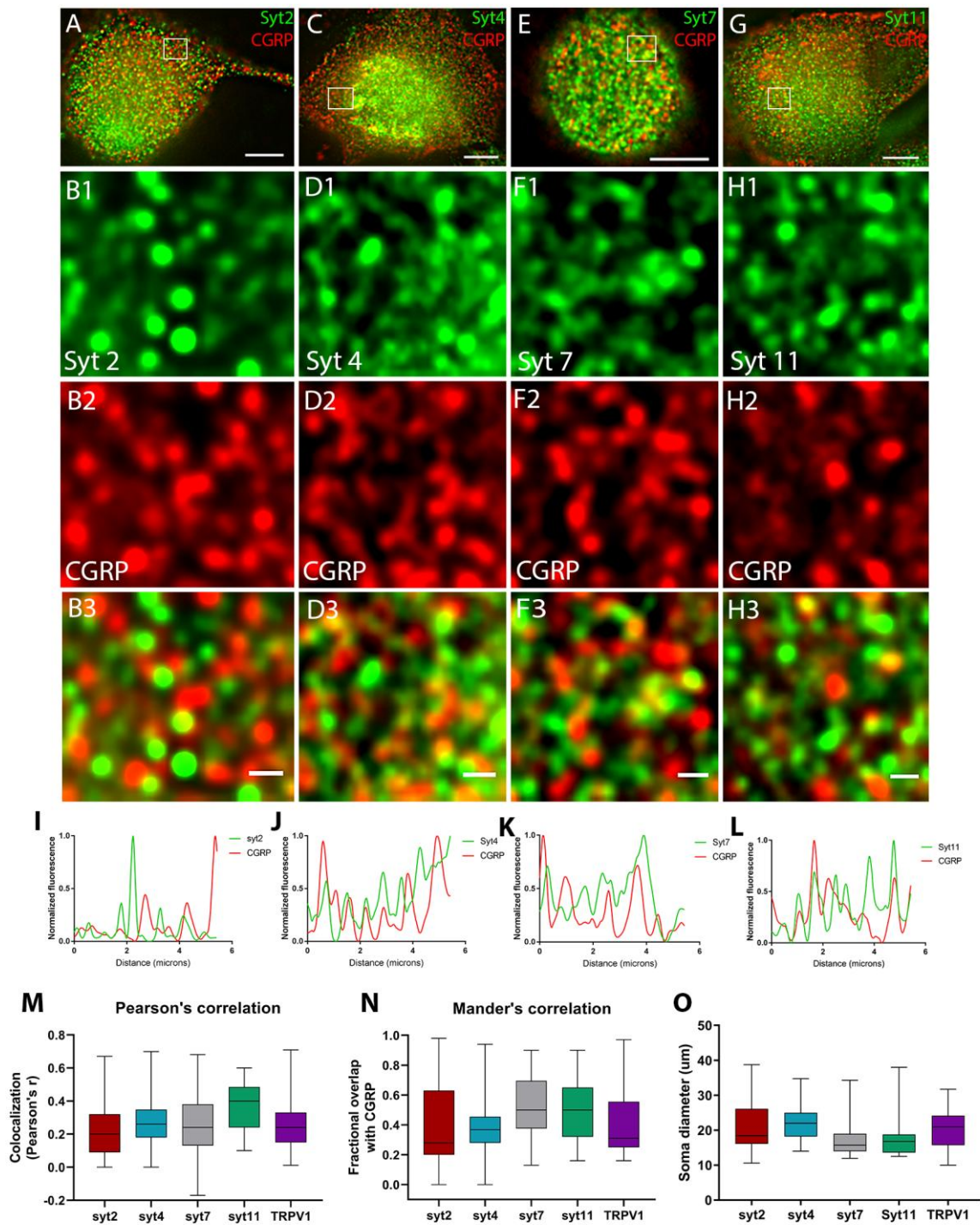


**Figure 3.4** Colocalization analysis of CGRP with syt2, 4, 7 and 11. **A, C, E, G** are representative deconvolved images of labelled DRG neuron somata, scale bars = 5  $\mu\text{m}$ . **B, D, F, H** are enlarged sections of the above images as indicated by white rectangles, scale bars = 0.5  $\mu\text{m}$ . All images have been contrast-enhanced by 5% for clarity. **I-L**, red and green fluorescence were measured along a 5  $\mu\text{m}$  line that was fitted along a representative ROI for each syt. Normalized fluorescence is shown against distance. **M-O**, Box-and-whiskers plot of Pearson's correlations, Manders' coefficients and soma sizes, averaged from across 2-3 cultures.

### 3.5. Syt4 or syt7 KO do not affect basic CGRP release

So far we found varying levels of colocalization and co-expression of the examined syt isoforms with CGRP in DRG neurons, suggesting that multiple syts are likely to contribute to the formation, trafficking and/or secretion of CGRP. To further evaluate the function(s) of syts in peptide secretion, we next measured CGRP secretion from DRG neurons isolated from KO mice. We narrowed our focus to syt4 and syt7 for the following reasons. Syt7 is a high affinity calcium sensor that is a major syt isoform on LDCVs in adrenal chromaffin cells and pancreatic islet cells (Gustavsson *et al.*, 2008; Schonn *et al.*, 2008) and has previously been reported to play a key role in sustained transmitter release by serving as a sensor of residual calcium that builds up after repetitive stimulation which is thought to regulate the fusion of LDCVs not tightly coupled to VGCCs (Liu *et al.*, 2014; Jackman *et al.*, 2016). These features make syt7 a possible candidate for regulating sustained peptide release during chronic pain states. Syt4 on the other hand is a non-calcium binding isoform that we found highly expressed in DRG neurons and is upregulated in neuropathic pain (section 3.1). It is also primarily found on LDCVs and known to interact with syt7 in pancreatic  $\beta$ -cells (Zhang *et al.*, 2009; Huang *et al.*, 2018). Syt7 and syt4 KO mice both survive well into adulthood, as opposed to syt2 KO mice that die around P21 (Pang *et al.*, 2006), making their use more accessible.

First, DRG neurons from Syt4 KO or heterozygous (HET) littermates were cultured and CGRP release was measured at 3 DIV using ELISA. Cells were stimulated either with external solution (basal release) or 40 mM KCl or 1  $\mu$ M capsaicin. KCl was chosen as a generic stimulant of excitable cells, while capsaicin only stimulates the TRPV1 positive cell population. 40 mM KCl induced a significant increase in CGRP release both in het and KO mice (figure 3.5 B-C). The mean increase in CGRP release was from  $0.4 \pm 0.1$  ng/ml to  $0.95 \pm 0.1$  ng/ml in the KO, and from  $0.3 \pm 0.1$  to  $1 \pm 0.2$  ng/ml in HET mice. The mean capsaicin evoked CGRP release was similar in the KO and HET mice ( $0.75 \pm 0.1$  ng/ml and  $0.8 \pm 0.1$  ng/ml respectively), and this was significant in the HET mice ( $p=0.02$ ) and nearly reached significance in the KO mice as well ( $p=0.08$ ). Exclusion of calcium in the solution blocked CGRP release, showing that it was via the regulated pathway. We confirmed the KO genotype by immunocytochemistry and PCR; syt4 staining was markedly reduced in cells

cultured from syt4 KO mice (figure 3.5 A). Absence of syt4 therefore did not have a significant effect on basal or evoked CGRP release.

The above experiments were repeated in Syt7 KO and wild type littermate mice. The mean KCl-induced CGRP release was from  $0.36 \pm 0.15$  ng/ml to  $1.4 \pm 0.5$  ng/ml in the wild type, and from  $0.38 \pm 0.3$  ng/ml to  $1.2 \pm 0.5$  ng/ml in KO cells, which was significant in the wild types, and nearly reached significance in the KOs ( $p = 0.06$ ) (figure 3.5 B, C). This lack of significance in the KOs was however likely due to lower n number in this group. Capsaicin induced CGRP release to similar levels in the wild type and KO cells: from  $0.36 \pm 0.15$  ng/ml to  $0.9 \pm 0.1$  ng/ml in the wild types, and from  $0.38 \pm 0.3$  ng/ml to  $0.9 \pm 0.2$  ng/ml in the KO cells, although this was only significant in the wild types (figure 3.5 D, E). Loss of syt7 therefore did not cause a pronounced defect in stimulated CGRP release. These experiments suggest that neither syt4 nor syt7 are critical regulators of stimulated CGRP secretion from DRG sensory neurons under 'normal' conditions.

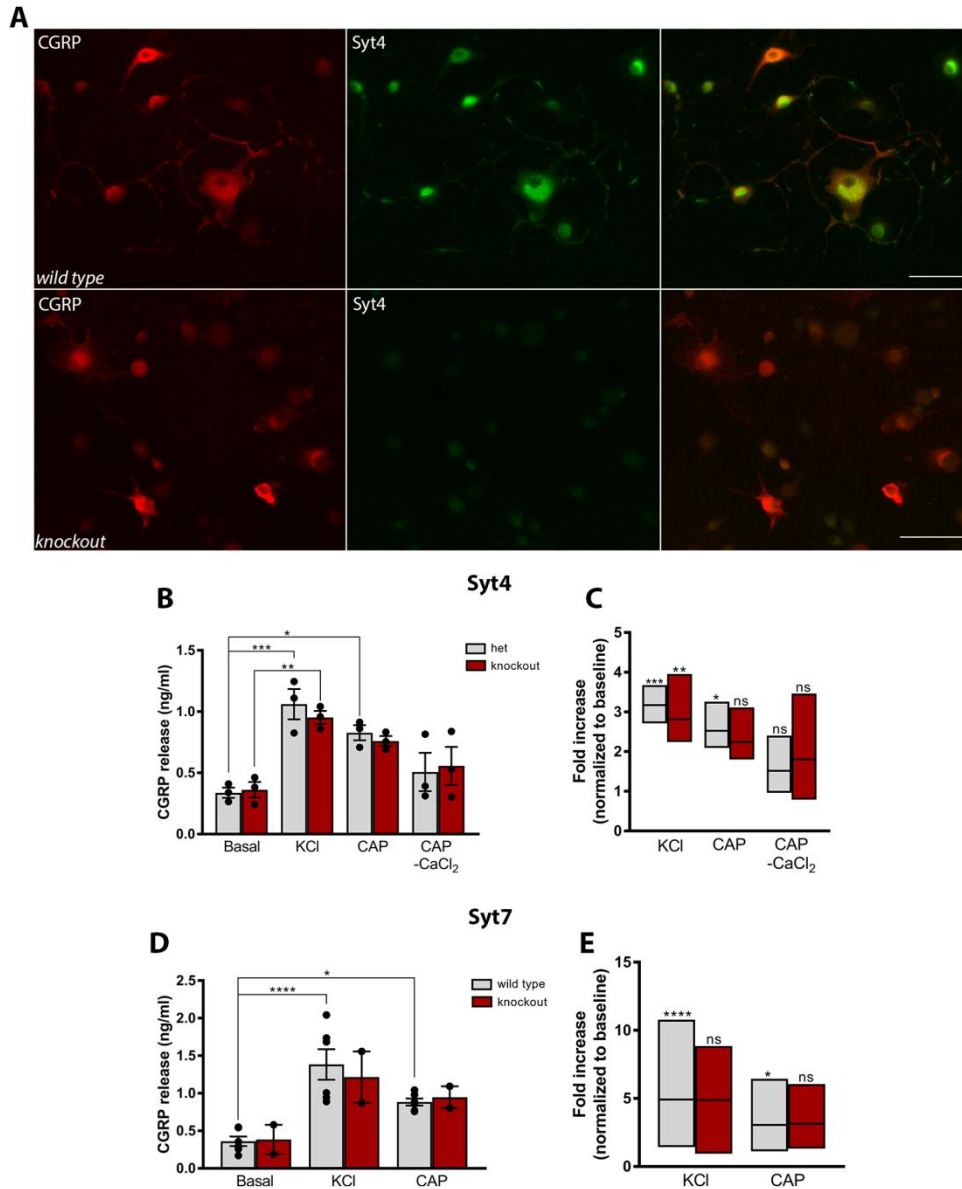


**Figure 3.5 Basal and evoked CGRP release are unaffected in *syt4* and *syt7* KO mice.** A, representative epifluorescent images of CGRP and *syt4* staining in *syt4* wild type and KO mice. *Syt4* staining disappears in the KOs. B, CGRP release (ng/ml) from *syt4* heterozygous (het) or KO mice after no stimulation (basal), 40 mM KCl, 1  $\mu$ M capsaicin (CAP) or 1  $\mu$ M capsaicin where CaCl<sub>2</sub> was replaced by equimolar EGTA. Mean  $\pm$  SEM are plotted, n = 3 KO and 3 heterozygous (het) mice). \*p = 0.023, \*\*p = 0.005, \*\*\*p = 0.0007, one-way ANOVA with Sidak's multiple comparisons. C, fold-change in CGRP release (min-max spread with mean), normalized to baseline. D, CGRP release as on B, from *syt7*<tm1b> KO or wild type mice. N = 2 KO and 6 wild type mice. \*p = 0.038, \*\*\*\*p < 0.0001, one-way ANOVA with Sidak's multiple comparisons. E, same as C.

### 3.6. Conclusions

Previously, several synaptotagmin isoforms were found in DRG neurons (section 3.1) but in this chapter we focused specifically on four isoforms: syt2, 4, 7 and 11. First the expression of each isoform was confirmed in DRG neurons cultured from syt4 KO and wild type mice by western blotting, and by immunofluorescence in cells cultured from C57BL/6 mice. Then, their expression and localization was correlated with that of the neuropeptide CGRP and found that multiple synaptotagmin isoforms are present on CGRP containing LDCVs, and finally functional ELISA experiments showed that syt4 and syt7 are not indispensable for CGRP release in cultured DRG neurons.

The western blots revealed high protein levels of syt4 and 11 in DRG neuron lysates and conversely lower protein levels of syt2 and syt7. The strong syt4 and syt11 expression is consistent with the result of Collins & Nassar (figure 3.1 B). Interestingly we also found lower protein levels of syt2, syt11 and syntaxin 1 in syt4 KO DRG lysates (figure 3.2.2 and 3.2.3). This could be explained by a potential disruption of the ubiquitin-proteasomal degradation pathway as all of the above proteins are degraded through ubiquitination (Chin, Vavalle and Li, 2002; Hakim *et al.*, 2016). Syt4 and syt11 are highly homologous, both can inhibit vesicle fusion and other synaptotagmin isoforms (Poser, Ichtchenko and Shao, 1997; Bhalla, Chicka and Chapman, 2008), and both have been identified as substrates of the E3 ubiquitin ligase parkin (Wang *et al.*, 2016). In the absence of parkin, Syt11 accumulates due to decreased degradation, which results in decreased dopamine release through impaired endocytosis and vesicle replenishment. This leads to the subsequent apoptosis of dopaminergic neurons and the developments of Parkinson's disease (Wang *et al.*, 2018). The protein levels of syt4 are similarly regulated by parkin and syt4 is also accumulated in the brains of parkin KO mice (Kabayama *et al.*, 2017). Thus, perhaps parkin and the ubiquitin-proteasomal degradation pathway are reversely affected in the syt4 KO mice towards increased activity, which could explain the observation of weaker syt11, as well as syt2 and syntaxin 1 western blot bands in the syt4 KO lysates.

The immunostaining experiments showed that syt4 was present in most neurons in our cultures, consistent with Usoskin *et al.* who found ubiquitous expression of syt4 in DRG neurons. Syt4 labelled Golgi-like structures as well as vesicles, as observed by punctate staining throughout the cell. As it has been established by multiple studies that syt4 labels

the Golgi and secretory vesicles in endocrine cells and neurons (Thomas *et al.*, 1999; Ibata *et al.*, 2000; Zhang *et al.*, 2009), we can safely assume that the staining pattern seen in our experiments indeed shows Golgi localization. However, future experiments could address the colocalization of syt4 with Golgi and mature/immature secretory vesicle markers (such as syntaxin 6, secretogranin II, TGN38, Rab3A (Ibata *et al.*, 2000; Fukuda *et al.*, 2003; Ahras, Otto and Tooze, 2006) to strengthen this finding. The ubiquitous nature of syt4 expression and its localization pattern suggests that, like in PC12 cells, syt4 also likely plays a role in LDCV maturation and trafficking in multiple DRG neuron populations (Fukuda *et al.*, 2003; Ahras, Otto and Tooze, 2006). It should also be noted however that syt4 expression is induced by neuronal activity (Vician *et al.*, 1995; Ferguson *et al.*, 1999), and as DRG isolation and dissociation is a major stress for cells and can even be considered as a model of nerve lesion (Malin, Davis and Molliver, 2007), the isolation procedure itself might as well induce the expression of syt4.

Immuno-colocalization with CGRP revealed that all of the synaptotagmin isoforms examined were expressed in peptidergic neurons, and this was expected based on their mRNA expression pattern from Usoskin *et al.* (figure 3.1A). A second observation of the immunostaining experiments was the weak fluorescence signal produced by syt2, 7 and 11 staining. A weak signal could arise due to low protein expression, which was confirmed by western blot for syt2 and 7, or from non-specific antibody staining. Indeed, the latter option was confirmed in western blots where the syt2, 4 and 7 antibodies all recognised non-specific bands in the knockout cells. Although the syt11 antibody could not be validated, the discrepancy between the strong western blot signal and weak immunocytochemistry signals suggest that this antibody may also have non-specific targets. Non-specific staining in immunocytochemistry can increase background and affect the quantification, as the threshold to decide whether a neuron was positive or negative for a given protein was set based on the fluorescence intensity of no-primary antibody controls, but the synaptotagmin signal was often only slightly higher than the threshold.

On the other hand, the weak staining is also likely the result of low protein expression in the case of syt2 and syt7, which might indicate that neurons do not need to express high copy numbers of these proteins as they serve highly specific functions inside the cells and their sorting onto vesicles is precisely controlled (Mutch *et al.*, 2011). Low signal caused by low protein levels could be improved by using signal amplification techniques, for example

by streptavidin-based detection of biotinylated primary antibodies (Ness *et al.*, 2003; Wang, Gibbons and Freeman, 2011). Nevertheless, these results indicate that syt2 and 7 are likely expressed in multiple DRG populations at low levels while the non-calcium binding syt4 and 11 are expressed in multiple populations but at higher level, and that there are also likely overlaps between the expression patterns of the different isoforms.

The subcellular colocalization analysis showed a similar picture to the population level, as all the synaptotagmin isoforms had vesicular staining but none colocalized strongly or exclusively with CGRP. The low colocalization of multiple syt isoforms with CGRP could suggest that they all play a role in regulating secretion. As the same staining procedure was used for these and the co-expression experiments, the same limitations also apply here. It was shown before that on average there are about 7-15 syt1 molecules on one SV, but much fewer, about 5-6 are sufficient to trigger  $\text{Ca}^{2+}$ -dependent release (Takamori *et al.*, 2006; Mutch *et al.*, 2011; Dittrich *et al.*, 2013). Though there might be more molecules on the larger LDCVs, due to the low copy number per vesicle one can expect low fluorescence signal even in high resolution images. Two types of colocalization algorithms were used in this thesis: Pearson's correlation is sensitive to low signal-to-noise ratio but does not require a threshold, while the MOC analysis requires the user to set a threshold on the images (Bolte and Cordelieres, 2006; Dunn, Kamocka and McDonald, 2011). This is automatically calculated by the program but if the fluorescent spots are not bright enough compared to the background, then the threshold is set too low and the program calculates false positive colocalization. The threshold can be adjusted by the user to only include brighter spots, this however introduces bias. All the above complications could have resulted in the high variability of colocalization seen in our results.

The difficulty of analysing colocalization of any subcellular structures smaller than 200 nm will remain when using diffraction-limited light microscopy. Significant advances have been made in the past ~ten years in developing super-resolution imaging methods that go far beyond the diffraction limit and can be used to precisely visualize the molecular architecture of small organelles such as secretory vesicles and quantify colocalization. These techniques include stimulated emission depletion (STED), stochastic optical reconstruction microscopy (STORM), structured illumination microscopy (SIM) (Sahl, Hell and Jakobs, 2017), and they can even be combined with electron microscopy (Schirra and Zhang, 2014; Peddie *et al.*, 2017). Such techniques could be utilized to visualize and accurately measure the cargo

content of vesicles harbouring one or multiple syt isoforms, and unambiguously answer the question whether multiple syt isoforms reside on the same vesicle and thus regulate vesicle fusion depending on which isoform is activated by local  $\text{Ca}^{2+}$  concentration, or whether different syt isoforms define distinct vesicle pools that possibly contain different cargoes or have different release probabilities (Schonn *et al.*, 2008; Gustavsson and Han, 2009; Rao *et al.*, 2014)

Besides investigating the colocalization of synaptotagmins with CGRP to give us hints about their role in peptide release, functional experiments were also used to assess syt4 and syt7 function. CGRP ELISA experiments on cells cultured from syt4 or syt7 KO mice did not find strong evidence that either of these isoforms affect basal or evoked CGRP release. Constitutive KO of genes can generate developmental changes that lead to functional compensation of the KO phenotype. Such effect has been observed for syt7 in SV exocytosis; neurons cultured from syt7 KO mice exhibited normal synaptic transmission in one study, but in a later study the same group showed that knockdown of syt7 eliminated asynchronous neurotransmitter release using multiple shRNAs and rescue experiments (Maximov *et al.*, 2008; Bacaj *et al.*, 2013). However, deletion of syt7 significantly reduces LDCV exocytosis in chromaffin cells and pancreatic B cells without genetic compensation (Gustavsson *et al.*, 2008; Schonn *et al.*, 2008). Thus further experiments using selective syt7 knockdown should reinforce our findings in DRG neurons.

A similar compensatory mechanism is possible in the case of syt4 as well, although studies done on syt4 KO mice consistently found enhanced LDCV exocytosis and secretion using different stimulation protocols. These studies found increased oxytocin secretion in the hypothalamus (70 mM KCl stimulation) (Zhang *et al.*, 2011), increased BDNF secretion in the hippocampus (unstimulated, basal release over 2-3 days) (Dean *et al.*, 2009), and increased LDCV exocytosis in low (but not high)  $\text{Ca}^{2+}$  concentration in the posterior pituitary nerve terminals (Zhang *et al.*, 2009). Although we did not find such increase in secretion in syt4 KO mice using our stimulus conditions (continuous 40 mM KCl or 1  $\mu\text{M}$  capsaicin), but different stimulations can induce different calcium signals and high frequency electrical stimulation induces more peptide and BDNF release in DRG neurons than continuous KCl depolarization (Balkowiec and Katz, 2000; Bost *et al.*, 2017). Overall, these ELISA experiments showed that syt4 and syt7 are not involved in basic and evoked CGRP release

from DRG neurons, but different stimulation paradigms (such as different KCl concentrations of electrical stimulation) could also be tested in syt4 and syt7 KO/KD cells.

So far we established that peptidergic DRG neurons express both Ca<sup>2+</sup>-binding and non-binding synaptotagmin isoform and that multiple isoforms are likely to be involved in regulating CGRP secretion as the colocalization analysis suggests. Deletion of syt4 or 7 did not significantly change basal or evoked CGRP release as measured by ELISA, but the increased syt4 gene expression in neuropathic pain models mirrors the increased neuropeptide expression (see section 3.1) and suggests that at least syt4 might be involved in pathological conditions. As syt4 is thought to serve its function at least partially by interacting with other isoforms, such as syt7 (section 1.2.6, (Mendez *et al.*, 2011; Huang *et al.*, 2018), subsequent experiments aimed to investigate the involvement of syt4 and syt7 in exocytosis in DRG neurons.

## 4. Studying single vesicle fusion in DRG neurons using pHluorin constructs

### 4.1. Introduction

Fluorescently tagged synaptic proteins (for example VAMP2, synaptophysin, VGLUT, synaptotagmins) coupled with high resolution imaging techniques provide a powerful tool for studying exo-endocytosis and, so long as the transfection protocol used to express the tagged proteins in target cells is properly optimized, this technique can be minimally invasive. Many different indicators of neuronal activity exist that are based on fluorescent proteins (Lee *et al.*, 2016; Lin and Schnitzer, 2016), but we decided to use the pH indicator pHluorin. This molecule was created from GFP by shifting its pH sensitivity which results in a decreased fluorescence at acidic pH (~5.5) and increased fluorescence at higher (~7.4) pH (Miesenböck, De Angelis and Rothman, 1998). When a pHluorin molecule is tagged to the luminal domain of a vesicular protein, the fluorescence inside the acidic vesicle lumen is quenched but is increased rapidly upon vesicle fusion (figure 1.4.2). Thus by tagging pHluorin to different vesicular proteins, one can study their function in exo-endocytosis. This technique has been widely used, especially in pancreatic islet cells and CNS neurons (Obermüller *et al.*, 2005; Rao *et al.*, 2014; Xu *et al.*, 2017), and in the recent years in DRG neurons as well (Bost *et al.*, 2017; Wang *et al.*, 2017; Shaib *et al.*, 2018).

The aim of these experiments was to establish a pHluorin-based assay of exocytosis in DRG neurons in our laboratory. Our first choice of fusion detector was VAMP2-pHluorin, which despite exhibiting relatively high surface expression (~ 15%) (Balaji and Ryan, 2007) has none the less been extensively used and well established.

## **4.2. Establishing exocytosis assay in DRG neurons using VAMP2-pHluorin**

We set out to optimize the imaging and analysis of pHluorin fusion events using TIRF microscopy. Neurons from C57/bL6 mice were transfected with VAMP2-pHluorin and imaged 2 days later on a TIRF microscope. Because of the microscope setup, electrical stimulation was not possible and thus cells were stimulated by perfusion of 40 mM KCl for 3 minutes. It should be noted that the number of cells that we could record from per culture was restricted (3-4 recordings could be made per dish or slide before the culture started perishing, times ~2-4 dishes or slides per experiment), and furthermore because the capsaicin sensitive (TRPV1 positive) neurons are only a fraction of the whole DRG culture and we could not identify those cells at the start of the experiment, we decided not to use capsaicin stimulation.

Individual fusion events were highly variable in their amplitude and decay time course but the fluorescence rise was almost always rapid (within  $\sim 0.2$  s) (figure 4.2.1). The HHD distribution (Figure 4.2.2 D) shows that the majority of events had a short ( $<1$  s) open time with a median of 0.66 s, and decayed fast with a median of 0.65 s with a few slower events (figure 4.2.2 E). Only 2 out of 178 events did not decay exponentially and thus could not be fit with an exponential decay curve, these events appear as a separate 40 s bin on figure 4.2.2 E. We then divided events according to cellular location (ie. soma or neurites) because there is evidence that pHluorin events differ on different locations (Dean et al., 2012) (figure 4.2.1). There were 165 events on the soma and only 13 on the neurites, but neurite events had significantly larger HHD (the median was 2.1 on the neurites compared to 0.65 on the soma, figure 4.2.2 B), but the decay times and amplitudes were similar (figure 4.2.2A, C). These results show for the first time in DRG neurons that VAMP2-pHluorin reports fusion events with a brief pore open time and fast decay, especially compared to the syt4 and syt7 pHluorin constructs (see below), and suggest some difference between somatic and neurite exocytosis.

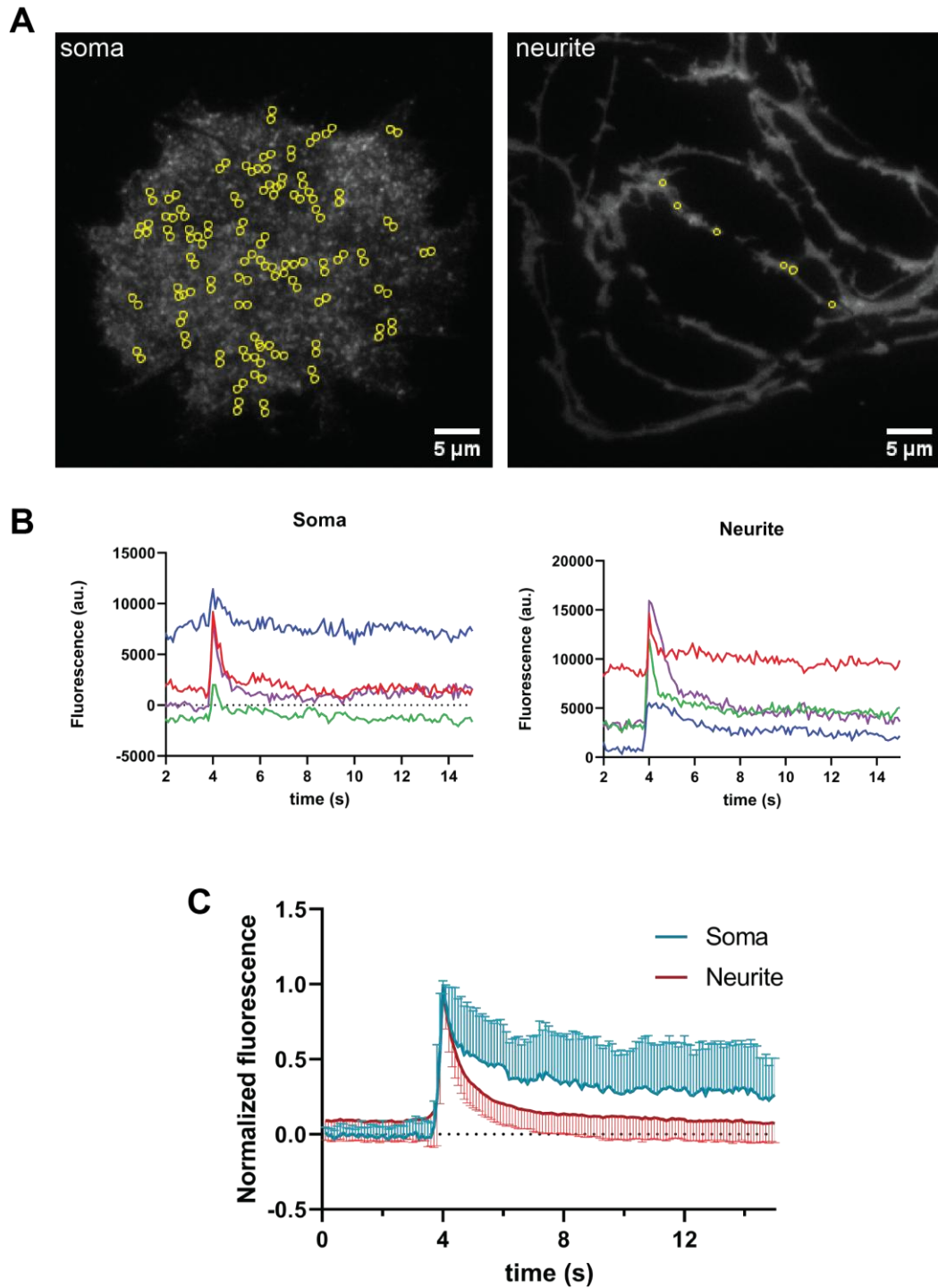


**Figure 4.2.1 Detection of VAMP2-pHluorin labelled vesicle fusion events using TIRF microscopy.** A, TIRF images of a representative soma and neurites, with yellow circles showing fusion events. B, representative examples of somatic and neurite events. C, average time-courses (mean  $\pm$  SD) of neurite (n=13 from three cells) and somatic (n=166 from two cells) events.

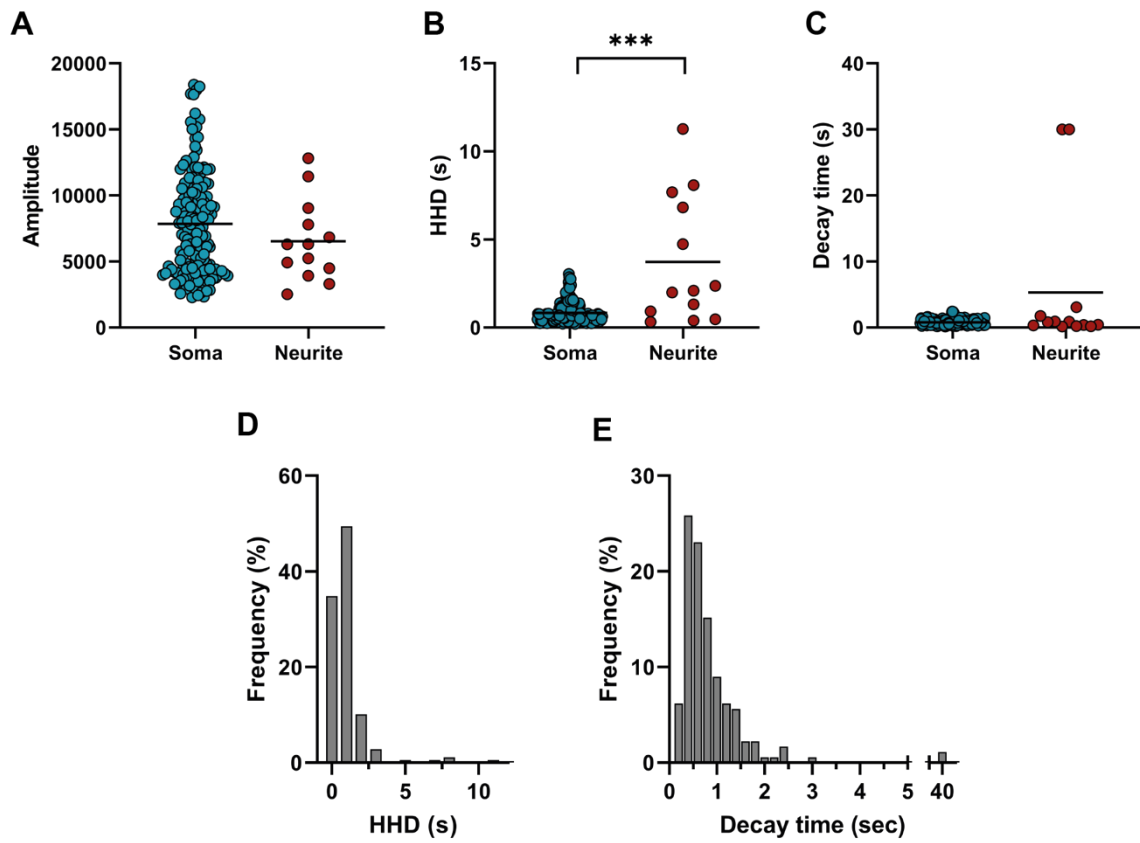


**Figure 4.2.2** Graphs of syt2-pHluo amplitude, HHD and decay time. A-C, scatter plots of VAMP2-pHluorin amplitudes, HHD and decay times on the soma and neurites. \*\*\* $p < 0.0001$ , two-tailed t test. D-E, frequency histograms of HHD (bin width=1 s) and decay time (bin width=0.2 s),  $n=178$  events.

### 4.3. Detecting peptide release using NPY-pHluorin

VAMP2 is an essential SNARE protein that may be present on different types of vesicles (SVs and LDCVs) and is therefore a nonselective vesicle marker. In order to correlate exocytosis to peptide release, we conducted experiments using NPY-pHluorin. Since the start of this PhD two studies have used NPY-pHluorin in DRG neurons to study the mechanism of exocytosis and found that NPY release occurs with fast kinetics ( $\sim 1$  s) but had conflicting findings with regard to the type of fusion (kiss-and-run or full fusion) that KCl stimulation induces (Bost *et al.*, 2017; Wang *et al.*, 2017). Thus here we aimed to explore the NPY-pHluorin release kinetics induced by our KCl stimulation.

We recorded 22 release events from three cells from C57/bL6 mice and analysed them similarly to VAMP2-pHluorin. All events were recorded from the soma, and were very fast, usually lasted only one frame in our recordings (figure 4.3 A-D). 13 events appeared diffuse, without a well-defined puncta at fusion, and their signal disappeared within one frame (100 ms) without detectable spreading of fluorescence (figure 4.3 B). In 6 cases there was visible diffusion of the signal for 2-3 frames after fusion which can be interpreted as a full fusion of the vesicle and total content release (figure 4.3 A), and in 2 cases it was unclear whether there was diffusion. It is possible that in the 13 events with diffuse profile but no visible signal spreading, the NPY-pHluorin release and signal diffusion was faster than our temporal resolution ( $< 100$  ms), while in those 6 cases where the spreading could be observed, content release was slower (2-300 ms). Indeed, the median decay time was 0.09 s, and the median HHD was 0.13 s (figure 4.3 E, F). There was one event that had a well-defined dot upon fusion which quickly disappeared without spreading, which could indicate a fast transient opening of the fusion pore (kiss-and-run) without NPY release and fast reacidification. The median fluorescence increase upon vesicle fusion was 1896 (figure 4.3 G). These results show that the neuropeptide NPY is secreted from the soma of sensory neurons with fast kinetics and varying fusion profiles.

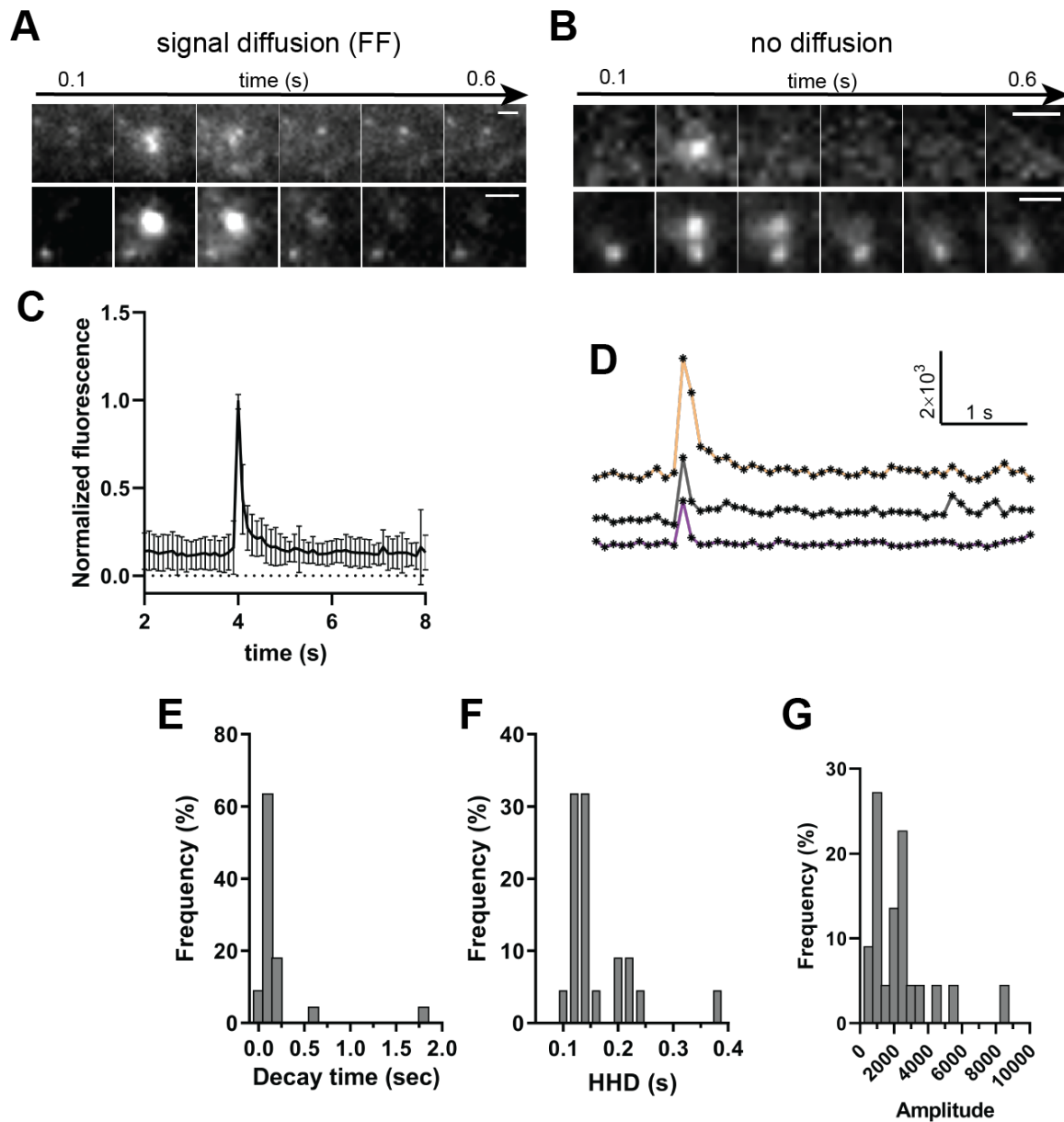


**Figure 4.3. Tracking peptide release using NPY-pHluorin.** A, examples of NPY-pHluorin release events. Top: two events are shown where the fluorescence signal visibly spreads out from the dot, probably indicating full fusion (FF) of the vesicle. Bottom: two events where the dot disappears without spreading of fluorescence (no diffusion), indicating fast release/pore closure. Scale bars = 1  $\mu\text{m}$ . B, schematic diagram of NPY-pHluorin. C, representative examples of NPY-pHluorin fluorescence time-courses. D, average NPY-pHluorin time-courses (mean  $\pm$  SD,  $n = 22$ ). E-G, distributions of event widths, decay times and amplitudes, events are shown as % frequency. Bin widths = 0.02 (E), 0.05 (F) and 0.4 (G).

#### **4.4. Syt2-pHluorin mediated exocytosis has distinct fusion kinetics between soma and neurites**

Thus far we have established that VAMP-pHluorin can be used as a reporter of exocytosis in DRG neurons and that these neurons release NPY after KCl stimulation. In order to start investigating the involvement of chosen synaptotagmins in regulated exocytosis in DRG neurons, first we transfected cells with syt2-pHluorin, which reports SV fusion in hippocampal neurons (Dean *et al.*, 2012), but has not been used in endocrine cells before to study LDCV exocytosis. 32 events were observed from four cells from across three transfections (syt4<sup>+/-</sup> mice); 56% (17/30) from neurites (figure 4.4.1 B) and 43% (13/30) from the soma (figure 4.4.1 A), example events for each category are shown in figure 4.4.1 C-D. The time-courses were normalized and averaged on figure 4.4.1 E, and this showed that averaged neurite and somatic events were only different in the late phase of decay. The amplitudes were similar on the soma and on the neurites, with mean increase of  $2284 \pm 908$  on the soma, and  $1762 \pm 1466$  on the neurites (figure 4.4.2 A). The fluorescence decay times were also similar between cellular locations and the mean decay time was  $1.53 \pm 1.3$  s on the soma and  $4 \pm 9$  s on the neurite, while the medians were 0.53 and 0.9 respectively (figure 4.4.2 C). On the neurites, there was one event that could not be fit with an exponential decay function, this appears in a separate 40 s bin on the pooled frequency histogram (figure 4.4.2 E). There was significant difference between the mean HHD on the soma and neurites; this was  $0.8 \pm 0.3$  s on the soma and  $2.8 \pm 2.2$  s on the neurites (figure 4.4.2 B). Overall, the characteristics of fusion events observed with syt2-pHluorin were different from those observed with VAMP2-pHluorin as revealed by longer decay times and HHD. Furthermore, the difference observed in the HHD between the neurites and the soma suggests possible differences between vesicle pools depending on cellular location.

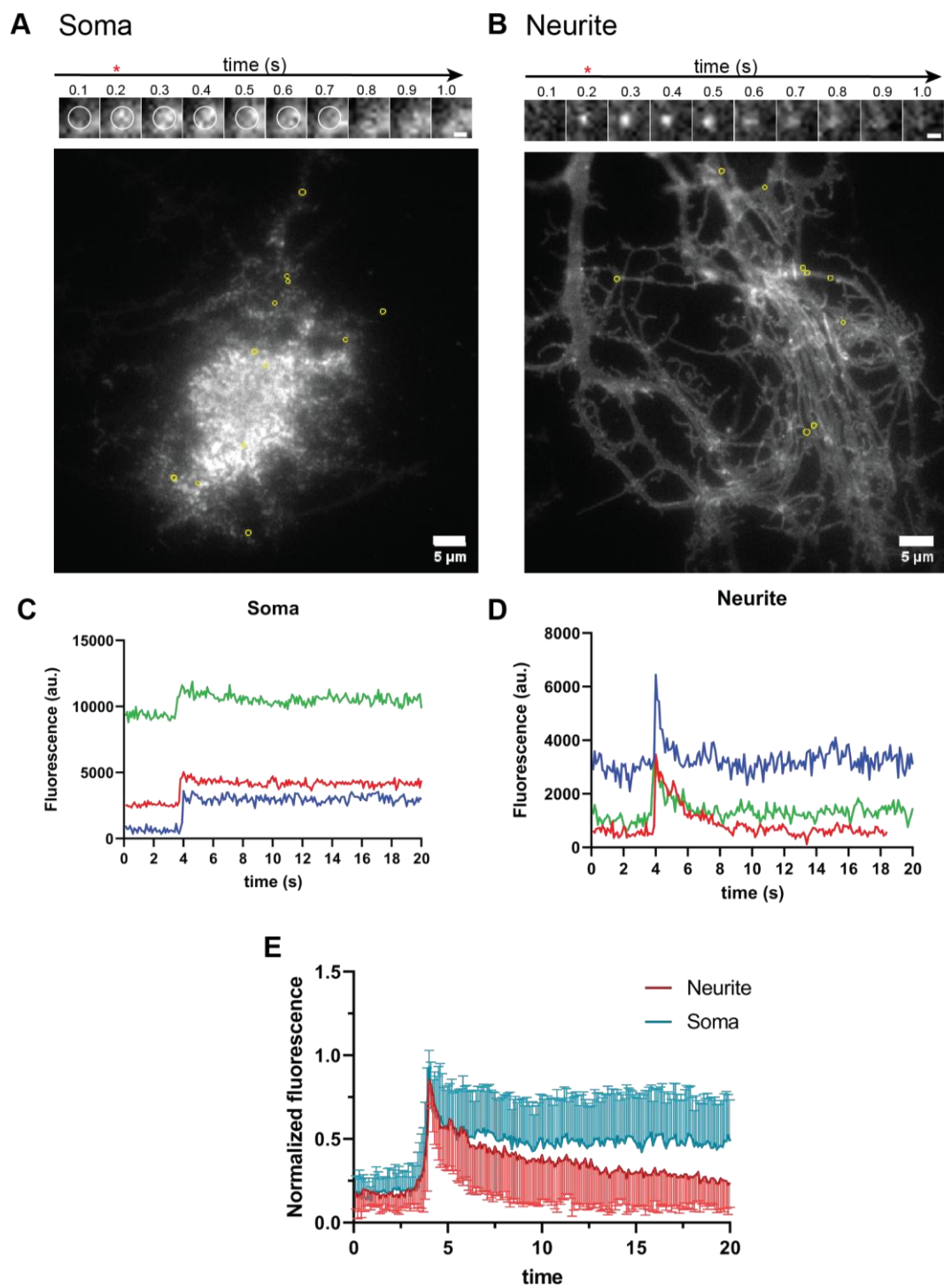


**Figure 4.4.1 Comparison of syt2-pHluorin fusion events on the soma and neurites.** A, montage of an example somatic event, red star above the 0.2 s frame indicates the initial time of fusion (scale bar=0.5  $\mu\text{m}$ ). TIRF image of the cell body underneath, yellow circles indicate syt2-pHluorin fusion events, scale bar=5  $\mu\text{m}$ . Corresponding graph on C shows example time courses. B-D, same for neurites. E, average time courses from neurites (n=19) and soma (n=13), mean  $\pm$  SD.

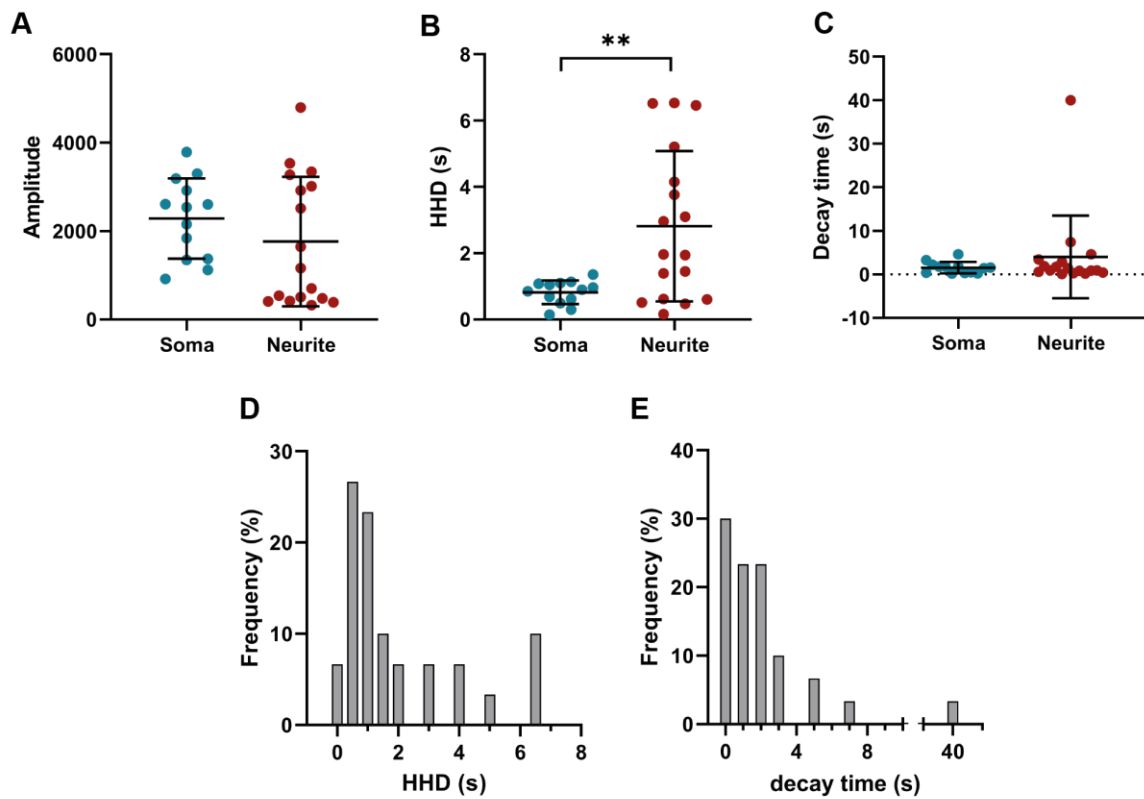


**Figure 4.4.2** Graphs of syt2-pHluo amplitude, HHD and decay time. A-C, scatter plots of syt2-pHluorin amplitudes, HHD and decay times on the soma and neurites. \*\*p=0.0041, two-tailed t test. D-E, frequency histograms of HHD (bin width=0.5 s) and decay time (bin width=1 s), n=30 events.

#### **4.5. Syt4-bearing vesicles can release NPY and have differences in their fusion kinetics between soma and neurites**

Next, we transfected DRG neurons with a syt4-pHluorin construct. The role of syt4 in regulated exocytosis is less well understood and cargo release from syt4 containing vesicles needs to be confirmed, thus we also transfected neurons with NPY-mCherry in these experiments.

Overall 33 syt4-pHluorin events were analysed from five cells from across four transfections. 57% (19/33) were observed on neurites and 42% (14/33) on the soma (figure 4.5.1 E, similar percentages as for syt2-pHluorin above). Generally, syt4 events were slow (ie. decayed slowly over time), example time-courses from neurites or soma are shown figure 4.5.1 C. The averaged syt4-pHluo time-courses on the soma and neurites appeared different (figure 4.5.1 D). Indeed the average HHD was significantly larger on the neurites,  $4.9 \pm 1.6$  s compared to  $3.5 \pm 1.3$  s on the soma (figure 4.5.2 C), although the fluorescence decay times were similar (figure 4.5.2 D). Most events had a short decay time of less than 2 second with a median of 1.4 s, and only 2 out of 33 (6 %) events did not decay exponentially (figure 4.5.2 F). There were some apparent differences between soma and neurite syt4-mediated fusion events and events with slower and faster kinetics were observed (examples are shown on figure 4.5.2 A), with the slower ones dominating on the neurites. These slower events also appeared as a second peak at  $\sim 7$  s on the pooled HHD histogram (figure 4.5.2 E). Additionally, somatic events were significantly smaller in amplitude; the fluorescence increase was  $1262 \pm 431$  on the soma compared to  $3218 \pm 2806$  on the neurites (figure 4.5.2 B).

One could expect that a longer HHD (and possibly more stable fusion pore) on neurites might correspond to more cargo release, however we observed the opposite as concomitant NPY release was observed less frequently on the neurites (figure 4.5.1 E). On the soma, eight out of 14 syt4 bearing fusing vesicles contained NPY and it was released from seven vesicles; on the neurites however only five out of the 19 fusing vesicles contained NPY and it was only successfully released in two cases. Thus, larger HHD does not necessarily allow more content release from vesicles. Overall this data shows that vesicles undergoing exocytosis and releasing neuropeptides are positive for syt4, and the apparent

differences in fusion and NPY release properties between the soma and neurites suggest possible differences between the exocytic machinery in these cellular locations.

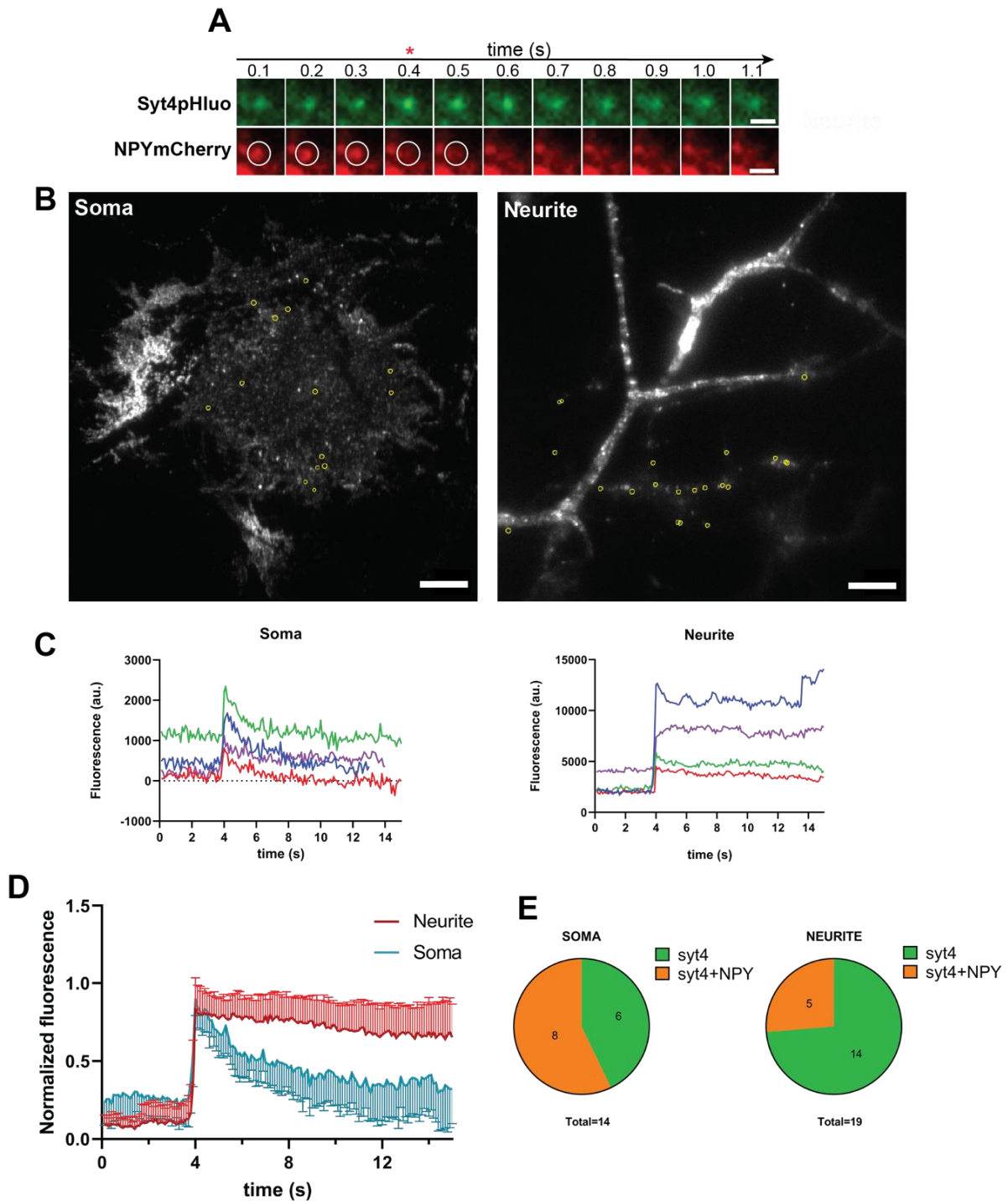


**Figure 4.5.1 Comparison of Syt4-pHluorin fusion events on the soma and neurites.** A, an example syt4pHluorin event with NPY release. Scale bars = 1  $\mu\text{m}$ , red star above the 0.4 s frame indicates the initial time of fusion. White circles highlight the NPY-mCherry puncta. B, TIRF images of a soma and neurites with yellow circles indicating fusion events. C, example time-courses of individual fusion events from the soma or neurites. D, average traces (mean  $\pm$  SD) of neurite ( $n = 19$ ) and somatic ( $n = 14$ ) events. E, Pie charts of syt4 and syt4 + NPY release events on the soma or neurites.

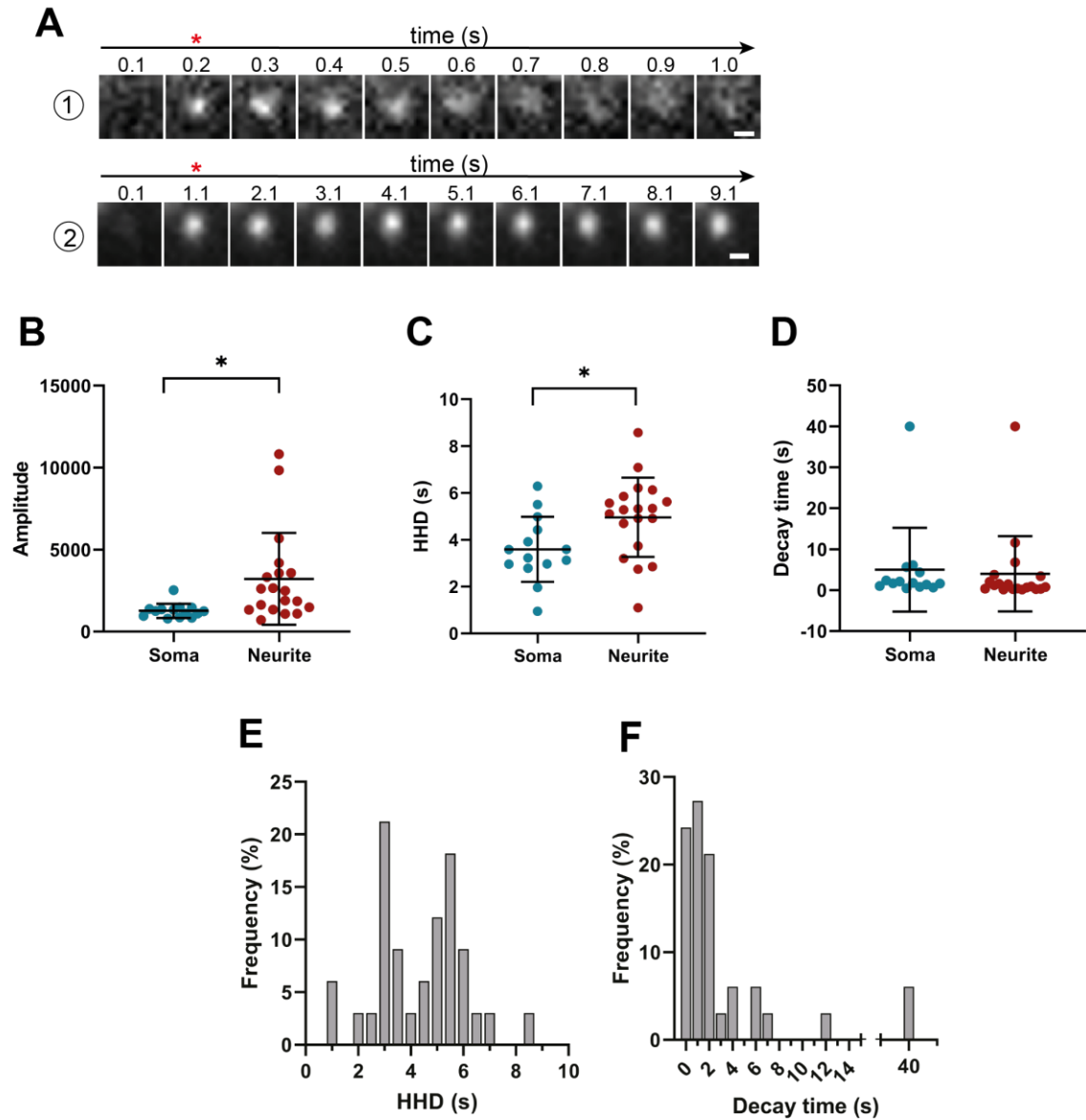


**Figure 4.5.2** Graphs of syt4-pHluo amplitude, HHD and decay time. A, Example montages of short (1) and long lasting (2) syt4-pHluorin events, scale bars=0.1  $\mu$ m. Red star indicates the initial time of fusion. B-D, scatter plots of syt4-pHluorin amplitudes, HHD and decay times on the soma and neurites. \* $p=0.01$ , two-tailed t test. E-F, frequency histograms of HHD (bin width=0.5 s) and decay time (bin width=1 s),  $n=33$  events.

## 4.6. Conclusions

In this chapter we established a pHluorin-based fusion assay and analysis in transfected DRG neurons using VAMP2-, NPY-, syt2- and syt4-pHluorin constructs. The first pHluorin based construct developed to study regulated exocytosis used VAMP2 as a putative selective tag for synaptic vesicles (Miesenböck, De Angelis and Rothman, 1998). Using bafilomycin, a V-type ATPase inhibitor that prevents the re-acidification of recycling vesicles, it was shown in hippocampal neurons that the decaying component of VAMP2-pHluorin and vGlut-pHluorin (another synaptic vesicle marker) events consists of endocytosis with average time constant of  $\sim 15$  s and reacidification with average time constant of  $\sim 4$  s (Atluri, 2006; Balaji and Ryan, 2007). Furthermore, Balaji & Ryan were able to distinguish three types of vGlut-pHluorin retrieval events: fast events that were only dictated by reacidification, slow events that had a dwell time ( $\tau \sim 13$  s) before start of fluorescence decay, and very slow events that lasted longer than 40 s; similar observations were reported earlier following analysis of the kinetics of VAMP2-pHluorin events (Gandhl and Stevens, 2003)

Subsequent studies in endocrine cells extended the use of the pHluorin tag to study LDCV exocytosis (Tsuboi and Rutter, 2003; Obermüller *et al.*, 2005; Felmy, 2007; Yuan *et al.*, 2015). These studies found lower values compared to the studies on SV exocytosis above, as they reported a plateau phase of around 1 s before decaying with a time constant of 1-2 s. We mostly observed fast VAMP2-pHluorin events with median decay time of 0.6 s and even the slowest ones had  $\tau < 4$  s. This, taken together with the low HHD values measured in our experiments (0.6-2.1 s), suggest that VAMP2-pHluorin mostly reported fast LDCV fusion events in DRG neurons. We cannot rule out the possibility that some of these fast decaying events represented full fusion and quick spreading of VAMP2-pHluorin outward from the fusion site, but bafilomycin could be used in future experiments to distinguish between these options, as only transient fusion with subsequent reacidification would be sensitive to bafilomycin.

While VAMP2-pHluorin and other membrane attached fusion proteins are useful to study fusion pore behaviours and vesicle endocytosis, several studies have used NPY-based fluorescent constructs to study cargo release as this isn't necessarily predicted by fusion (Tsuboi and Rutter, 2003). A study looking at NPY-Venus secretion from DRG neurons found

that KCl (60 mM) stimulation mostly induced transient (KR-type) fusion events (Bost *et al.*, 2017). The type and dynamics of vesicle fusion (ie. pore expansion or restriction, and vesicle retrieval or shrinking/collapsing) are likely regulated by the spatial and temporal properties of  $\text{Ca}^{2+}$  influx generated by different types of stimulation (section 1.2.5). In support of this, another recent study on DRG neurons found that high (70 mM) KCl stimulation was similar to repetitive electrical stimulation as they both induced large global  $\text{Ca}^{2+}$  influx through VGCCs, which lead to more full fusion, while the weaker capsaicin stimulation lead to smaller, localized  $\text{Ca}^{2+}$  increase at TRPV1 channels and to more KR type fusion (Wang *et al.*, 2017). The low (40 mM) and continuous KCl stimulation used in our experiments might have induced a more diffuse elevation of  $\text{Ca}^{2+}$  concentration (Xia, Lessmann and Martin, 2009) showed using Fluo-4 imaging that 30 mM KCl induced a much smaller  $\text{Ca}^{2+}$  increase in hippocampal neurons than 90 mM KCl), resulting in mixed full fusion / transient fusion events.

The above studies using NPY-pHluorin also showed that NPY release is fast and happens within <100 ms after fusion of vesicles in DRG neuron soma; this is in agreement with previous findings that NPY release can be as fast as 33 ms in bovine chromaffin cells (Chiang *et al.*, 2014), and similar decay times of NPY-pHluorin release were measured in DRG neurons before (Wang *et al.*, 2017). In the latter study, full fusion and KR events were distinguished by different HHD values (0.1 s for full fusion and 0.3 s for KR), but in our experiments most event widths were in the lower range (median was 0.13 s). The different fusion profiles that we saw with NPY-pHluorin might indicate differences in fusion pore dilation, as at least 6 events were full fusion as suggested by the signal diffusion, one event with well-defined puncta and no spreading might indicate narrow fusion pore without NPY release, and the rest of the events with a diffuse appearance but no visible signal spreading could indicate pore expansion with partial release, which was suggested to occur through kiss-and-run or kiss-and-stay type fusion in DRG neurons before (Bost *et al.*, 2017). An NPY-pHluorin molecule is  $\sim 40$  kDa, or its largest dimension is  $\sim 10$  nm (Barg, Olofsson and Rorsman, 2001), which would mean that if the events with no signal spreading mean fast KR with incomplete cargo release, then the fusion pore only expanded to around 10 nm in these cases. In conclusion, our results of NPY-pHluorin kinetics support previous findings from neurons and endocrine cells and 40 mM KCl stimulation induces mixed full fusion and

transient fusion events, but we cannot unequivocally conclude the ratio of these fusion types.

Compared to VAMP2-pHluorin, syt2 and syt4 reported fusion events with slower decay and longer HHD using the same stimulation (figure 4.4.2 and 4.5.2). One comprehensive study described the exo-endocytosis dynamics of almost all known synaptotagmin isoforms fused to pHluorin in hippocampal neurons (Dean *et al.*, 2012). When compared to synaptophysin-pHluorin fusion events, which exclusively marks synaptic vesicle exocytosis, they found that syt2 mediated fusion events exhibited SV-like features, consistent with its function mostly in SV exocytosis, and occurred exclusively in axons. Syt4 events on the other hand occurred in both axons and dendrites with slower kinetics than synaptophysin-pHluorin, and they were not always synchronised to the stimulation, consistent with LDCV-like features. An important difference between the above study and our system is that due to the lack of synaptic specializations, our experiments likely report predominantly LDCV fusion with different dynamics. Our results suggest that both of these syt isoforms mediate LDCV fusion with similarly slow vesicle retrieval times (pooled median  $\tau$  was  $\sim 1.4$  s for both syt2 and syt4). However, syt4-mediated fusion events had a longer HHD than syt2-mediated ones (1.1 s for Syt2 compared to 4.7 s for syt4), suggesting slower endocytosis kinetics. Studies in PC12 cells found that syt4 increased the duration of KR run events, but not of full fusion events (Wang *et al.*, 2003; Zhang, Zheng and Jackson, 2010). This agrees with the larger HHD seen in our experiments and might suggest that syt4 mediated events are mostly transient rather than full fusion events in the DRGs, which is supported by the finding that syt4 promotes KR in PC12 cells (Wang *et al.*, 2003). On the other hand, VAMP2-pHluorin HHD and decay times were both shorter, suggesting that VAMP2 drives vesicle fusion towards faster dynamics (short pore-open times and fast vesicle retrieval).

The difference between fusion parameters in different cellular locations might point at differences in the fusion machinery. The HHD was significantly larger on the neurites using each pHluorin construct, and the amplitudes were larger using syt4-pHluorin. One possible explanation for this observation is that there is a difference in the maturity and number of synaptotagmin molecules on the vesicles. Upon fusion pore opening, the proton exchange is instantaneous between the vesicle lumen and extracellular space, increasing the fluorescence of the pHluorin molecules inside the vesicles rapidly, thus in our analysis the

pHluorin signal amplitude likely reflects the number of pHluorin molecules inside the vesicle. If this is the case, it means that on the neurites more syt4 molecules were present on LDCVs, which could suggest the presence of more functionally mature vesicles in the neurites, as indeed LDCV maturation continues during trafficking from soma along the neurites (see section 1.2.1). Alternatively, controlling the number of synaptotagmins on LDCVs could have implications in stimulus-secretion coupling, and this could also explain the observation that VAMP2-pHluorin amplitudes were essentially the same between soma and neurites, as we can reasonably expect less variability in the vesicular copy number of an essential v-SNARE. Similar observations were made in hippocampal neurons, where exocytic events in neurites exhibited slower time course, prolonged fusion pore dilation and increased cargo release than on the soma, and the differences in fusion dynamics were attributed to differences in L-type  $\text{Ca}^{2+}$ -channel distribution and corresponding  $\text{Ca}^{2+}$ -signals (Matsuda *et al.*, 2009; Xia, Lessmann and Martin, 2009). It is possible that similar differences exist in cultured DRG neurons where LDCVs with different number of membrane synaptotagmins and/or different machinery would be needed in neurites compared to soma, to adjust to differences in  $\text{Ca}^{2+}$  signals. Future experiments should address the spatial relationship of LDCV fusion sites and  $\text{Ca}^{2+}$ -channels in DRG neurons.

Another, possible explanation for differences in amplitudes could be the occurrence of fast events that are below the temporal resolution of our acquisition rate (faster than 100 ms). Recently the pore expansion rate was determined for the first time to be  $> 8.9 \pm 1$  nm/ms in chromaffin cells (Shin *et al.*, 2018), meaning that it would be plausible for a fusion pore to expand enough within 100 ms that some of the pHluorin molecules could start diffusing away from the fusion site, resulting in a lower signal amplitude. This scenario would suggest that there are more ultrafast events occurring on the soma; however, the difference in amplitude was not observed with VAMP2-pHluorin.

The results of this study showed for the first time that syt4 mediates NPY release from both the soma and neurites, which provides further evidence toward syt4 being present on neuropeptide containing LDCVs. We have chosen NPY-based constructs to monitor peptide release in our live-cell imaging experiments because they have been widely used in the literature, while CGRP-based constructs have not been made or used before to our knowledge. However, peptides and specifically NPY and CGRP are mostly co-stored in DRG neurons (see section 1.2.1), and whether peptides and other transmitters are released

together or separately and whether this is regulated at the vesicle fusion stage or during packaging or maturation is still unclear (Merighi, 2018; Zhang *et al.*, 2019). The size of NPY and CGRP are very similar (NPY ~10 kDa, CGRP ~14 kDa) and thus information we learn about NPY release is likely applicable to CGRP as well in terms of release properties. In section 3.4, we established that syt4 does not play a major role in basic and KCl or capsaicin evoked CGRP release, but its presence on CGRP-containing vesicles (section 3.4), the NPY release observed from syt4-bearing vesicles (section 4.5) and that it was upregulated in neuropathic pain (section 3.1) prompted us to further investigate the involvement of syt4 in peptide release and exocytosis.

## 5. Investigating the effect of NGF on neuropeptide release

### 5.1. Introduction

NGF is produced during inflammation in peripheral tissues where it activates TrkA-expressing nociceptors, leading to increased synthesis and secretion of CGRP, BDNF and other neuropeptides which contribute to hyperalgesia (see section 1.1.4). This effect of NGF on CGRP release has been observed *in vitro* as well: Park et al. (2010) found that acute (30 minute) exposure to 100 ng/ml NGF increased capsaicin, but not KCl evoked CGRP release in DRG neurons. Long term NGF exposure (7 days, where cells were grown in the presence of NGF) also increased CGRP release compared to untreated cells that were not exposed to NGF, but this was due to increased CGRP content in the cells. In contrast, following acute NGF treatment the PI3/PKC pathway and Src family kinases mediated acute sensitization of sensory neurons, and the authors concluded that phosphorylation of TRPV1 channels by PKC activation after NGF treatment can explain the increased CGRP release (Park *et al.*, 2010).

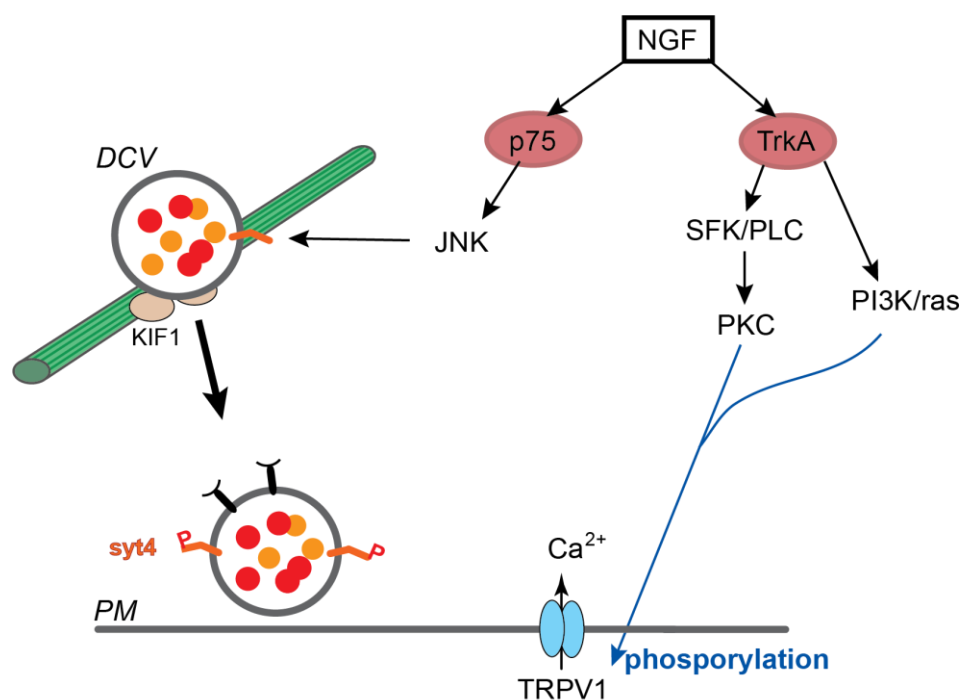


**Figure 5.1 NGF signalling pathways.** Acute NGF treatment and dimerization of the TrkA receptor leads to activation PKC and PI3K/ras pathways, which in turn phosphorylate TRPV1 and contribute to its sensitization in DRG neurons. Activation of the p75 receptor on the other hand activates JNK pathways. This pathway has been shown to result in the phosphorylation of syt4, which promotes the detachment of DCVs from KIF1 and microtubules (in green), and increases DCV capture at the plasma membrane (PM) in hippocampal neurons.

Other studies looking at the effect of acute NGF on exocytosis in PC12 cells provide evidence for the involvement of syt4 in NGF-induced potentiation of exocytosis. A group found that NGF induced the sorting of syt4 onto mature LDCVs, and this involved syt4 phosphorylation by c-Jun N-terminal kinases (JNK) (Fukuda *et al.*, 2003; Mori *et al.*, 2008). Syt4 phosphorylation was essential for the enhancement of KCl-induced transmitter release by NGF, but not for basal or depolarization induced release without NGF treatment (Mori *et al.*, 2008). In a more recent study, Bharat *et al.* found that JNK also phosphorylates syt4 in hippocampal neurons and this leads to decreased LDCV trafficking and increased capture of syt4 vesicles specifically at presynaptic sites (Bharat *et al.*, 2017). They concluded that Syt4 phosphorylation helps in vesicle tethering at synapses but has no effect on vesicle fusion; however previous findings indicate that overexpressing syt4 changes fusion pore dynamics and syt4-bearing vesicles favour KR fusion (Wang *et al.*, 2001, 2003). As we found strong and ubiquitous syt4 expression in cultured DRG neurons and our previous results suggest that it is present on neuropeptide containing LDCVs, we hypothesised that syt4 contributes to the pathway by which NGF enhances peptide release from DRG neurons, possibly through a mechanism involving its phosphorylation. Thus in this chapter we investigated syt4 phosphorylation in DRG neurons using mass spectrometry and its involvement in NGF induced potentiation of CGRP release using ELISA experiments.

## **5.2. 30 minutes NGF treatment enhances KCl induced CGRP release in wild type neurons**

First we set out to confirm the CGRP release potentiating effect of NGF in our culture conditions. For this, 3 DIV DRG neurons were treated with 100 ng/ml NGF for either 30 minutes or 2 hours and then stimulated with 40 mM KCl or 1  $\mu$ M capsaicin for 30 minutes. We chose a 30 minutes and 2 hour NGF treatment times because in the study of Mori et al. 2008, JNK/syt4 phosphorylation started after about 30 minutes of NGF exposure, and increased further in two hours. Our results showed that KCl stimulation increased CGRP release from  $0.32 \pm 0.13$  to  $1.27 \pm 0.6$  ng/ml in untreated cells (figure 5.2 and table 5.2), and this failed to reach significance ( $p = 0.13$ ) likely due to large standard deviations and small n numbers ( $n = 6$  data points from 2 experiments), as in other experiments KCl consistently induced significant increase (figure 3.5). However, following 30 minutes exposure to NGF, KCl induced significantly increased CGRP release, from  $0.29 \pm 0.16$  to  $1.67 \pm 0.96$ , and similarly 2 hours NGF treatment also induced significant potentiation, where  $0.23 \pm 0.14$  ng/ml CGRP was increased to  $1.53 \pm 1.04$  ng/ml (basal release in the NGF treated groups was unaffected) (table 5.2).

With the capsaicin stimulation there was a slight trend observed, but the increase was not significant in either condition ( $0.78 \pm 0.37$ ,  $1.06 \pm 0.56$  and  $0.92 \pm 0.75$  ng/ml CGRP release in the untreated, the 30-minute and the 2-hour NGF treated groups respectively, table 5.2). This somewhat contradicts the findings from Park et al. who only saw a significant potentiation in the capsaicin response (Park et al., 2010). Nevertheless, these results point towards the release potentiating effect of NGF in DRG neurons.

	Untreated control	30 min NGF	2 hr NGF
basal	0.32 ± 0.13	0.29 ± 0.16	0.23 ± 0.14
KCl	1.27 ± 0.6	1.67 ± 0.96	1.53 ± 1.04
Capsaicin	0.78 ± 0.37	1.06 ± 0.56	0.92 ± 0.75

**Table 5.2** CGRP release (ng/ml) as measured by ELISA in cells either untreated or treated with 100 ng/ml NGF for 30 minutes or 2 hours, followed by 30 minutes stimulation with KCl, capsaicin or no stimulation.

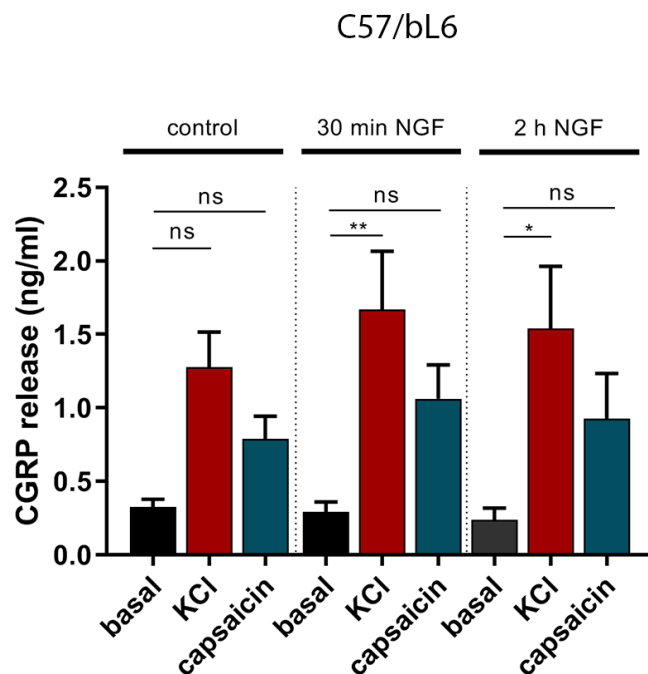


**Figure 5.2. Acute NGF treatment enhances KCl induced CGRP release.** ELISA result showing CGRP release from cells cultured from C57/bL6 mice that were either untreated or treated with NGF for 30 minutes or two hours, and then stimulated with external solution (basal), 40 mM KCl or 1 μM capsaicin for 30 minutes (mean ± SEM). n = 6 data points from 2 cultures, ns = not significant, \*p = 0.0161, \*\*p = 0.0052, one-way ANOVA with Sidak's multiple comparisons.

### 5.3. Syt4 is expressed in the majority of TrkA<sup>+</sup> neurons

NGF is only expected to affect those DRG neurons that express its receptor TrkA (or p75, though the latter can be activated by all neurotrophins, see section 1.1.4). Therefore, before examining the functional relationship between NGF and syt4, we assessed the percentage of cells that co-express TrkA and syt4. We also analysed the co-expression of CGRP with TrkA, which would be expected to be present in a largely overlapping population (Bennett, Dmietrieva, Priestley, Clary, & McMahon, 1996; Usoskin et al., 2014).

The results showed that TrkA and syt4 were co-expressed in ~33 % (27/82) of DRG neurons (figure 5.3B); nearly all TrkA<sup>+</sup> neurons however, expressed syt4 (figure 5.3C). This result agrees with our previous finding that syt4 is likely not restricted to a specific population but is widely expressed in DRG neurons. CGRP had a slightly higher colocalization with TrkA (42 %, 33/78, figure 5.3B), but 70% of TrkA<sup>+</sup> neurons were also positive for CGRP (figure 5.3C), confirming that TrkA is largely expressed in the peptidergic population. Moreover, analysis of soma diameters showed that the average diameters ranged between 13-17  $\mu\text{m}$  but the majority of TrkA<sup>+</sup> cells were small diameter neurons and these mostly expressed syt4 (figure 5.3D). CGRP/TrkA colocalization also largely marked small diameter neurons, while CGRP and syt4 alone marked a wider population of neurons. In conclusion, these results support the notion that NGF activates TrkA receptors on largely small diameter peptidergic neurons that express syt4. Whether there is a functional interaction between TrkA receptors and syt4 in these DRG neurons is unknown.

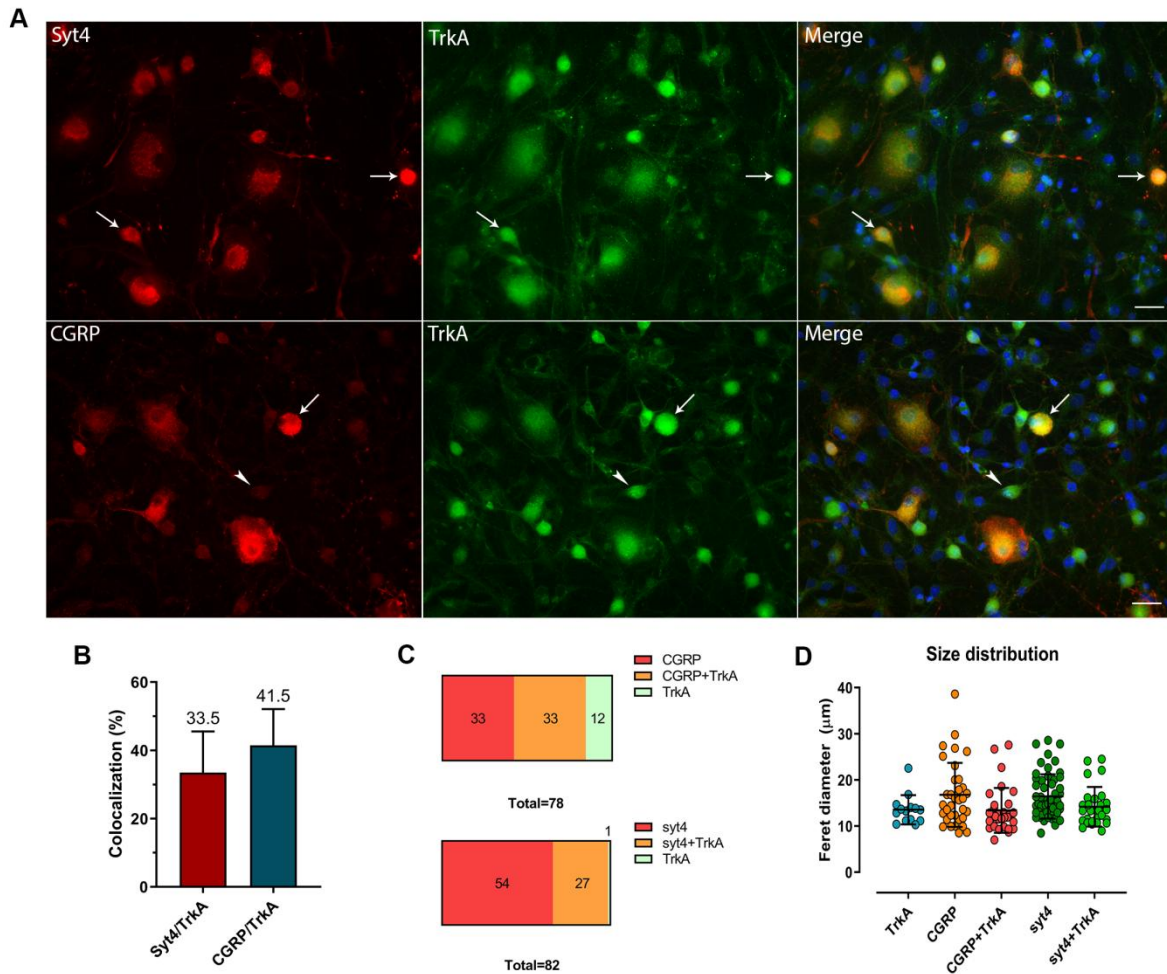


**Figure 5.3 Syt4 and CGRP are both co-expressed with TrkA.** A, representative epifluorescent images of DRG cultures immunostained for syt4, TrkA on the top and CGRP, TrkA on the bottom. Blue shows DAPI staining. Arrows show colocalization, arrowhead shows a cell only expressing TrkA. Scale bar = 25  $\mu\text{m}$ . B, percentage colocalization of either syt4 or CGRP with TrkA (number of co-expressing cells divided by total number of cells, mean  $\pm$  SD from two cultures). C, box charts showing the number of cells that were positive for the indicated proteins. Total numbers are shown from two cultures. D, scatter plot of the soma size distributions in the indicated groups (black lines show mean  $\pm$  SD).

## 5.4. NGF-enhancement of CGRP release is Syt4 dependent

In order to investigate whether syt4 contributes to NGF potentiation of CGRP release in DRG neurons (Figure 5.4D), we performed ELISA experiments in syt4 KO and heterozygous mice following 30 minutes NGF treatment. The results showed that in syt4<sup>+/-</sup> cells, there was a significant increase in both KCl and capsaicin evoked CGRP release in cells pre-treated with NGF compared to untreated controls (figure 5.4A). KCl evoked release increased from 0.47 ± 0.18 ng/ml to 0.77 ± 0.2 ng/ml, while capsaicin evoked release increased about two-fold, from 0.2 ± 0.15 to 0.54 ± 0.17 ng/ml. In DRG neurons isolated from syt4<sup>-/-</sup> mice, the potentiation of CGRP secretion by NGF was significantly reduced following both KCl and capsaicin stimulation (Figure 5.4B), indicating a requirement for syt4. The above results suggest that the NGF induced potentiation is reduced in the absence of syt4 and this is not restricted to a TRPV1<sup>+</sup> population, but is a more generic effect in all cells, as KCl induced release was equally affected. Taken together, the above experiments provide evidence for syt4 being involved in TrkA receptor potentiation of peptide secretion from DRG neurones.

	Syt4 <sup>+/-</sup>		Syt4 <sup>-/-</sup>	
	Untreated control	30 min NGF	Untreated control	30 min NGF
<b>Basal</b>	0.19 ± 0.07	0.29 ± 0.15	0.24 ± 0.15	0.23 ± 0.07
<b>KCl</b>	0.47 ± 0.18	0.77 ± 0.2	0.52 ± 0.18	0.68 ± 0.14
<b>capsaicin</b>	0.20 ± 0.15	0.54 ± 0.17	0.43 ± 0.18	0.59 ± 0.23

**Table 5.4** CGRP release (ng/ml) as measured by ELISA in cells cultured from syt4<sup>+/-</sup> or syt4<sup>-/-</sup> mice that were either untreated or treated with 100 ng/ml NGF for 30 minutes, followed by 30 minutes stimulation with KCl, capsaicin or no stimulation.

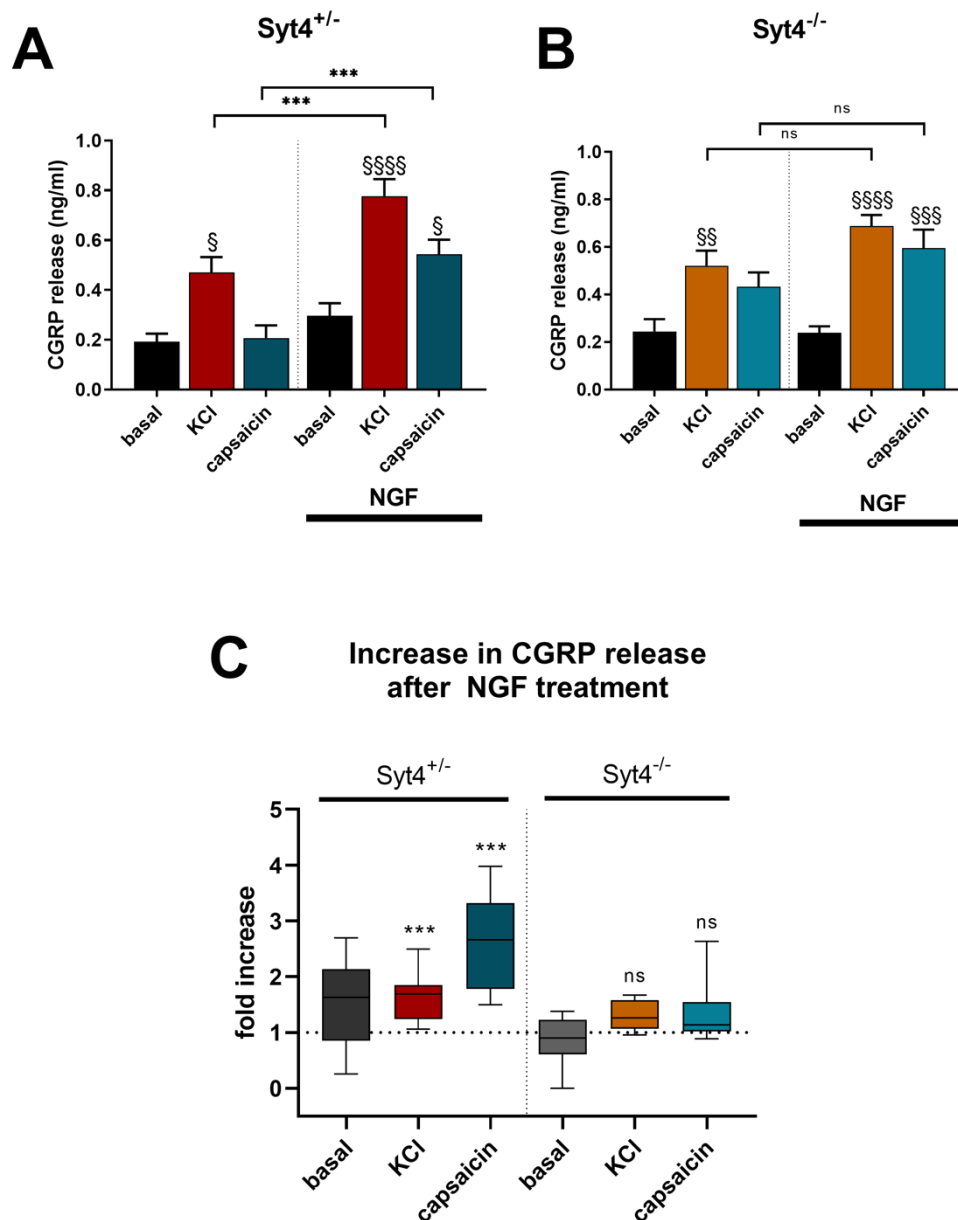


**Figure 5.4 The effects of NGF treatment on CGRP release is syt4 dependent.** A-B, CGRP release measured by ELISA from cells cultured from syt4<sup>-/-</sup> and syt4<sup>+/-</sup> mice that were either untreated or treated with NGF for 30 minutes, followed by stimulation as in A. n = 3 independent measurements from 3 cultures, \*\*\*p < 0.001, ns = not significant, §: p < 0.05, §§: p < 0.01, §§§: p < 0.001, §§§§: p < 0.0001, compared to “basal” in each group (NGF treated/untreated), one-way ANOVA with Sidak’s multiple comparisons. C, same as A-B but CGRP release *with* NGF treatment was normalized to CGRP release *without* NGF treatment in both genotypes to show the fold increase (box-and-whiskers graph showing 25th to 75th percentiles, min to max spread and median).

## 5.5. Identification of Syt4 phosphorylation sites in DRG neurons

As previous studies have indicated that Syt4 phosphorylation regulates its function (Mori *et al.*, 2008; Bharat *et al.*, 2017), we next examined whether the S135 site of syt4 is phosphorylated in DRG neurons after NGF treatment. As currently there are no available phosphospecific antibodies for syt4, we employed mass-spectrometry (MS) to explore phosphorylation sites. In order to do this, we performed syt4 immunoprecipitation (syt4-IP) on DRG neuron lysates prepared from four mice (figure 5.5A) to purify syt4 and then analysed the lysates with MS. DRG lysates were pooled from the four mice and were incubated with polyclonal syt4 antibody bound to sepharose beads to capture syt4. As a pull down control, some of the lysate was incubated with a control IgG antibody bound to sepharose beads which is not expected to bind syt4 specifically. Indeed, in the syt4 IP western blots, syt4 could be identified in the elution (E) while it was missing from the supernatant (S), while syt4 was detectable in the supernatant but not the elution when pulled down with the control IgG antibody (red rectangle on figure 5.5 A).

There was 14% sequence coverage of syt4 in the MS analysis. Nonetheless, we still managed to identify four phosphorylation sites on syt4, two of which were not previously described. All phosphorylation sites (like all other post-translational modification sites) fell between the transmembrane and the C2A domain in the cytoplasmic side (figure 5.5B, top). The known phosphorylation sites found were serine-114 and the putative TrkA target serine-135 (Mori *et al.*, 2008). The new phosphorylation sites found were serine-115 and threonine-122 (figure 5.5B, bottom). Both the S135 and S114 sites were previously identified in a high throughput phosphoproteomic study that used a shotgun approach to identify phosphorylation pathways involved in glucose secretion (Sacco *et al.*, 2016). Four additional high-throughput phosphoproteome profiling studies also identified the syt4 S135 site in murine brain (Huttlin *et al.*, 2010; Wiśniewski *et al.*, 2010; Goswami *et al.*, 2012; Lundby *et al.*, 2012). Two studies have investigated the functional role of S135 phosphorylation in PC12 cells and neurons (Bharat *et al.*, 2017; Mori *et al.*, 2008); however to date, the putative function of all other phosphorylation sites in syt4 are unexplored. While the above experiment was only carried out once and could not be repeated due to very limited amount of protein that we were able to purify from each mouse, but

nonetheless the Serine-135 phosphorylation site in syt4, which is the putative target of NGF/JNK signalling, was successfully identified in DRG lysates.

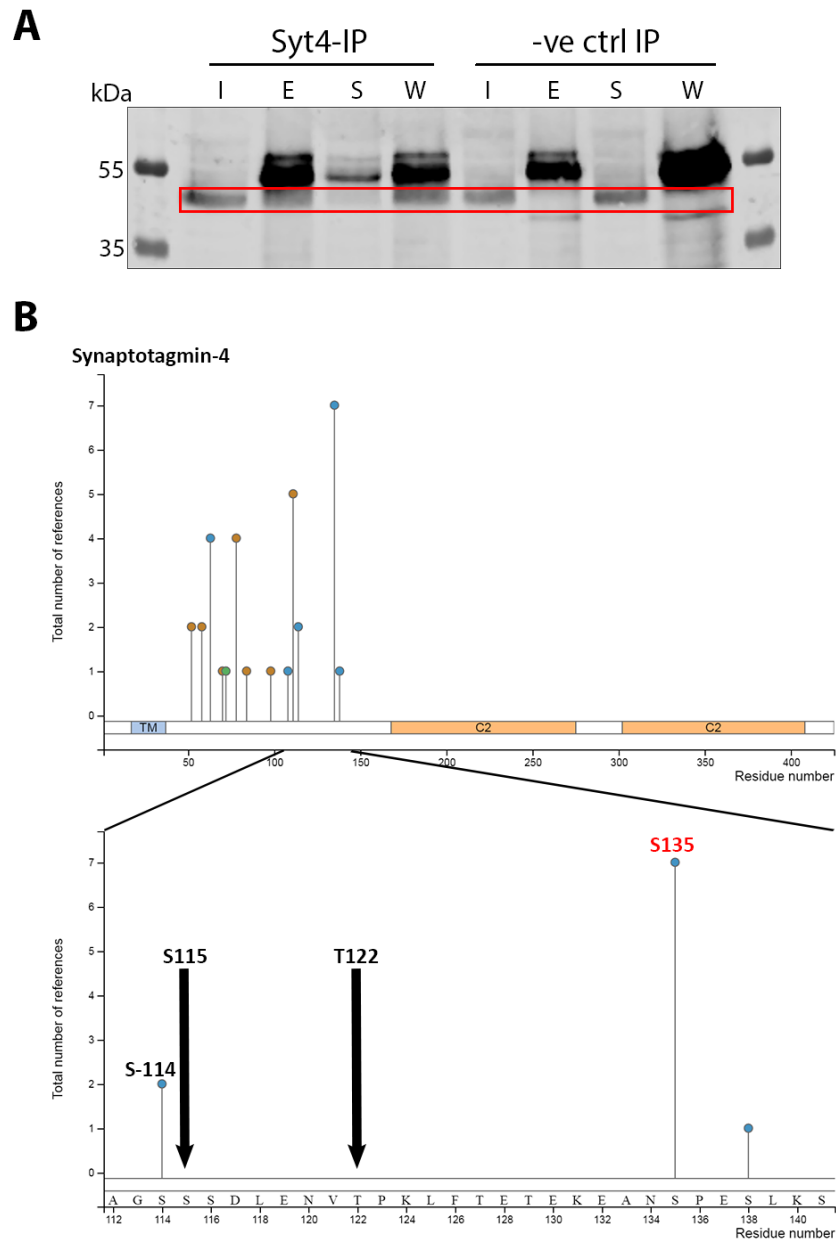


**Figure 5.5. Identification of the S135 and other phosphorylation sites in syt4 in DRG neurons.** A, western blot of a sy4-IP and a negative control IP, where the beads were incubated with a control IgG antibody. I = input from the original lysate, E = elution, S = supernatant, W = wash. Red rectangle marks the syt4 bands. (Note that syt4 is missing from the supernatant and is present in the elution and wash in the syt4-IP, while it is missing in the elution and is present in the supernatant in the control) B, structure of syt4 (exported from [www.phosphosite.org](http://www.phosphosite.org)). *Top image* shows the full length of the protein, lines indicate sites of posttranslational modification according to the number of references (Y axis) and the type of modification (blue circle: phosphorylation, green circle: acetylation, orange circle: ubiquitylation). TM = transmembrane domain. *Bottom*, enlarged section of the amino acid sequence as indicated, containing the identified phosphorylation sites from our experiment. Two black arrows indicate the novel phosphorylation sites identified in our studies.

## 5.6. Conclusions

From the experiments above, we can conclude that syt4 has a role in NGF induced potentiation of CGRP release in vitro. The molecular mechanisms that allow this increased exocytosis are unclear, but a study that looked at the effect of both chronic and acute NGF treatment on CGRP release provides some useful insights (Park *et al.*, 2010). According to this study, chronic (7 days) exposure to 30-250 ng/ml NGF activates a ras/MEK/ERK pathway, which leads to increased CGRP content in the neurons due to increased gene expression, but neither this nor the PI3-kinase/Akt pathway contribute to the increased CGRP release after acute (20 minute) exposure to 100 ng/ml NGF. PKC and src family kinases on the other hand are required for potentiated secretion after acute NGF treatment. PKC may be acting as a downstream phosphorylation target of src (Joseloff *et al.*, 2002) in this pathway, and phosphorylates TRPV1 channels to increase channel activity and peptide release (Bhave *et al.*, 2003; Wang *et al.*, 2015).

The low-affinity NGF receptor, p75 however also activates a number of signalling proteins, one of which is JNK. Others have demonstrated that JNK leads to the phosphorylation of syt4 at serine-135, and although we have preliminary data confirming this phosphorylation site in DRG neurons (section 4.5), further studies are needed to establish whether phosphorylation of S135 is regulated through NGF signalling, and should also determine the relative contribution of syt4 to PKC-dependent pathways as described above. As we found that deletion of syt4 reduced but did not abolish the NGF-potentiation of CGRP release, we can assume that multiple pathways may contribute an additive effect, the net outcome of which is increased CGRP release. It is also important to determine if syt4 is the downstream target of both receptors, or only of p75. Since p75 is a non-specific neurotrophin receptor, if syt4 phosphorylation happens through p75 activation then it is reasonable to assume that other neurotrophins could also engage this signalling pathway to increase peptide secretion. Therefore, here we showed for the first time that syt4 contributes to the increased CGRP release following acute NGF exposure in DRG neurons, and that syt4 is co-expressed with TrkA in small to medium sized neurons.

## 6. The effects of syt4 and its phosphorylation on syt7-mediated exocytosis and fusion kinetics

### 6.1. Introduction

To better understand the role of phosphorylation and the mechanisms by which syt4 may help enhance release, we looked at vesicle exocytosis using the previously established imaging methods (chapter 4). In this chapter we first show that syt4 and 7 are trafficked together to a population of vesicles. Syt4 and 7 were found to interact before using proximity ligation assay in pancreatic beta cells, where syt4 inhibited syt7-mediated insulin secretion in mature beta cells (C. Huang et al., 2018). To assess whether syt4 and syt7 colocalization has functional implications in sensory neurons, we analysed syt7 fusion events with or without syt4-mCherry, as well as in a syt4 knockout (KO) background. Additionally, to investigate the role of syt4 phosphorylation in the proposed NGF activated pathway, we double transfected cells with syt7-pHluorin and syt4 S135 phosphomutants that were created by site-directed mutagenesis (the target of NGF activation). The same syt4 mutation was tested previously in hippocampal neurons and was found to decrease mobility and increase capture of LDCVs at synapses (Bharat et al., 2017). Although multiple studies have examined the interaction of different synaptotagmin isoforms, and generally established that syt4 inhibits the function of other syts (section 1.2.6, also see (Bhalla et al., 2008; Littleton et al., 1999)), interestingly, one study found that syt4 did not have any effect on the secretion rate or decay time of syt7-mediated fusion in PC12 cells, only on that of syt1 and syt9, but it did inhibit syt7-mediated fusion in liposome fusion assays (Zhen Zhang et al., 2011). The study by Bharat et al. however only looked at the function of syt4 phosphorylation, not whether it interacts with other syts or whether phosphorylation affects these interactions. Thus, at the end of this chapter we aimed to study the effects of syt4-phosphorylation on syt7-mediated LDCV fusion.

## 6.2. Overexpressed syt7 and syt4 can be trafficked to the same vesicles, where syt4 may affect syt7-mediated fusion

We wanted to investigate directly if exogenously expressed syt4 and syt7 can be functionally targeted to the same secretory vesicles and whether this had any functional significance on syt7 mediated vesicle release. For this, Syt4<sup>+/-</sup> cells were transfected with syt7-pHluorin and wild type syt4-mCherry, and stimulated with 40 mM KCl while imaging on a TIRF microscope. Eight out of 28 co-transfected neurons examined responded to the stimulation, and overall 120 syt7-pHluorin fusion events were detected from across three transfections. First we examined their distribution according to cellular location and found that 24% (29/120) were on the soma while 76% (91/120) were in the neurites; a higher percentage of syt7 events colocalized with syt4 in the neurites (figure 6.2.1E). As was expected, syt4-mCherry fluorescence did not change at the time of fusion as can be seen on the example montage on figure 6.2.1 A. Thus, syt7 mediated exocytic events follow the trend that was observed with syt2 and syt4, namely that there are more events on the neurites compared to the soma.

Fusion of syt7-pHluorin vesicles showed varied kinetics in their rate of decay as well as amplitude depending on their cellular location. The averaged fluorescent traces of syt7-pHluorin showed different rates of decay between soma and neurites (figure 6.2.1 D). As was seen with syt2- and syt4-pHluorin, syt7-pHluorin events were significantly larger in amplitude on the neurites compared to the soma (median = 4985 and 1259 respectively, figure 6.2.1 F). Neurite syt7-pHluorin events decayed significantly slower (median = 7.1 compared to 1.5 at the soma, figure 6.2.1 H). Additionally, 24% of events on the neurites did not decay exponentially and were placed in a 40 s bin, while all somatic events could be fit with an exponential function (figure 6.2.1 H). With regards to HHD, this was also significantly larger on the neurites (median was 7.4 on the neurites and 4.5 on the soma, figure 6.2.1 F). These results support the evidence from chapter 4 that the kinetics of fusion events occurring at the soma of sensory neurons is different from those at neurites.

To investigate whether overexpression of syt4 alters syt7 fusion, we separated events according to presence or absence of syt4-mCherry at the fusion site. The majority of the syt7 events (76%, 89/120) had no syt4-mCherry associated with them compared with 24% (29/120) which clearly also had syt4-mCherry. In this analysis however we cannot rule

out the presence of endogenous syt4 on vesicles that had no syt4-mCherry signal; nonetheless the implication of this result is consistent with the view that trafficking of syt4 to vesicles inhibits their fusion. The analysis of the time courses of syt7-pHluorin events with or without syt4-mCherry revealed that those associated with syt4-mCherry decayed more slowly (figure 6.2.2 A). The median decay time was 16.8 s for the Syt7-pHluorin+Syt4-mCherry group and 4.7 s for the Syt7-pHluorin only group. It was observed that 44% of Syt7-pHluorin+Syt4-mCherry events could not be described by a single exponential, suggesting a very slow endocytosis/reacidification, while this was only observed in 17% of the Syt7-pHluorin only events. Syt7-pHluorin HHD was also significantly larger in the presence of syt4-mCherry (median = 9.1 s) than in its absence (median = 6.3s, figure 6.2.2 C). The HHD frequency distributions also showed a shift of syt7-pHluorin events towards larger HHD in the presence of syt4-mCherry (figure 6.2.2 E, F), which may suggest that overexpression of syt4 shifts syt7-mediated fusion towards slower kinetics. The median of syt7-pHluorin event amplitudes was also significantly larger in the presence (8569) than in the absence (2459) of syt4-mCherry (figure 6.2.1 B). These results suggest that the fusion kinetics of vesicles bearing syt7 can vary, and that co-expression with syt4 impacts upon this kinetics, favouring slower events.

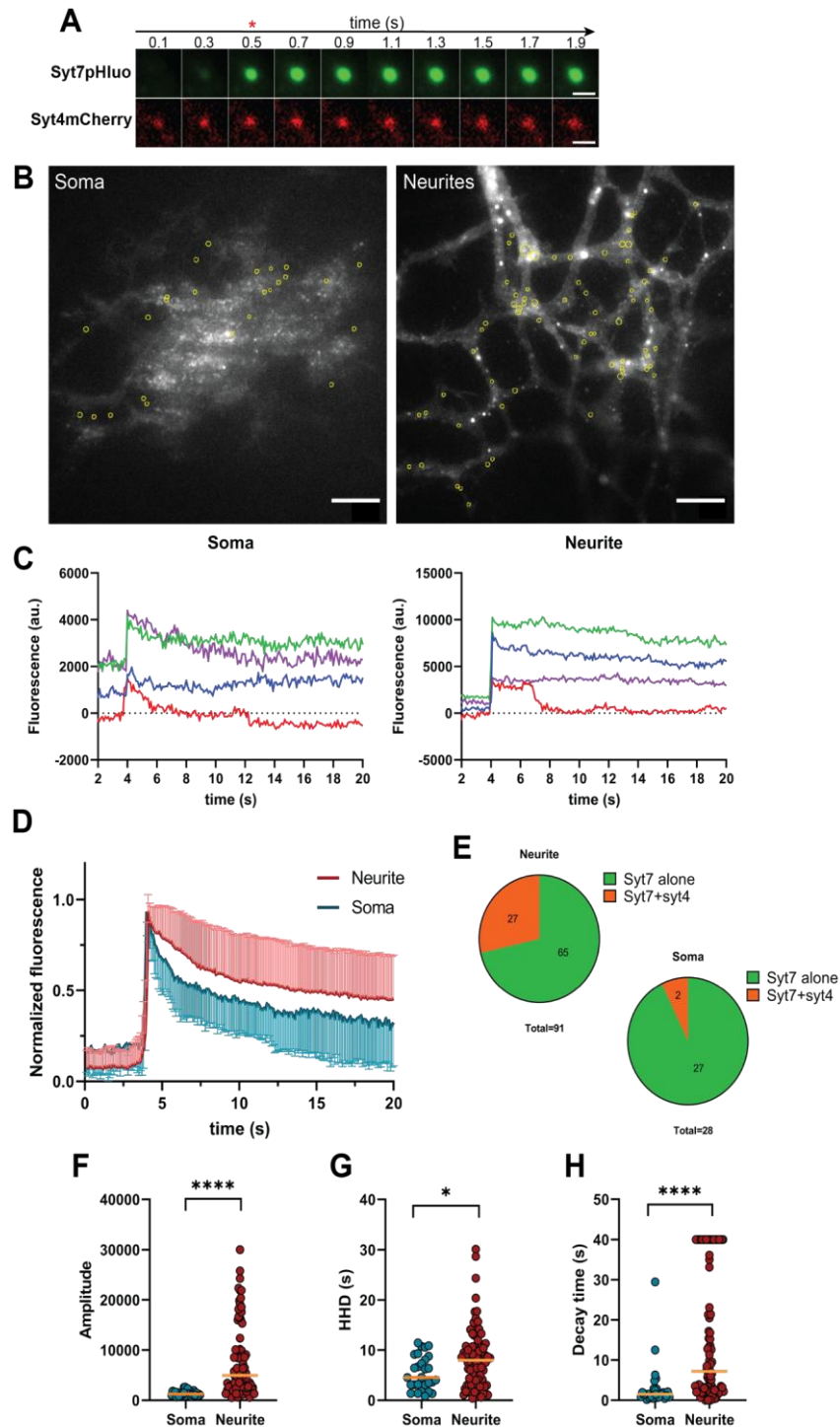


**Figure 6.2.1 Syt7-pHluorin fusion events differ on the soma and neurites.** A, montage of a syt7-pHluorin event with syt4-mCherry. Scale bar = 1  $\mu$ m, red star above the 0.6 s frame indicates the initial time of fusion. B, TIRF images of example soma or neurites, with yellow circles indicating fusion events. C shows corresponding examples of syt7-pHluorin events. D, averaged time-courses (mean  $\pm$  SD) of syt7-pHluorin events from neurites (n = 90) and soma (n = 29). E, pie charts showing the number of syt7-pHluorin events that occurred with or without syt4-mCherry on the same vesicle. F-H, scatter plots of syt7-pHluorin amplitudes, HHD and decay time on the soma and neurites. Orange lines indicate medians. \*\*\*\*p < 0.0001, \*p = 0.038, Mann-Whitney test.

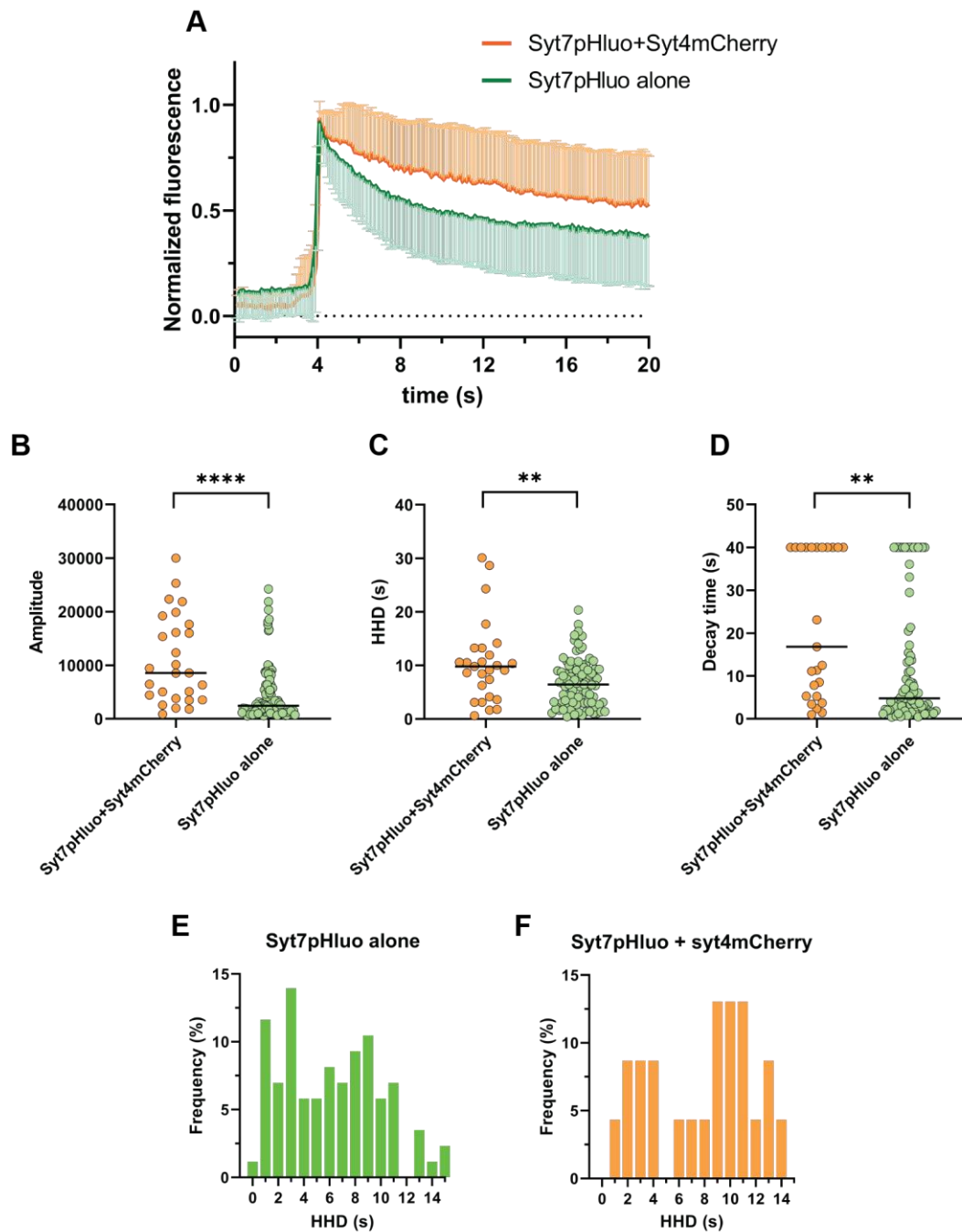


**Figure 6.2.2 Syt4-mCherry favours syt7-mediated events with slower kinetics.** A, averaged time-courses (mean  $\pm$  SD) of syt7-pHluorin events with (n = 29, orange symbols) or without (n = 91, green symbols) syt4-mCherry at the same vesicle. B-D, scatter plots of syt7-pHluorin amplitudes, HHD and decay time with or without syt4-mCherry. Black lines indicate medians. \*\*p=0.01 on C and 0.002 on D, \*\*\*\*p<0.0001, Mann-Whitney test. E-F, frequency histograms of syt7-pHluorin events with or without syt4-mCherry. Bin width = 1 s.

### 6.3. The kinetics of syt7-pHluorin events are altered in syt4<sup>-/-</sup> mice

In the previous experiments, the effects of overexpressing syt4-Cherry on syt7-mediated vesicle fusion were monitored in syt4<sup>+/-</sup> cells and found that the expression of syt4-mCherry slowed fusion kinetics. To better understand the possible impact of Syt4 on Syt7-mediated vesicle fusion, we transfected syt4<sup>-/-</sup> DRG neurons with syt7-pHluorin and compared these events to events recorded from syt4<sup>+/-</sup> neurons (see section 6.3). Due to the limited number of knockout mice in our colony, only two transfection experiments were possible; four out of 10 transfected neurons responded to KCl stimulation with measurable increases in pHluorin fluorescence. Similar to previous observations, the majority of fusion events (89%, n=18) were detected in the neurites; comparisons were made therefore between events observed in the neurites from DRG neurons isolated from syt4<sup>+/-</sup> and syt4<sup>-/-</sup> mice.

Analysis of the kinetics of syt7-pHluorin events in the neurites revealed that fusion events in syt4<sup>-/-</sup> DRGs have faster kinetics of decay than events in syt4<sup>+/-</sup> DRGs (figure 6.3 A). This was reflected in a shorter decay time (median = 3.6 s in the syt4<sup>-/-</sup> compared with 26.4 s in the syt4<sup>+/-</sup> cells, figure 6.3 D), while the HHD remained similar in both groups (8.5 and 8.8 s in the syt4<sup>+/-</sup> and syt4<sup>-/-</sup> cells, respectively). Analysis of the decay time frequency distributions showed that in the absence of syt4, there was a higher percentage of fast decaying events, while there was a higher percentage of events in the 40 s bin in the presence of syt4 (those that did not decay exponentially). This suggests that the presence of syt4 promotes syt7-pHluorin events with slower decay.

Comparison of the fluorescence amplitudes also revealed significantly lower values in the KO neurons (medians were 2529 and 9435 in the syt4<sup>-/-</sup> and syt4<sup>+/-</sup> cells respectively, figure 6.3 B). This is in agreement with the previous results (figure 6.2 B), but what this difference in the event amplitudes reflects exactly is unclear (see discussion, section 6.6). Taken together, the results of this and the previous section indicate that syt4 and syt7 can be trafficked to the same secretory vesicles in sensory neurons and provide evidence that syt4 alters the dynamics of exo/endocytosis of syt7 vesicles towards slower kinetics.

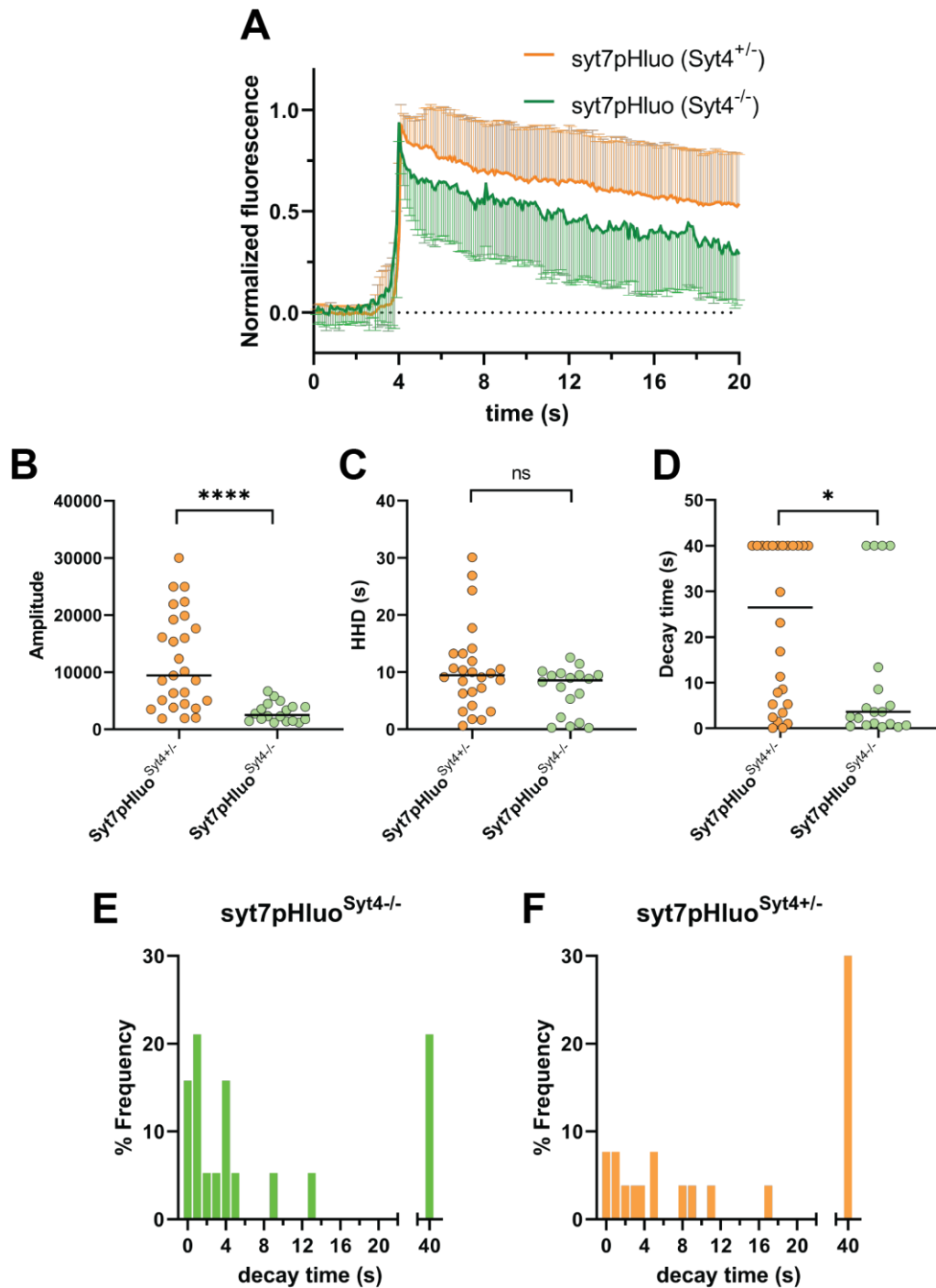


**Figure 6.3 The kinetics of syt7-pHluorin events is altered in syt4<sup>-/-</sup> mice.** A, averaged fluorescence time courses (mean  $\pm$  SD) of syt7-pHluorin fusion events in syt4<sup>-/-</sup> (n = 18) and syt4<sup>+/-</sup> (n = 27) cells. B-D, scatter plots of syt7-pHluorin amplitude, HHD and decay time in syt4<sup>-/-</sup> and syt4<sup>+/-</sup> cells. \*p=0.02, \*\*\*\*p < 0.0001, ns = not significant, Mann-Whitney test. Black lines indicate medians. E-F, frequency distribution of syt7-pHluorin decay times in syt4<sup>-/-</sup> and syt4<sup>+/-</sup> cells. Bin width is 1 s in the first section of the graph, the second section shows the 40 s bin containing those events that could not be fit with an exponential decay function.

## 6.4. Trafficking dynamics of Syt4-S135A and S135E-mCherry

Having established that syt4 favours longer lasting fusion events, we next investigated whether syt4 phosphorylation at the S135 site alters its influence on Syt7 fusion dynamics. We used the previously described phosphomutants: the phosphodeficient S135A and phosphomimetic S135E syt4 tagged to mCherry (Bharat et al., 2017). In these phosphomutants, a serine at the 135 site in the syt4 protein was changed to either an alanine or a glutamic acid to yield the phosphodeficient and phosphomimetic syt4 mutants respectively. First, we performed kymograph analysis to monitor their impact on vesicle trafficking dynamics. Kymographs and measurements of vesicle mobility (speed, pause duration, pause frequency) and the number of mobile vesicles were assessed and pooled from neurons imaged in the absence of any exogenous stimulus. Although information about directionality of vesicle movement (ie. anterograde or retrograde) has been extracted from the analysis, but we are unable to ascribe it as anterograde or retrograde, ie. whether the vesicle tracked was moving towards or away from the soma. This was because sensory neurons in culture often do not recapitulate the pseudounipolar morphology observed *in vivo* but instead grow complex and highly ramified neurites whose origins are difficult to identify. Thus, these vesicles were pooled into a “mobile vesicles” group, regardless of which way they moved. Frequency histograms of vesicle velocities revealed that S135A-syt4-mCherry and S135E-syt4-mCherry show similar distributions of speeds, but with more slow vesicles measured in cells expressing the S135E-syt4-mCherry mutant (figure 6.4.1F). This is reflected in a significantly lower mean speed of  $0.7 \pm 0.5 \mu\text{m/s}$  compared to  $0.8 \pm 0.5 \mu\text{m/s}$  in the S135A-syt4-mCherry mutant (figure 6.4.1B). Comparison of the pause frequencies between the two mutants (mean =  $1.6 \pm 1.9$  and  $1.5 \pm 1.4$  pauses/sec for S135A and S135E respectively) revealed no significant difference. The average pause duration however was significantly higher in the phosphomimetic s135E-syt4-mCherry ( $13.3 \pm 22.9$  s with 95% confidence limit (CL) of 1.8) compared to the s135A syt4-mCherry phosphodeficient mutant ( $10 \pm 19.5$  s with 95% confidence limit of 1.2, figure 6.4.1D). This suggests that vesicles bearing S135E-syt4-mCherry do not stop more frequently but their pauses last longer, consistent with vesicle capture and docking that would be needed to precede exocytosis. Additionally, there were also more mobile vesicles recorded on average in neurites expressing S135A-syt4-mCherry ( $7.8 \pm 7.6$ , with 95% CL of 1.7) than S135E-syt4-mCherry (4.5

$\pm 3.8$ , with 95% CL of 0.8, figure 6.4.1 E), suggesting that syt4 phosphorylation at S135 reduces vesicle mobility.

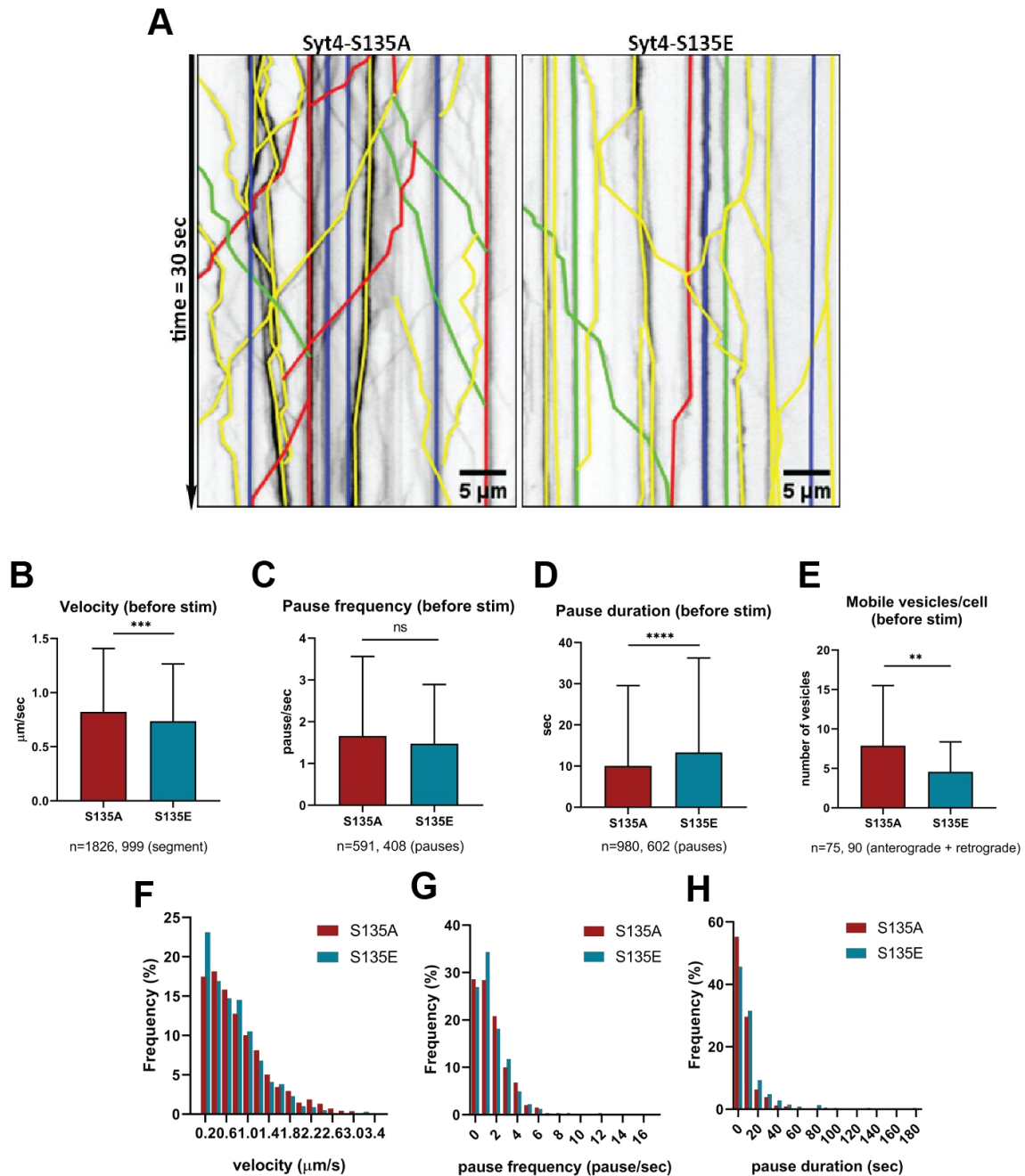


**Figure 6.4.1. Kymograph analysis of syt4-S135A and S135E before stimulation.** **A**, kymographs showing the tracks (coloured lines) of S135A-syt4-mCherry or S135E-ssyt4-mCherry labelled vesicles. Colours indicate the net directionality of the vesicle, ie. red = anterograde, green = retrograde, yellow = reversal, blue = stationary. **B-E**, pooled vesicle mobility parameters (velocity, pause duration, pause frequency, number of mobile vesicles, mean  $\pm$  SD) of the S135A and S134E phosphomutants from three experiments (mean  $\pm$  SD). n numbers and their meaning are indicated below the graphs. \*\*p = 0.0019, \*\*\*p = 0.0005, \*\*\*\*p < 0.0001, ns = not significant, Mann-Whitney test. **F, G, H**, distribution of indicated mobility parameters of both phosphomutants, bin width = 0.2  $\mu\text{m}/\text{s}$  on G, 1 on I, and 10 s on K.

We then asked the question whether 40 mM KCl stimulation affect the mobility of phosphomutant-syt4-mCherry bearing vesicles. For this, we compared the vesicle mobility parameters before and right after the onset of stimulation (representative kymographs are shown on figure 6.4.2A, B). This analysis revealed that both phosphomutants had reduced speed during the stimulation; the average reduction was 0.11 in the S135A- and 0.09  $\mu\text{m/s}$  in the S135E-syt4-mCherry mutant (figure 6.4.2C, G). Interestingly, the pause duration was slightly but significantly increased after the onset of stimulation in the S135A-syt4-mCherry phosphodeficient, but not in the S135E-syt4-mCherry phosphomimetic mutant (figure 6.4.2D, H), while the pause frequencies did not change (figure 6.4.2 E, I). Thus, it appears that while under 'resting' conditions, as has been shown in the analysis above (figure 6.4.1), the S135E-syt4-mCherry phosphomimetic mutant pauses for longer times than the S135A-syt4-mCherry phosphodeficient mutant (figure 6.4.2D, J), but during stimulation, vesicles bearing S135A-syt4-mCherry increase their pause duration to around the same level as the phosphomimetic S135E-syt4-mCherry bearing ones. The number of mobile vesicles significantly decreased with both phosphomutants during stimulation (figure 6.4.2F, J), suggesting increased vesicle capture. Taken together, these results suggest that stimulation reduces syt4 vesicle mobility regardless of phosphorylation at the S135 site, and instead this site might be more important for vesicle docking at potential release sites before the onset of stimulation.

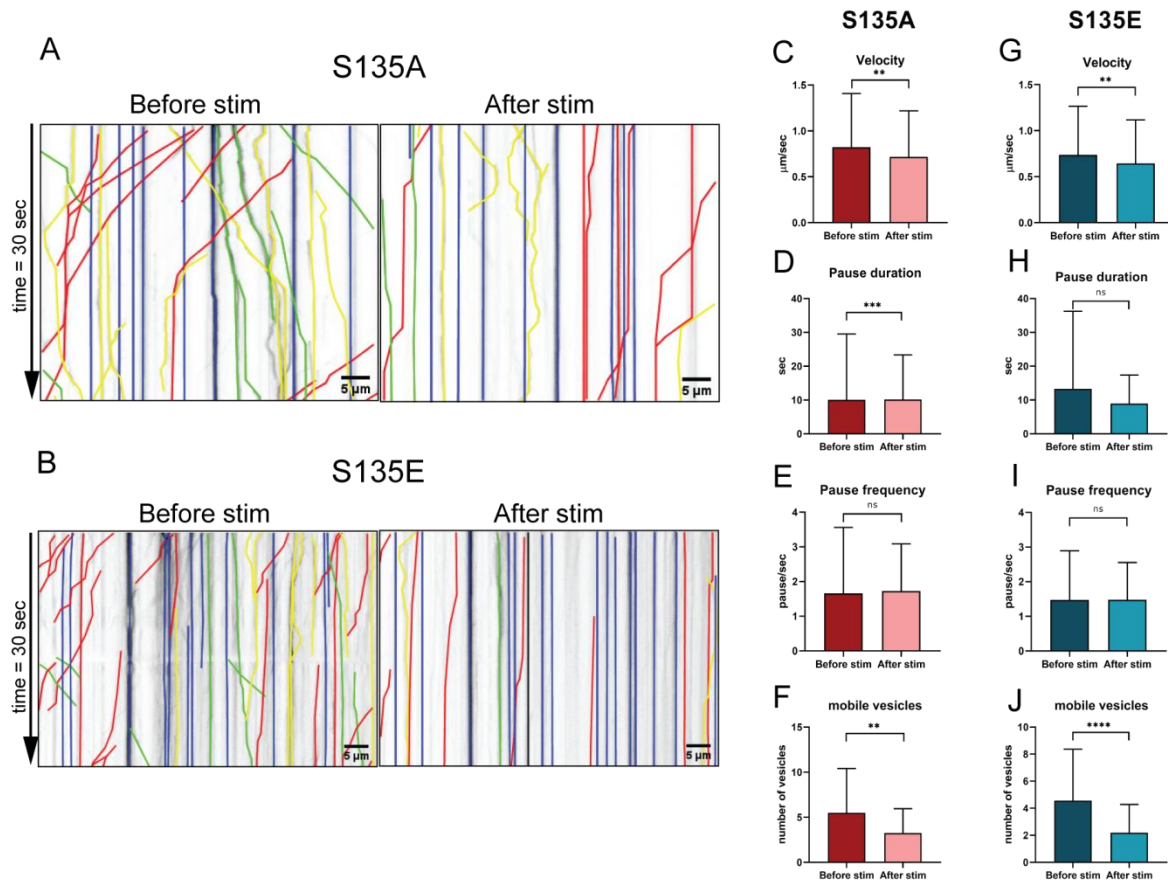


**Figure 6.4.2. Syt4 phosphomutants have reduced mobility after stimulation.** A-B, kymographs showing the tracks (coloured lines) of syt4-S135A or -S135E-labelled vesicles before and right after the onset of KCl stimulation. Colours indicate the net directionality of the vesicle, ie. red = anterograde, green = retrograde, yellow = reversal, blue = stationary. C-F, vesicle mobility parameters (mean  $\pm$  SD) of S135A before and during stimulation. \*\* $p < 0.005$ , \*\*\* $p = 0.0006$ , ns = not significant, Mann-Whitney test. G-J, same as C-F for S135E. \*\* $p < 0.005$ , \*\*\*\* $p < 0.0001$ .

## 6.5. S135 phosphorylation of syt4 shifts syt7 fusion events towards longer pore open time

Finally, to assess the potential effect of syt4 phosphorylation on syt7 mediated fusion, syt4<sup>+/-</sup> cells were transfected with syt7-pHluorin and with either S135E-syt4-mCherry or with 135A-syt4-mCherry. Syt7-pHluorin events were separated according to whether they also had phosphomutant-syt4-mCherry signal or not (therefore the three groups were syt7+S135A-syt4-mCherry, syt7+ S135E-syt4-mCherry, and syt7 alone).

In the syt7-pHluorin+S135A-syt4-mCherry co-transfection experiments, overall 170 syt7-pHluorin events were detected, 30% (52/170) of which also had S135A-syt4-mCherry signal (figure 6.5 A). In the syt7-pHluorin+S135E-syt4-mCherry experiments, 215 syt7-pHluorin events were detected, 17% (38/215) of which also had S135E-syt4-mCherry signal (figure 6.5 B). For further analysis, syt7-pHluorin alone events were pooled from the different experiments and compared to syt7-pHluorin+S135A/E-syt4-mCherry events. The averaged time-courses of syt7-pHluorin events were similar in the different groups (figure 6.5 C), with smaller differences in the later phase of fluorescence decay. Statistical analysis however revealed that there was no significant difference between either the event amplitudes or decay times (figure 6.5 D, F). The syt7-pHluorin amplitude medians were 3100, 3032 and 3007 with S135A-syt4-mCherry, S135E-syt4-mCherry or with no mCherry signal respectively (figure 6.5 D). The median decay time was the highest in the presence of the phosphodeficient S135A-syt4-mCherry mutant (3.2 s), while this was 1.9 s both in the presence of the phosphomimetic S135E-syt4-mCherry mutant and when syt7-pHluorin was not associated with either phosphomutants (figure 6.5 F). The percentage of slow events in the 40 s bin that could not be fit with an exponential decay was 5% in the syt7 alone group, 8% in the syt7-pHluorin+S135E-syt4-mCherry group and 19% in the syt7+S135A-syt4-mCherry group. This could suggest that the presence of the phosphodeficient S135A-syt4-mCherry mutant promotes a slower form of vesicle retrieval, but there was no significant difference in the decay times between groups.

Analysis of the syt7-pHluorin HHD showed that the median HHD was 4.8 s in the syt7 alone group, while it was 7 s in the presence of S135A-syt4-mCherry and 8.8 s in the presence of S135E-syt4-mCherry (figure 6.5 E). Although the median HHD in the latter two groups was significantly higher than in the syt7 alone group, this significance was weak (\*p

<0.05, non-parametric Kruskal-Wallis test) and was likely due to the much larger n number in the syt7 alone group, as the mean values in each group were similar and not significantly different ( $6.8 \pm 3.7$  s,  $7.4 \pm 4.6$  s and  $5.7 \pm 5$  s in the syt7+S135A-syt4-mCherry, syt7+ S135E-syt4-mCherry, and syt7 alone groups respectively, ordinary one-way ANOVA). In conclusion, these results suggest that the phosphorylation of syt4 at serine-135 does not affect syt7-pHluorin mediated fusion kinetics.

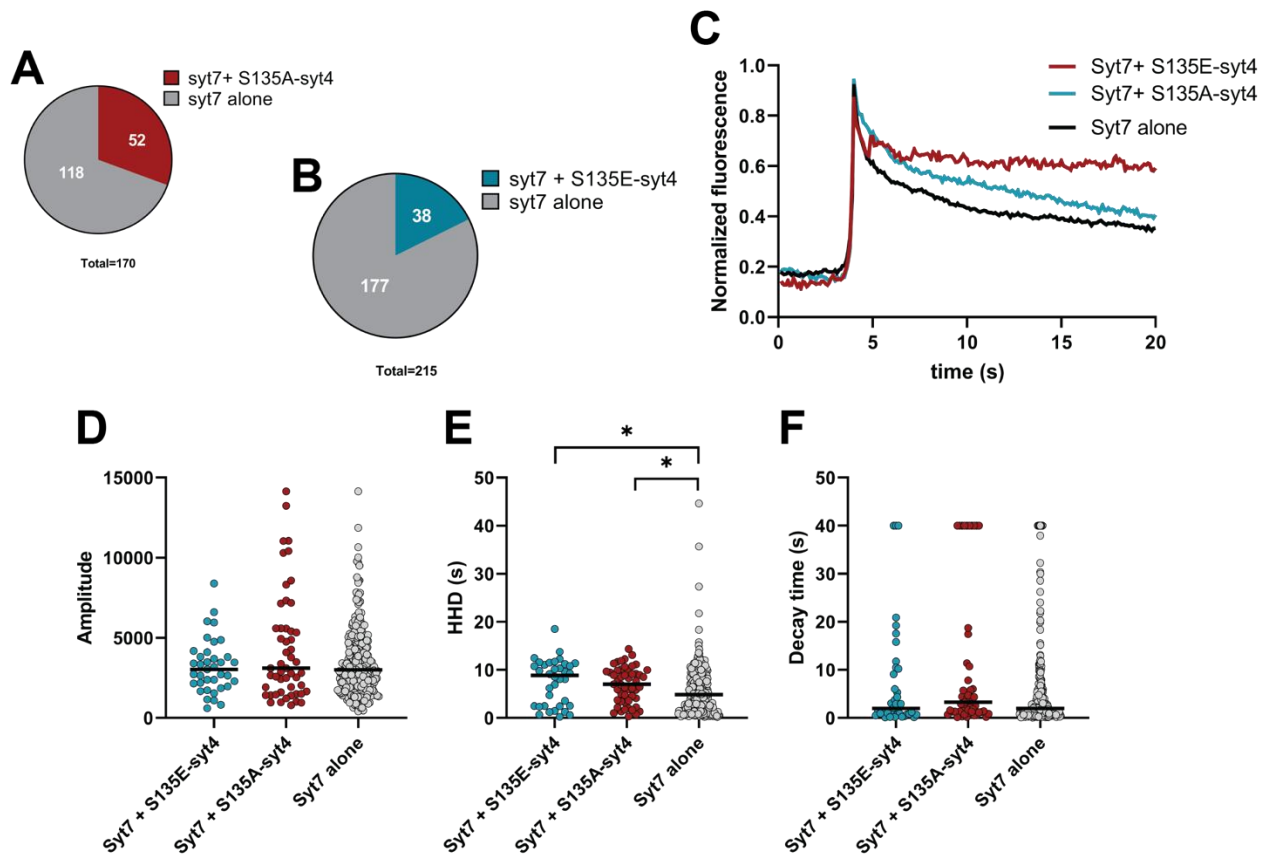


**Figure 6.5 Phosphorylation of syt4 at Serine-135 does not alter syt7-mediated fusion.** A-B, pie charts of syt7 events showing the fraction of events with S135A- or S135E-syt4-mCherry. B, averaged and normalized time-courses of syt7-pHluorin with S135A-syt4, S135E-syt4 or syt7-pHluorin alone. Error bars have been omitted for clarity. C-E, scatter plots of syt7-pHluorin amplitude, HHD and decay times with or without the syt4 phosphomutants. Horizontal black lines indicate median, \* $p < 0.05$ , Kruskal-Wallis test.

## 6.6. Conclusions

In this chapter, we set out to test whether the presence of syt4, or its phosphorylation at S135, affects the kinetics of syt7 mediated fusion. The main conclusion is that syt4 and 7 can be both trafficked to a subpopulation of vesicles, where syt4 alters syt7 mediated vesicle fusion by promoting slower/longer lasting fusion events. An observation was that syt7-pHluorin events had larger amplitudes in the presence of syt4-mCherry, or conversely had smaller amplitudes in syt4 KO cells. A possible explanation for this is that syt4 promotes the sorting of syt7 onto vesicles, which would result in more syt7-pHluorin molecules in the Syt4<sup>+/-</sup> cells, giving rise to larger amplitudes, while smaller amplitudes in syt4 KO cells. In support of this idea is that syt4 has a role in vesicle maturation in PC12 cells, and due to its ubiquitous expression in DRGs, we could assume a similar role in these cells too (see section 3.5). Nevertheless, we can conclude that syt4 promotes slower fusion and/or slower endocytosis, which has been shown in pituitary nerve terminals before (Zhang *et al.*, 2009)

We have also shown that syt4 phosphorylation at the S135 site does not appear to affect syt7 mediated fusion kinetics, nor the overall number of fusion events. Whether other phosphorylation sites on syt4 that were identified by us or others have any significance in syt4 function remains to be determined. Thus, it is the presence or absence of syt4 rather than its phosphorylation which alters syt7-mediated vesicle fusion by promoting slower fusion. How the slowed kinetics relates to content release would be important to address in further experiments. Though it is generally accepted that longer fusion allows for more content release whereas fast closure limits it, Shin *et al.* found that the majority of NPY release is fast, less than 2 s, and even as fast as 33 ms (Chiang *et al.*, 2014), but it can also be slow (~10 s) or even only partially released (Shin *et al.*, 2018). However, the true limiting factor is the size of the fusion pore, but we were unable to measure this in our experimental setup. If we consider the fusion pore to be dynamically changing, then during longer open times there is also a higher probability of a large enough fusion pore to allow fuller content release. To draw however any conclusion regarding cargo release, further experiments should employ the simultaneous monitoring of cargo (NPY or CGRP) release from syt7/syt4 tagged vesicles.

In chromaffin cells, syt7 regulates fusion pore dynamics and cargo release through its C2B domain, and  $\text{Ca}^{2+}$ -binding to this domain stabilizes the fusion pore (Segovia *et al.*, 2010; Bendahmane *et al.*, 2018). It is possible that in DRG neurons, syt4 forms complexes with syt7 to perhaps disrupt the  $\text{Ca}^{2+}$ -binding ability of Syt7 C2B domain, leading to more prolonged fusion pores (Chapman *et al.*, 1998; Bhalla, Chicka and Chapman, 2008). To understand the nature of a syt4-syt7 interaction in DRG neurons, future experiments should first confirm the direct interaction of these two proteins, although the imaging experiments showed that these two proteins can be sorted onto the same secretory vesicles. Furthermore, biochemical experiments could answer whether syt4 disrupts the  $\text{Ca}^{2+}$ -binding ability of the syt7 C2B domain or alters syt7 function in other ways.

The observation that syt7-pHluorin events were larger in magnitude on the neurites compared to the soma was consistent with the larger amplitudes and HHD seen on neurites with the VAMP2-, syt2- and syt4-pHluorin constructs (chapter 4). In hippocampal neurons, syt7 was found to exclusively recycle on axons with LDCV like characteristics, similar to syt4, and these syt7-pHluorin events were slow and had small amplitudes (Dean *et al.*, 2012). We observed syt7-pHluorin events on both the neurites and soma, but the ones on the neurites were larger in magnitude – these events had significantly larger amplitudes, slower decay and longer HHD (figure 6.2.1 F-H). pHluorin event amplitudes were consistently larger on the neurites with each syt construct, which supports the notion that these vesicles may be more mature or have got more synaptotagmin copies on them. The presence of more mature vesicles in axons/nerve terminals would also be consistent with the findings that the  $\text{Ca}^{2+}$  requirements of exocytosis are lower on nerve endings than on the soma (L. Y. M. Huang and Neher, 1996). The fact that more sy7 fusion events had syt4 associated with them on the neurites (figure 6.2.1 E) supports the notion that perhaps these were more mature vesicles. It should be noted here that although DRG neurons would not secrete peptides from their axons *in vivo*, the exocytic events we saw *in vitro* might represent the behaviour of vesicles that would normally be transported toward the axon endings and synapses.

Expression of the phosphomimetic S135E-syt4-mCherry mutant resulted in decreased vesicle mobility (velocity, pause duration, and the number of mobile vesicles, section 6.4). The values that we measured for these parameters are similar to what was measured before using the same constructs in hippocampal neurons (Bharat *et al.*, 2017).

Based on their results, Bharat et al. 2017 proposed a model whereby phosphorylation of syt4 by JNK breaks the interaction between syt4 and KIF1, the main anterograde motor protein in neurons, and this results in increased LDCV capture at synapses. After depolarization of the neurons with high KCl, the increased vesicle capture was dependent on the presence and phosphorylation of syt4. We found however that velocity and the number of mobile vesicles were similarly reduced in both phosphomutants after stimulation, but pause duration only decreased further with the phosphodeficient syt4 mutant, possibly because the phosphomimetic mutant already had decreased pause duration. This would imply that while syt4 phosphorylation at S135 increases the pause duration (and possibly vesicle capture) pre-stimulation, upon stimulation of the neurons both phosphodeficient and phosphomimetic syt4 have similar chance of being captured at release sites.

The main motors responsible for axonal trafficking in neurons are kinesins in the anterograde and dynein in the retrograde direction; LDCVs and SVs are thought to contain multiple kinesins and dyneins that dictate movement speed according to the “tug of war” model (Maday *et al.*, 2014). In DRG neurons, kinesin 1 and 3 control LDCV trafficking in a MAP2 dependent manner, where kinesin 1 acts as a “slower” motor with speeds of around 1  $\mu\text{m/s}$ , and kinesin 3 as a “fast” motor with a velocity of around 2  $\mu\text{m/s}$  and therefore the speed of a vesicle is thought to be generated by the interplay of these motor proteins (Gumy *et al.*, 2017). Syt4 was previously shown to be associated with kinesin 3 family protein Kif1a, however as in our experiments much slower Syt4 vesicle speed was measured compared to the average 2  $\mu\text{m/s}$  speed of Kif1a, it seems likely that other motor proteins, like kinesin 1 or dynein (which is also a slow motor protein) play a more dominant role in syt4 vesicle trafficking. Taken together, we have shown that syt4 and syt7 can be trafficked to the same vesicles in DRG neurons where they may interact, and provided evidence indicating that phosphorylation of syt4 at S135, a putative NGF signalling target, decreases vesicle mobility in DRG neurons.

## 7. General discussion

In this thesis, we set out to identify synaptotagmins controlling neuropeptide secretion from sensory neurons, to investigate their role in regulating LDCV exocytosis and in the process, establish methods for studying exocytosis directly in isolated DRG neurons. Four synaptotagmin isoforms have been described here in cultured DRG neurons for the first time: syt2, syt4, syt7 and syt11. Co-expression and colocalization analysis showed that these isoforms are expressed in peptidergic DRG neurons but are likely not limited to this single population, and that multiple isoforms may contribute to regulating CGRP release due to their presence on CGRP+ vesicles. Although ELISA experiments indicated that neither syt4 nor syt7 were indispensable for basal release, or release evoked by capsaicin or KCl, live-cell imaging clearly showed that syt4-bearing vesicles contained and released NPY. Syt4 could be involved in the maturation process of LDCVs in DRG neurons as supported by its Golgi-like localization (chapter 3), which could explain its presence on NPY-containing vesicles even if it does not directly regulate CGRP release under 'normal' conditions. However further CGRP ELISA experiments confirmed that syt4 has a role in NGF mediated potentiation of peptide release, as acute potentiation of KCl or capsaicin evoked CGRP release was decreased in the absence of syt4. The fact that this increased release was only reduced but not completely blocked suggests that there are probably multiple, parallel pathways involved in the NGF effect.

NGF is secreted during inflammation (see section 1.2), and binding to its main receptor TrkA leads to the activation of several signalling pathways. Activation of the PLC/PKC and Src family kinases (SFK) leads to the phosphorylation and sensitization of TRPV1 channels, while PI3 kinase/src signalling increases TRPV1 surface expression (Bhave et al., 2003; Zhang, Huang and McNaughton, 2005; Park et al., 2010). The increased TRPV1 activity leads to more  $Ca^{2+}$  influx which in turn increases peptide release (Park et al., 2010). Activation of the low affinity NGF receptor, p75, leads to the activation of JNK, which was shown in hippocampal neurons and PC12 cells to directly phosphorylate syt4 at Ser135 (Mori et al., 2008; Bharat et al., 2017), and in neurons, this caused the dissociation of syt4-bearing LDCVs from the microtubule motor Kif1a and increased capture at release sites. We have identified the same Ser135 phosphorylation site in DRG neurons in MS experiments, and found that phosphomimetic S135E-syt4-mCherry slowed vesicle mobility, increasing the

probability of capturing vesicles at release sites, but it did not affect syt7-mediated vesicle fusion. Syt7-pHluorin fusion events had however slower or faster kinetics in the presence or absence of syt4 respectively, implying that perhaps syt4 and syt7 interact in DRG neurons to modify vesicle fusion. Interaction of syt4 and syt7 was recently shown in pancreatic  $\beta$  cells (Huang *et al.*, 2018), and in these cells the calcium sensitivity of insulin secretion was altered by this interaction but individual fusion behaviour was not examined. Taken together, according to our results it seems likely that in DRG neurons, the main function of syt4 phosphorylation at S135 in the NGF pathway is to slow vesicle trafficking and increase vesicle capture without significantly affecting fusion.

Others previously showed that Kif1a is responsible for the trafficking of TrkA containing vesicles to the axon endings in DRG neurons (Tanaka *et al.*, 2016). The surface presentation of TrkA leads to a positive feedback loop, whereby upon NGF exposure, the increased TrkA-signalling leads to upregulation of Kif1a and increased TrkA transport to nerve endings. If syt4 is associated with Kif1a in DRG neurons, similarly to what was found in hippocampal neurons (Bharat *et al.*, 2017), then perhaps the same vesicles also contain TrkA (figure 7). Although we did not perform colocalization analysis of syt4 and TrkA, but we found that TrkA was mostly expressed in syt4 positive cells (section 5.3). In this case, the Ser135 phosphorylation of syt4 by JNK would lead to the reduced mobility and increased capture of these vesicles, as we have shown using kymograph analysis. Furthermore, live-cell imaging experiments showed that syt4 and syt7 are both present on a population of vesicles; further triple-labelling experiments would be needed to confirm whether these three proteins (syt4, syt7 and TrkA) actually reside on the same vesicles.

With regards to vesicle fusion behaviours as observed with pHluorin constructs, an important finding was that syt7 preferentially induces transient fusion events with stable fusion pores, as most of the syt7-pHluorin events were slow and stayed at the site of fusion for several seconds. The fact that syt7 preferentially promotes slow KR events agrees with results from chromaffin cells, where it also slowed down cargo release (Rao *et al.*, 2014; Bendahmane *et al.*, 2019). In DRG neurons, the activation of TRPV1 by capsaicin leads to weaker and more spatially restricted  $\text{Ca}^{2+}$  rise close to TRPV1 channels and more KR fusion, but all fusion events are near TRPV1 channels (Wang *et al.*, 2017). Stronger stimulation with KCl on the other hand leads to more robust and uniform  $\text{Ca}^{2+}$  rise near the membrane, resulting in more full fusion near VGCCs and importantly, KR events on the cell margins. This

study by Wang et al. provided evidence that differences in  $\text{Ca}^{2+}$  gradients near the membrane can control modes of fusion. As a high affinity calcium sensor with slow kinetics, syt7 is well-suited to trigger vesicle fusion following uniform  $\text{Ca}^{2+}$  rise or more distally from  $\text{Ca}^{2+}$  channels near the cell margins. These syt7-mediated events would be mostly KR as found by us and others (above), while at the same time syt4 may interact with syt7 to prolong the fusion pore lifetime, perhaps by stabilizing it (Figure 7). This could allow more time for peptide release or the diffusion of vesicular membrane proteins (such as TrkA, TRPV1 or other ion channels) into the plasma membrane. The increased surface presentation of TrkA in turn increases the NGF signalling in a positive feedback loop (Tanaka et al., 2016).

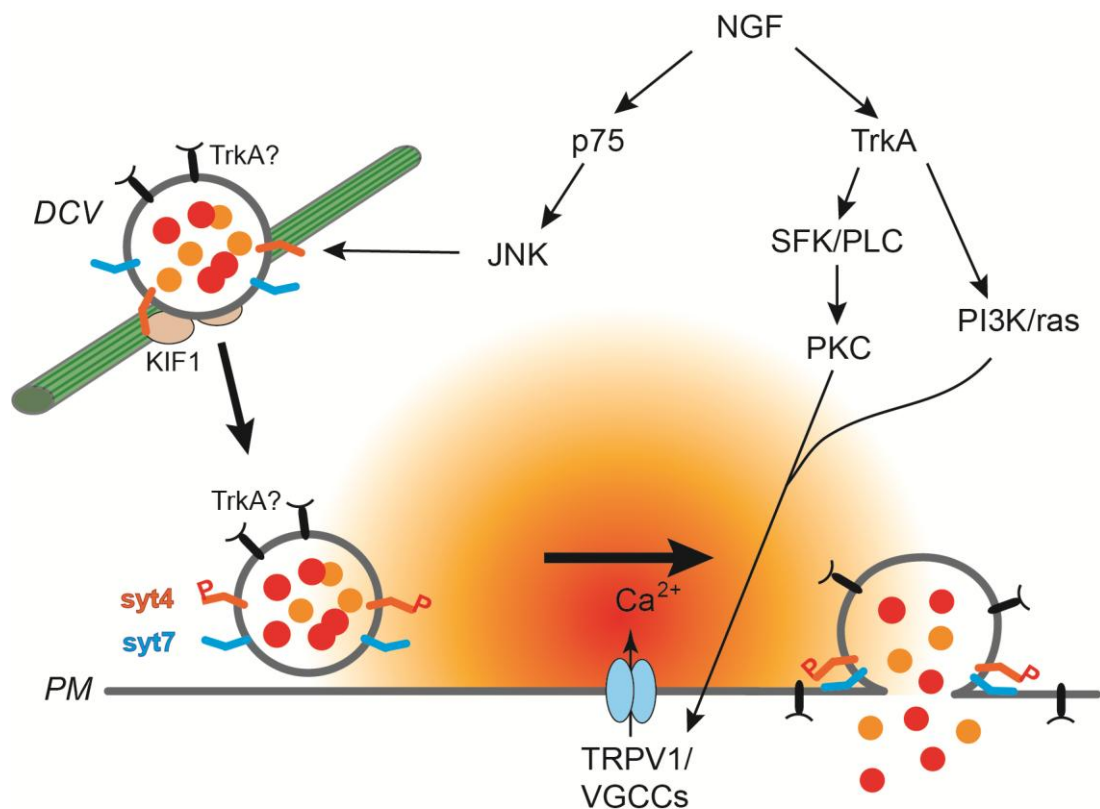


**Figure 7 Proposed pathways and mechanisms involved in NGF-induced increase of neuropeptide release in sensory neurons.** JNK activation through NGF/p75 leads to phosphorylation of syt4 (in orange, P tag = phosphorylation), reduced mobility of neuropeptide containing LDCVs (red and orange circles) inside the vesicle representing different co-stored neuropeptides (eg. CGRP, NPY), and dissociation from Kif1 and microtubules (green). TrkA (in black) may be present on the same vesicles, along with syt7 (in blue).  $\text{Ca}^{2+}$  influx through TRPV1 or VGCCs triggers syt7-mediated

transient fusion with long lasting fusion pores, allowing for more cargo release and surface presentation of TrkA receptors. Interaction of syt4 with syt7 may promote prolonged fusion, regardless of syt4 phosphorylation at S135E. The activation of TrkA receptors and related signalling pathways lead to further sensitization of TRPV1 channels.

As pointed out in sections 4.5 and 6.5, increased pore open time might not allow for more peptide release unless the pore is wide enough, and syt7 was found by several groups to restrict pore expansion and slow peptide release (Rao *et al.*, 2014; Bendahmane *et al.*, 2019). Keeping the fusion pore open for longer however might lead to slow and prolonged peptide release and their build-up at nerve terminals. This could contribute to windup, a form of short term synaptic plasticity where dorsal horn neurons respond with progressively increasing firing rates to repeated C-fibre inputs, and co-release of glutamate and neuropeptides are thought mediate the process (Ji *et al.*, 2003; D’Mello and Dickenson, 2008). It is also important to remember that LDCV recycling is slower than SV recycling, thus a slow but prolonged peptide release could compensate for the limited LDCV resupply at synapses and help to precisely regulate membrane recycling in neurons.

An important limitation of this work is that the results of syt4/7 mediated LDCV fusion in chapter 6 were not directly linked to peptide release or a peptidergic DRG population expressing TrkA or p75. In order to answer the question whether the possible interaction of syt4 and 7 plays a significant role in peptidergic neurons, imaging would have to be restricted to this population, using for example IB4 as a marker of non-peptidergic DRG neurons. This technique has been used historically, even though there is around 11-20% overlap on average between the IB4-binding and CGRP expressing populations (Li *et al.*, 2016; Shaib *et al.*, 2018). Identifying the peptidergic cells that also express NGF receptors and would be thus affected by NGF treatment is another level of complication, although according to our and others’ results, the majority of TrkA is expressed in the peptidergic population (sections 5.3 and 1.1).

The discrepancies in results from literature regarding exactly how syt4 and 7 regulate fusion pore might be better explained by a dynamic pore theory, rather than a simple choice between full fusion or KR (Shin *et al.*, 2018) (see section 1.2.5). Thus instead of readily distinguishing between two types of fusion, we measured the HHD and decay time of pFluorin-fusion events and related these to pore open time and vesicle retrieval. It should

be noted that the HHD values were measured by automatic peak detection of the Origin software, which may be inaccurate with very slowly decaying events, thus these are not exact measurements just approximations of the pore open/vesicle dwell times. According to our results and those from literature, syt7 triggers the fusion of LDCVs in lower/more generic elevation of calcium concentration, but the pore size and duration are differentially regulated based on other factors, such as stimulation strength/ $\text{Ca}^{2+}$  influx and interaction with other proteins, such as syt4 or actin cytoskeleton and microtubules.

To the best of our knowledge, syt4 or syt7 KO mice have not been tested for behavioural pain phenotypes, thus it would be pivotal to assess if the above model translates in vivo using mouse models of inflammatory pain. Though in this work we could only test the effects of NGF in syt4<sup>-/-</sup> animals, we would expect similar results in syt7 KO mice if the two proteins work together. The next step would be to confirm the interaction of syt4 and syt7 in biochemical experiments and link the changes in fusion pore dynamics to peptide release. Nevertheless, the results presented above provide insights into a possible mechanism by which nociceptive DRG neurons may increase neuropeptide release in the skin or the spinal cord during inflammation. Additionally, the live-imaging and analysis technique established here together with the results obtained on synaptotagmin-mediated fusion for the first time in DRG neurons provide valuable ground work for future research.

## References

- Acuna, C. *et al.* (2015) 'RIM-BPs Mediate Tight Coupling of Action Potentials to Ca(2+)-Triggered Neurotransmitter Release.', *Neuron*, 87(6), pp. 1234–47. doi: 10.1016/j.neuron.2015.08.027.
- Ahras, M., Otto, G. P. and Tooze, S. A. (2006) 'Synaptotagmin IV is necessary for the maturation of secretory granules in PC12 cells', *Journal of Cell Biology*, 173(2), pp. 241–251. doi: 10.1083/jcb.200506163.
- Albillos, A. *et al.* (1997) 'The exocytotic event in chromaffin cells revealed by patch amperometry', *Nature*. Nature Publishing Group, 389(6650), pp. 509–512. doi: 10.1038/39081.
- Alés, E. *et al.* (1999) 'High calcium concentrations shift the mode of exocytosis to the kiss-and-run mechanism.', *Nature cell biology*, 1, pp. 40–44. doi: 10.1038/9012.
- Amara, S. G. *et al.* (1985) 'Expression in brain of a messenger RNA encoding a novel neuropeptide homologous to calcitonin gene-related peptide', *Science*, 229(4718), pp. 1094–1097. doi: 10.1126/science.2994212.
- Anderson, L. E. and Seybold, V. S. (2004) 'Calcitonin gene-related peptide regulates gene transcription in primary afferent neurons', *Journal of Neurochemistry*, 91(6), pp. 1417–1429. doi: 10.1111/j.1471-4159.2004.02833.x.
- Andreev NYu *et al.* (1995) 'Peripheral administration of nerve growth factor in the adult rat produces a thermal hyperalgesia that requires the presence of sympathetic post-ganglionic neurones.', *Pain*, 63(1), pp. 109–15. doi: 10.1016/0304-3959(95)00024-m.
- Apfel, S. C. *et al.* (1996) 'Nerve growth factor regulates the expression of brain-derived neurotrophic factor mRNA in the peripheral nervous system', *Molecular and Cellular Neurosciences*, 7(2), pp. 134–142. doi: 10.1006/mcne.1996.0010.
- Atluri, P. P. (2006) 'The Kinetics of Synaptic Vesicle Reacidification at Hippocampal Nerve Terminals', *Journal of Neuroscience*, 26(8), pp. 2313–2320. doi: 10.1523/JNEUROSCI.4425-05.2006.

Axelrod, D. (2003) 'Total internal reflection microscopy in cell biology', *Methods in Enzymology*, 361(2), pp. 1–33.

Aziz, Q. *et al.* (2015) 'A classification of chronic pain for ICD-11', *Pain*, 156(6), pp. 1003–1007.

Bacaj, T. *et al.* (2013) 'Synaptotagmin-1 and Synaptotagmin-7 Trigger Synchronous and Asynchronous Phases of Neurotransmitter Release', *Neuron*, 80(4), pp. 947–959. doi: 10.1016/j.neuron.2013.10.026.

Bacaj, T. *et al.* (2015) 'Synaptotagmin-1 and -7 Are Redundantly Essential for Maintaining the Capacity of the Readily-Releasable Pool of Synaptic Vesicles', *PLOS Biology*, 13(10), p. e1002267. doi: 10.1371/journal.pbio.1002267.

Bacia, K. *et al.* (2004) 'SNAREs prefer liquid-disordered over "raft" (liquid-ordered) domains when reconstituted into giant unilamellar vesicles', *Journal of Biological Chemistry*. American Society for Biochemistry and Molecular Biology, 279(36), pp. 37951–37955. doi: 10.1074/jbc.M407020200.

Bai, J. *et al.* (2004) 'Fusion Pore Dynamics Are Regulated by Synaptotagmin•t-SNARE Interactions', *Neuron*, 41(6), pp. 929–942. doi: 10.1016/S0896-6273(04)00117-5.

Balaji, J. and Ryan, T. A. (2007) 'Single-vesicle imaging reveals that synaptic vesicle exocytosis and endocytosis are coupled by a single stochastic mode', *Proceedings of the National Academy of Sciences*, 104(51), pp. 20576–20581. doi: 10.1073/pnas.0707574105.

Balkowiec, A. and Katz, D. M. (2000) 'Activity-Dependent Release of Endogenous Brain-Derived Neurotrophic Factor from Primary Sensory Neurons Detected by ELISA In Situ', *The Journal of Neuroscience*, 20(19), pp. 7417–7423. doi: 10.1523/jneurosci.20-19-07417.2000.

Bannister, K., Kucharczyk, M. and Dickenson, A. H. (2017) 'Hopes for the Future of Pain Control', *Pain and Therapy*. Springer Healthcare, 6(2), pp. 117–128. doi: 10.1007/s40122-017-0073-6.

Bao, H. *et al.* (2016) 'Exocytotic fusion pores are composed of both lipids and

proteins', *Nature Structural and Molecular Biology*. Nature Publishing Group, 23(1), pp. 67–73. doi: 10.1038/nsmb.3141.

Bao, H. *et al.* (2018) 'Dynamics and number of trans-SNARE complexes determine nascent fusion pore properties', *Nature*. Nature Publishing Group, 554(7691), pp. 260–263. doi: 10.1038/nature25481.

Barber, C. F. *et al.* (2009) 'Postsynaptic regulation of synaptic plasticity by synaptotagmin 4 requires both C2 domains', *Journal of Cell Biology*, 187(2), pp. 295–310. doi: 10.1083/jcb.200903098.

Barg, S., Olofsson, C. S. and Rorsman, P. (2001) 'Delay between fusion pore opening and peptide release from insulin-containing granules in Ins-1 cells', *Diabetologia*, 44, pp. A61–A61.

Bauer, R. A. *et al.* (2004) 'Recycling of intact dense core vesicles in neurites of NGF-treated PC12 cells', *FEBS Letters*. John Wiley & Sons, Ltd, 571(1–3), pp. 107–111. doi: 10.1016/j.febslet.2004.05.086.

Bendahmane, M. *et al.* (2018) 'The synaptotagmin C2B domain calcium-binding loops modulate the rate of fusion pore expansion', *Molecular Biology of the Cell*. Edited by P. J. Brennwald, 29(7), pp. 834–845. doi: 10.1091/mbc.E17-11-0623.

Bendahmane, M. *et al.* (2019) 'Synaptotagmin-7 endows a population of chromaffin cell vesicles with enhanced calcium sensing and delayed content release properties', (7). doi: 10.1101/704205.

Bennett, D. L. H. *et al.* (1996) 'Postnatal changes in the expression of the trkA high-affinity NGF receptor in primary sensory neurons', *European Journal of Neuroscience*, 8(10), pp. 2204–2208. doi: 10.1111/j.1460-9568.1996.tb00742.x.

Berton, F. *et al.* (1997) 'Developmental regulation of synaptotagmin I, II, III, and IV mRNAs in the rat CNS.', *The Journal of neuroscience : the official journal of the Society for Neuroscience*, 17(4), pp. 1206–1216.

Betz, W. J. and Bewick, G. S. (1992) 'Optical analysis of synaptic vesicle recycling at the frog neuromuscular junction', *Science*. American Association for the Advancement of Science, 255(5041), pp. 200–203. doi: 10.1126/science.1553547.

Beuret, N. *et al.* (2004) 'Expression of Regulated Secretory Proteins Is Sufficient to Generate Granule-like Structures in Constitutively Secreting Cells\*'. doi: 10.1074/jbc.M310613200.

Bhalla, A., Chicka, M. C. and Chapman, E. R. (2008) 'Analysis of the Synaptotagmin Family during Reconstituted Membrane Fusion', *Journal of Biological Chemistry*, 283(31), pp. 21799–21807. doi: 10.1074/jbc.M709628200.

Bhalla, A., Tucker, W. C. and Chapman, E. R. (2005) 'Synaptotagmin Isoforms Couple Distinct Ranges of Ca<sup>2+</sup>, Ba<sup>2+</sup>, and Sr<sup>2+</sup> Concentration to SNARE-mediated Membrane Fusion', *Molecular Biology of the Cell*, 16(10), pp. 4755–4764. doi: 10.1091/mbc.e05-04-0277.

Bharat, V. *et al.* (2017) 'Capture of Dense Core Vesicles at Synapses by JNK-Dependent Phosphorylation of Synaptotagmin-4', *Cell Reports*. The Author(s), 21(8), pp. 2118–2133. doi: 10.1016/j.celrep.2017.10.084.

Bhave, G. *et al.* (2003) 'Protein kinase C phosphorylation sensitizes but does not activate the capsaicin receptor transient receptor potential vanilloid 1 (TRPV1)', *Proceedings of the National Academy of Sciences of the United States of America*, 100(21), pp. 12480–12485. doi: 10.1073/pnas.2032100100.

Bodmer, D., Ascaño, M. and Kuruvilla, R. (2011) 'Isoform-Specific Dephosphorylation of Dynamin1 by Calcineurin Couples Neurotrophin Receptor Endocytosis to Axonal Growth', *Neuron*, 70(6), pp. 1085–1099. doi: 10.1016/j.neuron.2011.04.025.

Bohannon, K. P. *et al.* (2017) 'Slow fusion pore expansion creates a unique reaction chamber for co-packaged cargo', *The Journal of General Physiology*, p. jgp.201711842. doi: 10.1085/jgp.201711842.

Bolte, S. and Cordelieres, F. P. (2006) 'A guided tour into subcellular colocalisation analysis in light microscopy', *Journal of Microscopy*, 224(3), pp. 13–232. doi: 10.1111/j.1365-2818.2006.01706.x.

Bonini, Sergio *et al.* (1996) 'Circulating nerve growth factor levels are increased in humans with allergic diseases and asthma', *Proceedings of the National Academy of*

*Sciences of the United States of America*, 93(20), pp. 10955–10960. doi: 10.1073/pnas.93.20.10955.

Bost, A. *et al.* (2017) 'Large dense-core vesicle exocytosis from mouse dorsal root ganglion neurons is regulated by neuropeptide Y', *Neuroscience*. IBRO, 346, pp. 1–13. doi: 10.1016/j.neuroscience.2017.01.006.

Brain, S. D. *et al.* (1985) 'Calcitonin gene-related peptide is a potent vasodilator', *Nature*, 313(5997), pp. 54–56. doi: 10.1038/313054a0.

Braun, M. *et al.* (2007) 'Corelease and Differential Exit via the Fusion Pore of GABA, Serotonin, and ATP from LDCV in Rat Pancreatic  $\beta$  Cells', *The Journal of General Physiology*, 129(3), pp. 221–231. doi: 10.1085/jgp.200609658.

Brose, N. *et al.* (1992) 'Synaptotagmin: A calcium sensor on the synaptic vesicle surface', *Science*, 256(5059), pp. 1021–1025. doi: 10.1126/science.1589771.

Carr, P. A., Yamamoto, T. and Nagy, J. I. (1990) 'Calcitonin gene-related peptide in primary afferent neurons of rat: Co-existence with fluoride-resistant acid phosphatase and depletion by neonatal capsaicin', *Neuroscience*, 36(3), pp. 751–760. doi: 10.1016/0306-4522(90)90017-X.

Carr, R. W. *et al.* (2009) 'Action potential initiation in the peripheral terminals of cold-sensitive neurones innervating the guinea-pig cornea', *Journal of Physiology*, 587(6), pp. 1249–1264. doi: 10.1113/jphysiol.2008.167023.

Chai, Z., Wang, C., Huang, R., Wang, Y., *et al.* (2017) 'Ca<sub>v</sub>2.2 Gates Calcium-Independent but Voltage-Dependent Secretion in Mammalian Sensory Neurons', *Neuron*, 96(6), pp. 1317–1326.e4. doi: 10.1016/j.neuron.2017.10.028.

Chai, Z., Wang, C., Huang, R., Wang, Y. Y., *et al.* (2017) 'Ca<sub>v</sub>2.2 Gates Calcium-Independent but Voltage-Dependent Secretion in Mammalian Sensory Neurons', *Neuron*, 96(6), pp. 1317–1326.e4. doi: 10.1016/j.neuron.2017.10.028.

Chanaday, N. L. and Kavalali, E. T. (2018) 'Optical detection of three modes of endocytosis at hippocampal synapses', *eLife*, 7. doi: 10.7554/eLife.36097.

Chanat, E., Weiß, U. and Huttner, W. B. (1994) 'The disulfide bond in chromogranin

B, which is essential for its sorting to secretory granules, is not required for its aggregation in the trans-Golgi network', *FEBS Letters*. John Wiley & Sons, Ltd, 351(2), pp. 225–230. doi: 10.1016/0014-5793(94)00865-5.

Chang, D. S. *et al.* (2016) 'Anti-nerve growth factor in pain management: Current evidence', *Journal of Pain Research*, 9, pp. 373–383. doi: 10.2147/JPR.S89061.

Chao, M. V. (2003) 'Neurotrophins and their receptors: A convergence point for many signalling pathways', *Nature Reviews Neuroscience*, 4(4), pp. 299–309. doi: 10.1038/nrn1078.

Chapman, E. R. *et al.* (1995) 'Ca<sup>2+</sup> regulates the interaction between synaptotagmin and syntaxin 1', *Journal of Biological Chemistry*, 270(40), pp. 23667–23671. doi: 10.1074/jbc.270.40.23667.

Chapman, E. R. *et al.* (1996) 'A novel function for the second C2 domain of synaptotagmin: Ca<sup>2+</sup>-triggered dimerization', *Journal of Biological Chemistry*, 271(10), pp. 5844–5849. doi: 10.1074/jbc.271.10.5844.

Chapman, E. R. *et al.* (1998) 'Delineation of the oligomerization, AP-2 binding, and synprint binding region of the C2B domain of synaptotagmin', *Journal of Biological Chemistry*, 273(49), pp. 32966–32972. doi: 10.1074/jbc.273.49.32966.

Chapman, E. R. and Jahn, R. (1994) 'Calcium-dependent Interaction of the Cytoplasmic Region of Synaptotagmin with Membranes: Autonomous Function of a Single C2-Homologous Domain', *Journal of Biological Chemistry*, 269(8), pp. 5735–5741.

Chiang, H. C. *et al.* (2014) 'Post-fusion structural changes and their roles in exocytosis and endocytosis of dense-core vesicles', *Nature Communications*. Nature Publishing Group, 5, pp. 1–15. doi: 10.1038/ncomms4356.

Chin, L. S., Vavalle, J. P. and Li, A. (2002) 'Staring, a novel E3 ubiquitin-protein ligase that targets syntaxin 1 for degradation', *Journal of Biological Chemistry*, 277(38), pp. 35071–35079. doi: 10.1074/jbc.M203300200.

Chiu, I. M. *et al.* (2014) 'Transcriptional profiling at whole population and single cell levels reveals somatosensory neuron molecular diversity.', *eLife*, 3, p. e04660. doi: 10.7554/eLife.04660.

Choksi, T. *et al.* (2002) 'Comparison of the expression of calcitonin receptor-like receptor (CRLR) and receptor activity modifying proteins (RAMPs) with CGRP and adrenomedullin binding in cell lines', *British Journal of Pharmacology*, 136(5), pp. 784–792. doi: 10.1038/sj.bjp.0704761.

Chow, R. H., von Rüden, L. and Neher, E. (1992) 'Delay in vesicle fusion revealed by electrochemical monitoring of single secretory events in adrenal chromaffin cells', *Nature*. Plenum, 356(6364), pp. 60–63. doi: 10.1038/356060a0.

Coleman, J. L. J. *et al.* (2015) 'Rapid knockout and reporter mouse line generation and breeding colony establishment using EUCOMM conditional-ready embryonic stem cells: A case study', *Frontiers in Endocrinology*, 6(JUN), p. 105. doi: 10.3389/fendo.2015.00105.

Craxton, M. (2004) 'Synaptotagmin gene content of the sequenced genomes', *BMC Genomics*, 5, pp. 1–14. doi: 10.1186/1471-2164-5-43.

D'Mello, R. and Dickenson, A. H. (2008) 'Spinal cord mechanisms of pain', *British Journal of Anaesthesia*, 101(1), pp. 8–16. doi: 10.1093/bja/aen088.

Dai, H. *et al.* (2004) 'Structural basis for the evolutionary inactivation of Ca<sup>2+</sup> binding to synaptotagmin 4', *Nat Struct Mol Biol*, 11(9), pp. 844–849. doi: 10.1038/nsmb817\rmsmb817 [pii].

Davletov, B. A. and Südhof, T. C. (1993) 'A single C2 domain from synaptotagmin I is sufficient for high affinity Ca<sup>2+</sup>/phospholipid binding.', *The Journal of biological chemistry*, 268(35), pp. 26386–90. Available at: [http://www.jbc.org/content/268/35/26386.abstract?ijkey=b2ee1b673df1af71318644be357e3487501c79cb&keytype2=tf\\_ipsecsha](http://www.jbc.org/content/268/35/26386.abstract?ijkey=b2ee1b673df1af71318644be357e3487501c79cb&keytype2=tf_ipsecsha).

Dean, C. *et al.* (2009) 'Synaptotagmin-IV modulates synaptic function and long-term potentiation by regulating BDNF release', *Nature Neuroscience*, 12(6), pp. 767–776. doi: 10.1038/nn.2315.

Dean, C. *et al.* (2012) 'Axonal and dendritic synaptotagmin isoforms revealed by a pHluorin-syt functional screen', *Molecular Biology of the Cell*. Edited by P. Brennwald, 23(9), pp. 1715–1727. doi: 10.1091/mbc.e11-08-0707.

Debus, K. and Lindau, M. (2000) 'Resolution of patch capacitance recordings and of fusion pore conductances in small vesicles', *Biophysical Journal*, 78(6), pp. 2983–2997. doi: 10.1016/S0006-3495(00)76837-8.

Delcroix, J.-D. *et al.* (2003) 'NGF Signaling in Sensory Neurons: Evidence that Early Endosomes Carry NGF Retrograde Signals', *Neuron*, 39(1), pp. 69–84. doi: 10.1016/S0896-6273(03)00397-0.

Deng, L. *et al.* (2011) 'RIM proteins activate vesicle priming by reversing autoinhibitory homodimerization of munc13', *Neuron*, 69(2), pp. 317–331. doi: 10.1016/j.neuron.2011.01.005.

Dhara, M. *et al.* (2016) 'v-SNARE transmembrane domains function as catalysts for vesicle fusion', *eLife*, 5. doi: 10.7554/eLife.17571.

Díaz-Vera, J. *et al.* (2010) 'Chromogranin B gene ablation reduces the catecholamine cargo and decelerates exocytosis in chromaffin secretory vesicles', *Journal of Neuroscience*, 30(3), pp. 950–957. doi: 10.1523/JNEUROSCI.2894-09.2010.

Díaz-Vera, J. *et al.* (2012) 'Chromogranins A and B are key proteins in amine accumulation, but the catecholamine secretory pathway is conserved without them', *The FASEB Journal*, 26(1), pp. 430–438. doi: 10.1096/fj.11-181941.

Dittié, A. S., Hajibagheri, N. and Tooze, S. A. (1996) 'The AP-1 adaptor complex binds to immature secretory granules from PC12 cells, and is regulated by ADP-ribosylation factor', *Journal of Cell Biology*. The Rockefeller University Press, 132(4), pp. 523–536. doi: 10.1083/jcb.132.4.523.

Dittman, J. S. and Kaplan, J. M. (2006) 'Factors regulating the abundance and localization of synaptobrevin in the plasma membrane', *Proceedings of the National Academy of Sciences of the United States of America*. National Academy of Sciences, 103(30), pp. 11399–11404. doi: 10.1073/pnas.0600784103.

Dittrich, M. *et al.* (2013) 'An excess-calcium-binding-site model predicts neurotransmitter release at the neuromuscular junction', *Biophysical Journal*. Biophysical Society, 104(12), pp. 2751–2763. doi: 10.1016/j.bpj.2013.05.023.

Dominguez, N. *et al.* (2018) 'Dense-core vesicle biogenesis and exocytosis in

neurons lacking chromogranins A and B', *Journal of Neurochemistry*, 144(3), pp. 241–254. doi: 10.1111/jnc.14263.

Domínguez, N. *et al.* (2012) 'The functional role of chromogranins in exocytosis', in *Journal of Molecular Neuroscience*, pp. 317–322. doi: 10.1007/s12031-012-9736-2.

Dong, X. *et al.* (2001) 'A Diverse Family of GPCRs Expressed in Specific Subsets of Nociceptive Sensory Neurons', *Cell*, 106(5), pp. 619–632. doi: 10.1016/S0092-8674(01)00483-4.

Du, W. *et al.* (2016) 'HID-1 is required for homotypic fusion of immature secretory granules during maturation', *eLife*, 5(OCTOBER2016), pp. 1–22. doi: 10.7554/eLife.18134.

Dunn, K. W., Kamocka, M. M. and McDonald, J. H. (2011) 'A practical guide to evaluating colocalization in biological microscopy', *AJP: Cell Physiology*, 300(4), pp. C723–C742. doi: 10.1152/ajpcell.00462.2010.

Dyck, P. J. *et al.* (1997) 'Intradermal recombinant human nerve growth factor induces pressure allodynia and lowered heat-pain threshold in humans.', *Neurology*, 48(2), pp. 501–5. doi: 10.1212/wnl.48.2.501.

Dzhashvili, Y. *et al.* (2007) 'Nodes of Ranvier and axon initial segments are ankyrin G-dependent domains that assemble by distinct mechanisms', *Journal of Cell Biology*, 177(5), pp. 857–870. doi: 10.1083/jcb.200612012.

Edvinsson, L. (2015) 'CGRP receptor antagonists and antibodies against CGRP and its receptor in migraine treatment', *British Journal of Clinical Pharmacology*, p. n/a-n/a. doi: 10.1111/bcp.12618.

Elhamdani, A. (2006) 'Double Patch Clamp Reveals That Transient Fusion (Kiss-and-Run) Is a Major Mechanism of Secretion in Calf Adrenal Chromaffin Cells: High Calcium Shifts the Mechanism from Kiss-and-Run to Complete Fusion', *Journal of Neuroscience*, 26(11), pp. 3030–3036. doi: 10.1523/jneurosci.5275-05.2006.

Emery, E. C. and Ernfors, P. (2018) 'Dorsal Root Ganglion Neuron Types and Their Functional Specialization', in Wood, J. N. (ed.) *The Oxford Handbook of the Neurobiology of Pain*. Oxford University Press, pp. 1–29. doi:

10.1093/oxfordhb/9780190860509.013.4.

Felmy, F. (2007) 'Modulation of cargo release from dense core granules by size and actin network', *Traffic*, 8(8), pp. 983–997. doi: 10.1111/j.1600-0854.2007.00583.x.

Ferguson, G. D. *et al.* (1999) 'Synthesis, degradation, and subcellular localization of synaptotagmin IV, a neuronal immediate early gene product', *Journal of Neurochemistry*, 72(5), pp. 1821–1831. doi: 10.1046/j.1471-4159.1999.0721821.x.

Ferguson, G. D. *et al.* (2000) 'Deficits in memory and motor performance in synaptotagmin IV mutant mice', *Proceedings of the National Academy of Sciences*, 97(10), pp. 5598–5603. doi: 10.1073/pnas.100104597.

Fernández-Chacón, R. *et al.* (2001) 'Synaptotagmin I functions as a calcium regulator of release probability.', *Nature*, 410(6824), pp. 41–49. doi: 10.1038/35065004.

Ferron, L. *et al.* (2014) 'Fragile X mental retardation protein controls synaptic vesicle exocytosis by modulating N-type calcium channel density', *Nature Communications*. Nature Publishing Group, 5, pp. 1–14. doi: 10.1038/ncomms4628.

Fukuda, M. *et al.* (2003) 'Nerve growth factor-dependent sorting of synaptotagmin IV protein to mature dense-core vesicles that undergo calcium-dependent exocytosis in PC12 cells', *Journal of Biological Chemistry*, 278(5), pp. 3220–3226. doi: 10.1074/jbc.M208323200.

Fukuda, M. *et al.* (2004) 'Synaptotagmin VII is targeted to dense-core vesicles and regulates their Ca<sup>2+</sup>-dependent exocytosis in PC12 cells', *Journal of Biological Chemistry*, 279(50), pp. 52677–52684. doi: 10.1074/jbc.M409241200.

Fulop, T. (2005) 'Activity-Dependent Differential Transmitter Release in Mouse Adrenal Chromaffin Cells', *Journal of Neuroscience*, 25(32), pp. 7324–7332. doi: 10.1523/jneurosci.2042-05.2005.

Fulop, T., Doreian, B. and Smith, C. (2008) 'Dynamin I plays dual roles in the activity-dependent shift in exocytic mode in mouse adrenal chromaffin cells', *Archives of Biochemistry and Biophysics*, 477(1), pp. 146–154. doi: 10.1016/j.abb.2008.04.039.

Fulop, T. and Smith, C. (2006) 'Physiological stimulation regulates the exocytic mode through calcium activation of protein kinase C in mouse chromaffin cells', *Biochemical Journal*, 399(1), pp. 111–119. doi: 10.1042/bj20060654.

Gandasi, N. R. *et al.* (2015) 'Survey of red fluorescence proteins as markers for secretory granule exocytosis', *PLoS ONE*, 10(6). doi: 10.1371/journal.pone.0127801.

Gandhl, S. P. and Stevens, C. F. (2003) 'Three modes of synaptic vesicular recycling revealed by single-vesicle imaging', *Nature*, 423(6940), pp. 607–613. doi: 10.1038/nature01677.

Gao, Z. *et al.* (2000) 'Synaptotagmin III/VII isoforms mediate Ca<sup>2+</sup>-induced insulin secretion in pancreatic islet B-cells', *Journal of Biological Chemistry*, 275(46), pp. 36079–36085. doi: 10.1074/jbc.M004284200.

Geppert, M. *et al.* (1994) 'Synaptotagmin I: A major Ca<sup>2+</sup> sensor for transmitter release at a central synapse', *Cell*, 79(4), pp. 717–727. doi: 10.1016/0092-8674(94)90556-8.

Goda, Y. and Stevens, C. F. (1994) 'Two components of transmitter release at a central synapse', *Proceedings of the National Academy of Sciences of the United States of America*, 91(26), pp. 12942–12946. doi: 10.1073/pnas.91.26.12942.

Gordon, S. L., Leube, R. E. and Cousin, M. a. (2011) 'Synaptophysin Is Required for Synaptobrevin Retrieval during Synaptic Vesicle Endocytosis', *Journal of Neuroscience*, 31(39), pp. 14032–14036. doi: 10.1523/JNEUROSCI.3162-11.2011.

Goswami, S. C. *et al.* (2014) 'Molecular Signatures of Mouse TRPV1-Lineage Neurons Revealed by RNA-Seq Transcriptome Analysis.', *The journal of pain : official journal of the American Pain Society*. Elsevier Ltd, 15(12), pp. 1338–59. doi: 10.1016/j.jpain.2014.09.010.

Goswami, T. *et al.* (2012) 'Comparative phosphoproteomic analysis of neonatal and adult murine brain', *Proteomics*, 12(13), pp. 2185–2189. doi: 10.1002/pmic.201200003.

Gould, H. J. *et al.* (2000) 'A possible role for nerve growth factor in the augmentation of sodium channels in models of chronic pain', *Brain Research*, 854(1–2),

pp. 19–29. doi: 10.1016/S0006-8993(99)02216-7.

Grabner, C. P. *et al.* (2006) *Regulation of large dense-core vesicle volume and neurotransmitter content mediated by adaptor protein 3*. Available at: [www.pnas.org/cgi/doi/10.1073/pnas.0509844103](http://www.pnas.org/cgi/doi/10.1073/pnas.0509844103) (Accessed: 28 February 2020).

Granseth, B. *et al.* (2006) 'Clathrin-Mediated Endocytosis Is the Dominant Mechanism of Vesicle Retrieval at Hippocampal Synapses', *Neuron*. Cell Press, 51(6), pp. 773–786. doi: 10.1016/j.neuron.2006.08.029.

Gumy, L. F. *et al.* (2017) 'MAP2 Defines a Pre-axonal Filtering Zone to Regulate KIF1- versus KIF5-Dependent Cargo Transport in Sensory Neurons', *Neuron*. Elsevier Inc., 94(2), pp. 347-362.e7. doi: 10.1016/j.neuron.2017.03.046.

Gustavsson, N. *et al.* (2008) 'Impaired insulin secretion and glucose intolerance in synaptotagmin-7 null mutant mice', *Proceedings of the National Academy of Sciences of the United States of America*. National Academy of Sciences, 105(10), pp. 3992–3997. doi: 10.1073/pnas.0711700105.

Gustavsson, N. and Han, W. (2009) 'Calcium-sensing beyond neurotransmitters: functions of synaptotagmins in neuroendocrine and endocrine secretion', *Biosci Rep*, 29(4), pp. 245–259. doi: 10.1042/BSR20090031.

Hakim, V. *et al.* (2016) 'The effects of proteasomal inhibition on synaptic proteostasis', *The EMBO Journal*, 35(20), pp. 2238–2262. doi: 10.15252/embj.201593594.

Han, S.-K. and Simon, M. I. (2011) 'Intracellular signaling and the origins of the sensations of itch and pain.', *Science signaling*, 4(185), p. pe38. doi: 10.1126/scisignal.2002353.

Han, Y. *et al.* (2015) 'RIM1 and RIM2 redundantly determine Ca<sup>2+</sup> channel density and readily releasable pool size at a large hindbrain synapse', *Journal of Neurophysiology*, 113(1), pp. 255–263. doi: 10.1152/jn.00488.2014.

Hartmann, J. and Lindau, M. (1995) 'A novel Ca<sup>2+</sup>-dependent step in exocytosis subsequent to vesicle fusion', *FEBS Letters*. John Wiley & Sons, Ltd, 363(3), pp. 217–220. doi: 10.1016/0014-5793(95)00318-4.

Hefti, F. F. *et al.* (2006) 'Novel class of pain drugs based on antagonism of NGF', *Trends in Pharmacological Sciences*, 27(2), pp. 85–91. doi: 10.1016/j.tips.2005.12.001.

von Hehn, C. A., Baron, R. and Woolf, C. J. (2012) 'Deconstructing the Neuropathic Pain Phenotype to Reveal Neural Mechanisms', *Neuron*. Elsevier Inc., 73(4), pp. 638–652. doi: 10.1016/j.neuron.2012.02.008.

Heuser, J. E. and Reese, T. S. (1981) 'Structural changes after transmitter release at the frog neuromuscular junction.', *The Journal of cell biology*. Rockefeller University Press, 88(3), pp. 564–80. doi: 10.1083/jcb.88.3.564.

Hinners, I. *et al.* (2003) 'AP-1 recruitment to VAMP4 is modulated by phosphorylation-dependent binding of PACS-1', *EMBO reports*. John Wiley & Sons, Ltd, 4(12), pp. 1182–1189. doi: 10.1038/sj.embor.7400018.

Hökfelt, T. *et al.* (2000) 'Neuropeptides - An overview', *Neuropharmacology*, 39(8), pp. 1337–1356. doi: 10.1016/S0028-3908(00)00010-1.

Hosaka, M. *et al.* (2002) 'Identification of a Chromogranin A Domain That Mediates Binding to Secretogranin III and Targeting to Secretory Granules in Pituitary Cells and Pancreatic-Cells', *Molecular Biology of the Cell*, 13, pp. 3388–3399. doi: 10.1091/mbc.02-03-0040.

Huang, C. *et al.* (2018) 'Synaptotagmin 4 Regulates Pancreatic  $\beta$  Cell Maturation by Modulating the Ca<sup>2+</sup> Sensitivity of Insulin Secretion Vesicles', *Developmental Cell*. Elsevier Inc., pp. 1–15. doi: 10.1016/j.devcel.2018.03.013.

Huang, L. Y. M. and Neher, E. (1996) 'Ca<sup>2+</sup> -dependent exocytosis in the somata of dorsal root ganglion neurons.', *Neuron*, 17, pp. 135–145.

Huang, L. Y. and Neher, E. (1996) 'Ca(2+)-dependent exocytosis in the somata of dorsal root ganglion neurons.', *Neuron*, 17(1), pp. 135–45. doi: S0896-6273(00)80287-1 [pii].

Hui, E. *et al.* (2005) 'Three distinct kinetic groupings of the synaptotagmin family: candidate sensors for rapid and delayed exocytosis.', *Proceedings of the National Academy of Sciences of the United States of America*, 102(14), pp. 5210–4. doi: 10.1073/pnas.0500941102.

Huttlin, E. L. *et al.* (2010) 'A Tissue-Specific Atlas of Mouse Protein Phosphorylation and Expression', *Cell*, 143(7), pp. 1174–1189. doi: 10.1016/j.cell.2010.12.001.

Ibata, K. *et al.* (2000) 'Synaptotagmin IV is present at the Golgi and distal parts of neurites', *Journal of Neurochemistry*, 74(2), pp. 518–526. doi: 10.1046/j.1471-4159.2000.740518.x.

Iyengar, S., Ossipov, M. H. and Johnson, K. W. (2017) 'The role of calcitonin gene-related peptide in peripheral and central pain mechanisms including migraine.', *Pain*, 158(4), pp. 543–559. doi: 10.1097/j.pain.0000000000000831.

Jackman, S. L. *et al.* (2016) 'The calcium sensor synaptotagmin 7 is required for synaptic facilitation', *Nature*. Nature Publishing Group, 529(7584), pp. 88–91. doi: 10.1038/nature16507.

Jackson, M. B. (2007) 'In search of the fusion pore of exocytosis', *Biophysical Chemistry*, 126(1–3), pp. 201–208. doi: 10.1016/j.bpc.2006.05.022.

Jaiswal, J. K. *et al.* (2004) 'Synaptotagmin VII restricts fusion pore expansion during lysosomal exocytosis', *PLoS Biology*, 2(8). doi: 10.1371/journal.pbio.0020233.

Jean Husten, E. and Eipper, B. A. (1994) 'Purification and characterization of PAM-1, an integral membrane protein involved in peptide processing', *Archives of Biochemistry and Biophysics*, 312(2), pp. 487–492. doi: 10.1006/abbi.1994.1336.

Jensen, T. S. *et al.* (2011) 'A new definition of neuropathic pain', *Pain. International Association for the Study of Pain*, 152(10), pp. 2204–2205. doi: 10.1016/j.pain.2011.06.017.

Ji, R.-R., Xu, Z.-Z. and Gao, Y.-J. (2014) 'Emerging targets in neuroinflammation-driven chronic pain.', *Nature reviews. Drug discovery*. Nature Publishing Group, 13(7), pp. 533–48. doi: 10.1038/nrd4334.

Ji, R. R. *et al.* (2002) 'p38 MAPK activation by NGF in primary sensory neurons after inflammation increases TRPV1 levels and maintains heat hyperalgesia', *Neuron*, 36(1), pp. 57–68. doi: 10.1016/S0896-6273(02)00908-X.

Ji, R. R. *et al.* (2003) 'Central sensitization and LTP: Do pain and memory share similar mechanisms?', *Trends in Neurosciences*, pp. 696–705. doi: 10.1016/j.tins.2003.09.017.

Johnson, S. L. *et al.* (2010) 'Synaptotagmin IV determines the linear Ca<sup>2+</sup> dependence of vesicle fusion at auditory ribbon synapses', *Nature Neuroscience*. Nature Publishing Group, 13(1), pp. 45–52. doi: 10.1038/nn.2456.

Joseloff, E. *et al.* (2002) 'Src family kinases phosphorylate protein kinase C  $\delta$  on tyrosine residues and modify the neoplastic phenotype of skin keratinocytes', *Journal of Biological Chemistry*, 277(14), pp. 12318–12323. doi: 10.1074/jbc.M111618200.

Kabayama, H. *et al.* (2017) 'Parkin promotes proteasomal degradation of synaptotagmin IV by accelerating polyubiquitination', *Molecular and Cellular Neuroscience*. Elsevier Inc., 80, pp. 89–99. doi: 10.1016/j.mcn.2017.02.006.

Kavalali, E. T. and Jorgensen, E. M. (2014) 'Visualizing presynaptic function.', *Nature neuroscience*. Nature Publishing Group, 17(1), pp. 10–6. doi: 10.1038/nn.3578.

Kerr, B. J. *et al.* (2001) 'A role for the TTX-resistant sodium channel Nav 1.8 in NGF-induced hyperalgesia, but not neuropathic pain', *NeuroReport*, 12(14), pp. 3077–3080. doi: 10.1097/00001756-200110080-00019.

Khan, N. and Smith, M. T. (2015) 'Neurotrophins and neuropathic pain: Role in pathobiology', *Molecules*, 20(6), pp. 10657–10688. doi: 10.3390/molecules200610657.

Kim, D. K. and Catterall, W. A. (1997) 'Ca<sup>2+</sup>-dependent and -independent interactions of the isoforms of the  $\alpha$ 1A subunit of brain Ca<sup>2+</sup> channels with presynaptic SNARE proteins', *Proceedings of the National Academy of Sciences of the United States of America*, 94(26), pp. 14782–14786. doi: 10.1073/pnas.94.26.14782.

Kim, T. *et al.* (2005) 'Chromogranin A deficiency in transgenic mice leads to aberrant chromaffin granule biogenesis', *Journal of Neuroscience*, 25(30), pp. 6958–6961. doi: 10.1523/JNEUROSCI.1058-05.2005.

Kim, T. *et al.* (2006) 'Dense-core secretory granule biogenesis', *Physiology*, 21(2), pp. 124–133. doi: 10.1152/physiol.00043.2005.

Klingauf, J., Kavalali, E. T. and Tsien, R. W. (1998) 'Kinetics and regulation of fast endocytosis at hippocampal synapses', *Nature*, 394(6693), pp. 581–585. doi: 10.1038/29079.

Kung, L. H. *et al.* (2013) 'Evidence for Glutamate as a Neuroglial Transmitter within Sensory Ganglia', *PLoS ONE*, 8(7). doi: 10.1371/journal.pone.0068312.

Latremoliere, A. and Woolf, C. J. (2009) 'Central Sensitization: A Generator of Pain Hypersensitivity by Central Neural Plasticity', *Journal of Pain*. Elsevier Ltd, 10(9), pp. 895–926. doi: 10.1016/j.jpain.2009.06.012.

Lee, H. *et al.* (2016) 'Advanced fluorescence protein-based synapse-detectors', *Frontiers in Synaptic Neuroscience*, 8(JUN), pp. 1–12. doi: 10.3389/fnsyn.2016.00016.

Li, C.-L. *et al.* (2016) 'Somatosensory neuron types identified by high-coverage single-cell RNA-sequencing and functional heterogeneity', *Cell Research*, 26(1), pp. 83–102. doi: 10.1038/cr.2015.149.

Li, C. *et al.* (1995) 'Ca<sup>2+</sup>-dependent and -independent activities of neural and non-neural synaptotagmins', *Nature*, pp. 594–599. doi: 10.1038/375594a0.

Li, C. *et al.* (2018) 'Somatosensory Neuron Typing with High-Coverage Single-Cell RNA Sequencing and Functional Analysis', *Neuroscience Bulletin*. Springer Singapore, 34(1), pp. 200–207. doi: 10.1007/s12264-017-0147-9.

Li, C., Davletov, B. a and Südhof, T. C. (1995) 'Distinct Ca<sup>2+</sup> and Sr<sup>2+</sup> Binding Properties of Synaptotagmins.', *The Journal of Biological Chemistry*, 270(42), pp. 24898–24902.

Li, Y. *et al.* (2007) 'Regulation of insulin secretion and GLUT4 trafficking by the calcium sensor synaptotagmin VII', *Biochemical and Biophysical Research Communications*, 362(3), pp. 658–664. doi: 10.1016/j.bbrc.2007.08.023.

Li, Y. C. *et al.* (2017) 'Synaptotagmin-1- and Synaptotagmin-7-Dependent Fusion Mechanisms Target Synaptic Vesicles to Kinetically Distinct Endocytic Pathways', *Neuron*. Elsevier, 93(3), pp. 616–631.e3. doi: 10.1016/j.neuron.2016.12.010.

Lin, M. Z. and Schnitzer, M. J. (2016) 'Genetically encoded indicators of neuronal

activity', *Nature neuroscience*, 19(9), pp. 1142–53. doi: 10.1038/nn.4359.

Lindsay, R. M. (1988) 'Nerve growth factors (NGF, BDNF) enhance axonal regeneration but are not required for survival of adult sensory neurons.', *The Journal of neuroscience : the official journal of the Society for Neuroscience*, 8(7), pp. 2394–405. Available at: <http://www.ncbi.nlm.nih.gov/pubmed/3249232> (Accessed: 29 July 2019).

Lindsay, R. M. and Harmar, A. J. (1989) 'Nerve growth factor regulates expression of neuropeptide genes in adult sensory neurons', *Nature*, 337(6205), pp. 362–364. doi: 10.1038/337362a0.

Littleton, J. T. *et al.* (1999) 'Synaptic function modulated by changes in the ratio of synaptotagmin I and IV', *Nature*, 400(6746), pp. 757–760. doi: 10.1038/23462.

Liu, H. *et al.* (2014) 'Synaptotagmin 7 functions as a Ca<sup>2+</sup>-sensor for synaptic vesicle replenishment', *eLIFE*, pp. 1–18. doi: 10.7554/eLife.01524.

Lollike, K., Borregaard, N. and Lindau, M. (1995) 'The exocytotic fusion pore of small granules has a conductance similar to an ion channel.', *The Journal of cell biology*. Rockefeller University Press, 129(1), pp. 99–104. doi: 10.1083/jcb.129.1.99.

López-Benito, S. *et al.* (2018) 'Regulation of BDNF Release by ARMS/Kidins220 through Modulation of Synaptotagmin-IV Levels', *The Journal of Neuroscience*, 38(23), pp. 5415–5428. doi: 10.1523/jneurosci.1653-17.2018.

Lundby, A. *et al.* (2012) 'Quantitative maps of protein phosphorylation sites across 14 different rat organs and tissues', *Nature Communications*, 3(1), p. 876. doi: 10.1038/ncomms1871.

Luo, F., Bacaj, T. and Südhof, T. C. (2015) 'Synaptotagmin-7 Is Essential for Ca<sup>2+</sup>-Triggered Delayed Asynchronous Release But Not for Ca<sup>2+</sup>-Dependent Vesicle Priming in Retinal Ribbon Synapses.', *The Journal of neuroscience : the official journal of the Society for Neuroscience*, 35(31), pp. 11024–33. doi: 10.1523/JNEUROSCI.0759-15.2015.

Luo, F. and Südhof, T. C. (2017) 'Synaptotagmin-7-Mediated Asynchronous Release Boosts High-Fidelity Synchronous Transmission at a Central Synapse', *Neuron*, 94(4), pp. 826–839.e3. doi: 10.1016/j.neuron.2017.04.020.

MacDougall, D. D. *et al.* (2018) 'The high-affinity calcium sensor synaptotagmin-7 serves multiple roles in regulated exocytosis', *The Journal of General Physiology*, 150(6), pp. 783–807. doi: 10.1085/jgp.201711944.

Machado, H. B. *et al.* (2004) 'Synaptotagmin IV Overexpression Inhibits Depolarization-Induced Exocytosis in PC12 Cells', *Journal of Neuroscience Research*, 76(3), pp. 334–341. doi: 10.1002/jnr.20072.

Maday, S. *et al.* (2014) 'Axonal Transport: Cargo-Specific Mechanisms of Motility and Regulation', *Neuron*. Cell Press, 84(2), pp. 292–309. doi: 10.1016/j.neuron.2014.10.019.

Malarkey, E. B. and Parpura, V. (2011) 'Temporal characteristics of vesicular fusion in astrocytes: Examination of synaptobrevin 2-laden vesicles at single vesicle resolution', *Journal of Physiology*, 589(17), pp. 4271–4300. doi: 10.1113/jphysiol.2011.210435.

Malin, S. a, Davis, B. M. and Molliver, D. C. (2007) 'Production of dissociated sensory neuron cultures and considerations for their use in studying neuronal function and plasticity.', *Nature protocols*, 2(1), pp. 152–160. doi: 10.1038/nprot.2006.461.

Mamet, J., Lazdunski, M. and Voilley, N. (2003) 'How nerve growth factor drives physiological and inflammatory expressions of acid-sensing ion channel 3 in sensory neurons.', *The Journal of biological chemistry*, 278(49), pp. 48907–48913. doi: 10.1074/jbc.M309468200.

Marquèze, B. *et al.* (1995) 'Cellular localization of synaptotagmin I, II, and III mRNAs in the central nervous system and pituitary and adrenal glands of the rat.', *The Journal of neuroscience : the official journal of the Society for Neuroscience*, 15(July), pp. 4906–4917.

Martinez, I. *et al.* (2000) 'Synaptotagmin vii regulates Ca<sup>2+</sup>-dependent exocytosis of lysosomes in fibroblasts', *Journal of Cell Biology*, 148(6), pp. 1141–1149. doi: 10.1083/jcb.148.6.1141.

Matsuda, N. *et al.* (2009) 'Differential Activity-Dependent Secretion of Brain-Derived Neurotrophic Factor from Axon and Dendrite', *Journal of Neuroscience*, 29(45),

pp. 14185–14198. doi: 10.1523/jneurosci.1863-09.2009.

Matsuda, S. *et al.* (1996) 'Dorsal root ganglion neuron development in chick and rat', *Anatomy and Embryology*, 193(5), pp. 475–480. doi: 10.1007/BF00185878.

Matteoli, M. *et al.* (1988) 'Differential effect of  $\alpha$ -latrotoxin on exocytosis from small synaptic vesicles and from large dense-core vesicles containing calcitonin gene-related peptide at the frog neuromuscular junction', *Proceedings of the National Academy of Sciences of the United States of America*, 85(19), pp. 7366–7370. doi: 10.1073/pnas.85.19.7366.

Matthew, W. D. (1981) 'Identification of a synaptic vesicle-specific membrane protein with a wide distribution in neuronal and neurosecretory tissue', *The Journal of Cell Biology*, 91(1), pp. 257–269. doi: 10.1083/jcb.91.1.257.

Mattheyses, A. L., Simon, S. M. and Rappoport, J. Z. (2010) 'Imaging with total internal reflection fluorescence microscopy for the cell biologist', *Journal of Cell Science*, pp. 3621–3628. doi: 10.1242/jcs.056218.

Maximov, A. *et al.* (2008) 'Genetic analysis of synaptotagmin-7 function in synaptic vesicle exocytosis', *Proceedings of the National Academy of Sciences*, 105(10), pp. 3986–3991. doi: 10.1073/pnas.0712372105.

Mendez, J. A. *et al.* (2011) 'Somatodendritic dopamine release requires synaptotagmin 4 and 7 and the participation of voltage-gated calcium channels', *Journal of Biological Chemistry*, 286(27), pp. 23928–23937. doi: 10.1074/jbc.M111.218032.

Meng, J. *et al.* (2007) 'Synaptobrevin I mediates exocytosis of CGRP from sensory neurons and inhibition by botulinum toxins reflects their anti-nociceptive potential.', *Journal of cell science*, 120(Pt 16), pp. 2864–2874. doi: 10.1242/jcs.012211.

Meng, J. *et al.* (2009) 'Activation of TRPV1 Mediates Calcitonin Gene-Related Peptide Release, Which Excites Trigeminal Sensory Neurons and Is Attenuated by a Retargeted Botulinum Toxin with Anti-Nociceptive Potential', *Journal of Neuroscience*, 29(15), pp. 4981–4992. doi: 10.1523/JNEUROSCI.5490-08.2009.

Meng, J. *et al.* (2016) 'TNF $\alpha$  induces co-trafficking of TRPV1/TRPA1 in VAMP1-containing vesicles to the plasmalemma via Munc18–1/syntaxin1/SNAP-25 mediated

fusion', *Scientific Reports*. Nature Publishing Group, 6(February), p. 21226. doi: 10.1038/srep21226.

Meng, J., Dolly, J. O. and Wang, J. (2014) 'Selective Cleavage of SNAREs in Sensory Neurons Unveils Protein Complexes Mediating Peptide Exocytosis Triggered by Different Stimuli.', *Molecular neurobiology*, pp. 574–588. doi: 10.1007/s12035-014-8665-1.

Merighi, A. *et al.* (2011) 'Neuromodulatory function of neuropeptides in the normal CNS', *Journal of Chemical Neuroanatomy*, 42(4), pp. 276–287. doi: 10.1016/j.jchemneu.2011.02.001.

Merighi, A. (2017) 'Neuropeptides and Coexistence', in *Encyclopedia of Neuroscience*. Elsevier, pp. 843–849. doi: 10.1016/B978-008045046-9.01467-4.

Merighi, A. (2018) 'Costorage of High Molecular Weight Neurotransmitters in Large Dense Core Vesicles of Mammalian Neurons', *Frontiers in Cellular Neuroscience*, 12(August), pp. 1–7. doi: 10.3389/fncel.2018.00272.

Miesenböck, G., De Angelis, D. a and Rothman, J. E. (1998) 'Visualizing secretion and synaptic transmission with pH-sensitive green fluorescent proteins.', *Nature*, 394(6689), pp. 192–5. doi: 10.1038/28190.

Mittelstaedt, T., Alvaréz-Baron, E. and Schoch, S. (2010) 'RIM proteins and their role in synapse function', *Biological Chemistry*, 391(6), pp. 599–606. doi: 10.1515/BC.2010.064.

Mohrmann, R. *et al.* (2013) 'Synaptotagmin interaction with SNAP-25 governs vesicle docking, priming, and fusion triggering', *Journal of Neuroscience*, 33(36), pp. 14417–14430. doi: 10.1523/JNEUROSCI.1236-13.2013.

Di Mola, F. F. *et al.* (2000) 'Nerve growth factor and Trk high affinity receptor (TrkA) gene expression in inflammatory bowel disease', *Gut*, 46(5), pp. 670–678. doi: 10.1136/gut.46.5.670.

Molliver, D. C. *et al.* (1997) 'IB4-binding DRG neurons switch from NGF to GDNF dependence in early postnatal life', *Neuron*, 19(4), pp. 849–861. doi: 10.1016/S0896-6273(00)80966-6.

Montesinos, M. S. *et al.* (2008) 'The crucial role of chromogranins in storage and exocytosis revealed using chromaffin cells from chromogranin A null mouse', *Journal of Neuroscience*, 28(13), pp. 3350–3358. doi: 10.1523/JNEUROSCI.5292-07.2008.

Moore-Dotson, J. M., Papke, J. B. and Harkins, A. B. (2010) 'Upregulation of synaptotagmin IV inhibits transmitter release in PC12 cells with targeted synaptotagmin I knockdown.', *BMC Neuroscience*, 11(1), p. 104. doi: 10.1186/1471-2202-11-104.

Morenilla-Palao, C. *et al.* (2004) 'Regulated exocytosis contributes to protein kinase C potentiation of vanilloid receptor activity', *Journal of Biological Chemistry*, 279(24), pp. 25665–25672. doi: 10.1074/jbc.M311515200.

Mori, Y. *et al.* (2008) 'JNK phosphorylates synaptotagmin-4 and enhances Ca<sup>2+</sup>-evoked release', *The EMBO Journal*, 27(1), pp. 76–87. doi: 10.1038/sj.emboj.7601935.

Mutch, S. A. *et al.* (2011) 'Protein quantification at the single vesicle level reveals that a subset of synaptic vesicle proteins are trafficked with high precision', *Journal of Neuroscience*, 31(4), pp. 1461–1470. doi: 10.1523/JNEUROSCI.3805-10.2011.

Nanavati, C. *et al.* (1992) 'The exocytotic fusion pore modeled as a lipidic pore', *Biophysical Journal*. Elsevier, 63(4), pp. 1118–1132. doi: 10.1016/S0006-3495(92)81679-X.

Nascimento, A. I., Mar, F. M. and Sousa, M. M. (2018) 'The intriguing nature of dorsal root ganglion neurons: Linking structure with polarity and function', *Progress in Neurobiology*. Elsevier, 168(May), pp. 86–103. doi: 10.1016/j.pneurobio.2018.05.002.

Nelson, M. T. *et al.* (1990) 'Arterial dilations in response to calcitonin gene-related peptide involve activation of K<sup>+</sup> channels.', *Nature*, 344(6268), pp. 770–3. doi: 10.1038/344770a0.

Ness, J. M. *et al.* (2003) 'Combined tyramide signal amplification and quantum dots for sensitive and photostable immunofluorescence detection', *Journal of Histochemistry and Cytochemistry*, 51(8), pp. 981–987. doi: 10.1177/002215540305100801.

Neumann, S. *et al.* (2017) 'KymoAnalyzer: a software tool for the quantitative analysis of intracellular transport in neurons', *Traffic*. John Wiley & Sons, Ltd (10.1111),

18(1), pp. 71–88. doi: 10.1111/tra.12456.

Nilsson, G. and Pernow, B. (1975) 'Substance P : Localization in the Central Nervous System and in Some Primary Sensory Neurons single fluorescent-positive fibers were seen Induction of F1 Hybrid Antiparent Cytotoxic Effector Cells : under the epithelium , and a network of', *Science (New York, N.Y.)*, 100(13), pp. 889–891.

Obermüller, S. *et al.* (2005) 'Selective nucleotide-release from dense-core granules in insulin-secreting cells', *Journal of Cell Science*, 118(18). doi: 10.1242/jcs.02549.

Obermüller, S. *et al.* (2010) 'Defective secretion of islet hormones in chromogranin-B deficient mice', *PLoS ONE*. Edited by K. Maedler. Public Library of Science, 5(1), p. e8936. doi: 10.1371/journal.pone.0008936.

Osborne, S. L. *et al.* (1999) 'Calcium-dependent oligomerization of synaptotagmins I and II: Synaptotagmins I and II are localized on the same synaptic vesicle and heterodimerize in the presence of calcium', *Journal of Biological Chemistry*, 274(1), pp. 59–66. doi: 10.1074/jbc.274.1.59.

Owen, D. E. and Egerton, J. (2012) 'Culture of Dissociated Sensory Neurons from Dorsal Root Ganglia of Postnatal and Adult Rats', in *Neurodegenerative Diseases: Neurobiology, Pathogenesis and Therapeutics*, pp. 179–187. doi: 10.1007/978-1-61779-536-7\_16.

Pang, Z. P. *et al.* (2006) 'Synaptotagmin-2 is essential for survival and contributes to Ca<sup>2+</sup> triggering of neurotransmitter release in central and neuromuscular synapses', *J Neurosci*, 26(52), pp. 13493–13504. doi: 10.1523/JNEUROSCI.3519-06.2006.

Park, K. A. *et al.* (2010) 'Signaling pathways that mediate nerve growth factor-induced increase in expression and release of calcitonin gene-related peptide from sensory neurons', *Neuroscience*. Elsevier Inc., 171(3), pp. 910–923. doi: 10.1016/j.neuroscience.2010.09.027.

Pasqua, T. *et al.* (2016) 'Impact of Chromogranin A deficiency on catecholamine storage, catecholamine granule morphology and chromaffin cell energy metabolism in vivo', *Cell and Tissue Research*, 363(3), pp. 693–712. doi: 10.1007/s00441-015-2316-3.

Patapoutian, A. and Reichardt, L. F. (2001) 'Trk receptors: mediators of neurotrophin action', pp. 281–286. doi: 10.1016/S0959-4388(00)00208-7.

Patel, T. D. *et al.* (2000) 'Development of sensory neurons in the absence of NGF/TrkA signaling in vivo', *Neuron*, 25(2), pp. 345–357. doi: 10.1016/S0896-6273(00)80899-5.

Peddie, C. J. *et al.* (2017) 'Correlative super-resolution fluorescence and electron microscopy using conventional fluorescent proteins in vacuo', *Journal of Structural Biology*. The Authors, 199(2), pp. 120–131. doi: 10.1016/j.jsb.2017.05.013.

Perin, M. S. *et al.* (1990) 'Phospholipid binding by a synaptic vesicle protein homologous to the regulatory region of protein kinase C', *Nature*, 345(6272), pp. 260–263. doi: 10.1038/345260a0.

Perin, M S *et al.* (1991) 'Domain structure of synaptotagmin (p65)', *The Journal of biological chemistry*, 266(1), pp. 623–9. Available at: <http://www.ncbi.nlm.nih.gov/pubmed/1985919>.

Perin, M.S. *et al.* (1991) 'Structural and functional conservation of synaptotagmin (p65) in *Drosophila* and humans', *The Journal of biological chemistry*, 266(January 5), pp. 615–622. Available at: <https://linkinghub.elsevier.com/retrieve/pii/S0169743910002248>.

Perrais, D. *et al.* (2004) 'Recapture after exocytosis causes differential retention of protein in granules of bovine chromaffin cells', *Journal of Physiology*. Wiley-Blackwell, 560(2), pp. 413–428. doi: 10.1113/jphysiol.2004.064410.

Pezet, S. and McMahon, S. B. (2006) 'NEUROTROPHINS: Mediators and Modulators of Pain', *Annual Review of Neuroscience*, 29(1), pp. 507–538. doi: 10.1146/annurev.neuro.29.051605.112929.

Le Pichon, C. E. and Chesler, A. T. (2014) 'The functional and anatomical dissection of somatosensory subpopulations using mouse genetics', *Frontiers in Neuroanatomy*. Frontiers Research Foundation, p. 21. doi: 10.3389/fnana.2014.00021.

Pinheiro, P. S., Houy, S. and Sørensen, J. B. (2016) 'C2-domain Containing Calcium Sensors in Neuroendocrine Secretion', *Journal of Neurochemistry*, pp. 1–16. doi:

10.1111/jnc.13865.

Poser, C. Von, Ichtchenko, K. and Shao, X. (1997) 'The Evolutionary Pressure to Inactivate', *the Journal of Biological Chemistry*, 272(22), pp. 14314–14319.

Price, T. J. and Flores, C. M. (2007) 'Critical Evaluation of the Colocalization Between Calcitonin Gene-Related Peptide, Substance P, Transient Receptor Potential Vanilloid Subfamily Type 1 Immunoreactivities, and Isolectin B4 Binding in Primary Afferent Neurons of the Rat and Mouse', *Journal of Pain*, 8(3), pp. 263–272. doi: 10.1016/j.jpain.2006.09.005.

Rao, T. C. *et al.* (2014) 'Distinct fusion properties of synaptotagmin-1 and synaptotagmin-7 bearing dense core granules.', *Molecular biology of the cell*, 25(16), pp. 2416–27. doi: 10.1091/mbc.E14-02-0702.

Rao, T. C. *et al.* (2017) 'Synaptotagmin isoforms confer distinct activation kinetics and dynamics to chromaffin cell granules', *The Journal of General Physiology*, p. jgp.201711757. doi: 10.1085/jgp.201711757.

Reinhold, A. K. *et al.* (2015) 'Differential transcriptional profiling of damaged and intact adjacent dorsal root ganglia neurons in neuropathic pain', *PLoS ONE*, 10(4), pp. 1–17. doi: 10.1371/journal.pone.0123342.

Rhee, J. S. *et al.* (2005) 'Augmenting neurotransmitter release by enhancing the apparent Ca<sup>2+</sup> affinity of synaptotagmin 1', *Proceedings of the National Academy of Sciences of the United States of America*, 102(51), pp. 18664–18669. doi: 10.1073/pnas.0509153102.

Richards, D. A., Guatimosim, C. and Betz, W. J. (2000) 'Two endocytic recycling routes selectively fill two vesicle pools in frog motor nerve terminals', *Neuron*. Cell Press, 27(3), pp. 551–559. doi: 10.1016/S0896-6273(00)00065-9.

Rizo, J., Chen, X. and Araç, D. (2006) 'Unraveling the mechanisms of synaptotagmin and SNARE function in neurotransmitter release', *Trends in Cell Biology*. Elsevier Ltd, 16(7), pp. 339–350. doi: 10.1016/j.tcb.2006.04.006.

Rizo, J. and Xu, J. (2015) 'The Synaptic Vesicle Release Machinery', *Annual Review of Biophysics*, 44(1), pp. 339–367. doi: 10.1146/annurev-biophys-060414-034057.

Rouwette, T. *et al.* (2016) 'Standardized profiling of the membrane-enriched proteome of mouse dorsal root ganglia provides novel insights into chronic pain.', *Molecular & cellular proteomics : MCP*, pp. 2152–2168. doi: 10.1074/mcp.M116.058966.

Russell, F. A. *et al.* (2014) 'Calcitonin Gene-Related Peptide: Physiology and Pathophysiology', *Physiological Reviews*, 94(4), pp. 1099–1142. doi: 10.1152/physrev.00034.2013.

Sacco, F. *et al.* (2016) 'Glucose-regulated and drug-perturbed phosphoproteome reveals molecular mechanisms controlling insulin secretion', *Nature Communications*, 7. doi: 10.1038/ncomms13250.

Sahl, S. J., Hell, S. W. and Jakobs, S. (2017) 'Fluorescence nanoscopy in cell biology', *Nature Reviews Molecular Cell Biology*. Nature Publishing Group, 18(11), pp. 685–701. doi: 10.1038/nrm.2017.71.

Salio, C. *et al.* (2006) 'Neuropeptides as synaptic transmitters', *Cell and Tissue Research*, 326(2), pp. 583–598. doi: 10.1007/s00441-006-0268-3.

Salio, C. *et al.* (2007) 'Costorage of BDNF and neuropeptides within individual dense-core vesicles in central and peripheral neurons', *Developmental Neurobiology*, 67(3), pp. 326–338. doi: 10.1002/dneu.20358.

Schirra, R. T. and Zhang, P. (2014) 'Correlative Fluorescence and Electron Microscopy', in *Current Protocols in Cytometry*. Hoboken, NJ, USA: John Wiley & Sons, Inc., pp. 12.36.1-12.36.10. doi: 10.1002/0471142956.cy1236s70.

Schneggenburger, R. and Rosenmund, C. (2015) 'Molecular mechanisms governing Ca<sup>2+</sup> regulation of evoked and spontaneous release', *Nature Neuroscience*, 18(7), pp. 935–941. doi: 10.1038/nn.4044.

Schonn, J. S. *et al.* (2008) 'Synaptotagmin-1 and -7 are functionally overlapping Ca<sup>2+</sup> sensors for exocytosis in adrenal chromaffin cells', *Proc Natl Acad Sci U S A*, 105(10), pp. 3998–4003. doi: 10.1073/pnas.0712373105

Segovia, M. *et al.* (2010) 'Push-and-pull regulation of the fusion pore by synaptotagmin-7.', *Proceedings of the National Academy of Sciences of the United States of America*, 107(44), pp. 19032–19037. doi: 10.1073/pnas.1014070107.

Shaib, A. H. *et al.* (2018) 'Paralogs of the Calcium-Dependent Activator Protein for Secretion Differentially Regulate Synaptic Transmission and Peptide Secretion in Sensory Neurons', *Frontiers in Cellular Neuroscience*, 12(September), pp. 1–17. doi: 10.3389/fncel.2018.00304.

Sharma, S. and Lindau, M. (2018) 'The fusion pore, 60 years after the first cartoon'. doi: 10.1002/1873-3468.13160.

Sheng, Z. U. H., Yokoyama, C. T. and Catterall, W. A. (1997) 'Interaction of the synprint site of N-type Ca<sup>2+</sup> channels with the C2B domain of synaptotagmin I', *Proceedings of the National Academy of Sciences of the United States of America*, 94(10), pp. 5405–5410. doi: 10.1073/pnas.94.10.5405.

Shin, W. *et al.* (2018) 'Visualization of Membrane Pore in Live Cells Reveals a Dynamic-Pore Theory Governing Fusion and Endocytosis', *Cell*. Elsevier Inc., 173(4), pp. 934-945.e12. doi: 10.1016/j.cell.2018.02.062.

Skarnes, W. C. *et al.* (2011) 'A conditional knockout resource for the genome-wide study of mouse gene function', *Nature*. Nature Publishing Group, 474(7351), pp. 337–344. doi: 10.1038/nature10163.

Sørensen, J. B. *et al.* (2003) 'Examining synaptotagmin 1 function in dense core vesicle exocytosis under direct control of Ca<sup>2+</sup>', *Journal of General Physiology*, 122(3), pp. 265–276. doi: 10.1085/jgp.200308855.

South, S. M. *et al.* (2003) 'A Conditional Deletion of the NR1 Subunit of the NMDA Receptor in Adult Spinal Cord Dorsal Horn Reduces NMDA Currents and Injury-Induced Pain', *The Journal of Neuroscience*, 23(12), pp. 5031–5040. doi: 10.1523/JNEUROSCI.23-12-05031.2003.

Spruce, A. E. *et al.* (1990) 'Properties of the fusion pore that forms during exocytosis of a mast cell secretory vesicle', *Neuron*. Cell Press, 4(5), pp. 643–654. doi: 10.1016/0896-6273(90)90192-I.

Stanzel, R. D. P., Lourenssen, S. and Blennerhassett, M. G. (2008) 'Inflammation causes expression of NGF in epithelial cells of the rat colon', *Experimental Neurology*, 211(1), pp. 203–213. doi: 10.1016/j.expneurol.2008.01.028.

Steenbergh, P. M. *et al.* (1986) 'Structure and expression of the human calcitonin/CGRP genes', *FEBS Letters*, 209(1), pp. 97–103. doi: 10.1016/0014-5793(86)81091-2.

Steiner, D. F. *et al.* (1992) 'The new enzymology of precursor processing endoproteases', *Journal of Biological Chemistry*, 267(33), pp. 23435–23438.

Stucky, C. L. and Lewin, G. R. (1999) 'Isolectin B(4)-positive and -negative nociceptors are functionally distinct.', *The Journal of neuroscience*, 19(15), p. 505. Available at: <http://www.ncbi.nlm.nih.gov/pubmed/10414978>.

Südhof, T. C. (2002) 'Synaptotagmins: Why so many?', *Journal of Biological Chemistry*, 277(10), pp. 7629–7632. doi: 10.1074/jbc.R100052200.

Südhof, T. C. (2013) 'Neurotransmitter release: The last millisecond in the life of a synaptic vesicle', *Neuron*, 80(2009), pp. 675–690. doi: 10.1016/j.neuron.2013.10.022.

Sugita, S. *et al.* (2001) 'Synaptotagmin VII as a plasma membrane Ca(2+) sensor in exocytosis.', *Neuron*, 30(2), pp. 459–73. doi: 10.1016/S0896-6273(01)00290-2.

Sugita, S. *et al.* (2002) 'Synaptotagmins form a hierarchy of exocytotic Ca<sup>2+</sup> sensors with distinct Ca<sup>2+</sup> affinities', *The EMBO Journal*, 21(3), pp. 270–280. doi: 10.1093/emboj/21.3.270.

Sun, J. *et al.* (2007) 'A dual-Ca<sup>2+</sup>-sensor model for neurotransmitter release in a central synapse', *Nature*, 450(7170), pp. 676–682. doi: nature06308 [pii]\r10.1038/nature06308.

Sun, M. *et al.* (2013) 'Multiple Sorting Systems for Secretory Granules Ensure the Regulated Secretion of Peptide Hormones', *Traffic*. John Wiley & Sons, Ltd, 14(2), pp. 205–218. doi: 10.1111/tra.12029.

Takamori, S. *et al.* (2006) 'Molecular Anatomy of a Trafficking Organelle', *Cell*, 127(4), pp. 831–846. doi: 10.1016/j.cell.2006.10.030.

Tanaka, Y. *et al.* (2016) 'The Molecular Motor KIF1A Transports the TrkA Neurotrophin Receptor and Is Essential for Sensory Neuron Survival and Function', *Neuron*. Elsevier Inc., 90(6), pp. 1215–1229. doi: 10.1016/j.neuron.2016.05.002.

Taraska, J. W. *et al.* (2003) 'Secretory granules are recaptured largely intact after stimulated exocytosis in cultured endocrine cells', *Proceedings of the National Academy of Sciences of the United States of America*, 100(4), pp. 2070–2075. doi: 10.1073/pnas.0337526100.

Thomas, D. M. *et al.* (1999) 'Functional and biochemical analysis of the C2 domains of synaptotagmin IV.', *Molecular biology of the cell*, 10(7), pp. 2285–2295.

Todd, A. J. (2010) 'Neuronal circuitry for pain processing in the dorsal horn.', *Nature reviews. Neuroscience*, 11(12), pp. 823–36. doi: 10.1038/nrn2947.

Tooze, J. and Tooze, S. A. (1986) 'Clathrin-coated vesicular transport of secretory proteins during the formation of ACTH-containing secretory granules in AtT20 cells', *Journal of Cell Biology*, 103(3), pp. 839–850. doi: 10.1083/jcb.103.3.839.

Tooze, S. A. (1991) 'Characterization of the immature secretory granule, an intermediate in granule biogenesis', *The Journal of Cell Biology*, 115(6), pp. 1491–1503. doi: 10.1083/jcb.115.6.1491.

Tsuboi, T. and Rutter, G. A. (2003) 'Multiple Forms of "Kiss-and-Run" Exocytosis Revealed by Evanescent Wave Microscopy', *Current Biology*, 13(7), pp. 563–567. doi: 10.1016/S0960-9822(03)00176-3.

Ullrich, B. *et al.* (1994) 'Functional properties of multiple synaptotagmins in brain', *Neuron*, 13(6), pp. 1281–1291. doi: 10.1016/0896-6273(94)90415-4.

Usoskin, D. *et al.* (2014) 'Unbiased classification of sensory neuron types by large-scale single-cell RNA sequencing', *Nature Neuroscience*. Nature Publishing Group, 18(1), pp. 145–153. doi: 10.1038/nn.3881.

Vasquez, J. K. *et al.* (2014) 'Lateral Diffusion of Proteins on Supported Lipid Bilayers: Additive Friction of Synaptotagmin 7 C2A–C2B Tandem Domains'. doi: 10.1021/bi5012223.

Verhage, M *et al.* (1991) 'Characterization of the release of cholecystokinin-8 from isolated nerve terminals and comparison with exocytosis of classical transmitters', *Journal of Neurochemistry*, 56, pp. 1394–1400.

Verhage, Matthijs *et al.* (1991) 'Differential release of amino acids, neuropeptides, and catecholamines from isolated nerve terminals', *Neuron*. Cell Press, 6(4), pp. 517–524. doi: 10.1016/0896-6273(91)90054-4.

Vician, L. *et al.* (1995) 'Synaptotagmin IV is an immediate early gene induced by depolarization in PC12 cells and in brain.', *Proceedings of the National Academy of Sciences of the United States of America*, 92(6), pp. 2164–2168.

Voets, T. *et al.* (2001) 'Intracellular calcium dependence of large dense-core vesicle exocytosis in the absence of synaptotagmin I.', *Proceedings of the National Academy of Sciences of the United States of America*, 98(20), pp. 11680–11685. doi: 10.1073/pnas.201398798.

Volynski, K. E. and Krishnakumar, S. S. (2018) 'Synergistic control of neurotransmitter release by different members of the synaptotagmin family', *Current Opinion in Neurobiology*. Elsevier Ltd, 51, pp. 154–162. doi: 10.1016/j.conb.2018.05.006.

Wang, C. *et al.* (2016) 'Synaptotagmin-11 inhibits clathrin-mediated and bulk endocytosis', *EMBO reports*, 17(1), pp. 47–63. doi: 10.15252/embr.201540689.

Wang, C. *et al.* (2018) 'Synaptotagmin-11 is a critical mediator of parkin-linked neurotoxicity and Parkinson's disease-like pathology', *Nature Communications*. Springer US, 9(1), pp. 1–14. doi: 10.1038/s41467-017-02593-y.

Wang, C. T. *et al.* (2001) 'Synaptotagmin modulation of fusion pore kinetics in regulated exocytosis of dense-core vesicles', *Science*, 294(5544), pp. 1111–1115. doi: 10.1126/science.1064002\r294/5544/1111 [pii].

Wang, C. T. *et al.* (2003) 'Different domains of synaptotagmin control the choice between kiss-and-run and full fusion', *Nature*, 424(6951), pp. 943–947. doi: 10.1038/nature01857\rnature01857 [pii].

Wang, N., Gibbons, C. H. and Freeman, R. (2011) 'Novel immunohistochemical techniques using discrete signal amplification systems for human cutaneous peripheral nerve fiber imaging', *Journal of Histochemistry and Cytochemistry*, 59(4), pp. 382–390. doi: 10.1369/0022155410396931.

Wang, S. *et al.* (2015) 'Modality-specific mechanisms of protein kinase C-induced hypersensitivity of TRPV1: S800 is a polymodal sensitization site', *Pain*, 156(5), pp. 931–941. doi: 10.1097/j.pain.000000000000134.

Wang, Y. Y. *et al.* (2017) 'Ligand- and voltage-gated Ca<sup>2+</sup> channels differentially regulate the mode of vesicular neuropeptide release in mammalian sensory neurons', *Science Signaling*, 10(484), pp. 1–8. doi: 10.1126/scisignal.aal1683.

Weber, T. *et al.* (1998) 'SNAREpins: Minimal Machinery for Membrane Fusion', *Cell*, 92(6), pp. 759–772. doi: 10.1016/S0092-8674(00)81404-X.

Weiss, A. N. *et al.* (2014) 'Luminal Protein within Secretory Granules Affects Fusion Pore Expansion', *Biophysical Journal*. Cell Press, 107(1), pp. 26–33. doi: 10.1016/J.BPJ.2014.04.064.

Wen, H. *et al.* (2010) 'Distinct roles for two synaptotagmin isoforms in synchronous and asynchronous transmitter release at zebra fish neuromuscular junction.', *Proceedings of the National Academy of Sciences*, 107(31), pp. 13906–13911. doi: 10.1073/pnas.1008598107/-  
/DCSupplemental.www.pnas.org/cgi/doi/10.1073/pnas.1008598107.

Wen, P. J. *et al.* (2016) 'Actin dynamics provides membrane tension to merge fusing vesicles into the plasma membrane', *Nature Communications*, 7(1). doi: 10.1038/ncomms12604.

Wendler, F. *et al.* (2001) 'Homotypic Fusion of Immature Secretory Granules During Maturation Requires Syntaxin 6', *Molecular Biology of the Cell*. American Society for Cell Biology, 12(6), pp. 1699–1709. doi: 10.1091/mbc.12.6.1699.

White, F. A. *et al.* (1996) 'Synchronous onset of NGF and TrkA survival dependence in developing dorsal root ganglia', *Journal of Neuroscience*. Society for Neuroscience, 16(15), pp. 4662–4672. doi: 10.1523/jneurosci.16-15-04662.1996.

Wiesenfeld-Hallin, Z. *et al.* (1984) 'Immunoreactive calcitonin gene-related peptide and substance P coexist in sensory neurons to the spinal cord and interact in spinal behavioral responses of the rat', *Neuroscience Letters*, 52(1–2), pp. 199–204. doi: 10.1016/0304-3940(84)90374-4.

Winter, J. *et al.* (1988) 'Nerve growth factor (NGF) regulates adult rat cultured dorsal root ganglion neuron responses to the excitotoxin capsaicin', *Neuron*, 1(10), pp. 973–981. doi: 10.1016/0896-6273(88)90154-7.

Wiśniewski, J. R. *et al.* (2010) 'Brain phosphoproteome obtained by a fasp-based method reveals plasma membrane protein topology', *Journal of Proteome Research*, 9(6), pp. 3280–3289. doi: 10.1021/pr1002214.

de Wit, H. *et al.* (2009) 'Synaptotagmin-1 Docks Secretory Vesicles to Syntaxin-1/SNAP-25 Acceptor Complexes', *Cell*, 138(5), pp. 935–946. doi: 10.1016/j.cell.2009.07.027.

de Wit, J., Toonen, R. F. and Verhage, M. (2009) 'Matrix-Dependent Local Retention of Secretory Vesicle Cargo in Cortical Neurons', *Journal of Neuroscience*. Society for Neuroscience, 29(1), pp. 23–37. doi: 10.1523/jneurosci.3931-08.2009.

Woolf, C. J. (2011) 'Central sensitization: Implications for the diagnosis and treatment of pain', *Pain*. International Association for the Study of Pain, 152(SUPPL.3), pp. S2–S15. doi: 10.1016/j.pain.2010.09.030.

Wu, M. M. *et al.* (2001) 'Mechanisms of pH Regulation in the Regulated Secretory Pathway', *Journal of Biological Chemistry*, 276(35), pp. 33027–33035. doi: 10.1074/jbc.M103917200.

Wu, Y. *et al.* (2009) 'Biophysical characterization of styryl dye-membrane interactions', *Biophysical Journal*, 97(1), pp. 101–109. doi: 10.1016/j.bpj.2009.04.028.

Xia, X., Lessmann, V. and Martin, T. F. J. (2009) 'Imaging of evoked dense-core-vesicle exocytosis in hippocampal neurons reveals long latencies and kiss-and-run fusion events', *Journal of Cell Science*, 122(1), pp. 75–82. doi: 10.1242/jcs.034603.

Xiao, H.-S. *et al.* (2002) 'Identification of gene expression profile of dorsal root ganglion in the rat peripheral axotomy model of neuropathic pain.', *Proceedings of the National Academy of Sciences of the United States of America*, 99(12), pp. 8360–5. doi: 10.1073/pnas.122231899.

Xie, Z. *et al.* (2017) 'Molecular Mechanisms for the Coupling of Endocytosis to Exocytosis in Neurons', *Frontiers in Molecular Neuroscience*, 10(March), pp. 1–8. doi:

10.3389/fnmol.2017.00047.

Xu, J. *et al.* (2009) 'Synaptotagmin-1 functions as a Ca<sup>2+</sup> sensor for spontaneous release', *Nature Neuroscience*, 12(6), pp. 759–766. doi: 10.1038/nn.2320.

Xu, J., Mashimo, T. and Südhof, T. C. (2007) 'Synaptotagmin-1, -2, and -9: Ca(2+) sensors for fast release that specify distinct presynaptic properties in subsets of neurons.', *Neuron*, 54(4), pp. 567–81. doi: 10.1016/j.neuron.2007.05.004.

Xu, Y. *et al.* (2011) 'Dual-mode of insulin action controls GLUT4 vesicle exocytosis', *Journal of Cell Biology*, 193(4), pp. 643–653. doi: 10.1083/jcb.201008135.

Xu, Y. *et al.* (2017) 'Excess cholesterol inhibits glucose-stimulated fusion pore dynamics in insulin exocytosis', *Journal of Cellular and Molecular Medicine*, XX(X), pp. 1–13. doi: 10.1111/jcmm.13207.

Xue, M. *et al.* (2010) 'Structural and Mutational Analysis of Functional Differentiation between Synaptotagmins-1 and -7', *PLoS ONE*. Edited by B. Kobe, 5(9), p. e12544. doi: 10.1371/journal.pone.0012544.

Yoo, S. H. (1996) 'pH- and Ca<sup>2+</sup>-dependent aggregation property of secretory vesicle matrix proteins and the potential role of chromogranins A and B in secretory vesicle biogenesis', *Journal of Biological Chemistry*, 271(3), pp. 1558–1565. doi: 10.1074/jbc.271.3.1558.

Yoshihara, M. *et al.* (2005) 'Retrograde signaling by Syt 4 induces presynaptic release and synapse-specific growth', *Science*, 310(5749), pp. 858–863. doi: 10.1126/science.1117541.

Young, S. M. and Neher, E. (2009) 'Synaptotagmin Has an Essential Function in Synaptic Vesicle Positioning for Synchronous Release in Addition to Its Role as a Calcium Sensor', *Neuron*. Elsevier Ltd, 63(4), pp. 482–496. doi: 10.1016/j.neuron.2009.07.028.

Yuan, T. *et al.* (2015) 'Spatiotemporal detection and analysis of exocytosis reveal fusion "hotspots" organized by the cytoskeleton in endocrine cells', *Biophysical Journal*. Biophysical Society, 108(2), pp. 251–260. doi: 10.1016/j.bpj.2014.11.3462.

Yuen, E. C. *et al.* (1996) 'Nerve growth factor and the neurotrophic factor hypothesis', *Brain and Development*, 18(5), pp. 362–368. doi: 10.1016/0387-7604(96)00051-4.

Zeisel, A. *et al.* (2018) 'Molecular Architecture of the Mouse Nervous System', *Cell*, 174(4), pp. 999-1014.e22. doi: 10.1016/j.cell.2018.06.021.

Zhang, C. *et al.* (2004) 'Calcium- and dynamin-independent endocytosis in dorsal root ganglion neurons', *Neuron*, 42(2), pp. 225–236. doi: 10.1016/S0896-6273(04)00189-8.

Zhang, C. and Zhou, Z. (2002) 'Ca<sup>2+</sup>-independent but voltage-dependent secretion in mammalian dorsal root ganglion neurons', *Nature Neuroscience*. Nature Publishing Group, 5(5), pp. 425–430. doi: 10.1038/nn845.

Zhang, G. *et al.* (2011) 'Neuropeptide Exocytosis Involving Synaptotagmin-4 and Oxytocin in Hypothalamic Programming of Body Weight and Energy Balance', *Neuron*. Elsevier Inc., 69(3), pp. 523–535. doi: 10.1016/j.neuron.2010.12.036.

Zhang, Q. *et al.* (2019) 'Differential Co-release of Two Neurotransmitters from a Vesicle Fusion Pore in Mammalian Adrenal Chromaffin Cells', *Neuron*, 102(1), pp. 173-183.e4. doi: 10.1016/j.neuron.2019.01.031.

Zhang, X. *et al.* (2007) 'Neuronal somatic ATP release triggers neuron-satellite glial cell communication in dorsal root ganglia', *Proceedings of the National Academy of Sciences of the United States of America*, 104(23), pp. 9864–9869. doi: 10.1073/pnas.0611048104.

Zhang, X., Huang, J. and McNaughton, P. A. (2005) 'NGF rapidly increases membrane expression of TRPV1 heat-gated ion channels', *EMBO Journal*, 24(24), pp. 4211–4223. doi: 10.1038/sj.emboj.7600893.

Zhang, Z. *et al.* (2009) 'Synaptotagmin IV: a multifunctional regulator of peptidergic nerve terminals.', *Nature neuroscience*, 12(2), pp. 163–171. doi: 10.1038/nn.2252.

Zhang, Z., Zheng, Z. and Jackson, M. B. (2010) 'Synaptotagmin IV Modulation of Vesicle Size and Fusion Pores in PC12 Cells', *Biophysical Journal*. Biophysical Society,

98(6), pp. 968–978. doi: 10.1016/j.bpj.2009.11.024.

Zhao, B. *et al.* (2011) 'Transport of receptors, receptor signaling complexes and ion channels via neuropeptide-secretory vesicles.', *Cell research*. Nature Publishing Group, 21(5), pp. 741–53. doi: 10.1038/cr.2011.29.

Zhao, W. D. *et al.* (2016) 'Hemi-fused structure mediates and controls fusion and fission in live cells', *Nature*. Nature Publishing Group, 534(7608), pp. 548–552. doi: 10.1038/nature18598.

Zheng, H. *et al.* (2009) 'Action potential modulates Ca<sup>2+</sup>-dependent and Ca<sup>2+</sup>-independent secretion in a sensory neuron.', *Biophysical journal*, 96(6), pp. 2449–56. doi: 10.1016/j.bpj.2008.11.037.

Zhou, Q. *et al.* (2017) 'The primed SNARE–complexin–synaptotagmin complex for neuronal exocytosis', *Nature*. Nature Publishing Group, 548(7668), pp. 420–425. doi: 10.1038/nature23484.

Zhu, W. *et al.* (2004) 'A Developmental Switch in Acute Sensitization of Small Dorsal Root Ganglion (DRG) Neurons to Capsaicin or Noxious Heating by NGF', *Journal of Neurophysiology*. American Physiological Society, 92(5), pp. 3148–3152. doi: 10.1152/jn.00356.2004.

Zhu, W. and Oxford, G. S. (2011) 'Differential gene expression of neonatal and adult DRG neurons correlates with the differential sensitization of TRPV1 responses to nerve growth factor', *Neuroscience Letters*. Elsevier, 500(3), pp. 192–196. doi: 10.1016/j.neulet.2011.06.034.